

Investigation of biogenesis of the  
presynaptic compartments  
using human iPSC-derived neurons

Inaugural-Dissertation

to obtain the academic degree

Doctor rerum naturalium (Dr. rer. nat)

submitted to the Department of Biology, Chemistry, Pharmacy of

the

Freie Universität Berlin

by

**Filiz Sila Rizalar**

born in

Samsun, Turkey

Berlin, 2022

Period of doctorate studies: September 2017 to March 2022

Supervisor: Prof. Dr. Volker Haucke

Institute: Leibniz-Forschungsinstitut für Molekulare  
Pharmakologie (FMP), Berlin

1st Reviewer: Prof. Dr. Volker Haucke

2nd Reviewer: Prof. Dr. Stephan J. Sigrist

Date of defense: 22.06.2022

Affidavit

I declare that my PhD thesis at hand has been written independently and with no other sources and aids then quoted.

I also declare that I have not applied for an examination procedure at any other institution and that I have not submitted the dissertation in this or any other form to any other faculty as a dissertation

Berlin, March 24th, 2022

*to my father, Prof. Rıza Rızalar*

## Acknowledgement

Firstly, I would like to express my sincere gratitude to my research supervisor, Prof. Volker Haucke for the continuous support during my PhD study, for his guidance, motivation, inspiring discussions and immense knowledge.

I would like to thank Prof. Stephan Sigrist from the Free University for the great and productive collaboration we had over the last years. I would like to thank Dr. Astrid Petzoldt for lively and thorough discussions. I thank Dr. Sebastian Diecke from the MDC for a wonderful collaboration. I also wish to thank Dr. Martin Lehmann for being a great help for all my imaging-related issues and opening up new experimental possibilities for answering crucial questions in my project.

I would like to thank my subgroup colleagues: Shuhan Kong, Max Lucht, Julia Riedlberger, Dr. Dmytro Puchkov and Dr. Miaomiao Tian for great discussions and their constructive feedback. I also acknowledge Dr. Christoph Ott and Dr. Anela Vukoja who worked on this subject before me and provided the basis for my project. I would like to thank my colleagues Dr. Domenico Azarnia Tehran, Dr. Marijn Kuijpers, Dr. Tolga Soykan, Philipp A. Koch and Kristine Oevel, Dr. Gillian Dornan and Dr. Tania Lopez-Hernandez for fantastic scientific (and non-scientific) discussions, great suggestions and motivation.

I would like to thank our secretaries Alexandra Chylla and Sebastian Kramer for their great organizational help. I also thank our technicians, especially Delia Löwe, for their continuous technical support.

I would like to acknowledge all past and present members of the AG Haucke who created a cheerful, collaborative and supportive atmosphere inside as well as outside the laboratory. Working with you made this journey very much enjoyable and much easier- thank you for your endless support!

Finally, I would like to thank my (other) friends, especially Nazmiye Özkan and Dr. Cansu Akkaya. In particular, I wish to thank Dr. Alexander Wallroth for his continuous and full support.

Most importantly, I want to express my deepest gratitude to my family for supporting me throughout my studies, my thesis and my life in general.

# I Table of Contents

I Table of Contents.....	5
II Summary.....	9
III Zusammenfassung.....	10
1. Introduction.....	1
1.1. Building a synapse.....	1
1.2. Components and assembly of the presynapse.....	2
1.2.1. Synaptic cell adhesion molecules.....	4
1.2.2. The Cytomatrix of the AZ.....	5
1.2.3. Calcium channels.....	7
1.2.4. Synaptic vesicles and the machinery for neurotransmitter release.....	8
1.3. Mechanisms of axonal transport of precursor vesicles.....	10
1.3.1. Morphology and cell biological identity of presynaptic transport vesicles.....	11
1.3.2. Kinesins as primary motors for anterograde axonal transport.....	14
1.4. Kinesins implicated in presynaptic precursor transport.....	15
1.4.1. KIF1A and the associated presynaptic precursor transport machinery.....	18
1.5. Arl8: a small GTPase regulating lysosomal motility.....	20
1.5.1. Role of Arl8 in presynapse formation.....	24
1.6. Phosphoinositide identity of presynaptic precursor vesicles.....	26
1.6.1. Phosphoinositides as signposts of compartmental membrane identity.....	26
1.3.3. Phosphatidylinositol 3-phosphates and the endolysosomal system.....	28
1.3.4. PI(3,5)P2 in the endolysosomal system.....	29
2. Objectives.....	33
3. Material and Methods.....	34
3.1. Materials.....	34
3.1.1. Chemicals.....	34
3.1.2. Buffers, Media and Solutions.....	34
3.1.3. Enzymes and kits.....	38
3.1.4. Molecular weight standards.....	39
3.1.5. Small hairpin RNA oligonucleotides.....	39
3.1.6. Plasmid vectors.....	42

3.1.7. Antibodies.....	44
3.2. Molecular Biology Methods.....	46
3.2.1. Cloning strategies .....	46
3.2.2. Polymerase chain reaction .....	46
3.2.3. Agarose gel electrophoresis of DNA fragments .....	47
3.2.4. Sequencing of DNA .....	48
3.2.5. Transformation of chemically competent <i>E.coli</i> Top10 cells .....	48
3.2.6. Glycerol Stocks.....	48
3.2.7. Purification of plasmid DNA from <i>E. coli</i> cultures.....	48
3.2.8. RNA extraction from iPSCs and iNs.....	49
3.2.9. Reverse transcription of RNA.....	49
3.2.10. RNA quantification using quantitative real-time PCR.....	49
3.2.11. Isolation of genomic DNA (gDNA) from iPSCs.....	50
3.2.12. Genotyping of iPS clones .....	50
3.3. Cell Culture Methods .....	51
3.3.1. Human induced pluripotent stem cell (iPSC) culture .....	51
3.3.2. Differentiation of human iPSCs into cortical neurons .....	52
3.3.3. Generating genome-edited isogenic iPSC lines using CRISPR.....	53
3.3.4. Lentiviral production in HEK-293TN cells.....	56
3.3.5. Preparation and culture of primary mouse glia.....	56
3.3.6. Culture of HEK293T and HeLa cells .....	57
3.3.7. jetPRIME transfection of HeLa cells for immunofluorescence analysis.....	57
3.3.8. Calcium phosphate transfection of primary hippocampal neurons and iNs.....	57
3.3.9. Immunocytochemistry.....	58
3.4. Microscopy and Image Analysis.....	59
3.4.1. Confocal microscopy .....	59
3.4.2. Spinning disc confocal microscopy and analysis of axonal transport dynamics ...	59
3.4.4. pHluorin live-cell imaging .....	60
3.5. Biochemical Methods.....	61
3.5.1. Protein preparation from cells .....	61
3.5.2. Determining protein concentration in cell lysates.....	61
3.5.3. Immunoprecipitation using magnetic nanobeads.....	62
3.5.4. Expression of recombinant proteins in <i>E.coli</i> .....	62
3.5.5. Affinity-purification of GST-fusion proteins.....	63
3.5.6. Liposome sedimentation assay.....	63
3.5.6. SDS polyacrylamide gel electrophoresis (SDS-PAGE).....	65

3.5.8. Coomassie staining of SDS-polyacrylamide gels.....	66
3.5.9. PIP-strip .....	67
3.5.10. Mass Spectrometry analysis of the immunoprecipitation experiment.....	67
4. Results.....	68
4.1. Human induced pluripotent stem (iPS) cell-derived neurons (iNs) as a model system to study presynaptic biogenesis.....	68
4.1.1. Human iPS cells can be efficiently differentiated into excitatory cortical neurons.....	68
4.1.2. Characterization of developing and mature iNs .....	69
4.3. KIF1A is the main kinesin driving anterograde transport of presynaptic vesicles .....	78
4.3.1. KIF1A co-traffics with presynaptic proteins in the developing axon.....	78
4.3.2. Lentiviral shRNA-mediated knockdown of KIF1A depletes SV and AZ proteins from presynapses in iNs.....	79
4.3.3. Genetically engineered <i>KIF1A</i> <sup>-/-</sup> iNs phenocopy the KIF1A knockdown phenotype .....	82
4.3.4. Immunoprecipitation of KIF1A followed by MS/MS reveals interaction partners of KIF1A in developing iNs.....	85
4.4. Arl8 is a marker of PVs and regulates their axonal trafficking.....	87
4.4.1. PVs co-transport with lysosomal membrane proteins in the developing axon .....	87
4.4.2. PV transport is regulated by Arl8 but is not dependent on KIF5B/BORC/SKIP complex.....	90
4.4.3. Arl8a/b double KO iPSCs validate the presynaptic loss observed in Arl8 knockdown iNs.....	94
4.4.4. Loss of Arl8 results in decreased calcium influx in iNs .....	97
4.6. KIF1A drives the transport of synaptic PVs via its interaction with Arl8 and PI(3,5)P <sub>2</sub> .....	99
4.6.1. The PH domain of KIF1A is essential for driving anterograde transport of PVs ...	99
4.6.2. PIP Kinase inhibitor screen reveals specific phosphoinositides recognized by the PH domain of KIF1A .....	100
4.6.3. Lentiviral knockdown of PIKfyve verifies that PI(3,5)P <sub>2</sub> is essential for PV transport.....	106
4.6.4. Liposome sedimentation assays show that the KIF1A PH domain directly binds to PI(3,5)P <sub>2</sub> .....	107
4.7. PIKfyve activity is required for anterograde PV transport .....	109
4.7.1. KIF1A requires Arl8 and PI(3,5)P <sub>2</sub> to drive anterograde transport of PVs in developing neurons.....	109
4.7.2. Loss of BORC induces anterograde PV transport by increasing PI(3,5)P <sub>2</sub> levels .....	112
5. Discussion.....	117

5.1. Different components of the presynaptic compartment are delivered collectively to axon terminals.....	117
5.2. Arl8a and Arl8b regulate PV motility in developing human neurons .....	121
5.3. PVs have a lysosomal identity although they are different than <i>bona fide</i> lysosomes .....	123
5.4. KIF1A PH domain is essential to drive anterograde transport of PVs .....	126
5.5. PIKfyve activity is required for KIF1A to drive efficient transport of PVs .....	129
6. Conclusion .....	134
7. References.....	135
8. Appendix .....	148
8.1. Appendix A: Abbreviations .....	148
8.2. Appendix B: Supplemental Figures .....	151
8.3. Appendix C: List of Figures and Tables.....	154
8.3.1. List of Tables.....	154
8.3.2. List of Figures .....	154

## II Summary

Synapse formation starts during development as axons establish contacts with dendrites and neuronal cell bodies. Having a single elongated axon and multiple dendrites derived from the cell body attribute neurons an exceptional polarity, resulting in synapses being located distant to the cell body where most protein synthesis takes place. Thus, to ensure stoichiometric assembly of functional presynaptic units, components of the presynaptic compartment, synaptic vesicle (SV) and active zone (AZ) proteins as well as synaptic cell adhesion molecules (sCAMs), need to be delivered to nascent synapses in a coordinated manner. Mechanisms regulating the efficient delivery of presynaptic proteins to axon terminals as well as the cellular identity of presynaptic transport organelles are incompletely understood. This thesis therefore focused on elucidating the axonal transport machinery of presynaptic protein carrying vesicles, referred to as precursor vesicles (PVs) in developing neurons.

During the course of this thesis I established, that PVs transport not only SV proteins but also AZ proteins and the sCAM protein Neurexin 1 $\beta$  collectively to the nascent presynapse in developing human iPSC-derived neurons. Anterograde trafficking of PVs is driven by the kinesin motor protein KIF1A and is regulated by the lysosomal small GTPase Arl8. Double loss of Arl8a and Arl8b in human neurons results in a significantly decreased number of anterogradely moving PVs in developing neurons and, consequently, a drastic loss in presynaptic protein levels at mature synapses. Interestingly, despite being regulated by Arl8, PVs are distinct from mature degradative lysosomes: They are non-acidic, do not harbor cathepsin activity, and use a transport machinery that is distinct from the classical KIF5B-dependent lysosomal transport machinery. Live imaging and biochemical experiments indicate that PVs presumably originate from the endolysosomal system, as they have a specific PI(3,5)P2 lipid identity which is recognized by the PH domain of KIF1A. Arl8 and PI(3,5)P2 provide a coincidence detection mechanism for KIF1A to drive PV transport by interacting directly with Arl8 via its CC3 domain and with PI(3,5)P2 through its lipid binding PH domain. PV transport is further regulated by a multi-subunit complex named BORC, which regulates lysosomal motility upstream of Arl8. BORC activity can mediate PV transport independent of Arl8 by negatively regulating PI(3,5)P2 levels. Taken together, my data unravels the lipid identity of presynaptic transport organelles and sheds light on their biogenesis and the mechanisms that underlying the regulation of the machinery for PV transport.

### III Zusammenfassung

Die Synapsenbildung beginnt während der Neuronal-Entwicklung, wenn Axone Kontakte mit Dendriten und neuronalen Zellkörpern herstellen. Ein einzelnes verlängertes Axon und mehrere Dendriten, die aus dem Zellkörper stammen, verleihen Neuronen eine außergewöhnliche Polarität, was dazu führt, dass sich Synapsen weit entfernt vom Zellkörper befinden, in die Proteinsynthese hauptsächlich stattfindet. Um den stöchiometrischen Aufbau von funktionellen präsynaptischen Einheiten sicherzustellen, müssen Komponenten des präsynaptischen Kompartiments, synaptische Vesikel (SV) und „Active-Zone“ Proteine (AZ) sowie synaptische Zelladhäsionsmoleküle (sCAMs) koordiniert an sich entwickelnde Synapsen geliefert werden. Mechanismen, die den effizienten Transport von präsynaptischen Proteinen zu Axon-Enden regulieren, sowie die zelluläre Identität von präsynaptischen Transportorganellen waren bisher weitestgehend unerforscht. Das Ziel dieser Dissertation war daher die Aufklärung der axonalen Transportmaschinerie für präsynaptische proteinhaltige Vesikel -die als Vorläufer-Vesikel (PVs) bezeichnet werden- in sich entwickelnden Neuronen.

Im Zuge dieser Arbeit wurde etabliert, dass PVs neben SV-Proteinen auch AZ-Proteine und das sCAM-Protein Neurexin 1 $\beta$  gemeinsam zur entstehenden Präsynapse in sich entwickelnden humanen aus iPSC (induzierte pluripotente Stammzellen) differenzierten Neuronen transportieren. Der anterograde Transport von PVs wird durch das Kinesin-Motorprotein KIF1A angetrieben und durch die lysosomale kleine GTPase Arl8 reguliert. Genetischer Verlust von beiden Isoformen - Arl8a und Arl8b - in menschlichen Neuronen führte zu einer signifikant verringerten Anzahl an anterograd transportierten PVs während der Neuronen-entwicklung und in der Konsequenz zu einem drastischen Verlust der präsynaptischen Proteinen in reifen Synapsen. Obwohl sie ebenfalls durch Arl8 reguliert werden, unterscheiden sich PVs interessanterweise von reifen Lysosomen: Sie haben keinen sauren pH-Wert, keine Cathepsin-Aktivität und verwenden eine Transportmaschinerie, die sich von der klassischen KIF5B-abhängigen lysosomalen Transportmaschinerie unterscheidet. Live-Mikroskopie und biochemische Experimente zeigten, dass PVs vermutlich trotzdem aus dem endo-lysosomalen System stammen, da sie eine spezifische PI(3,5)P2-Lipid-Identität haben, die von der KIF1A PH-Domäne erkannt wird. KIF1A erkennt Arl8 und PI(3,5)P2 per Koinzidenz, indem es direkt mit Arl8 über seine CC3-Domäne und mit PI(3,5)P2 über seine lipidbindende PH-Domäne interagiert und somit den PV-Transport initiiert. Der PV-Transport wird weiter durch einen Komplex aus mehreren Untereinheiten namens BORG reguliert, der Arl8 und darüber die Motilität von Lysosomen reguliert. BORG kann den PV-Transport unabhängig von Arl8 negativ regulieren, indem PI(3,5)P2-Level auf PVs indirekt

durch BORC minimiert werden. Alles in allem entschlüsseln die Daten meiner Arbeit die Lipididentität von präsynaptischen Transportorganellen und beleuchten ihre Biogenese und die Mechanismen, die der Regulation der Maschinerie für den PV-Transport zugrunde liegen.

# 1. Introduction

## 1.1. Building a synapse

Neurons are highly polarized brain cells, consisting of a single axon and multiple dendrites deriving from the cell body to form tightly associated pre- and postsynaptic compartments. Axons transmit action potentials (APs) arising at the axon initial segment (AIS) towards their tip, where the presynaptic compartment is built. Dendrites specialize in receiving signals coming from other neurons through the postsynaptic compartment and forwarding them to the soma and further. Synaptic connections are built as asymmetric intercellular junctions between the presynaptic and postsynaptic compartments. These two processes are precisely juxtaposed to each other in order to enable swift and precise information transmission between cells. Synapses define the sites where neuronal communication takes place and therefore are critical for various processes such as information processing, learning and memory. When an AP reaches the presynapse, it induces the release of neurotransmitters that diffuse through the synaptic cleft and bind to the receptors on the postsynapse of another neuron, mediating the transfer of information. This process is dependent on various molecular machineries (which will be discussed in the next chapter) that have to be added to not only generate but also maintain a functional synapse. Thus, synaptic biogenesis takes place during neuronal development to establish nascent synapse formation and continues in mature neuronal networks to maintain neuronal plasticity (Südhof, 2017a).

In contrast to the significant progress that has been made in understanding synaptic transmission and retrieval of information at the post-synapse (Maritzen and Haucke, 2018; Soykan et al., 2016; Takamori et al., 2006b), remarkably little is known regarding the formation of the presynaptic compartment. Neuronal cell body contains the cell nucleus and the biosynthetic machinery necessary for protein synthesis, including the endoplasmic reticulum (ER), ribosomes and the Golgi apparatus. This restricts protein biosynthesis mainly to the somatodendritic region with exceptions of local protein translation proximal to synaptic sites (Hafner et al., 2019; Sigrist et al., 2000). This indicates that following their synthesis in the neuronal soma, presynaptic components are packaged into synaptic precursor vesicles (PVs) and carried along the axon to sites of presynaptic biogenesis.

A major challenge for PVs is logistical, as the presynaptic compartment can be meters away from the neuronal cell body (Guedes-Dias and Holzbaaur, 2019). Half-lives of presynaptic

## Introduction

---

proteins have been estimated on the time scale of days, with approximately 0.7% of synaptic protein content being degraded per hour (Cohen et al., 2013). In addition, as few as 1-5 PVs are thought to provide sufficient presynaptic components to assemble a functional bouton in cultured neurons (Ahmari et al., 2000; Maas et al., 2012a; Shapira et al., 2003), resulting in very low numbers of PVs passing the axon initial segment in mature neurons. Therefore, studying morphological or biochemical characterization of PVs has had limitations due to not only extreme transport challenge they undergo, but also their transient nature and low abundance.

The cell biological origin and molecular composition of synaptic PVs remain unknown. Moreover, mechanisms that direct their formation in the neuronal cell body, their transport and maturation along developing axons, and the assembly of the complex molecular machines that make up a functional presynapse are still debated. These elements, however, are essential to understand since they will provide new insights into human neurological diseases related to defective presynaptic biogenesis and/or impaired axonal transport.

### 1.2. Components and assembly of the presynapse

The presynaptic compartment is defined as a specialized region of the axonal membrane and may originate either at the axonal terminal (resulting in a terminal bouton) or along the axon shaft (resulting in an *en passant* bouton). Neurons initiate formation of their presynaptic compartments prior to postsynaptic compartments. Moreover, presynaptic compartments have been reported to form in the absence of postsynaptic targets (Prokop et al., 1996), suggesting that presynaptic biogenesis may be a cell-autonomous process and does not require transsynaptic contact (Südhof, 2017b).

During neurotransmission, an AP is propagated along the axonal shaft to the presynapse to open voltage-gated calcium channels (Cavs), allowing the release of neurotransmitters by exocytosis of synaptic vesicles (SVs) at the active zone (AZ). Neurotransmitters that are released into the synaptic cleft then interact with postsynaptic transmembrane receptors to further propagate the signal. Thus, precise spatio-temporal establishment of the presynaptic compartment is required for the fast and accurate transmission of nerve impulses. To this end, the presynaptic compartment not only serves for

## Introduction

the confined recruitment and anchoring of SVs and Cavs at the AZ, but also for the establishment of transsynaptic adhesions with postsynaptic densities.

There are three main building blocks of a functional presynapse: (i) Synaptic cell-adhesion molecules (sCAMs), trans-cellular signaling factors that hold the pre- and postsynaptic compartments together, (ii) an active zone cytomatrix (CAZ) which is built by AZ proteins, and (iii) neurotransmitter-filled SVs and the associated machinery at or nearby Cav-containing release sites (**Figure 1.1**).

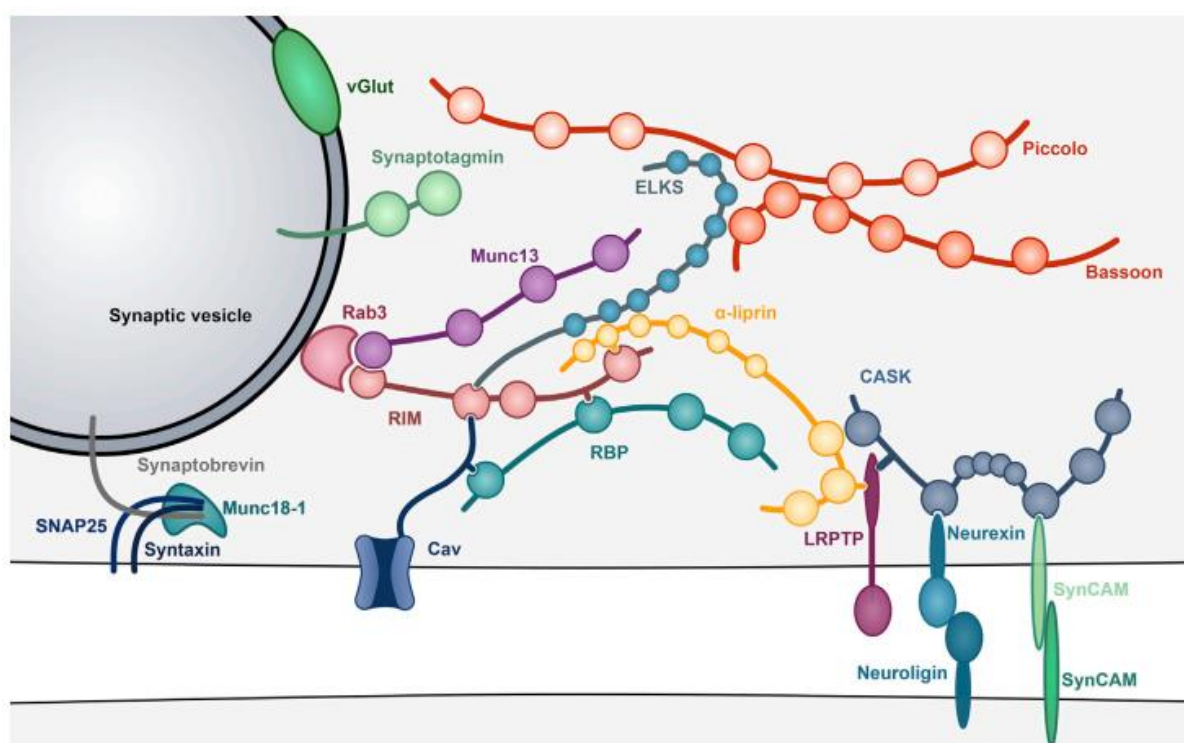


**Figure 1.1. Key components of the presynaptic machinery for neurotransmitter release.** Schematic representation of presynaptic components including protein domains and their interactions, including sCAMs (shown SynCAM, Neuroligin, Neurexin and LRPTP); CAZ proteins (shown RIM, RBP, α-liprin, CASK, ELKS, Munc13, Piccolo, Bassoon); Cavs; SV proteins (shown Synaptobrevin, Rab3, Synaptotagmin, vesicular glutamate transporter [vGlut]); and SV-associated fusion machinery (SNAP25, Syntaxin, Munc18-1) (Rizalar et al., 2021).

## Introduction

---

### 1.2.1. Synaptic cell adhesion molecules

Formation of a chemical synapse is preceded by the establishment of physical axodendritic contact and is initiated by transmembrane synaptic cell adhesion molecules (sCAMs). sCAMs mediate interneuronal junctions bridging the synaptic cleft via their extracellular domains, thereby establishing sites of presynapse. Transsynaptic adhesions by sCAMs hold pre- and postsynaptic compartments together and ensure the precise nano-alignment of the AZ with the postsynaptic density. Transsynaptic junctions are also required for bi-directional intercellular signaling that instruct an 'assembly signal' for the biogenesis and differentiation of nascent synapses.

sCAMs comprise multiple gene families, including neurexins, neuroligins, cadherins and Ig-containing cell adhesion molecules (IgCAMs) (Sanes and Zipursky, 2020). Given the asymmetric nature of the synapse, the initial transsynaptic contact is likely mediated by heterophilic axodendritic interactions, e.g. between the presynaptic Neurexin and postsynaptic Neuroligin, or between different SynCAM isoforms (Biederer et al., 2002; Fogel et al., 2007; Stagi et al., 2010; Südhof, 2017b; Thomas et al., 2008). Neurexins, through interaction with neuroligins, also trigger the recruitment of SVs (Dean et al., 2003) and clustering of Cavs at the presynaptic AZ (Luo et al., 2020), indicating that Neurexin-Neuroligin interaction is not only important for initiating of axodendritic contact and defining the site of biogenesis, but also for the recruitment of synaptic machinery for presynaptic differentiation.

Cell-based co-culturing systems of neurons with non-neuronal cells expressing postsynaptic sCAMs showed that expression of Neuroligin or SynCAM in non-neuronal cells is sufficient to recruit and assemble presynaptic specializations in neurons (Biederer et al., 2002; Sara et al., 2005; Scheiffele et al., 2000), indicating the instructive role of sCAMs in driving assembly of nascent presynaptic compartments. In addition to instructing the assembly signal, sCAMs can also serve as wiring molecules mediating the recruitment of presynaptic machinery to the transsynaptic nanocolumn. LAR (leukocyte associated receptor)-type receptor phospho-tyrosine phosphatases (LRPTP)s, presynaptic sCAMs that interact a multitude of postsynaptic targets, are central players in the local recruitment of presynaptic components, ensuring their close proximity to postsynaptic density (Horn et al., 2012; Sclip and Südhof, 2020).

## Introduction

### 1.2.2. The Cytomatrix of the AZ

Following the initial axodendritic contact, presynaptic components are rapidly assembled at the AZ on a timescale of minutes, prior to the assembly of the post-synaptic density (Friedman et al., 2000; Okabe et al., 2001; Petzoldt et al., 2016). Proper assembly of the active zone requires the transport of AZ material along axons, its assembly into an active zone protein complex in presynaptic nerve terminals and anchoring of this complex at the target membrane (**Figure 1.2**). The CAZ serves as a scaffold for recruiting and positioning of Caves and SVs within the presynaptic compartment (Emperador-Melero and Kaeser, 2020; Petzoldt et al., 2016; Scheiffele et al., 2000).

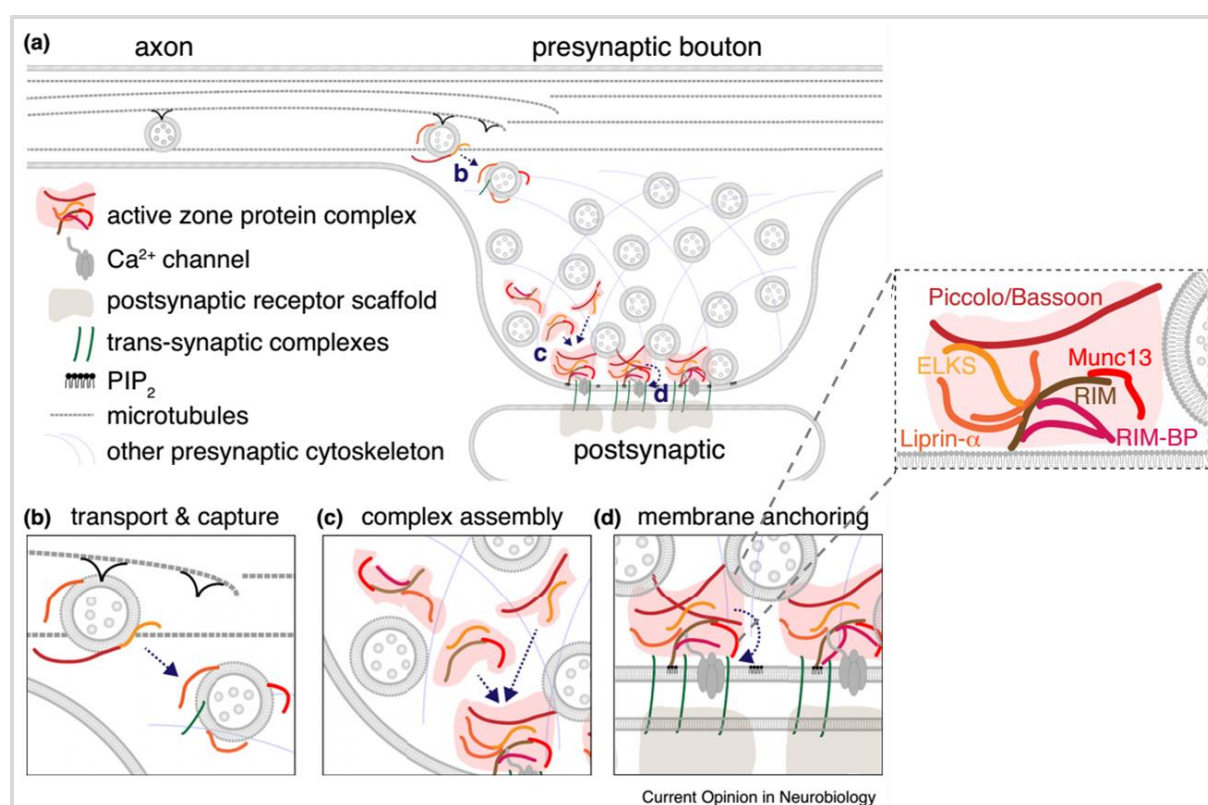


**Figure 1.2. Main processes in Active Zone assembly.** Schematic illustration demonstrating the main processes that are necessary for AZ assembly. These processes are initiated by the transport of AZ material and its capture in presynaptic nerve terminals (b), continued with the assembly of the material into an active zone protein complex (c), and finalizes by the anchoring of this complex at the target membrane (d). Higher magnification of an AZ protein complex formed by RIM, RIM-BP, ELKS, Liprin-α, Munc-13, and Piccolo/Bassoon is shown on the right hand side. (Adapted from (Emperador-Melero and Kaeser, 2020))

## Introduction

---

RIM (for Rab3-Interacting Molecules), RBP (RIM Binding Proteins) and Munc13 form a tripartite complex: RIM-RBP complex forms dense condensates to cluster Cav by liquid-liquid phase separation at the AZ, RIM-Munc13 complex positions SVs in close proximity to Cavs (Miki et al., 2017; Nakamura et al., 2015; Tang et al., 2016; Wu et al., 2019). Knockout of either RIMs or RBP only partially impairs AZ function whereas their combined loss impairs the alignment of the AZ with the PSD and completely blocks clustering of Cavs and vesicle priming. This indicates that by forming interactions, RIM and RBPs act as a group of main organizers of the AZ (Acuna et al., 2016).

$\alpha$ -liprin, CASK (Calcium/Calmodulin-dependent Serine protein Kinase) and ELKS (proteins rich in amino acids E, L, K and S) are conserved CAZ protein families that provide an interconnected molecular network at the presynapse by not only interacting with each other but also linking RIM, RBP, Munc13 tripartite complex to transsynaptic adhesion molecules for precise alignment with the PSD (Biederer et al., 2002; Hata et al., 1996; Ko et al., 2003; Ohtsuka et al., 2002; Schoch et al., 2002).

Piccolo and Bassoon, two large AZ scaffolds specific to the vertebrate nervous system, serve as a presynaptic skeleton that stabilize the presynaptic compartment. Apart from interacting with each other, Piccolo and Bassoon also interact other CAZ proteins ELKS, Munc13, RIM and RBPs to form an interconnected molecular network for physical and functional integration of the AZ (Davydova et al., 2014; Dresbach et al., 2006; Fujimoto et al., 2002; Maas et al., 2012a; Takao-Rikitsu et al., 2004; Wang et al., 2009).

Although synapse numbers or SV pool size are not extremely affected by the loss of AZ proteins, in many cases neurotransmission and the nanoscale localization of key presynaptic components are depleted, due to failure in formation of required interactions at the CAZ (Jin and Garner, 2008; Südhof, 2017b).

## Introduction

### 1.2.3. Calcium channels

Cavs are heteromultimeric protein complexes. Each of their subunits can be encoded by multiple genes that can undergo alternative splicing and differential RNA processing, giving rise to a multitude of Cavs (Simms and Zamponi, 2014). Most synapses depend on P/Q-type (Cav2.1), N-type (Cav2.2) or R-type (Cav2.3) Cavs for neurotransmitter release (Gasparini et al., 2001; Li et al., 2007; Simms and Zamponi, 2014). Cavs open in response to the action potential-driven membrane polarization. The resulting influx of  $\text{Ca}^{2+}$  to the presynaptic compartment sets a wide range of  $\text{Ca}^{2+}$ -dependent processes in motion - including the fusion of SVs with subsequent neurotransmitter release. Clustering of Cavs at the AZ is critical for the precise control of the speed and strength of neurotransmitter release. The number of Cav clusters correlates with the number of SV docking sites and the strength of transmission (Miki

et al., 2017). The physical distance between Cav clusters to  $\text{Ca}^{2+}$ -sensors and docked SVs further determines the speed and amount of neurotransmitters released in each nerve pulse (Biederer et al., 2017; Eggemann et al., 2012).

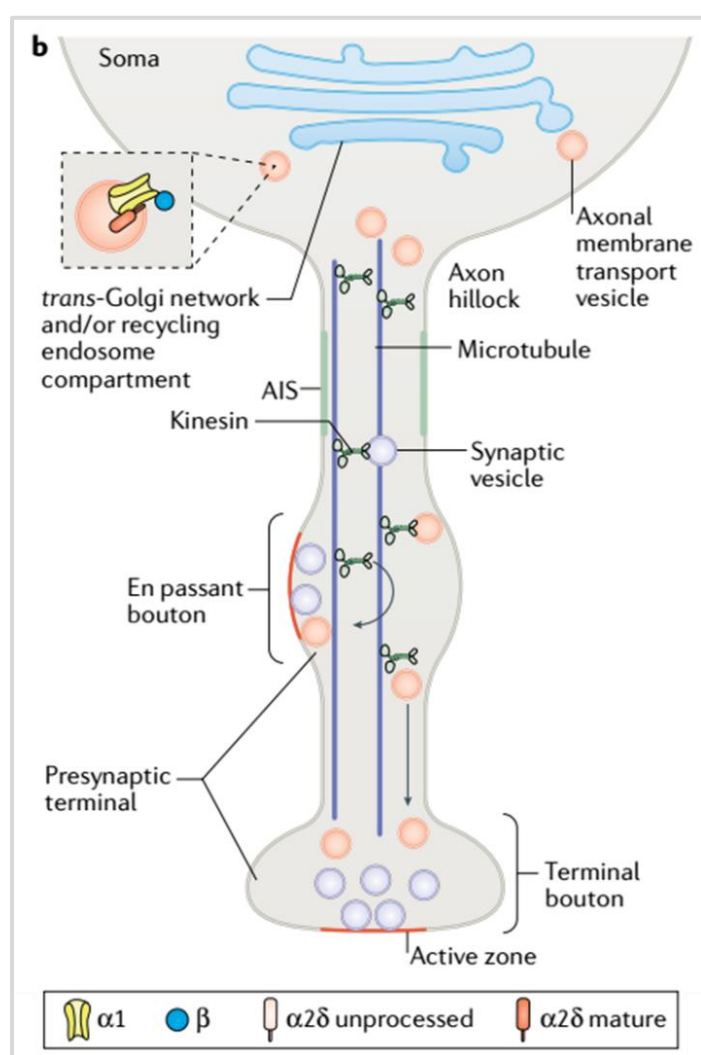


**Figure 1.3. Illustration of axonal transport mechanism of Cav channel-carrier vesicles destined for active zone membranes.** Axonal cargo-containing transport vesicles from the trans-Golgi network/recycling endosome compartment bind to microtubules at the axon hillock. The cargo destined for *en passant* or *terminal* boutons is attached by axonal kinesins to microtubules and is released from the microtubules at presynaptic sites, similar to synaptic vesicles. (Adapted from (Dolphin and Lee, 2020)).

## Introduction

---

Cavs are recruited at the AZ via simultaneous interaction with the AZ scaffolding RIM/RBP proteins (Graf et al., 2012; Han et al., 2011; Kaeser et al., 2011; Liu et al., 2011; Miki et al., 2017; Nakamura et al., 2015; Tang et al., 2016; Wu et al., 2019). Moreover, RIMs can directly regulate activity of Cavs by modulating their opening (Kaeser et al., 2012). MINT and CASK also contribute to the recruitment of Cavs to the presynapse (Maximov and Bezprozvanny, 2002; Spafford and Zamponi, 2003). In addition, Cavs can also interact with the sCAM Neurexin which enables the tight coupling of Cav clusters to SV release sites (Luo et al., 2020). Although there is very limited information on how Cavs are transported along the developing axons to the nascent presynapse, it is conceivable that their transport in the axons as well as their precise localization and clustering within the presynaptic sites rely on multiple coordinated mechanisms and protein interactions (**Figure 1.3**).

### 1.2.4. Synaptic vesicles and the machinery for neurotransmitter release

SVs contain approximately 80 different integral membrane proteins with 40 known SV residents, with relatively tightly controlled copy numbers of these proteins (Takamori et al., 2006b; Wilhelm et al., 2014) (**Figure 1.4**). Some of the SV proteins mediate neurotransmitter uptake such as neurotransmitter transporters, e.g. the vacuolar ATP-dependent proton pump vATPase (vGlut1), some are primarily involved in exocytic fusion, e.g. synaptobrevin 2 (Syb2) and synaptotagmin 1 (Syt1), and some are partly involved in these processes, such as Synaptophysin (Syp) which has a role in Syb2 sorting (Gordon et al., 2011).

## Introduction

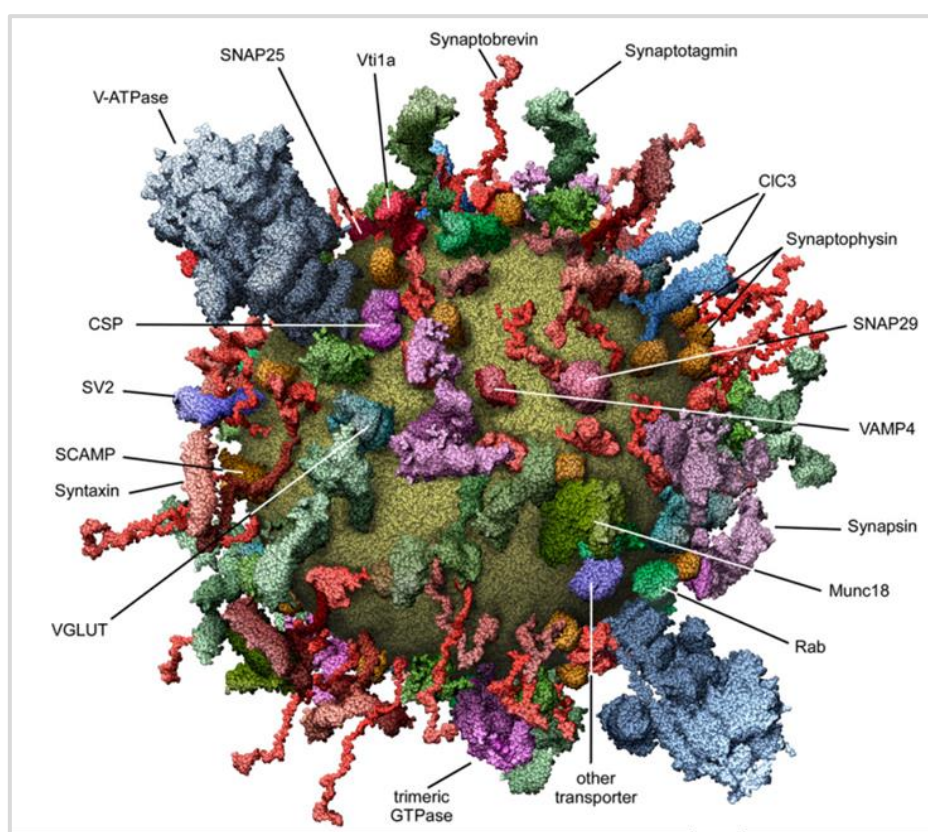


**Figure 1.4. Molecular model of an average synaptic vesicle.** Schematic illustration demonstrating the main processes that are necessary for AZ assembly. These processes are initiated by the transport of AZ material and its capture in presynaptic nerve terminals (b), continued with the assembly of the material into an active zone protein complex (c), and finalizes by the anchoring of this complex at the target membrane (d). Higher magnification of an AZ protein complex formed by RIM, RIM-BP, ELKS, Liprin-a, Munc-13, and Piccolo/Bassoon is shown on the right hand side. (Adapted from (Takamori et al., 2006a))

SVs need to position in close proximity to Cavs to allow tight coupling of action potential-driven calcium-currents to neurotransmitter release via SV fusion. SVs are spatially segregated within presynaptic boutons, resulting with docked SV clusters at each AZ (Kaeser et al., 2011; Maschi and Klyachko, 2017; Park et al., 2012; Tang et al., 2016; Watanabe et al., 2013). SVs that are in the readily releasable pool (RRP) are anchored at AZ release sites through interactions with Bassoon, Piccolo and ELKS/ BRP proteins (Hallermann et al., 2010; Mukherjee et al., 2010). SV proteins Rab3 and Rab27 also interact with RIM /Munc13 heterodimers, which further position docked SVs in close proximity to clustered Cavs (Fukuda, 2003; Lu et al., 2006; Wang et al., 1997).

## Introduction

---

The principal SV fusion machinery constitutes the plasma membrane SNAREs Syntaxin and SNAP25 that form a complex with the vesicular SNARE Synaptobrevin, present on SVs. The SNARE complex also requires Munc18-1 to achieve successful fusion of SVs at the AZ (Dulubova et al., 2007; Hata et al., 1993; Khvotchev et al., 2007). Previously, plasma-membrane SNAREs Syntaxin and SNAP25 have been shown to be co-transported with the AZ proteins Piccolo and Bassoon, however SV proteins have been suggested to not be a part of these transport units (Shapira et al., 2003; Zhai et al., 2001). Thus, it is conceivable that plasma-membrane resident release machinery assembles prior to the recruitment of SVs to nascent synapses.

To conclude, proper delivery and assembly of these components are essential to form a functional presynaptic compartment. However, in which order and by which transport machineries these basic building blocks are delivered to and assembled into a nascent presynaptic compartment remains unknown.

### 1.3. Mechanisms of axonal transport of precursor vesicles

Assembly of a functional presynaptic unit requires key presynaptic components to be delivered to the nascent presynapse in a timely and spatially coordinated manner. Synaptic adhesion proteins, calcium channels and SV proteins are transmembrane proteins predominantly synthesized in the neuronal soma by the rough endoplasmic reticulum (ER). Subsequently they are exported to the Golgi complex and the trans-Golgi-network (TGN), both of which are largely absent from the axon and from presynaptic nerve terminals (Horton et al., 2005). Thus, presynaptic biogenesis requires the formation of precursor vesicles carrying presynaptic proteins so that they can be shuttled along microtubule tracks (Ahmari et al., 2000; Goldstein et al., 2008; Okada et al., 1995; Simms and Zamponi, 2014). AZ proteins which are initially synthesized on cytoplasmic ribosomes may later associate with Golgi membranes in the neuronal soma before being transported to nascent synapses (Jin and Garner, 2008; Maas et al., 2012a; Shapira et al., 2003; Zhai et al., 2001).

Due to the low numbers and transient nature of PVs, many important questions regarding their axonal transport remain unanswered. For instance, the molecular mechanisms for tight coordination of axonal transport machinery to ensure the stoichiometric assembly of functional presynaptic compartments have not been fully resolved (Ahmari et al., 2000;

## Introduction

---

Goldstein et al., 2008; Okada et al., 1995; Shapira et al., 2003). Likewise, major questions regarding the morphology and biological identity of the PVs also remain to a large extent unresolved.

### 1.3.1. Morphology and cell biological identity of presynaptic transport vesicles

Coordinated vesicular delivery of presynaptic Cavs, AZ and SV proteins is required for formation of a functional presynapse (Ahmari et al., 2000; Maeder et al., 2014; Zhai et al., 2001; Ziv and Garner, 2004). However, it is currently unclear how the delivery of stoichiometric amounts of presynaptic material is ensured and whether the different presynaptic components assemble in parallel or as separate modules.

Various types of organelles that may transport the presynaptic proteins along axonal microtubules to axon terminals have been mentioned in previous literature. According to one model, each of the different presynaptic units, namely AZ proteins, Cavs, and SVs, are transported on distinct classes of precursor organelles and assemble as separate modules at the presynapse. According to this '**multiple distinct carrier model**', transport of the SV-proteins is regulated by kinesin-3 family of motor proteins KIF1A (*Unc104* in *C. elegans*, *Imac* in *D. melanogaster*) and its paralog KIF1B $\beta$  (Hall and Hedgecock, 1991; Jin and Garner, 2008; Okada et al., 1995; Pack-Chung et al., 2007). Studies using KIF1A KO mice or the *C. elegans* ortholog of KIF1A, *Unc104*, have reported that mutant axons have smaller AZs and significantly fewer SVs at the presynapse, with concurrent large surfeits of small and uniform vesicles (30-50 nm) in the neuronal cell bodies, resembling SVs, but with generally denser cores (Okada et al., 1995; Pack-Chung et al., 2007). These vesicles which accumulate at the soma of KIF1A KO mice are tethered together as in synaptic boutons but are distinct from the clusters around Golgi, nor are they associated with the cell membrane (Hall and Hedgecock, 1991; Yonekawa et al., 1998). According to this model, AZ proteins Piccolo, Bassoon and ELKS-2/CAST, as well as the synaptic cell-cell adhesion molecule N-cadherin and the synaptic t-SNARE proteins Syntaxin and SNAP-25 are transported as pre-assembled complexes to presynaptic sites on dense-core granules of 80 nm diameter termed Piccolo-Bassoon transport vesicles (PTVs). In contrast, other constituents of the AZ, such as Munc-13 and Munc-18 are transported via different routes (Jin and Garner, 2008; Maas et al., 2012a; Shapira et al., 2003; Zhai et al., 2001). PTVs were thought to be derived from the Golgi apparatus since endogenous Bassoon and Piccolo proteins co-localize with markers of the

## Introduction

---

trans-Golgi network (TGN) in neuronal cell bodies. Possibly, further maturation steps are required to bring additional CAZ proteins (e.g. RIM1a and Munc13) together in a post-Golgi step. Subsequent mature PTVs carry a comprehensive set of AZ materials, such that very small numbers of PTVs (<5) are able to provide sufficient Bassoon, Piccolo and RIM content of a functional AZ (Bresler et al., 2004; Maas et al., 2012a; Shapira et al., 2003). Importantly, this model suggests that components of the perisynaptic plasma membrane and SVs do not associate with PTVs but are packaged into and transported along the axon on different types of transport vesicles (Jin and Garner, 2008; Zhai et al., 2001).

Contrary to the multiple distinct carrier model, a second model, named **‘transport packet model’**, argues that proteins of different synaptic modules are transported by the same precursor organelle or organelle clusters (Ahmari et al., 2000; Bury and Sabo, 2011; Wu et al., 2013). This transport of different proteins would require a coordinated mechanism to be developed prior to synapse development and would provide significant advantage to neurons by ensuring the delivery of stoichiometric amounts of presynaptic material. Studies by Ahmari and colleagues have described mobile ‘transport packets’ which carry many (and possibly all) of the components required for the formation of an active presynapse, and have observed varied dense-core (with 70 nm diameter) and pleiomorphic small (with 40 nm diameter) vesicles as well as tubulovesicular structures at nascent synapses (Ahmari et al., 2000). Perhaps the existence of multiple vesicular intermediates can be advantageous for rapid and efficient presynaptic assembly. EM immunolabeling experiments by Tao-Cheng et al. have identified a type of vesicle-aggregate, rather than an individual type of dense-core vesicle as carriers of Bassoon- and Piccolo in developing rat hippocampal axons (Tao-Cheng, 2007). Importantly, many SV and associated proteins have been found to localize in these carrier aggregates. However, not all vesicles containing these SV-related proteins also contained Bassoon and Piccolo. This suggests that, these vesicle aggregates consisting of one or two dense core vesicles containing AZ proteins and several clear core vesicles rich in SV proteins together represent a preassembled transport unit that is sufficient to form a stable presynaptic active zone (Maeder et al., 2014; Tao-Cheng, 2007). More recent studies have provided further evidence that SV and AZ proteins are present and transported together in the axon, whether carried by one type of vesicle or by multiple vesicles (Bury and Sabo, 2011; Klassen et al., 2010; Vukoja et al., 2018). For instance, time-lapse confocal microscopy on rat cortical cultures or *Drosophila* motoneurons have shown that a significant proportion of presynaptic SV and AZ proteins are transported together prior to a stable terminal (Bury and Sabo, 2011; Vukoja et al., 2018). Along the same line, *C. elegans* and *Drosophila* mutant animals lacking

## Introduction

---

the small GTPase Arl8, a kinesin adaptor regulating organelle motility, show proximally mislocalized presynaptic cargo containing both SV and AZ proteins in the axons (Klassen et al., 2010; Vukoja et al., 2018). Together, these findings suggest that presynaptic SV and AZ proteins are sorted into precursor vesicles, which then likely undergo further maturation steps while being transported toward distal axons, and are assembled into functional SVs and AZ compartments only after their delivery to the nascent presynapse. However, it remains to be elucidated to what extent these proteins are co-trafficked in developing neurons, whether they are present homogeneously in one type of carrier or are distributed in multiple subgroups of vesicles, and whether Cavs are co-transported with AZ and SV proteins.

Unlike the considerable amount of speculations on the morphology of the transported precursor organelles, their cell biological identity has remained largely elusive. As discussed earlier, precursor vesicles carrying AZ proteins and Cavs are thought to be derived from Golgi compartment (Dolphin and Lee, 2020; Maas et al., 2012a). However, limiting ER-to-Golgi transport impairs membrane supply from dendrites, whereas the supply of presynaptic components to axons remains sustained (Ye et al., 2007). Furthermore, even when post-Golgi trafficking is inhibited, axons continue to grow, arguing that obstructions in post-Golgi trafficking selectively suppress dendritic growth (Horton et al., 2005). Thus, it is likely that other membrane sources are also involved in presynaptic biogenesis. In line with this, Vukoja and colleagues have recently made the surprising discovery that presynaptic precursor organelles contain lysosomal membrane proteins such as Spinster and Lamp1, as well as the lysosomal kinesin adaptor Arl8 (Vukoja et al., 2018). These vesicles, however, seem to be devoid of degradative lysosomal proteases. Hence, they identify a lysosome-related vesicle that is probably distinct from mature degradative lysosomes involved in protein turnover. Electron micrographs confirm that closely packed perinuclear arrays of presynaptic lysosome-related precursor vesicles, named PLVs, accumulate in neuronal somata of Arl8 mutant larvae. PLVs are homogeneously sized (around 70 nm diameter), comparably uniform vesicles of varying electron densities and are clearly distinct from other organelles such as SVs, degradative lysosomes or the ER present in the soma. Whether Arl8 is also required for the axonal transport of PVs in the mammalian central nervous system has remained unanswered and will be addressed in this thesis and therefore will be discussed extensively in the following chapters.

## Introduction

---

### 1.3.2. Kinesins as primary motors for anterograde axonal transport

Microtubules are polarized tubulin polymers that form part of the cytoskeleton. Directed long-range transport of membranous organelles, lipids, proteins, RNA and signaling molecules along the axon is achieved by molecular motors on the microtubules. While the microtubule polarity is rather complex in dendrites, in the axon parallel microtubules are organized in a uniformly polarized network with fast-growing plus ends directed towards axon tips and relatively stable minus ends pointed towards the soma (Burton and Paige, 1981; Kwan et al., 2008; Stepanova et al., 2003). This form of microtubule network in the axon enables cargos to be continuously transported by the cytoplasmic motor proteins kinesins and dyneins (Yu and Baas, 1994). Kinesins are responsible for anterograde movements of newly synthesized proteins and lipids from the cell body towards periphery, including synaptic components, whereas dyneins direct the retrograde transport of molecules for their removal from the axon or synapse and sends them back to the soma for degradation to maintain cellular homeostasis (Maday et al., 2012). Directionality of axonal movements requires tight regulation for proper neuronal development and function.

Cargo transport in the axon can be achieved by fast (50-400 mm/day) or slow (maximum 8 mm/day) axonal transport, depending on the cargo type, motor proteins involved in the transport and the associated machinery (Roy, 2014). Transport of membranous vesicles or organelles is mostly based on fast axonal transport which exhibit frequent pauses and changes in transport directionality due to different motors being present on axonal microtubules that can take over the cargo (Hendricks et al., 2010; Lasek et al., 1984).

Kinesins are drivers of fast cargo transport. The kinesin superfamily includes 45 mammalian genes that give rise to a myriad of proteins by undergoing alternative splicing (Lawrence et al., 2004; Miki et al., 2001). Kinesins are grouped into 15 classes which can be broadly grouped into three types: N-kinesins (N-KIFs) have their motor domain at their amino-terminal end and drive plus-end motility, C-kinesins (C-KIFs) have their motor domain at their carboxy-terminal region and generally drive minus-end motility, and M-kinesins (M-KIFs) contain their motor domains at the central domain and they depolymerize microtubules. N-KIFs make up the major type of kinesins expressed in neurons (Hirokawa et al., 2010). Motor domains of kinesins bind the microtubule tracks in an ATP-dependent manner, whereas tail or stalk domains (depending on the specific type of kinesin) are responsible of cargo recognition and binding (**Figure 1.5**).

## Introduction

---

### 1.4. Kinesins implicated in presynaptic precursor transport

Two kinesin motor protein families, kinesin 1 and kinesin 3, have been implicated in axonal transport of presynaptic precursor vesicles in various model organisms. Therefore, they will be discussed in further detail.

**KIF5** (KHC, Unc-116), often referred as the classical kinesin, is the first member of kinesin-1 family which has been identified. The KIF5 motor complex consists of two KIF5 motors, also known as kinesin heavy chains (KHCs). KIF5 can also build tetramers where two kinesin light chains (KLCs) associate with the tail domains of the two KIF5 motors. Gene duplications have led to three KIF5 subtypes in mammals: neuron-specific KIF5A and KIF5C and ubiquitously expressed KIF5B.

KIF5 motors have role in the transport of many different cargoes, including mitochondria, synaptic vesicle precursors, PTVs, Jun N-terminal kinase (JNK)-interacting proteins (JIPs),  $\beta$ -Amyloid precursor protein (APP), mRNA, cargoes of slow axonal transport such as neurofilament proteins and even the dynein complex (reviewed in (Hirokawa et al., 2009)). In non-neuronal cells KIF5B has been identified as the main driver of lysosomal transport via a KIF5B-KLC2-SKIP complex (Guardia et al., 2016). KIF5 (KHC) mutant flies show dystrophic axonal terminals and focal organelle-filled swellings along the length of the axon, although synapse formation and function remains unaffected (Hurd and Saxton, 1996).

A previous study using *C. elegans* has suggested that, two SV-associated proteins, Syt1 and Syb2, might be transported via kinesin-1 motor protein, due to their mislocalization upon loss of a JNK-Signaling Scaffold Protein Unc-16 which associates directly with kinesin-1 (Byrd et al., 2001). However, a direct association between SV proteins and conventional kinesin could not be revealed. On the other hand, direct interaction between KIF5 motors and membrane proteins Syntaxin1 (via Syntabulin) (Su et al., 2004) and SNAP-25 (Diefenbach et al., 2002) have been successfully shown, making them more probable cargoes of KIF5B. In another study, KIF5B motor and its adaptor Syntabulin have been co-purified with Bassoon and Piccolo as well as with Syntaxin in rat brain, suggesting that vesicular intermediates carrying AZ proteins may rely on conventional kinesin motors for transport to the nascent presynapse (Cai et al., 2007). However, Bassoon co-purifies not only with AZ proteins but also with the SV protein Syp and this interaction is not affected by the loss of Syntabulin or KIF5B. Moreover, recent data report that disrupting Unc-116 (kinesin heavy chain homolog) in *C.*

## Introduction

---

*elegans* only mildly perturbs the localization of CAZ proteins (Sakamoto et al., 2005) and does not result in a presynaptic phenotype (Wu et al., 2013). Overall, KIF5B associates with Syntaxin and SNAP-25 via Syntabulin, might be involved in the transport of AZ proteins Bassoon and Piccolo, and albeit less likely also other proteins such as Syp, Syt1 and Syb2.

**KIF1** (*imac*, *Unc-104*) is an atypical member of the kinesin superfamily and exists in a monomeric form although it can dimerize to reach higher speeds (average 1 $\mu$ m/s) and processivity (Tomishige et al., 2002; Zhou et al., 2001) (**Figure 1.6**). The kinesin-3 family contains three KIF1 genes in mammals (KIF1A, KIF1B and KIF1C), one in *C. elegans* (*Unc-104*) and in *D. melanogaster* (*immaculate connections*, *imac*), respectively. Many motor proteins including KIF1A, can be auto inhibited, as this process prevents futile ATP hydrolysis when motors do not bind to cargoes (Verhey and Hammond, 2009).

The CC1 domain of KIF1A regulates its auto inhibition, while the CC2 domain regulates motor dimerization (Hummel and Hoogenraad, 2021). Importantly, KIF1A and KIF1B $\beta$ , which is generated by a splicing variation in the cargo binding domain of the KIF1B gene, both contain a forkhead homology-associated (FHA) and a canonical pleckstrin homology (PH) domain which are located after the motor and stalk domain towards the N-terminus. FHA domains are phosphopeptide recognition domains, specifically for phosphothreonine epitopes on proteins. PH domains can bind phosphoinositides with high affinity and specificity but they may also have protein binding ability. Through their interactions, they can drive membrane translocation of proteins: They can recruit them to different membranes or enable them to interact with other components of the signal transduction pathways (Maffucci et al., 2003). The PH domain of KIF1A is thought to be necessary to achieve proper cargo binding and dictating cargo specificity, although it is not sufficient for axonal transport of cargo. Recent studies show that both the CC3 and PH domains are required for efficient cargo binding (Hirokawa et al., 2010; Hummel and Hoogenraad, 2021). (**Figure 1.6**)

## Introduction

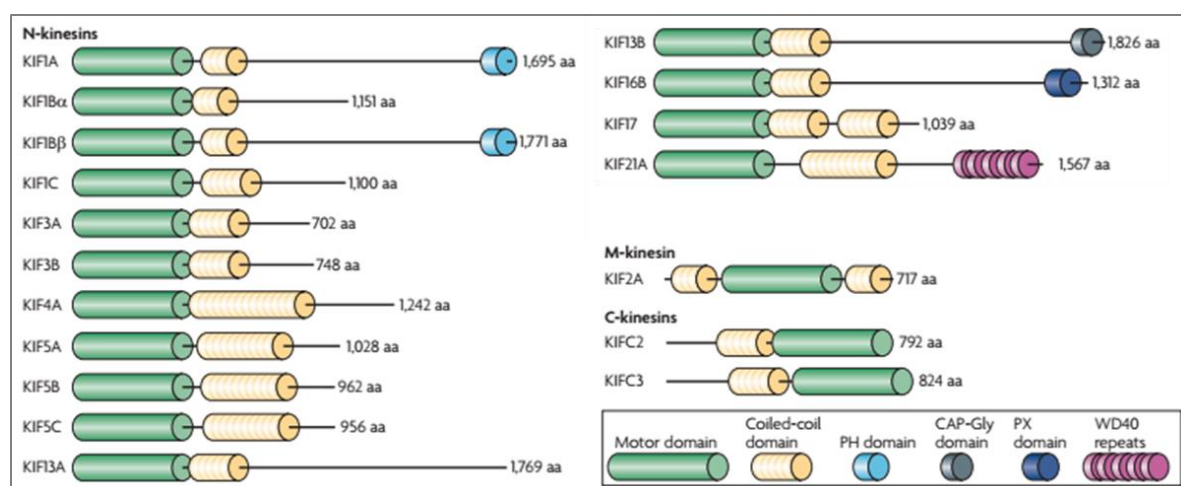


**Figure 1.5. Domain structures of major kinesins.** In general, kinesins comprise a kinesin motor domain and a coiled-coil domain. There are also gene specific domains, such as the pleckstrin homology (PH) domain of KIF1A and KIF1B $\beta$ , the CAP-Gly domain of KIF13B and the WD40 repeats of KIF21A. N-kinesins, M-kinesins and C-kinesins contain their motor domain at the amino terminus, in the center or at the carboxyl terminus, respectively. aa, amino acids; PX, phox homology. (Adapted from (Hirokawa et al., 2009))

KIF1A and KIF1B $\beta$  have been implicated in the transport of SV proteins including Syp, Syt1 and Rab3a; dense-core vesicles (DCVs), brain-derived neurotrophic factor (BDNF) and recently the presynaptic adhesion protein Neurexin (NRX-1) through association with multiple adaptors (Gabrych et al., 2019; Hirokawa et al., 2010; Oliver et al., 2022) (**Figure 1.6**). Therefore, they are essential for neuronal survival and function. In both non-neuronal and neuronal cells KIF1A, together with the classical kinesin KIF5B, has been shown to drive anterograde lysosome transport (Guardia et al., 2016). Additionally, KIF1A has been identified as the main motor protein to drive the anterograde transport of DCVs in invertebrate and vertebrate systems (Hummel and Hoogenraad, 2021; Lo et al., 2011). Altered KIF1A activity conceivably interferes with growth factor transport and secretion, particularly through regulating the transport of vesicles containing the neurotrophin BDNF (Carabalona et al., 2016). KIF1A haploinsufficient mice showed sensory neuronal defects and depleted number of nociceptive neurons expressing the NGF receptor TrkA, which led to the discovery that KIF1A transports TrkA to enhance PI3K signaling (Tanaka et al., 2016). Roles of KIF1A and KIF1B $\beta$  in neurons, along with the interactions they form with their adaptors, will be discussed in detail in the next section.

## Introduction

### 1.4.1. KIF1A and the associated presynaptic precursor transport machinery

Earlier work has indicated that the kinesin-3 family of neuron-specific motor proteins KIF1A and its paralog KIF1B $\beta$  are responsible for transporting presynaptic PVs (Hall and Hedgecock, 1991; Jin and Garner, 2008; Okada et al., 1995; Pack-Chung et al., 2007; Zhao et al., 2001). Nerve ligation experiments by Okada and colleagues have shown that KIF1A associates with membranous organelles containing SV proteins, including Syt1, Syp and Rab3a, but not others (e.g. SV2 or presynaptic membrane proteins Syntaxin 1a and SNAP25) (Okada et al., 1995). Complete loss of KIF1A or KIF1B $\beta$  in mice is postnatally lethal (Xu et al., 2018; Yonekawa et al., 1998; Zhao et al., 2001). Cultured neurons from KIF1A-deficient mice show reduced numbers of SVs in nerve terminals and abnormal accumulation of clusters of SV-like vesicles in cell bodies, indicating decreased presynaptic protein transport (Yonekawa et al., 1998). Of note, similar reduction in the density of SVs in the nerve terminals, among other neurological abnormalities, has also been reported in KIF1B $\beta$  KO mice (Zhao et al., 2001). In addition, SV and AZ proteins in Unc-104 mutant *C. elegans* are also almost completely absent from the axon and instead mislocalized to soma and dendrites (Klassen et al., 2010).

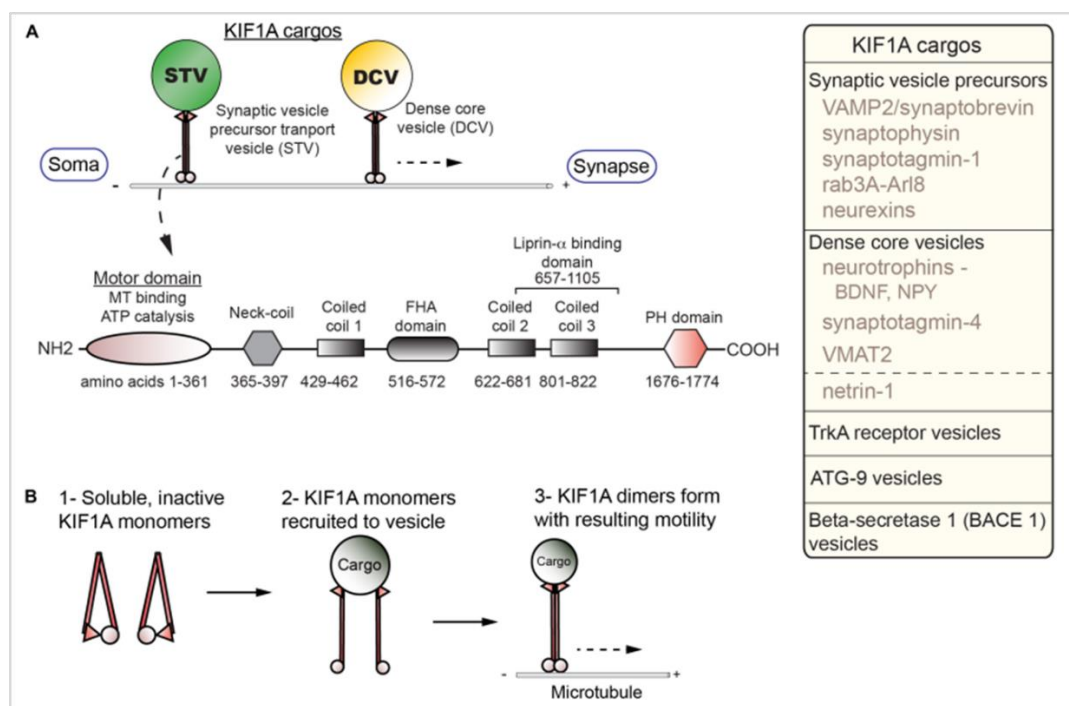


**Figure 1.6. Cargos, structure, and regulation of KIF1A.** (A) KIF1A is a homodimer that traffics a number of cargos (box; right) from the soma to distal portions of the axon including synapses. Schematic illustration indicates the domains identified in KIF1A. (B) Diagram of activation steps of KIF1A to be recruited to its cargo. (Taken from (Gabrych et al., 2019))

## Introduction

---

Cultured hippocampal neurons from embryonic KIF1B $\beta$  knockout mice show severe neuronal death and impaired axon elongation (Zhao et al., 2001). Recently, IGF1R-containing vesicles were identified as a cargo of KIF1B $\beta$  and specific mutations in the *KIF1B $\beta$*  gene disrupting its IGF1R binding capacity were linked to Charcot-Marie-Tooth (CMT) disease, an inherited peripheral neuropathy (Xu et al., 2018). Interestingly, although KIF1A or KIF1B $\beta$  are structurally very similar to each other, certain phenotypes of KIF1B $\beta$  cannot be rescued by re-introduction of KIF1A, which when combined with the fact that loss of these two proteins cause at least partially different neuronal phenotypes, indicates that the physiological roles of KIF1A and KIF1B $\beta$  seem to be non-identical.

Both KIF1A and KIF1B $\beta$  bind to the SV-associated small GTPase Rab3 through its upstream activator protein mitogen-activated protein kinase (MAPK)-activating death domain (MADD; also known as DENN and hereafter referred to as DENN/MADD) (Niwa et al., 2008) and this interaction has been suggested to constitute an important part in the PV transport machinery (Hummel and Hoogenraad, 2021). Genetic loss of DENN/MADD in mice is postnatally lethal. It results in reduced number of SVs at the neuromuscular junctions and impairment in neurotransmitter release (Yamaguchi et al., 2002). Loss of AEX-3, the ortholog of DENN/MADD in *C. elegans*, on the other hand, only impairs Rab3 transport in the axons but does not alter the delivery of other SV proteins to nerve terminals (Iwasaki et al., 1997). Interestingly, Rab3A-D KO mice appear to develop milder phenotypes, for instance the number of SVs at nerve terminals remain unchanged compared to WT mice (Schonn et al., 2010). Perhaps the compensation of function by other Rabs may explain the absence of a strong phenotype in Rab3A-D KO mice. For instance, Rab6 and Rab27 can be candidates for such a compensation mechanism since they have both been shown to associate with vesicular cargo in the axons (Nyitrai et al., 2020; Takamori et al., 2006a). On the other hand it is also possible that another subset of SV proteins is transported by a mechanism that is independent of Rab3, perhaps using different motor proteins (Byrd et al., 2001). Unc-16/Kinesin-1 interaction, elaborated in the previous section, can be counted among such mechanisms.

The lysosomal small GTPase Arl8 has been identified as an interactor of KIF1A in *C. elegans* (Wu et al., 2013) and has been shown to regulate axonal transport of presynaptic proteins in this model system (Klassen et al., 2010). Arl8 deficiency causes the presynaptic cargo to mislocalize in the proximal axon in *C. elegans*. JNK (c-Jun N-terminal Kinase) pathway has been implicated as another regulator of this transport machinery by working antagonistically to Arl8 (Wu et al., 2013). A similar mislocalization of presynaptic proteins is

## Introduction

---

observed in Arl8 mutant flies, suggesting the conservation of roles of Arl8 in the presynapse formation (Vukoja et al., 2018). Arl8 and effects of its loss in cells and organisms in terms of organelle motility will be discussed in more detail in the following chapters.

### 1.5. Arl8: a small GTPase regulating lysosomal motility

Arl8 (ADP-ribosylation factor-like protein 8) is an evolutionarily highly conserved small GTPase. Whereas Arl8 is encoded from a single gene in invertebrates, it exists as two related paralogs in vertebrates, named Arl8a and Arl8b, which have 91% amino acid sequence identity with each other. Arl8 belongs to Ras superfamily of guanine nucleotide-binding proteins which function as molecular switches in a variety of cellular processes, such as cellular organization and signaling or protein or membrane transport. Many of the diverse members of the Ras superfamily require the contribution of co-factors including GEFs (guanine nucleotide exchange factors) to help dissociate strongly bound GDP, GAPs (GTPase activating proteins) to accelerate GTP hydrolysis, or GDI (guanine dissociation inhibitor) that help maintain some of the small monomeric GTPases in an inactive state by building soluble complexes with them and thus preventing exchange of GDP to GTP (Cherfils and Zeghouf, 2013). In their GTP-bound state Ras proteins interact with effectors which are proteins having high affinity to the GTP- and low affinity to the GDP-bound state of Ras proteins. Although they display functional diversity, Ras superfamily proteins are rather conserved in their size (between 20 and 25 kDa) and structural and biochemical properties. They are classified into several subgroups by sequence homology, which are: Arf/Sar, Rho, Rab, Ras and Ran which all together correspond to 167 human proteins (Rojas et al., 2012).

Members of Arf/Sar family of the Ras superfamily have several important roles in vesicular trafficking and organelle structure: they recruit coat proteins that promote sorting of vesicle cargos, modulate membrane phospholipid metabolism, regulate enzymes by interacting with regulators of other G proteins and interact with cytoskeletal factors. In this family there are 6 mammalian Arf proteins which are classified into 3 groups based on sequence homology: Class I (ARF1, ARF2 and ARF3), Class II (ARF4 and ARF5) and Class III (ARF6) (Rojas et al., 2012). In addition, there are over 20 ARF-like (ARL) proteins, which make up the functionally most diverse group of ARFs and seem to have broader roles than ARFs. ARL and ARF proteins both display a conserved amphiphatic helix at their C-terminus.

## Introduction

---

However, unlike ARF proteins, ARLs are generally not myristoylated at their amphiphatic site. In some cases they lack any post-translational modification at this site, and in others (for instance Arl8a and Arl8b) this helical domain is acetylated (Hofmann and Munro, 2006). Similar to other members of Ras superfamily, ARF or ARL family members also cycle between an active (GTP bound) and inactive (GDP bound) conformation aided by GEFs and GAPs thereby selectively binding their effector proteins. Interestingly, in contrast to Rab and Rho G-proteins, ARF family members such as ARF6 might stay constitutively membrane-bound which might be key to coordinate distinct signaling pathways (Chun et al., 2008).

Arl8a and Arl8b were identified as the first small GTP-binding proteins reported to be localized to lysosomes in mammalian cell lines, showing very high co-localization with lysosomal membrane proteins such as CD63 and Lamp2, whereas not co-localizing with the early endosome marker EEA1 (Hofmann and Munro, 2006). In a dextran pulse-chase experiment, the fluid-phase endocytic marker dextran accumulated in Arl8-positive structures, further proving that Arl8a and Arl8b predominantly localized to lysosomes. As mentioned earlier, Arl8a or Arl8b are not N-terminally myristoylated but acetylated. Mutations at their N terminal site result in a diffuse cytoplasmic distribution, indicating that this site is essential for membrane targeting. Further mutations at the hydrophobic site of the amphiphatic helix domain showed that the helix is required for membrane binding, similar to other ARFs and ARLs (Antonny et al., 1997; Hofmann and Munro, 2006). After being targeted to lysosomes, Arl8 regulates kinesin-dependent lysosomal motility in different cell types (Hofmann and Munro, 2006; Rosa-Ferreira and Munro, 2011), causing lysosomes to disperse from the perinuclear site and accumulate at the cell periphery (**Figure 1.7**). The lysosomal targeting of Arl8 and its role in lysosomal motility have also been confirmed in *C. elegans* (Nakae et al., 2010) and *D. Melanogaster* (Rosa-Ferreira and Munro, 2011; Vukoja et al., 2018) model systems.

SKIP/PLEKHM2 has been identified as an Arl8 effector protein by using affinity chromatography (Rosa-Ferreira and Munro, 2011). SKIP binds specifically to the GTP form of Arl8a and Arl8b through their N terminal site containing the RUN domain. Furthermore, SKIP directly binds to kinesin-1 on its light chain KLC2 (Boucrot et al., 2005; Dumont et al., 2010). Through these interactions, Arl8 recruits SKIP to lysosomes and together Arl8 and SKIP act on anterograde transport of lysosomes (**Figure 1.7**). In further studies, a multisubunit complex named BORC (BLOC-one-related complex), which is composed of three subunits common to BLOC-1 complex (BLOS1, BLOS2, and Snapin) and five unshared subunits (KXD1,

## Introduction

LOH12CR1/myrlysin, C17orf59/lypersin, C10orf32/diaskedin, and MEF2BNB), was discovered to recruit Arl8 to lysosomes (Pu et al., 2015) (**Figure 1.8**). Therefore, BORG works as a master regulator and the produced BORG-Arl8-SKIP-kinesin ensemble promotes microtubule-guided transport of lysosomes toward the cell periphery.

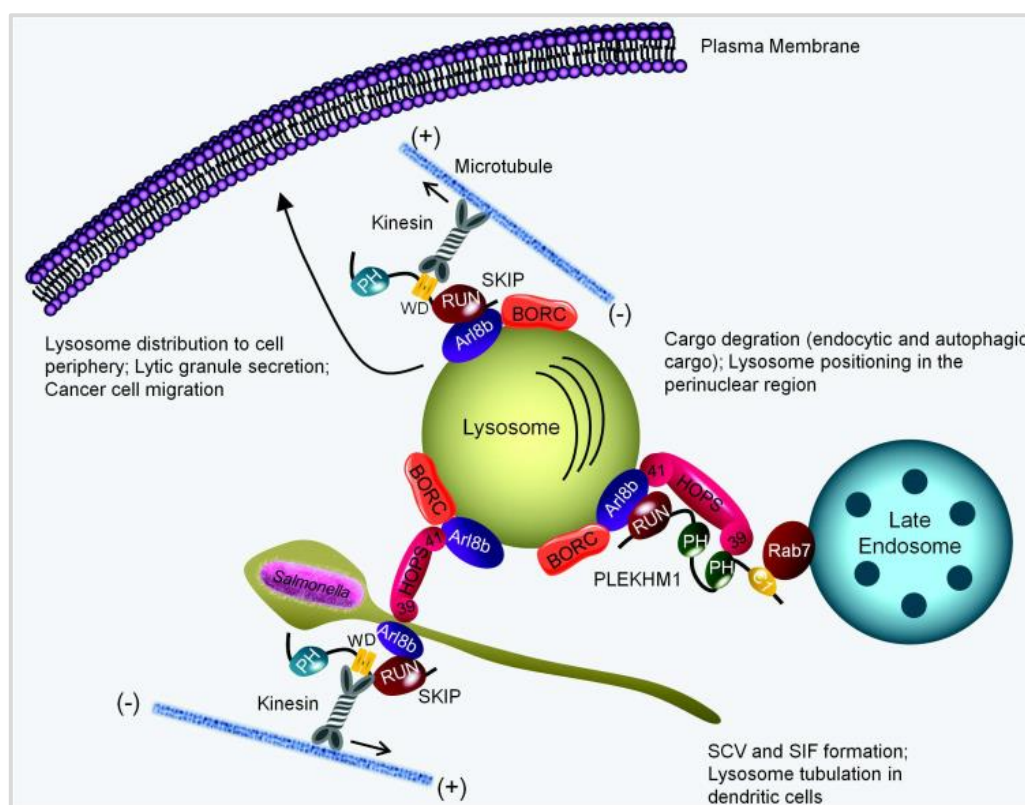


**Figure 1.7. Arl8 interacts with its upstream regulator BORG and its downstream effectors SKIP, HOPS complex and PLEKHM1 to regulate lysosome positioning and cargo degradation.** Arl8b localizes to the lysosomal membranes in the presence of multi-subunit complex BORG. When Arl8b is on the membranes and in its GTP-bound state, it interacts with its downstream effectors SKIP, HOPS complex or PLEKHM1 to regulate lysosome motility and cargo degradation. The Arl8b-SKIP-HOPS complex machinery is exploited by pathogens like Salmonella for establishing infection in host cells. (Taken from (Sharma, 2019))

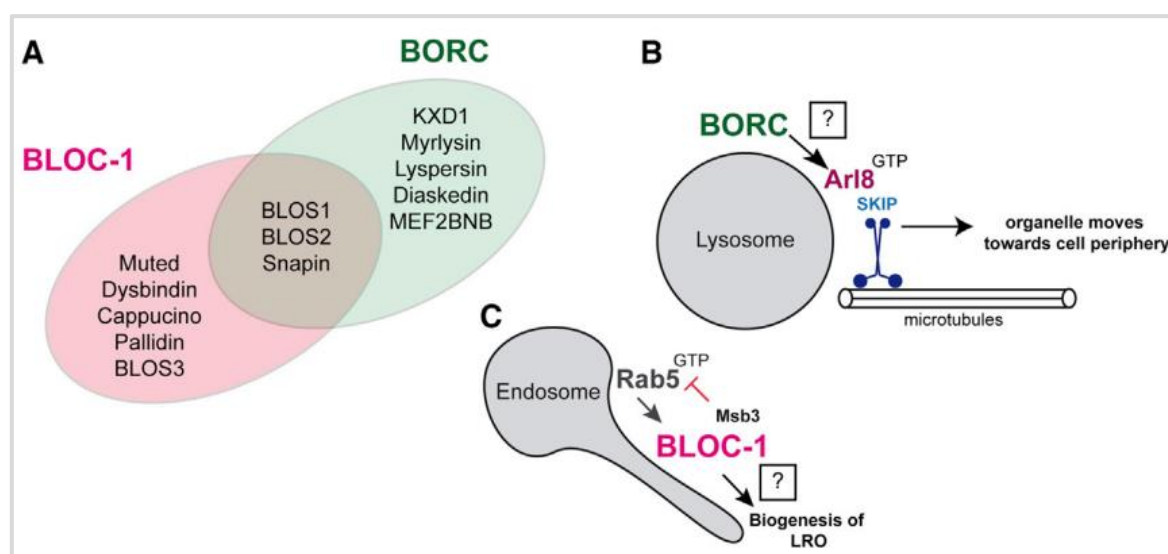


**Figure 1.8. Compositions and roles of BORC and BLOC-1 multisubunit complexes.** (A) Subunit compositions of BLOC and BORC. Three subunits of each complex are shared. (B) BORC is a resident lysosomal complex that promotes Arl8 recruitment and thereby microtubule-dependent lysosomal positioning. (C) BLOC-1 localizes to tubular endosomes and is required for the biogenesis of lysosome-related organelles (LROs). (Taken from (Langemeyer and Ungermann, 2015))

Critical impact of Arl8 on regulation of organelle motility have been shown in several studies using loss of function experiments. Arl8 mutant *C. elegans* show increased number of late endosomal/lysosomal compartments which are smaller in size, suggesting that Arl8 directs the trafficking of endocytosed macromolecules to lysosomes by facilitating late endosome-lysosome fusion (Nakae et al., 2010). In parallel with this observation, in a yeast two-hybrid assay Arl8b has been found to bind the VPS41 subunit of the HOPS (homotypic fusion and protein sorting) complex, a multi-subunit complex which regulates late endosome and lysosome fusion (Khatter et al., 2015; Sharma, 2019) (**Figure 1.7**). Arl8b recruits the HOPS complex to lysosomes, thereby regulating the function of this tethering complex in endocytic degradation. Complete loss of Arl8 in flies is lethal in the larval third instar stage (Vukoja et al., 2018). Similarly, complete loss of either Arl8a or Arl8b in mice is also late embryonically or postnatally lethal (Hashimoto et al., 2019). Arl8b knockout embryos display growth retardation phenotypes with defective brain development (Hashimoto et al., 2019). The fact that complete loss of Arl8 causes a drastic consequence in both flies and mice highlights its importance in normal development and, possibly, synapse maintenance.

## Introduction

---

### 1.5.1. Role of Arl8 in presynapse formation

The role of Arl8 in axonal transport of PVs has first been described in *C. elegans*, where Arl8 deficiency causes premature accumulation of presynaptic cargo within the proximal axon and a consequent failure in the assembly of presynapses in distal segments (Klassen et al., 2010). A subsequent study used a forward genetic screen and revealed another regulator of this transport machinery as the JNK (c-Jun N-terminal Kinase) pathway. The JNK pathway functions antagonistically to Arl8 and promotes SV clustering whereas Arl8 limits the degree of premature clustering thereby facilitating formation of presynapses in distal segments (Wu et al., 2013). Importantly, Arl8 mutant phenotype in *C. elegans* has been only incompletely suppressed upon inactivation of JNK pathway, indicating that the regulatory mechanism directing the anterograde axonal movement of PVs is much more complex than this. It is likely that multiple pathways need to work collectively in regulating presynaptic protein transport and clustering.

Lysosome movement by both KIF5B-KLC2-SKIP and KIF1A motors is regulated by Arl8a/b and BORC in both neuronal and non-neuronal cells, indicating that Arl8 can interact both with KIF5B machinery and KIF1A (Guardia et al., 2016). In *C. elegans*, Arl8 binds to Unc-104 at its CC3 domain and unlocks its auto inhibition, enabling Unc-104 to bind its cargo vesicles through its tail domain and initiate their transport (Niwa et al., 2016; Wu et al., 2013). These findings reveal that direct interaction with Arl8 is essential for full activation of KIF1A.

The crucial role of Arl8 in coordinating PV transport has been further investigated using the model system *D. melanogaster*, where genetic loss of Arl8 causes a significant depletion of SV and AZ components including bona fide SVs from presynaptic sites and a corresponding impairment of evoked neurotransmission at NMJ synapses (Vukoja et al., 2018). In contrast, genetic upregulation of PV transport by overexpressing Arl8 in motoneurons facilitates neurotransmitter release, suggesting that Arl8 is a limiting factor for efficient delivery of presynaptic proteins. The reduced delivery of presynaptic proteins to axon terminals in Arl8 mutant animals is paralleled by the somatic accumulation of PLVs in neuronal cell bodies, similar to observations in a KIF1A KO mouse model. However, the accumulating vesicles in KIF1A deficient mice were much smaller than PLVs and their morphology resembled that of mature SVs (Yonekawa et al., 1998).

## Introduction

---

In mice, Arl8b knockout embryos display defective neural fold development and impaired roof plate formation, with decreased expression levels of Sox9, an early marker of prospective neural crest, and Gdf7 (growth differentiation factor 7) and Msx1 (msh homeobox1), midline marker genes (Hashimoto et al., 2019). Though these observations indicate the importance of Arl8 for mammalian brain development, future studies involving conditional loss of Arl8a and Arl8b will be of great importance in understanding the cellular and molecular mechanisms underlying these developmental phenotypes.

Lastly, although Arl8 has been identified as a crucial regulator of presynaptic biogenesis, the fact that Arl8 deficient neurons are still able to assemble functional presynaptic units suggests the presence of additional regulators in presynaptic protein trafficking in developing neurons. Further studies are needed to reveal such regulators and thus to provide a better understanding of presynaptic assembly.

### 1.6. Phosphoinositide identity of presynaptic precursor vesicles

Phosphoinositides (PIs) are a minor class of comparably short-lived membrane phospholipids. Each of the PI species has a unique subcellular distribution with a predominant localization in subsets of membrane. PVs, being specific organelles in neurons carrying presynaptic material, might potentially have a specific PI identity which has not been addressed before. Conceivably, PI identity of these organelles might be related to the organelle PVs are derived from.

#### 1.6.1. Phosphoinositides as signposts of compartmental membrane identity

Inositol phospholipids are concentrated at the cytosolic surface of membranes. Phosphatidylinositol (PtdIns), the precursor of PIs, is synthesized mainly in the endoplasmic reticulum (ER) and is then delivered to other membranes by vesicular transport or by using cytosolic PtdIns transfer proteins. Phosphorylation of its inositol ring at positions 3, 4 and 5 results in the generation of seven different PI species. These species can be interconverted by specific PI kinases and phosphatases (**Figure 1.9**). Each PI species possesses a predominant localization in subsets of membrane. Importantly, the localization of specific PIs can be heterogeneous within a given membrane. This distinct intracellular distribution of PIs, together with their high turnover, constitutes these lipids as mediators of signaling events in various cellular compartments. Apart from cell signaling, PIs also mediate other crucial cellular and organismal functions such as gating of ion channels, cytoskeleton regulation and motility, development, as well as the regulation of intracellular membrane traffic (Balla, 2013; Di Paolo and De Camilli, 2006).

The subcellular distributions of different PI species are distinct. PI 4-phosphates such as phosphatidylinositol 4-phosphate [PI(4)P] and phosphatidylinositol 4,5-bisphosphate [PI(4,5)P<sub>2</sub>] are concentrated along the exocytic pathway: predominantly in the Golgi complex, the trans-Golgi network (TGN), and at the plasma membrane. In contrast, PI 3-phosphates such as PI(3)P and PI(3,5)P<sub>2</sub> are hallmarks of the endo-lysosomal system, being located primarily within early and late endosomes or lysosomes (Balla, 2013; Raiborg et al., 2013). Being distributed to distinct subcellular locations, PIs carry out critical functions for the specific organelles or membrane domains they are located at (Balla, 2013; Di Paolo and De Camilli, 2006). PIs serve as signposts for the organelles or membrane transport intermediates (e.g.

## Introduction

vesicles and tubules). Therefore, when these organelles reach maturity, undergo fusion events or acquire different cellular functions, their PI content changes.

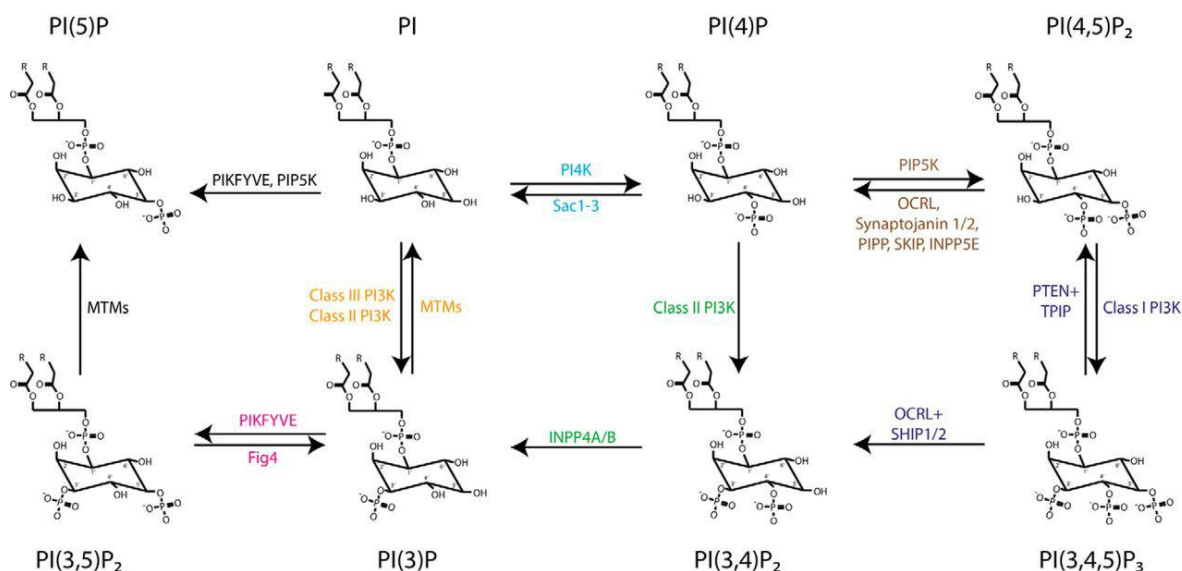


**Figure 1.9. Interconversion pathways of seven phosphoinositides by kinases and phosphatases.** Phosphorylation of phosphatidylinositol by PI4K produces PI(4)P. PIP5K further phosphorylates PI(4)P to yield PI(4,5)P<sub>2</sub>, which serves as a substrate for class I PI 3-kinases (Class I PI3K) to produce PI(3,4,5)P<sub>3</sub>. Class III PI 3-kinase (termed Vps34) (Class III PI3K) phosphorylates PI at its 3-OH position and synthesizes PI(3)P. PIKFYVE can phosphorylate PI(3)P to produce PI(3,5)P<sub>2</sub> and may also synthesize PI(5)P from PI. Class II PI 3-kinases (Class II PI3K) can phosphorylate PI(4)P to yield PI(3,4)P<sub>2</sub> and PI to yield PI(3)P. Removal of phosphate groups to reverse the reactions are catalyzed by phosphatases. Myotubularins (MTMs) are 3-phosphatases that hydrolyze PI(3)P and PI(3,5)P<sub>2</sub>. OCRL, synaptojanin 1/2, PIPP, SKIP, and INPP5E are PI(4,5)P<sub>2</sub> 5-phosphatases, Fig4 is a 5-phosphatase for PI(3,5)P<sub>2</sub>. PTEN and TPIP are 3-phosphatases which yield PI(4,5)P<sub>2</sub> and OCRL and SHIP1/2 are 5-phosphatases which yield PI(3,4)P<sub>2</sub> from PI(3,4,5)P<sub>3</sub>. The 4-phosphatases Sac1–3 dephosphorylate PI(4)P and INPP4A/B dephosphorylate PI(3,4)P<sub>2</sub> (Wallroth and Haucke, 2018).

## Introduction

---

### 1.3.3. Phosphatidylinositol 3-phosphates and the endolysosomal system

Phosphorylation of the inositol ring of phosphatidylinositol and its derivatives at the 3-position generates phosphatidylinositol 3-phosphates, thereby producing phosphatidylinositol 3-phosphate [PI(3)P], phosphatidylinositol 3,4-bisphosphate [PI(3,4)P<sub>2</sub>], phosphatidylinositol 3,5-bisphosphate [PI(3,5)P<sub>2</sub>], and phosphatidylinositol 3,4,5-trisphosphate [PI(3,4,5)P<sub>3</sub>]. Phosphatidylinositol 3-phosphate species are pivotal regulators of processes at intracellular membranes, not only because of their distinctive subcellular localizations but also due to their phosphorylation being rapidly reversible. The latter feature renders phosphatidylinositol 3-phosphates important players in signaling cascades and intracellular membrane trafficking (Balla, 2013; Raiborg et al., 2013).

Three classes of PI 3-kinases (PI3Ks) generate a membrane identity tag for the endosomal system by phosphorylating the phosphatidylinositol D3 OH group either at the plasma membrane or at endosomes. Additionally, a single PI 5-kinase, PIKfyve, catalyzes the synthesis of PI(3,5)P<sub>2</sub> from PI(3)P (Balla, 2013; Raiborg et al., 2013). Several types of PI phosphatases, primarily the myotubularin family of PI 3-phosphatases, accomplish turnover of PI 3-phosphates (Hsu and Mao, 2015). Class I PI3Ks predominantly produce PI(3,4,5)P<sub>3</sub> *in vivo*. The assembled class I PI3Ks play role in signaling cascades that regulate cell growth, metabolism, proliferation and survival (Vanhaesebroeck et al., 2010). Class II PI3Ks generate PI(3,4)P<sub>2</sub> and a minor portion of PI(3)P. The majority of PI(3)P, a hallmark of the endosomal system, is generated by class III PI3K VPS34. PI(3)P is of key importance for endosome function since it recruits various downstream effectors such as early endosome autoantigen 1 (EEA1), the ESCRT component hepatocyte growth factor-regulated tyrosine kinase substrate (Hrs), and endosomal SNXs. These effectors bind to PI(3)P directly via their FYVE or PX domains and the resulting complexes regulate endosomal fusion, intraluminal vesicle formation and maturation (Raiborg and Stenmark, 2009; Schoneberg et al., 2017).

In addition to PI(3)P, endosomes, multivesicular bodies (MVBs), lysosomes and autophagic compartments contain a functionally important pool of PI(3,5)P<sub>2</sub> on their limiting membranes synthesized by the PI 5-kinase PIKfyve (termed Fab1 in yeast) (Ikonomov et al., 2002; Mayinger, 2012; McCartney et al., 2014; Sbrissa et al., 1999). PIKfyve is a protein that is conserved in all eukaryotes and is recruited to endosomes by its FYVE (Fab1, YOTB, Vac1 and EEA1) domain-mediated interaction with PI(3)P. This conversion of PI(3)P to PI(3,5)P<sub>2</sub> at the limiting membrane of late endosomes is crucial for endosomal maturation along the late

## Introduction

---

endosome/lysosome pathway. Importantly, PI(3,5)P<sub>2</sub> turnover at MVBs and/or lysosomes is mediated by myotubularin phosphatases, specifically by myotubularin-related 2 (MTMR2), which removes the 3-phosphate from PI(3,5)P<sub>2</sub>, as well as Fig4, which removes the 5-phosphate (Bolino et al., 2004; Vaccari et al., 2011).

### 1.3.4. PI(3,5)P<sub>2</sub> in the endolysosomal system

PI(3,5)P<sub>2</sub> is more scarce than most of the PIs in cells and comprises only 0.05-0.1% of total cellular PI (Jin et al., 2016). It has been reported to be essential in many processes in endolysosomal system, including sorting of degradative cargo into MVBs and formation of intraluminal vesicles through its association with the ESCRT-III component Vps24 (Odorizzi et al., 1998; Whitley et al., 2003).

PI(3,5)P<sub>2</sub> was initially identified as a component of the yeast vacuole and mammalian cells (Dove et al., 1997; Whiteford et al., 1997). Reduction of PI(3,5)P<sub>2</sub> in yeast resulted in an enlarged vacuole due to defects in vacuole fission and retrograde traffic to the Golgi (Gary et al., 2002). Reduction of PI(3,5)P<sub>2</sub> in mammalian cells, achieved either by expressing a dominant negative mutant of the PIKfyve kinase or using an siRNA knockdown approach of Vac14 in different studies (Ikonomov et al., 2002; Sbrissa et al., 2004), also resulted in cell vacuolization indicating that the role of PI(3,5)P<sub>2</sub> is conserved in eukaryotic cells. In parallel to these findings, acute inhibition of PIKfyve by a selective inhibitor YM-201636 has been shown to block late endosomal protein sorting or turnover as well as the ESCRT machinery dependent retroviral budding (Jefferies et al., 2008). Later, the discovery of another specific PIKfyve inhibitor, Apilimod, has greatly contributed to studies on the roles of PIKfyve, reporting enlarged lysosome formation upon depletion of PI(3,5)P<sub>2</sub> (Cai et al., 2013). Besides, lysosomal PI(3,5)P<sub>2</sub> has also been mentioned in regulation of calcium release from the lysosome lumen and activation of the v-ATPase (Dong et al., 2010; Li et al., 2014).

Given the multiple functions of PI(3,5)P<sub>2</sub> at late endosomes/lysosomes, the activity of PIKfyve must be tightly regulated. The PIKfyve kinase is in fact part of a larger protein complex, which includes a lipid phosphatase of the Sac family, Fig4 (also called Sac3) that is held together by the scaffold protein Vac14 (also called ArPIKfyve). A recent study has revealed that Vac14 pentamerizes into a star-shaped structure, to which, a single copy each of PIKfyve and Fig4 can bind (Lees et al., 2020) (**Figure 1.10**). This intriguing Vac14 pentamerization

## Introduction

---

conceivably serves as a scaffold that coordinates Fig4 and PIKfyve activities to avoid futile cycles of ATP hydrolysis, although additional roles for this unusual stoichiometry cannot be ruled out. Interestingly, in the intact complex, the lipid phosphatase Fig4 has been found to be active whereas the kinase activity of PIKfyve is suppressed due to a conformational restraint, with its active site being located away from the membrane. This observation indicates opposite roles of PIKfyve and Fig4. However, previous studies report that loss of either PIKfyve, Fig4, or Vac14 causes depletion of PI(3,5)P<sub>2</sub> in various model systems (Duex et al., 2006; Ikononov et al., 2011; Jin et al., 2008). The recent study by Lees and colleagues provides further insights on these contradicting observations by reporting that Fig4, in addition to its activity on lipids, is a serine phosphatase that acts on PIKfyve to increase its lipid kinase activity (Lees et al., 2020). Indeed, PIKfyve is primed by Fig4 to reach its maximal activity following a conformational change upon stimulus. This elegant interplay between PIKfyve and Fig4 allows for tight regulation of endosomal PI(3,5)P<sub>2</sub> levels and affect phosphoinositide metabolism.

Loss-of-function studies in various models associate PIKfyve with developmental defects and embryonic lethality (Nicot et al., 2006; Rusten et al., 2006). Complete loss of phosphatidylinositol phosphate kinase 3 (PPK-3), the *C. elegans* orthologue of PIKfyve/Fab1, results in enlarged lysosomes and possible accumulation of autophagosomes, indicating a defect in membrane trafficking in *ppk-3* mutants (Nicot et al., 2006). *Drosophila fab1* mutants show giant lysosomal structures, impaired lysosomal acidification and tissue outgrowth, the latter suggesting a crucial role of Fab1 in controlling negative cell size (Rusten et al., 2006). Complete loss of PIKfyve in mice is embryonically lethal at very early developmental stages, indicating that sufficient PI(3,5)P<sub>2</sub> or PI(5)P levels are required in embryonic and postnatal stages (Ikononov et al., 2011). Complete loss of Fig4 in mice causes death within 6 weeks after birth, with a clear vacuolization phenotype in cultured neurons and defective myelination in both CNS and PNS (Chow et al., 2007). Conditional Fig4 knockout mice display massive brain defects: spongiform degeneration of the brain, movement disorder, and tremor, all of which demonstrate the necessity of Fig4 expression in neurons for survival. Similarly, a conditional knockout of PIKfyve also reports spongiform degeneration of the brain and vacuole formation in other tissues (Zolov et al., 2012).

## Introduction

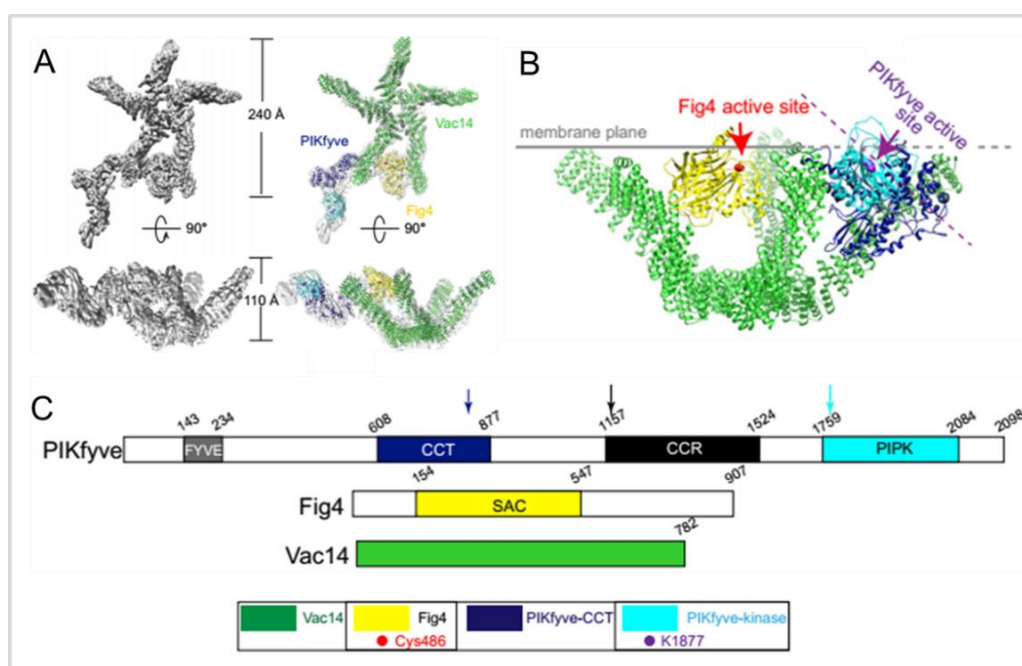


**Figure 1.10. Cryo-EM Reconstruction and domain organization of the human PIKfyve lipid kinase complex.** (A) The composite reconstruction demonstrating that intact PIKfyve complex comprises one copy of PIKfyve and Fig4 and a pentameric Vac14 scaffold. The left panels show the maps only; the right panels also show docked protein models. (B) During membrane interaction of PIKfyve complex, Fig4 active site is oriented to face the membrane, while PIKfyve active site has an approximately 45° twist, hindering its access to membrane-incorporated phosphoinositides. (C) Schemes demonstrating the domain organization of PIKfyve, Fig4, and Vac14. (Adapted from (Lees et al., 2020))

Mutations in PIKfyve and thus PI(3,5)P<sub>2</sub> production have been linked to several neurological diseases, most commonly to the Charcot–Marie–Tooth (CMT) disease. Mice lacking MTMR2, the phosphatase that removes the 3-phosphate from PI(3,5)P<sub>2</sub>, are models of peripheral neuropathy CMT4B1 (Bolino et al., 2004), and are thought to accumulate excess PI(3,5)P<sub>2</sub>. Using genetically engineered mice, Vaccari and colleagues have shown that MTMR2 and Fig4 access the same subcellular pool of PI(3,5)P<sub>2</sub> and that MTMR2 hydrolyzes PI(3,5)P<sub>2</sub> *in vivo* (Vaccari et al., 2011). Moreover, in another severe type of CMT, CMT4J, patients inherit a mutation on Fig4 which causes an amino acid change from isoleucine to threonine (I41T). As a result, delay in motor development and reduced nerve conduction velocity are observed in patients (Chow et al., 2007). This I41T mutation renders Fig4 unstable and blocks its interaction with the scaffolding protein Vac14, confirming the

## Introduction

---

importance of the Fig4-Vac14 interaction (Lenk et al., 2011). Therefore, the PIKfyve-Vac14-Fig4 complex is linked to human neurological disorders and many specific mutation in this complex have yet to be uncovered (Hasegawa et al., 2017; McCartney et al., 2014)

PIs mediate both signaling events in cellular compartments and various cellular and organismal functions including cytoskeleton regulation, motility and development. Investigating the PI identity of presynaptic PVs would give important insight into their biogenesis. For instance, their PI(3)P, PI(4)P or PI(3,5)P<sub>2</sub> identity could identify them as early endosome, Golgi or late endosome derived, respectively. Additionally revealing the lipid identity of these organelles might assist the characterization of the transport machinery. For example, if PVs have PI(3)P identity there is a high chance that Rab5 is involved in their transport. Alternatively, PVs might interact with an adaptor protein or a kinesin motor protein through a specific PI. For instance the neuronal kinesins KIF1A and KIF1B $\beta$  have been suggested to bind PI(4,5)P<sub>2</sub>, which raises the possibility that PVs might have this identity. Overall, studying the lipid identity of PVs would uncover the organelle they are derived from and provides insight into which other players might be involved in PV transport.

### 2. Objectives

Neurons are highly specialized brain cells containing a single elongated axon and multiple dendrites. Therefore, presynaptic compartments can be located very distant from the neuronal cell body where the protein synthesis machinery resides. To ensure stoichiometric assembly of functional presynaptic units, delivery of presynaptic proteins to nascent synapses must be tightly coordinated. To date, molecular mechanisms required for presynaptic biogenesis remain incompletely understood. **Using a combination of genetic, biochemical and cell biological approaches in human stem cell-derived neurons, I aimed to investigate the presynaptic transport machinery and identify presynaptic precursor organelles during neuronal development.**

### 3. Material and Methods

#### 3.1. Materials

##### 3.1.1. Chemicals

If not indicated otherwise chemicals were purchased from Carl Roth (Germany), Life Technologies (USA), Merck (Germany), Sigma-Aldrich (USA) and Thermo Fisher (USA). Consumables were obtained from B. Braun (Germany), Biozym (Germany), GE Healthcare (UK), Greiner (Germany), Millipore (USA), Sarstedt (Germany) and Schott (Germany).

All chemicals and inhibitors which were used in live-imaging or confocal imaging experiments are: DMSO (Sigma-Aldrich, D8418), VPS34-IN1 (kind gift from James Hastie, 1  $\mu$ M working concentration), SAR405 (MedChemExpress, CAS No 1523406-39-4, 3  $\mu$ M working concentration), Compound 19 (Selleckchem, CAS No 1383716-46-8, 3  $\mu$ M working concentration), Apilimod (Echelon Biosciences, 100 nM working concentration), PI4KIIIbeta-IN-10 (MedChem Express, CAT No 1881233-39-1, 2  $\mu$ M working concentration), CVM-05-002 (PI5P4K $\alpha$  inhibitor, kind gift from Dr. Nathanael S. Gray, 10  $\mu$ M working concentration), THZ-P1-2 (pan-PI5P4K inhibitor, kind gift from Dr. Nathanael S. Gray, 1  $\mu$ M working concentration) and Compound 13 (TM-04-176-01) (pan-PI5P4K inhibitor, kind gift from Dr. Nathanael S. Gray, 10  $\mu$ M working concentration). GNE3511 (DLK inhibitor, CalBiochem, 10  $\mu$ M working concentration). All stocks were prepared in DMSO.

##### 3.1.2. Buffers, Media and Solutions

All buffers and solutions were prepared using ultrapure water. The pH was adjusted by addition of NaOH or HCl unless otherwise specified. Buffers used for specific protocols are further explained in detail in the respective methods section.

## Materials and Methods

---

**Table 3.1.** Composition of buffers and media used in molecular biology experiments

Buffer / Solution / Medium	Composition
LB Medium	1 % (w/v) Yeast extract, 0.5 % (w/v) NaCl, 0.5 % (w/v) Trypton, pH 7.4
LB Plates	LB medium, 15 g/l Agar-agar
2xYT Medium	1.0% (w/v) Yeast extract, 1.6% (w/v) Trypton, 0.5 % (w/v) NaCl, pH 7.4
Antibiotics (stock solutions)	100 mg/ml Ampicillin, sterile filtered (1000x) 50 mg/ml Kanamycin, sterile filtered (1000x)
50x Tris-Acetate-EDTA buffer (TAE)	200 mM Tris, 100 mM Glacial acetic acid, 50 mM EDTA, pH 8.2 – 8.4
6x DNA loading dye	0.03 % (w/v) Bromophenol blue, 0.03 % (w/v), Xylene cyanol FF, 60 % (v/v) Glycerol, 60 mM EDTA

**Table 3.2.** Buffers and solutions used in cell biological and imaging experiments

Buffer / Solution / Medium	Composition
DMEM (Lonza)	Dulbecco's modified eagles medium, 4.5 g/l glucose (Gibco), 10% (v/v) Fetal bovine serum (heat-inactivated, Gibco) 100 U/ml Penicillin, 0.1 mg/ml Streptomycin
F12/N2 iN differentiation medium	1x DMEM/F12 (Dulbecco's Modified Eagle Medium/Nutrient Mixture F-12, 1x N2 supplement, 1x NEAA (Gibco), 10 ng/ml Human BDNF, 10 ng/ml Human NT-3, 0.2 ug/ml Mouse laminin, 2.5 µg/ml Dox, 100 U/ml Penicillin, 0.1 mg/ml Streptomycin

## Materials and Methods

---

Buffer / Solution / Medium	Composition
NB/B27 iN differentiation medium	1x NBA (Neurobasal™-A Medium), 1x B27 supplement, 1x GlutaMax (Gibco), 10 ng/ml Human BDNF, 10 ng/ml Human NT-3 0.2 µg/ml Mouse laminin, 2.5 µg/ml Dox, 100 U/ml Penicillin, 0.1 mg/ml Streptomycin
Basic medium for hippocampal neurons	1 x MEM (Minimum Essential Media; Gibco), 5 g/l Glucose, 200 ml/l NaHCO <sub>3</sub> , 100 mg/l Transferrin
Growth medium for hippocampal neurons and iNs	1 x Basic medium, 5 % (v/v) FCS (Biochrom), 0.5 mM L-glutamine (Lonza), 2 % (v/v) B27-supplement (Gibco), 50 U/ml Penicillin, 50 µg/ml Streptomycin
10 x PBS	1.37 M NaCl, 43 mM Na <sub>2</sub> HPO <sub>4</sub> , 14 mM NaH <sub>2</sub> PO <sub>4</sub> , 27 mM KCl, pH 7.4
PFA fixative	4 % (w/v) Paraformaldehyde (PFA) 4 % (w/v) Sucrose, 1x PBS, pH 7.4
10 x Imaging stock solution	1.2 M NaCl, 35 mM KCl, 40 mM KH <sub>2</sub> PO <sub>4</sub> , 200 mM TES, 50 mM NaHCO <sub>3</sub> , 50 mM Glucose, 12 mM Na <sub>2</sub> SO <sub>4</sub> , pH 7.4
1 x Imaging buffer	1x Imaging stock solution 50 mM NaCl, 1.2 mM MgCl <sub>2</sub> , 1.3 mM CaCl <sub>2</sub> , 50 µM APV, 10 µM CNQX

## Materials and Methods

---

**Table 3.3.** Compositions of solutions used for biochemical experiments

Buffer / Solution	Composition
Lysis Buffer	20 mM Hepes pH 7.4, 100 mM KCl, 2 mM MgCl <sub>2</sub> , 1 % (v/v) Triton X-100, 1 mM PMSF, 0.3 % (v/v) Protease inhibitor cocktail
Purification Buffer	50mM Hepes pH7.5, 150mM NaCl, 1 mM PMSF, 1mM MgCl <sub>2</sub> , 0.3 ul/ml cyanase, 1mM EDTA, 2mM DTT, 0.3 % (v/v) Protease inhibitor cocktail 1% (v/v) Triton X-100, 1mg/ml of T4 lysozyme
4 x SDS–PAGE sample buffer	40% Glycerol, 240 mM Tris/HCl pH 6.8, 8% SDS, 0.04% bromophenol blue, 5% beta-mercaptoethanol
4 x SDS–PAGE separation gel buffer	0.4% SDS, 1.5 M Tris base, pH 8.8
4 x SDS–PAGE stacking gel buffer	0.4% SDS, 0.5 M Tris base, pH 6.8
10 x SDS–PAGE running buffer	0.246 M Tris, 1.92 M Glycin, 10% SDS
Coomassie–blue staining solution	0.1% (w/v) Coomassie 250G, 10% Acetic acid, 25% Methanol
Coomassie–blue destaining solution	10% Acetic acid, 25% Methanol
Ponceau staining solution	0.3% (w/v) Ponceau S, 1% Acetic acid
Ponceau destaining solution	1% Acetic acid

## Materials and Methods

---

Buffer / Solution	Composition
Transfer buffer	25 mM Tris, 192 mM Glycine, 20% (v/v) MeOH
10 x TBS	0.2 M Tris pH 7.6, 1.4 M NaCl
2 x Bradford solution	200 ml 85% H <sub>3</sub> PO <sub>4</sub> , 100 ml Ethanol, 140 g/ml Coomassie 250G

### 3.1.3. Enzymes and kits

Phusion high fidelity DNA polymerase, restriction enzymes, calf intestinal alkaline phosphatase (CIP) and Proteinase K were purchased from New England Biolabs (NEB). T4 DNA Ligase and Dream Taq DNA Polymerase were purchased from Thermo Fisher Scientific.

Plasmid DNA was purified from *Escherichia coli* (*E. coli*) overnight cultures in small scale using NucleoSpin Plasmid kit from Macherey-Nagel. For large scale plasmid DNA isolation the endotoxin free plasmid DNA purification kit (NucleoBond Xtra Midi EF kit) from Macherey-Nagel was used. DNA purification from agarose gels and PCR reactions was performed using NucleoSpin Gel and PCR Clean-up kits from Macherey-Nagel. Total RNA was isolated from cells using RNeasy Mini Kit from Qiagen. RNA was reverse-transcribed to cDNA using Invitrogen™ SuperScript™ IV First-Strand Synthesis System and quantified using SYBR Green Master Mix from Thermo Fisher Scientific.

For transfection of iPSCs Lipofectamine Stem transfection system was obtained from Thermo Fisher Scientific. For transfection of iNs and mouse primary hippocampal cultures the calcium phosphate transfection kit was purchased from promega (ProFection Mammalian Transfection system).

## Materials and Methods

---

### 3.1.4. Molecular weight standards

**Table 3.4.** Molecular weight standards

Marker	Marker band	Source
Generuler 1 kbp DNA ladder	kbp marker band: 10, 8, 6, 5, 4, 3.5, 3, 2.5, 2, 1.5, 1, 0.75, 0.5, 0.25	Thermo Scientific #SM311
Prestained protein standard	kDa marker bands: 175, 80, 58, 46, 30, 25, 17, 7	New England Biolabs #7708
PageRuler Prestained Plus Protein Ladder	kDa marker bands: 250, 130, 100, 70, 55, 35, 25, 15, 10	Thermo Scientific #26616

### 3.1.5. Small hairpin RNA oligonucleotides

**Table 3.5.** Sequences of shRNAs used in this study

Targeted gene	Species	Sequence Antisense 5' – 3'	Source
None (scrambled)	human	CCACGAAGTAGGGTGCGAA	Dharmacon
Arl8a	human	TGAATAAGCCACTGTAGGG	Dharmacon
Arl8b	human	TTAGGAAGGACCGTATTCT	Dharmacon
KIF1A	human	GAACACATGGCTCTTACCC	Dharmacon
KIF5B	human	TGGATCATGAAGTTTACCC	Dharmacon
Myrlysin sh1	human	TTAGTCTCAAGGTGTCTGC	Dharmacon
Myrlysin sh2	human	TGGCGTATCTTTTCTGGCG	Dharmacon
SKIP sh1	human	TCGAGCTCCGTGCAGGCAT	Dharmacon
SKIP sh2	human	CGCTTGAGCTGGCAGAGAA	Dharmacon

## Materials and Methods

---

Targeted gene	Species	Sequence Antisense 5' – 3'	Source
Diaskedin sh1	human	TAACTTGATGATTGGACAA	Dharmacon
Diaskedin sh2	human	ATGAACACAGACAAACATC	Dharmacon
PIKfyve sh1	human	TGCGTTCTCAACCAGTAGC	Dharmacon
PIKfyve sh2	human	AATTGCTATAGCTTGTGCC	Dharmacon
PIKfyve sh3	human	AACCAGATCTATCCAGTGA	Dharmacon
MADD sh1	human	GACATGGAGAGTGCATTGT	Dharmacon
MADD sh2	human	CTCGATGTCTACTCGCTTC	Dharmacon
MADD sh3	human	AACCGTACCATGGCAACCC	Dharmacon
FYCO1 sh1	human	TAGCGAATAAATGCTCTTC	Dharmacon
FYCO1 sh2	human	CACATGTTGGCTCACCTGT	Dharmacon
BLOS1 sh1	human	CACCTCATGGTCCAGCTTT	Dharmacon
BLOS1 sh2	human	GGTAGGAGGGATAGGGTTG	Dharmacon
BLOC1S4 sh1	human	CAGCATGCCACGAACTCG	Dharmacon
BLOC1S4 sh2	human	TTCAGTTTGATTCCCCATG	Dharmacon

All DNA oligonucleotides used as primers for polymerase chain reactions (PCRs) were purchased from BioTez as lyophilized powder and dissolved in autoclaved ultrapure water to obtain a 100  $\mu$ M stock concentration. For experiments the stock was further diluted to 10  $\mu$ M. All were stored at -20 °C. Primers which were used for cloning are listed in Table 3.6.

## Materials and Methods

**Table 3.6.** Primer sequences used for cloning

Primer	Sequence
SNAPVAMP2_Sy1_fw	tcgctagcccagagctctggattaaatggcgcgccATGGACAAAGACTGCGA AATG
SNAPVAMP2_Sy1_rv	gatatcgaattctagagtcgcgcccttaattaaCTAAGTGCTGAAGTAAACGAT GATG
SypSNAP_Sy1_fw	ctagcccagagctctggattaaatggcgcgccATGGACGTGGTGAATCAGC
SypSNAP_Sy1_rv	gatatcgaattctagagtcgcgcccttaattaaTTAACCCAGCCCAGGCTTG
KIF1A-eGFP_Sy1_fw	tcgctagcccagagctctggattaaatggcgcgccatggccggggcctctgtg
KIF1A_eGFP_Sy1_rv	agaggttgattatcgataagcttgatatcgaattcttactgtacagctcgtccatg
Arl8b_mCh_Sy1_fw	tcgctagcccagagctctggattaaatggcgcgccatgtggcgtcatctcc
Arl8b_mCh_Sy1_rv	agaggttgattatcgataagcttgatatcgaattcttactgtacagctcgtccatg
FYCO1shRES_fwd1	ggatccgaattcgatatccagcacagtggcggcccatggcctccaccaatgcag
FYCO1shRES_rev1	gcgaatgaaagcacgtccttccccaaggatgttc
FYCO1shRES_fwd2	tcctggggaaaggacgtgcttcattcgctactccttggtg
FYCO1shRES_rev2	gaggctgatcagcgggttaaaccggccctctagattacaggaaatcacttccatcg
FYCO1deltaRUN_fwd	ggatccgaattcgatatccagcacagtggcggcccatggcagatacggcatcagac
FYCO1deltaRUN_rev	gaggctgatcagcgggttaaaccggccctctagattacaggaaatcacttccatcg
FYVE-LIR-GOLD-Fwd	ggatccgaattcgatatccagcacagtggcggcccgctggaattccagcagaagc
FYVE-LIR-GOLD-Rev	gaggctgatcagcgggttaaaccggccctctagattacaggaaatcacttccatcg
FYCO1_FYVE1-Fwd	ggatccgaattcgatatccagcacagtggcggcccgatgccctggaattccag
FYCO1_FYVE1-Rev	cagggcatcactaccgcctcactgagcttctg
FYCO1_FYVE2-Fwd	aagctcagtgaggcggtagtgatgccctggaattccag
FYCO1_FYVE2-Rev	gaggctgatcagcgggttaaaccggccctctagattagcctcactgagcttctg
KIF1A_PH1_fw	cagatccgctagcgtaccggactcagatctcgagatggtcgggcaacagagacagag
KIF1A_PH1_rev	ctctgtgcccgaacgaccgcatctgcgagatc
KIF1A_PH2_fw	gcgagatgcgggtcgctcgggcaacagagacagag
KIF1A_PH2_rev	gctcctcgccctgctcaccatggtggcgaccggtcgaccgcatctgcgagatc
KIF1A_dPH_fw	cagatccgctagcgtaccggactcagatctcgagatggccggggcctctgtg
KIF1A_dPH_rev	gctcctcgccctgctcaccatggtggcgaccggtcaggggagggagtcttcttagatc
GFP-GST-fwd	atctggaagtctgttccaggggcccctgggatccATGGTGAGCAAGGGCGAG
GFP-GST-rev	tgttggccgaaccattgatccCTTGTACAGCTCGTCCATG
GST-2xPH-fwd	ctgtacaaggatcaATGGTTCGGGCAACAGAGAC
GST-2xPH-rev	cagatcgtcagtcagtcacgatgcggccgctcgagttaGACCCGCATCTGCGCA GATC
Syp-RFP-lenti-fwd	ggagctgtgctgctgagagcgcagtcgctagcatggacgtggtgaatcagctggtggc
Syp-RFP-lenti-rev	agaggttgattatcgataagcttgatatcgaattcttaggcgggtggagtggcggc
Lamp1-SNAP-fwd	ttcgatgtggagcttctaaaactggaaccaccgggtggatcaggttctatggacaaagactgc
Lamp1-SNAP-rev	gtggtatggctgattatgatctagagtcgcgggccgacccagcccaggcttgcc

## Materials and Methods

---

### 3.1.6. Plasmid vectors

All bacterial and mammalian expression vectors used in this study are described in Table 3.7. All plasmid DNA were stored at -20 °C at a concentration of 1 µg/µl.

**Table 3.7.** Vector backbones used for cloning and protein expression

Plasmid backbone	Properties	Source
pcDNA3.1	Mammalian expression vector; CMV promoter	Thermo Fisher Scientific
pEGFP-N	Mammalian expression vector for fusion proteins with C-terminally tagged eGFP; CMV promoter	Clontech
pFUGW with hSy1 promoter	Mammalian lentiviral expression vector; human Synapsin1 promoter	Viral Core Facility of Charite
BL-360 f(U6)sNLS-RFP	Mammalian lentiviral expression vector with dual promoters, U6 promoter for shRNA, Synapsin promoter for nuclear RFP	Rosenmund lab
pGEX-6P-1	Bacterial expression vector with N-terminally tagged GST proteins; thrombin cleavage site; IPTG inducible Taq promoter	Pharmacia

**Table 3.8.** Plasmid DNA constructs used for recombinant protein expression

Construct	Species	Backbone	Tag	Source/Comments
eGFP	Jellyfish	pFUGW	eGFP	Baltimore D. (Lois et al., 2002)
SYP-eGFP	Rat	pcNEO	eGFP	Haucke V.
SYP-RFP	Rat	LivinColorsN1	mRFP	Wienisch M.
Syt1-RFP	Rat	mcherryC1	mRFP	Haucke V.
vGlut1-venus	Rat	pEGFP-N	eGFP	Haucke V.

## Materials and Methods

Construct	Species	Backbone	Tag	Source/Comments
vGlut1-RFP	Rat	pEGFP-N	mRFP	Haucke V.
Bsn-GFP	Rat	pEGFP-C	GFP	Gundelfinger et al.
Munc13-GFP	Rat	pEGFP-N	eGFP	Haucke V.
Munc13-SNAP	Rat	pSNAP-N1	SNAP	Haucke V.
Nrxn1 $\beta$ -GFP	Rat	pEGFP-N	eGFP	Perrais D.
Arl8b-GFP	Human	pcDNA-DEST47	GFP	Kahn R. (Addgene # 67404)
Arl8b-mCherry	Human	pcmCherry-MK	mCherry	Haucke V.
Arl8b-mCh-LV	Human	pFUGW	mCherry	Haucke V.
Arl8b(TN)-GFP	Human	pEGFP-N1	eGFP	Haucke V.
Arl8b(QL)-GFP	Human	pEGFP-N1	eGFP	Haucke V.
Arl8a-Myc	Human	pDS_Myc-X	Myc	Kahn R. (Addgene # 67361)
Arl8b-Myc	Human	pDS_Myc-X	Myc	Kahn R. (Addgene # 67362)
Lamp1-GFP	Human	pEGFP-N3	mGFP	Falcon-Perez JM.
Lamp1-mCherry	Human	pEGFP-N3	mCherry	Haucke V.
Rab7-GFP	Human	pEGFP-C2	eGFP	Van der Sluis, P. (UMC)
CD63-GFP	Human	pEGFP C2	eGFP	Luzio P. (Addgene # 62964)
Mito-RFP	Human	pcDNA3	RFP	Haucke V.
KIF1A-EGFP	Mouse	Clontech N1	eGFP	Hirokawa N.
KIF1A-EGFP-LV	Mouse	pFUGW	eGFP	Haucke V.
KIF1A-mCh-LV	Mouse	pFUGW	mCherry	Haucke V.
Syp-2x-pH	Rat	pcDNA3	pHluorin	Haucke V.
NGN2 (neuronal differentiation)	Human	na	-	Sudhof T. (Stanford Uni.)
rtTA (neuronal differentiation)	Human	na	-	Sudhof T. (Stanford Uni.)
GFP (neuronal differentiation)	Jellyfish	na	-	Sudhof T. (Stanford Uni.)
pRSV-Rev	Human	pRSV-Rev	-	Addgene (12253)
pRRE	Human	pMD	-	Addgene (12251)
VSV-G	Human	pCMV	-	Addgene (8454)

## Materials and Methods

---

### 3.1.7. Antibodies

All primary and secondary antibodies used in this study are listed in Table 3.9 and Table 3.10, respectively. All antibodies were stored at -20 °C for long-term or at 4 °C for short-term periods. Antibodies were diluted with 50 % (v/v) for long-term storage. All specified dilutions refer to the 1:1 glycerol-diluted antibody stocks.

**Table 3.9.** Primary antibodies used in this study.

Antigen	Host	Source	Clone/ Cat #	Dilution WB	Dilution ICC
Bassoon	Guinae pig	SySy	141004	-	1:100
Homer 1	Mouse	SySy	160003	-	1:200
Homer 1	Guinae pig	SySy	160011	-	1:200
Synapsin 1/2	Rabbit	SySy	106002	1:250	1:500
Synaptophysin	Rabbit	SySy	101002	1:500	1:200
Synaptotagmin 1	Mouse	SySy	105 011	1:500	1:300
Syntaxin 1	Mouse	SySy	110111	1:500	1:250
SNAP 25	Mouse	SySy	111011	1:1000	1:250
Piccolo	Rabbit	SySy	142002	-	1:100
PSD95	Mouse	ThermoFisher	MA1-045	1:500	1:500
$\beta$ -3-Tubulin	Rabbit	SySy	302302	-	1:300
MAP2	Guinae pig	SySy	188004	-	1:500
NeuN	Mouse	Merck	MAB377	1:500	1:200
Lamp1	Rabbit	Cell Signaling	9091P	-	1:100
Arl8	Rabbit	ProteinTech	17060-1-ap	1:500	-
Arl8	Rabbit	SCBT	sc-398635 (H-8)	-	1:50
KIF1A	Rabbit	Abcam	ab180153	1:500	1:50
KIF5B	Rabbit	Abcam	ab167429	1:500	-
SKIP	Rabbit	Abcam	ab91581	1:250	-
Myrlysin	Mouse	Abnova	H00118426-B01	1:250	-

## Materials and Methods

Antigen	Host	Source	Clone/ Cat #	Dilution WB	Dilution ICC
Diaskedin	Rabbit	Abnova	PAB23142	1:250	-
BLOS1	Mouse	SCBT	sc-515444	1:100	-
BLOC1S4 (CNO)	Mouse	Avantor (vwr)	ABGEAT1570A	1:250	-
PIKfyve	Mouse	SCBT	sc-100408	1:100	-
GST	Mouse	ThermoFisher	MA4-004	1:500	-
$\beta$ -Actin	Mouse	Sigma	A5441	1:2000	-
GFP	Chicken	Abcam	ab13970	1:5000	1:2000
GFP	Mouse	Clontech	632381	1:2500	1:500
RFP	Rabbit	Biozol	MBL-PM005	1:1000	1:500

**Table 3.10.** Secondary antibodies used in this study

Antigen	Host	Conjugate	Source	Cat #	Dilution
Rabbit	goat	AlexaFluor 488	Invitrogen	A11034	1:500
Mouse	goat	AlexaFluor 488	Invitrogen	A11029	1:500
Mouse	goat	Alexa Fluor568	Thermo	A11004	1:500
Rabbit	goat	Alexa Fluor568	Invitrogen	A11036	1:500
Rabbit	donkey	Alexa Fluor647	Invitrogen	A31573	1:500
Mouse	goat	Alexa Fluor647	Thermo	A21236	1:500
Chicken	goat	AlexaFluor 488	Abcam	ab150169	1:500
Guinae pig	goat	Alexa Fluor568	Thermo	A11075	1:500
Guinae pig	donkey	AlexaFluor 488	Jackson	706-545-148	1:500
Mouse	goat	HRP	Jackson	115-035-003	1:5000
Rabbit	goat	HRP	Jackson	111-035-003	1:5000
Mouse	goat	IRDye 800CW	LICOR	P/N 926-32210	1:5000
Rabbit	goat	IRDye 800CW	LICOR	P/N 925-32211	1:5000

## Materials and Methods

---

### 3.2. Molecular Biology Methods

#### 3.2.1. Cloning strategies

Cloning strategies were designed with the ApE (A Plasmid Editor) software. Primers were designed to have a 15-18 bp overlap with the target sequence in order to ensure specific amplification of the target sequence.

Target sequence was inserted into the plasmid vector of interest either using the corresponding restriction enzyme or using Gibson Assembly strategy. In both cases, the melting temperatures of primers were kept between 50°C and 70°C. At the end of each cloning procedure, the complete DNA construct was controlled *in silico* to guarantee the absence of unwanted frame shifts, stop codons or incompatibilities of restriction enzyme recognition sites.

#### 3.2.2. Polymerase chain reaction

For reasons of lower error rate, the high fidelity Phusion polymerase (New England Biolabs) was used for polymerase chain reaction (PCR) amplification for cloning of constructs or for amplifying parts of genomic DNA (gDNA).

**Table 3.11:** Phusion High-Fidelity PCR 25 µl reaction mix.

Components	Volume
Phusion High-Fidelity Polymerase	0.25 µl
Phusion High-Fidelity Buffer (5x)	5 µl
forward primer (10 µM)	1.25 µl
reverse primer (10 µM)	1.25 µl
dNTPs (10mM)	0.5 µl
DMSO	1 µl
template DNA	250 ng
H <sub>2</sub> O	ad 25 µl

## Materials and Methods

---

**Table 3.12:** Phusion High-Fidelity Touchdown PCR program.

Step	Temperature	Time	Repeat cycle
Initial denaturation	98 °C	3 min	-
Denaturation	98 °C	10 sec	10x
Primer annealing	68 °C (dT=-1C/cycle)	30 sec	
Extension	72 °C	60 sec	
Denaturation	98 °C	10 sec	30x
Primer annealing	60 °C	30 sec	
Extension	72 °C	60 sec	
Extension	72 °C	10 min	-
Hold	4 °C	∞	-

### 3.2.3. Agarose gel electrophoresis of DNA fragments

Agarose gel electrophoresis was used for separating DNA fragments by size for analysis and purification. Depending on the size of the DNA fragments 0.7 – 2 % (w/v) agarose gels were prepared by dissolving agarose in 1x TAE buffer supplemented with 100 ng/ml ethidiumbromide (Roth) to detect DNA by UV light. DNA samples with 1x loading buffer were loaded on the agarose gel. Subsequently, the gel was run in a horizontal chamber (Perfect Blue from PeqLab) filled with 1x TAE buffer at 100 V for 20 - 30 min. DNA fragments were visualized by UV light on a UV table (UVT-28 LV from Herolab) and documented with G:Box gel documenting system (Syngene).

If the DNA fragments were used for further cloning steps, UV light exposure was minimized, bands were cut under the UV light and DNA was purified using NucleoSpin Gel and PCR clean-up kit (Macherey Nagel) according to manufacturer's instructions.

## Materials and Methods

---

### 3.2.4. Sequencing of DNA

Following purification of PCR products using PCR clean-up kit (Macherey Nagel), ten µl of PCR product, together with their specific sequencing primers were sent for sequencing. Sanger sequencing was performed by LGC Genomics GmbH. Sequences were analysed using the DNASTar SeqMan Software Version 13.0.0.

### 3.2.5. Transformation of chemically competent *E.coli* Top10 cells

Chemically competent *E.coli* (50 µl of CaCl<sub>2</sub> competent TOP10 or BL21 CodonPlus strains) were transformed with the ligation reaction or plasmid DNA following the heat shock protocol. First, competent *E.coli* were thawed on ice and incubated 30 min on ice with 10 µl of the ligation reaction or 1 µg of plasmid DNA. Next, the bacterial culture was heat shocked for 50 s at 42 °C, chilled on ice for 5 min and incubated with 500 µl LB without antibiotics at 37 °C for 1 hour. For selection, 250ul of the bacterial cultures were plated on pre-warmed LB agar plates with antibiotics corresponding to their selective resistance. The LB plates were incubated at 37 °C overnight.

### 3.2.6. Glycerol Stocks

For long term storage of *E.coli* clones, glycerol stocks of overnight cultures were prepared by mixing bacterial overnight cultures in LB medium in 1:1 volume ratio with 50% (w/v) sterile glycerol. The stocks were stored in cryotubes, frozen and stored at -80°C.

### 3.2.7. Purification of plasmid DNA from *E. coli* cultures

Plasmid DNA was purified from small-scale overnight *E. coli* cultures using the NucleoSpin Plasmid kit from Macherey-Nagel according to manufacturer's instructions (Mini-prep). Bacteria were lysed in an alkaline and SDS containing buffer, cell debris and genomic DNA were removed by centrifugation, further contaminations were removed by washing steps and the plasmid DNA was detected in the supernatant bound to a silica column and eluted from the column.

## Materials and Methods

---

For large scale DNA purification, NucleoBond® Xtra endotoxin free (EF) plasmid purification kit from Macherey-Nagel was used following the manufacturer's instructions. Here, eluted plasmid DNA was precipitated with isopropanol and reconstituted with sterile ultrapure water to 1 µg/µl.

### 3.2.8. RNA extraction from iPSCs and iNs

Total RNA was extracted from cells using the RNeasy Mini Kit (Qiagen) according to manufacturer's instructions. Samples were treated with DNase directly on the purification column by addition of 80 µl RNase-free DNase I (Qiagen) which was prepared according to manufacturer's instructions and incubated for 15 min at room temperature after the first washing step. RNA concentrations were determined using a nanodrop spectrophotometer.

### 3.2.9. Reverse transcription of RNA

Reverse transcription of the isolated RNA into complementary DNA (cDNA) was performed using the SuperScript IV kit (Thermo Fisher) according to manufacturer's instructions. A total RNA amount of 50 ng to 1 µg was used for cDNA synthesis.

### 3.2.10. RNA quantification using quantitative real-time PCR

Quantitative real-time PCR (qRT-PCR) was performed using DNA oligonucleotides flanking the target region and SYBR Green master mix (Thermo Fisher) according to manufacturer's instructions.

## Materials and Methods

---

### 3.2.11. Isolation of genomic DNA (gDNA) from iPSCs

For isolating genomic DNA from iPSCs, NucleoSpin Tissue XS kit was used according to manufacturer's instructions. DNA concentrations were determined using a Nanodrop spectrophotometer.

### 3.2.12. Genotyping of iPS clones

To genotype the successfully CRISPR/Cas9 genome engineered iPS clones, primers were designed to amplify the region targeted by Cas9. *Arl8a/b* dKOs were identified with Sanger sequencing as described in 3.2.4. Genotyping of Syp-EGFP KI cells was performed by amplifying the 5' and 3' regions surrounding the EGFP tag. After positive clones were initially identified by PCR, their nucleotide sequences were further confirmed similarly by Sanger sequencing.

### 3.3. Cell Culture Methods

#### 3.3.1. Human induced pluripotent stem cell (iPSC) culture

The feeder-free iPSC line BIHi005-A which has been generated at Berlin Institute of Health (BIH) and contains Doxycycline-inducible Ngn2-EGFP-Puromycin expression cassette at its safe harbor locus was used in all experiments involving iPSCs. The cell line was generated from fibroblast of dermis in the OLS and was reprogrammed using the CytoTune™-iPS 2.0 Sendai Reprogramming Kit (Thermo Fisher). The non-transmissible Sendai virus vector encoded for the four pluripotency factors (SOX2, KLF-4, OCT4, c-MYC), known to efficiently reprogram somatic cells into iPSCs (Takahashi and Yamanaka, 2006). The reprogrammed iPSCs were characterized by immunofluorescence staining for the pluripotency markers OCT4, SOX2, NANOG and SSEA4 and SNP karyotyping was carried out at Berlin Institute of Health (BIH). iPSC line was tested for the absence of human pathogenic viruses (HIV, HBV, HCV) by the Leibniz-Institute DSMZ, German Collection of Microorganisms and Cell Cultures, Braunschweig, Germany. The line AICS-0022-037 (LAMP1-mEGFP Knock-in iPSCs) was purchased from Allen Institute, USA.

Human iPSC cultures were maintained on plates coated with Matrigel™ (BD Biosciences) in StemFlex medium (Thermo Fisher) at 37 °C in humidified atmosphere containing 5% CO<sub>2</sub>. The coating solution was prepared by dissolving 400 µl Matrigel in 20 ml OPTI-MEM™ and kept in the fridge. Plates were coated by adding 1.5 ml of Matrigel™ solution per one well of a 6-well plate and incubating at 37 °C for 1h. After the coating, matrigel solution was re-collected for later use. The iPSC medium StemFlex was changed every second day. For regular passaging (twice a week), cells at 80% confluency were incubated with 1 ml dissociation solution (1x PBS containing 0.5 M EDTA) per one well of a 6-well plate for 5 min at 37 °C. Afterwards, the dissociation solution was removed, and cell clumps carefully resuspended in StemFlex medium and transferred onto Matrigel™-coated plates at a ratio of 1:4-1:10. For single cell seeding and counting, cells were dissociated by incubation in 1 ml StemPro™ Accutase™ (Thermo Fisher) for 5 min at 37 °C. The single cell suspension was diluted with 5 ml StemFlex medium and centrifuged at 200 x g for 5 min at RT. The cell pellet was resuspended in StemFlex supplemented with 10 µM ROCK-1 inhibitor Y-27632 (LC Laboratories) to reduce apoptosis of single iPSCs after dissociation. Cells were counted and seeded on Matrigel™-coated plates. iPSCs were cryopreserved by dissociating 80-90 % confluent cell wells using StemPro™ Accutase™ as described above. Cell pellets were

## Materials and Methods

---

resuspended in 1 ml Bambanker™ freezing medium (Lymphotec Inc.), transferred to cryovials, and frozen at -80°C in Nalgene™ cryo freezing containers. Cells were thawed at 37 °C, diluted with 10 ml StemFlex medium and centrifuged at 200 x g for 5 min. Cell pellets were then resuspended in StemFlex supplemented with 10 µM ROCK-1 inhibitor and cells were plated on plates coated with Matrigel™. Plasmid DNA transfections were performed using Lipofectamine Stem™ Transfection Reagent (Thermo Fisher) according to manufacturer's instructions.

### 3.3.2. Differentiation of human iPSCs into cortical neurons

Human iPSCs were differentiated into cortical neurons using an optimised method based on the rapid neuronal differentiation protocol described in (Zhang et al., 2013) (see also Figure 4.1).

Ngn2 cassette-containing iPSCs were plated on Matrigel™-coated 6-wells cells (2 x 10<sup>5</sup> iPSCs / well) (day -1) in StemFlex medium containing 10 µM ROCK-1 Inhibitor (Y-27632). If the plated cells did not contain the differentiation cassette in their genome, the cassette was administered to iPSCs by lentiviral delivery 6 hours post-seeding and cells were incubated with the lentivirus overnight. The next day (day 0), neuronal differentiation was initiated by changing the iPSC medium to F12-N2 medium which contained 2.5 µg/ml doxycycline to induce Ngn2 expression (Table 3.2). The day after (day 1), the medium was changed to F12-N2 medium containing fresh doxycycline. On this day, nuclear GFP signal in the differentiating cells was visible under the fluorescent microscope. On day 2, F12-N2 medium containing fresh doxycycline was supplemented with 10 µg/ml puromycin to apply a negative selection and enrich for cells in which the Ngn2 expression cassette has been successfully activated. Puromycin selection was applied for a minimum of 24 hours, until no undifferentiated cells were observed in wells. On day 3, differentiating iNs were co-cultured with mouse astrocytes to support neuronal growth. Glia cultures prepared from P0/P1 mouse cortices and passaged at least one time after their preparation (see Section 3.3.5) were detached by 5 minute incubation with Trypsin at 37 °C. They were spun-down at 300g or 5 minutes, cell pellet was resuspended in 1 ml NB-B27 medium (Table 3.2) and cells were counted. iNs were washed once with 1x PBS to remove dead cells and puromycin and detached by 3 minute incubation with Accutase at 37 °C. Following centrifugation at 200g for 5 minutes, cell pellet was resuspended in NB-B27 medium (max. 500 µl to achieve higher cell density) and cells were

## Materials and Methods

---

counted. iNs and mouse astrocytes were seeded in a 5:1 ratio respectively. Of note, this ratio might change depending on the particular experiment and astrocytes could be completely omitted for biochemical experiments requiring iNs to develop no longer than 13 days. iN-astrocyte mix cells were seeded on matrigel-coated plates or coverslips. To achieve dense iN cultures, only the center of the coverslips were coated with Matrigel™ and a total number of 80 – 150 x 10<sup>3</sup> cells were seeded per coverslip in a 30 – 50 µl drop. When using this technique, plates were first incubated at 37 °C for 1 hour until iNs and astrocytes attached to coverslips, and then NB-B27 medium containing fresh doxycycline was added (2 ml per one well of a 6-well plate). After day 3, medium of iNs was never changed completely. On day 6 and 8, half of the NB-B27 medium was replaced with NB-B27 medium containing fresh doxycycline and on day 10 half of the NB-B27 media was replaced with Growth Medium containing FBS (Table 3.2). After this point doxycycline was no longer added to the medium, and instead Ara-C was included to inhibit overgrowth of mitotic glial cells. After day 10, iN cultures were fed only weekly, by removing 100 µl of the old media and adding 150 µl of fresh Growth media. Mature neurons were harvested after day 28.

### 3.3.3. Generating genome-edited isogenic iPSC lines using CRISPR/Cas9

pX330-U6-Chimeric\_BB-CBh-hSpCas9 was obtained from Addgene (#42230). All guide RNA sequences used in Crispr experiments are shown in Table 3.13. Primers for Arl8a KO guide RNA generation were: forward 1: 5'- CACC G CGCGATCACGTTGACGAAGG -3'; reverse 1: 5'- AAAC CCTTCGTCAACGTGATCGCG C -3'; forward 2: 5'- CACC G TGTTGAACAAAGCGATCATA -3'; reverse 2: 5'- AAAC TATGATCGCTTTGTTCAACA C -3'. Primers for Arl8b KO guide RNA generation were: forward 1: 5'- CACC G AGAGATGGAGCTGACGCTCG -3'; reverse 1: 5'- AAAC CGAGCGTCAGCTCCATCTCT C -3'; forward 2: 5'- CACC G CGCGATGACATTGACGAAGG -3'; reverse 2: 5'- AAAC CCTTCGTCAATGTCATCGCG C -3'. Primers for Syp-EGFP-KI guide RNA generation were: forward: 5'- CACC GCTCACCAGACTACATCTGAT -3'; reverse: 5'- AA ACATCAGATGTAGTCTGGTGAGC -3'. The primers were annealed and cloned into the px330 plasmid using the Bpil site. For the generation of the Syp-EGFP cell line via insertion of a GFP tag before the stop-codon of *SYP*, a vector was generated containing the original genomic sequence of human *SYP* approximately 1200 bp up- and downstream of the start-codon including the sequence of eGFP before the stop-codon of *SYP*. The homology regions and the eGFP sequence were joined together via gene synthesis (Absea gene synthesis).

## Materials and Methods

---

**Table 3.13:** guide RNA sequences used in Crispr/Cas9.

sgRNA	Gene/ Targets	Sequence
Arl8a-sg1	Arl8a/ Exon 1	CGCGATCACGTTGACGAAGG
Arl8a-sg2	Arl8a/ Exon 1	TGTTGAACAAAGCGATCATA
Arl8b-sg1	Arl8b/ Exon 1	AGAGATGGAGCTGACGCTCG
Arl8b-sg2	Arl8b/ Exon 1	CGCGATGACATTGACGAAGG
KIF1A-sg1	KIF1A/ Exon 4	CAACTACGCGTCGCAGAAGC
Syp-KI-sg1	SYP/ Exon 7	GAAATCAGACTACATCTGAT

For generating CRISPR KO clones, px330-plasmid containing the gRNA was transfected into iPSCs using Lipofectamine Stem™ Transfection Reagent (Thermo Fisher) according to manufacturer's instructions. For generating Syp-eGFP KI clones, px330-plasmid containing the gRNA and the homology recombination vector were co-transfected into iPSCs by the same method. In this case, 4 hours after transfection, an HDR enhancer was added in the cell medium (IDT, 1081072) and incubated overnight. Two days after transfection, transfected cells were selected by their GFP expression and were pooled in one well of a 6-well plate by FACS sorting. After the sorted cells recovered, they were plated in Matrigel™-coated 10cm plates very sparsely (approximately 6000 iPSCs/plate) and cells were observed until cell colonies had formed. Colonies were expanded and genomic DNA was isolated.

Arl8a/b dKO clones were generated sequentially: first Arl8a KO clones were generated and single cell derived colonies were sequenced for frameshifts using primer pairs shown on Table 3.14. Subsequently, single KO clones were transfected with px330-plasmid containing the gRNA for Arl8b and the same selection protocol was applied. Generated double KO clones were initially identified by Western Blot, where the complete lack of Arl8 signal was detected in double KO samples. Selected clones were further sequenced for Arl8b KO using primer pairs shown on Table 3.14, correct cell clones were expanded and cryopreserved.

Syp-eGFP knock in iPS clones were identified by PCR amplification and Sanger sequencing. To test for integration of the HR cassette, the genomic DNA was amplified using a set of three primers (specified in Table 3.14), two of them binding in the genomic region, not included in the homology arms of the vector, and one of them binding in the vector's selection

## Materials and Methods

---

cassette. PCR products were analyzed on 1 % agarose gels to identify wildtype (WT, 0.25 kb) and homology cassette integrated (HR, 1 kb) alleles (see Figure 4.5.). Cell clones with integration of the homology cassette in both alleles (absence of WT band) were sequenced to ensure integrity of left and right homology arms and correct introduction of the eGFP tag. Correct cell clones were expanded and cryopreserved in liquid nitrogen.

**Table 3.14.** Primer pairs used for amplification of Crispr-targeted regions.

Primer name	Gene	Sequence
Arl8a-F1	Arl8a	GATTCCGGGGCAGCGAGTCGT
Arl8a-R1	Arl8a	TATGCCAGGCGGCGACCC
Arl8a-R2	Arl8a	TACTAGGCCCCAAGCGCTCG
Arl8b-F1	Arl8b	GGCGAGTCATATGATCCGCTCGG
Arl8b-R1	Arl8b	GGCGCTCACCGCGATGACAT
Arl8b-R2	Arl8b	TTCCGCTGCCGATCTCAGTGCTACT
Syp-EGFP-F1	SYP	CCTGACTATGGTCAACCAG
Syp-EGFP-F2	SYP	ACTATGGGCAGCAAGGCTA
Syp-EGFP-R1	SYP	GCTCTTAGCAGGTAGTTCTG
Syp-EGFP-R2	SYP	AGTCCTTACTTGCCCCAGTA
Syp-EGFP-F3-int.	SYP	ATCTTCTTCAAGGACGACGG

## Materials and Methods

---

### 3.3.4. Lentiviral production in HEK-293TN cells

For production of lentiviruses,  $2 \times 10^6$  HEK-293TN cells were seeded in DMEM containing 5 % FBS in 10 cm plates. The next day, the viral construct of interest was co-transfected with two packaging plasmids using Calcium Phosphate transfection. Next morning, cells were washed with 2x PBS and medium was replaced with 6 ml of fresh DMEM. Cells were incubated for an additional 24 h. After incubation, the medium was collected and stored at 4 °C, while the incubation of the transfected cells with 6 ml of DMEM was repeated for the next day. After 12 ml of medium containing virus was harvested, dead cells were removed from the medium by centrifugation at 2000 x g for 5 min at 4 °C. The cleared medium was transferred to Amicon Columns (size 100K) to enable virus concentration without ultracentrifugation. Lentivirus-containing supernatants were centrifuged at 5000 x g for 20 min at 4 °C. The supernatant collected on the filter (approximately 250ul) was aliquoted and snap frozen in liquid nitrogen. Aliquoted virus preparations were stored at -80 °C.

### 3.3.5. Preparation and culture of primary mouse glia

Astrocytes were prepared from mouse pups on post-natal day 1-3. Briefly, after skull was opened, cortices were dissected meninges was removed. Cortices were collected in a 5-cm dish in HBSS, cut into small pieces with scalpel and collected into a falcon tube. Following removal of supernatant, cortices were washed three times with 5ml HBSS. After the last wash, 5 ml Trypsin (37°C) and 10 µl DNase were added and the tissues were incubated at 37°C for 15 min. After trypsinization, cortices were again washed three times with 5 ml of HBSS. Tissue was resuspended in 2ml DMEM + FCS + P/S and 10 µl DNase and triturated first using 1ml pipette tips and then using glass Pasteur pipettes with narrowed pore size until no particles were observed. Then the cells were divided into falcon tubes in DMEM and centrifuged for 8 min at 200 g (1000 rpm) at 4°C. Cell pellets were resuspended in 1 ml medium and plated onto 10 cm dishes in DMEM + FCS + P/S.

One day after preparation, astrocytes were washed with 1X PBS to remove debris and medium was changed to fresh DMEM containing 1% FCS and P/S. Culture became confluent approximately 7 days after preparation. Glia was kept in culture until passage 3 and discarded afterwards. Before their usage in iN preparations, they were trypsinized at least one time to make sure there were no residual mouse neurons contaminating human neurons preparation.

## Materials and Methods

---

### 3.3.6. Culture of HEK293T and HeLa cells

Cell lines used for immunoprecipitation and immunofluorescence staining experiments were human embryonic kidney (HEK) 293T and HeLa (human cervical carcinoma) cells, respectively. Both cell lines were grown in Dulbecco's modified Eagle's medium (DMEM) high glucose supplemented with 10 % (v/v) fetal calf serum (FCS) and 1 % (v/v) penicillin/streptomycin (Gibco). Cells were passaged twice a week by brief washing with PBS and incubation with 0.05 % (v/v) trypsin/EDTA (Gibco) for 5 min at 37 °C. After cells were resuspended in an excess of medium with FCS for trypsin inactivation, they were then plated in 1:3-10. After 20 passages cells were discarded.

### 3.3.7. jetPRIME transfection of HeLa cells for immunofluorescence analysis

HeLa cells were transfected with plasmid DNA using jetPRIME (PolyPlus Transfection). jetPRIME is a cationic reagent which facilitates DNA uptake into cells by forming complexes with negatively charged DNA. Briefly, per well of a 6-well plate 2 µg of plasmid DNA was mixed in 200 µl jetPRIME buffer and 4 µl of jetPRIME was added into this mix. The transfection solution was vortexed for one second and incubated for 10 min at RT before it was added to the cells.

### 3.3.8. Calcium phosphate transfection of primary hippocampal neurons and iNs

Primary hippocampal neurons were transfected on DIV7 - 9 with calcium phosphate using ProFection Mammalian Transfection System (Promega). This method is based on complex formation between DNA and calcium phosphate, which are then taken up via endocytosis. Endocytic uptake of plasmids is induced by 20 minute starvation in the starvation medium Neurobasal-A (Gibco, Life technologies). Incubation in calcium- and magnesium-free HBSS is required to remove residual precipitates at the end of the process. Thus, both Neurobasal A medium and HBSS had to be adjusted with D-Mannitol to the same osmolarity as the neuronal culture medium and equilibrated at 37 °C and 5 % CO<sub>2</sub>.

## Materials and Methods

---

For transfection of one coverslip with 25 mm in diameter a maximum amount of 6 µg plasmid DNA and were used. Plasmid DNA and 250 mM CaCl<sub>2</sub> were mixed with nuclease free water to a final volume of 100 µl. This mixture was then added drop-wise to an equal amount of 2x Hepes buffered saline in a second tube while constant vortexing. Subsequently the mix was incubated for 20 minutes at RT to allow complex formation. Neurons were starved at the same time in 1 ml of osmolarity adjusted and equilibrated Neurobasal-A medium. 200 µl of the DNA-calcium phosphate precipitate were added drop-wise to each coverslip, and neurons were incubated for 25 minutes at 37 °C in incubators containing 5 % CO<sub>2</sub>. Finally, cells were washed two times with 2 ml of osmolarity adjusted and equilibrated HBSS and transferred back into their original medium. When 18 mm coverslips were used, all amounts were reduced by a third.

### 3.3.9. Immunocytochemistry

Cultured primary hippocampal neurons or human iNs were fixed with 4 % (w/v) PFA and 4 % (w/v) sucrose for 15 min on ice and washed three times with PBS. To stain for intracellular proteins fixed neurons were blocked and permeabilized for 1 h with 10 % (v/v) NGS and 0.3 % (v/v) Triton-X 100 in PBS at RT. Primary antibody (Table 3.9.) was diluted in 5% (v/v) NGS and 0.03 % (v/v) Triton-X 100 in PBS, centrifuged at 17000g for 10 minutes before use, applied on the coverslips and incubated for 1 h at room temperature. Cells were washed three times with PBS to remove unbound antibody and bound antibody was decorated with corresponding secondary antibodies (Table 3.10.) for 45 minutes as described above. Neurons were washed three times with 1X PBS and mounted in Immu-Mount (Thermo Fisher) mounting solution on microscopy slides. To visualize DNA containing nuclei, 1 µg/ml DAPI (4'-6-diamidino-2-phenylindole, Sigma) was introduced in the second wash in 1X PBS. Immunofluorescent stainings of HEK 293T or HeLa cells were performed as described for neuronal cultures. In case of the stainings for STED microscopy, appropriate secondary antibodies were used in 1:200 dilution and prolong Gold Antifade (Invitrogen) was used as a mounting solution.

## Materials and Methods

---

### 3.4. Microscopy and Image Analysis

#### 3.4.1. Confocal microscopy

All fixed and immunofluorescently stained cell cultures were imaged at a resolution of 1,024 × 1,024 on a Zeiss laser scanning confocal microscope LSM710 controlled by Zeiss software and equipped with Plan-Apochromat x63 NA 1.40 oil DIC and EC Plan-Neofluar x40 NA1.30 Oil DIC objectives.

All acquisition settings were set equally for all groups within each immunostaining. Image processing and quantitative analysis was performed in ImageJ. For quantitative analysis of fluorescent intensities in the soma, the total area of the soma was manually selected and measured using ImageJ selection tools. For quantitative analysis of fluorescent intensities in the synaptic regions, average intensities of fluorescent puncta (synapses) were measured by centering 9 × 9 pixel (~1 × 1 μm) regions on maxima determined by ImageJ processing function. Sites of synapses were determined via colocalization of postsynaptic (Homer1 or PSD95) and presynaptic (Synaptophysin or Bassoon) regions in traced neurites, as described previously (Mata et al., 2016).

#### 3.4.2. Spinning disc confocal microscopy and analysis of axonal transport dynamics

For live-cell imaging experiments, a spinning disc confocal microscope (CSU-X1, Nikon) equipped with a Plan Apo VC x60 NA 1.40 oil objective was used. Image processing and quantitative analysis was performed in ImageJ.

Developing iNs (day 12-14) or mouse primary hippocampal neurons (DIV 6-8) were grown on 25mm coverslips. Before imaging, 1X imaging buffer (Table 3.2.) was prepared and osmolarity was equilibrated to the medium levels. Coverslips mounted in a metal ring and supplemented in the imaging medium were imaged in an incubation chamber that maintains optimal temperature and CO<sub>2</sub> (37 °C and 5% CO<sub>2</sub>). To visualize proteins with a specific fluorescent tag for single-color acquisition, a laser channel was exposed for 100–200 ms while for dual-color acquisition, different laser channels were exposed for 100–200 ms sequentially, by using a Quad filter which enabled swift switch between channels. Neurons were imaged

## Materials and Methods

---

every 200 to 300 ms for 120 or 300 s depending on the specific experiment. To identify the axon, neurons were pre-incubated with a CF640R-conjugated antibody against the AIS protein neurofascin (NF-640R) for 30 min before live-cell imaging. Regions of interests (ROI)s containing at least 50  $\mu\text{m}$  of axon length were chosen for imaging. Areas of axons proximal to the axonal initial segment (AIS) were preferentially chosen for analysis.

Live imaging data obtained from neurons were exported as .tiff files for further analysis using ImageJ plug-in Kymotoolbox (Zala et al., 2013). A line was drawn spanning the middle of the respective image and a kymograph was generated. Kymographs from each channel were saved under separate folders named C1 and C2, and the images were processed using an ImageJ plug-in DualChannelKymoAnalysis (Schmied, C. unpublished). This plug-in first used KymoButler kymograph analysis tool which identified tracks of individual vesicles on each kymograph and calculated the speed, pause duration and directionality of vesicles, then analysed all vesicle transport data by identifying each individual transport event with their corresponding speed and directionality information and filtering out stationary events, and finally highlighted co-anterograde or retrograde transport events on the original kymographs belonging to each channel (C1 and C2).

### 3.4.4. pHluorin live-cell imaging

In order to monitor SV exo- and endocytosis, a green fluorescent protein (GFP) variant named pHluorin, which is fused to the luminal domain of synaptic vesicle proteins, was used. pHluorin was genetically modified to have a higher pH sensitivity with a pKa of 7.1, providing pHluorin molecules with the ability to be protonated at low pH, and this results in quenching of their fluorescence (Miesenbock et al., 1998). SVs acidify by the vATPase generating a proton gradient for neurotransmitter uptake. Upon expression of pHluorin tagged SV proteins in neurons, all pHluorins tagged SV proteins residing on SVs will be in a quenched state, whereas surface-stranded SV proteins with a pHluorin tag will be fluorescent. Upon depolarization, SVs will fuse with the plasma membrane, which will expose the luminal pHluorin to the extracellular solution with a neutral pH and thus will become un-quenched. This method provides real-time observation of the SV release by an increase of fluorescence and the subsequent SV endocytosis during which SVs are re-acidified and the fluorescent signal is re-quenched (Figure 10).

## Materials and Methods

---

Human iNs were transfected on day 28 as described in section 3.3.8 with pHluorin constructs and imaged on day 33-34 in physiological imaging buffer at room temperature. The coverslips were assembled in a stimulation chamber with two lateral electrodes (RC-47FSLP, Warner Instruments) connected to a stimulator (MultiStim SYSTEM-D330, Harvard Apparatus) providing electrical field stimulation of neurons at 100 mA and varying frequency and duration. Postsynaptic NMDA and AMPA receptors were inhibited by 50  $\mu$ M APV (Abcam) and 10  $\mu$ M CNQX (Sigma) to prevent action potential propagation. Images were acquired with 0.5 Hz frame rate with the epifluorescent microscopes. 30 to 50 responding boutons per recording were selected as regions of interest (ROI) and analyzed with the ImageJ plugin 'Time Series Analyzer' (RRID:SCR\_014269). The mean fluorescent intensities of responding boutons were background corrected. To compare the apparent release of SVs the mean fluorescent intensities (F) were normalized to their initial fluorescence (F<sub>0</sub>) prior to electrical stimulation, and F/F<sub>0</sub> traces were plotted. The endocytic retrieval was analyzed by normalizing the fluorescent time courses subtracted by F<sub>0</sub> (obtaining  $\Delta$ F) to their maximum peak fluorescence.  $\Delta$ F/F curves were plotted and the endocytic time constant  $\tau$  was determined by fitting a monoexponential decay curve using Prism (Graphpad) software.

### 3.5. Biochemical Methods

#### 3.5.1. Protein preparation from cells

Confluent cells were briefly washed with PBS on ice and harvested in 100  $\mu$ l 1X lysis buffer for one well of a 6-well dish. After the lysates were collected with a cell scraper, they were centrifuged at 17,000 x g for 20 min at 4 °C to remove cell debris. Soluble proteins were diluted in SDS sample buffer and stored at -20 °C.

#### 3.5.2. Determining protein concentration in cell lysates

Protein concentrations in cell lysates were determined using the Pierce™ BCA Protein Assay Kit (Thermo Fisher) according to manufacturer's instructions. In short, 2  $\mu$ l of cell lysate was mixed with 23  $\mu$ l ddH<sub>2</sub>O and 200  $\mu$ l of the kit's reagent mix (reagent A : reagent B, 50:1) in a 96-well plate. BSA solutions with a total protein content ranging from 2  $\mu$ g to 0  $\mu$ g were used

## Materials and Methods

---

as a standard curve and also mixed with reagent A and B. After preparing all samples, the 96-well plate was spin-down, top part was covered with Parafilm and the plate was incubated at 37 °C for 30 min. After incubation, absorbance was measured using a plate reader at 562 nm wavelength.

### 3.5.3. Immunoprecipitation using magnetic nanobeads

Cells (either HEK 293Ts or developing iNs) were plated on Matrigel™-coated 10cm dishes. When cells were already transduced with lentiviral constructs prior to the experiment, IP experiment was started 24 hours after plating the cells. When cells were to be transfected, they were transfected with appropriate plasmids using JetPrime transfection method (see 3.3.7) and IP experiment was held 24 hours after transfection.

Plates were washed twice with ice-cold 1X PBS. 1ml of IP lysis buffer (0,05% saponin, 20mM HEPES pH7,4, 130mM NaCl, 10mM NaF, Protease Inhibitor) was added per plate, lysates were scraped into a tube and were centrifuged for 10 minutes at 10 000xg at 4°C. Soluble fraction of the lysate was kept and pellet was discarded. 75µl of lysate were transferred into a clean tube and mixed with 25ul of 4x SDS-buffer to be used as the input on WB. Rest of the supernatant was mixed with 15 ul of previously washed GFP- or RFP-trap Magnetic Agarose beads (ChromoTek) and the mix was incubated for 3h at 4°C on a rotator. Beads were then washed 3-5 times in lysis buffer on a magnetic stand and were eluted in 25 ul of 2x SDS sample buffer.

### 3.5.4. Expression of recombinant proteins in E.coli

*E. coli* BL21 strain was transformed with pET28a or pGEX6P-1 plasmid, and a small scale culture of 10 ml of were grown overnight at 37 °C with the respective antibiotics. The following day the overnight culture was transferred into 500 ml of 2x YT protein expression medium with appropriate antibiotics and grown at 37 °C at 180 rpm until an optical density OD600 of 0.6 was approximately reached. Protein expression was induced with 0.5 mM isopropyl thiogalactoside (IPTG). Bacteria were incubated at 20 °C or 16 °C (depending on the fusion protein) for 16 hours before they were harvested at 4 °C with 4000 x g for 20 min. The bacterial

## Materials and Methods

---

pellets were resuspended in HBS buffer (50mM Hepes pH7.5, 150mM NaCl), aliquoted and stored at -20 °C.

### 3.5.5. Affinity-purification of GST-fusion proteins

The HBS-suspension of bacterial cells overexpressing the GST-fused protein (see 3.5.4) was supplemented with 1 mM phenylmethylsulfonyl fluoride (PMSF), 1mM MgCl<sub>2</sub>, 0.3 ul/ml cyanase (DNase), 1mM EDTA, 2mM DTT, 1 tabled of PIC (Roche, cOmplete™, Mini Protease Inhibitor Cocktail) per 50ml of HBS solution, 1% (v/v) Triton-x-100 and 1mg/ml of T4 lysozyme was added to degrade bacterial cell walls and remove nucleic acids.

After 15 min incubation on ice, the cells were crack opened by sonification (total 2min at 70% power, pulse on 1s, pulse off 5s) and the tube was placed on a rotator to allow for cell lysis for another 15 min at 4 °C. Cell debris was sedimented by centrifugation at 35,000 x g for 20 min at 4 °C. The bacterial supernatant was then transferred to clean tubes containing 500µl 50% prewashed GST-binding resin slurry (Novagen, glutathione coupled beads) and incubated on a rotation wheel at 4°C for 2h. After the incubation, the beads were run through an open column which was previously washed with the HBS buffer, and were washed three times before they were eluted in 2ml of HBS buffer containing 30 mM reduced glutathione (pH 7.5). The concentration on the eluted protein was measured by Bradford assay. The eluted protein was loaded on a SDS-PAGE gel and subsequently Coomassie stained in order to verify the correct size of the recombinant protein as well as the grade of degradation.

### 3.5.6. Liposome sedimentation assay

To identify which phosphoinositides interact with the purified PH domain of KIF1A, liposomes of different compositions were prepared. All liposomes contained 60-70% DOPC (1,2-dioleoyl-sn-glycero-3-phosphocholine), 20% DOPE (1,2-dioleoyl-sn-glycero-3-phosphoethanolamine) and 10% Cholesterol. Amounts of components needed for each liposome sample were calculated (Table 3.15).

## Materials and Methods

---

**Table 3.15.** Liposome compositions for sedimentation assay

% lipid	lipid	MW	stock mg/ml	stock (mM)	umole	volume (μL)
70 (no PI)- 60	DOPC	786.15	10	12.7202	1.2	94.338
20	DOPE	744.03	10	13.4402	0.4	29.76136
10	Cholesterol	386.66	10	25.8625	0.2	7.7332
10	PI(3)P	977.147	1	1.0234	0.2	195.4294
10	PI(3,5)P <sub>2</sub>	1074.16	1	0.9310	0.2	214.8316
10	PI(4,5)P <sub>2</sub>	1096.39	1	0.9121	0.2	219.277

All components were pipetted using glass syringes and glass tubes under the fume hood. The glass tubes were placed in a desiccator. After 30 minutes, stop the vacuum and tubes were left overnight for drying. Next morning a lipid film formed around the glass tubes. Using a long tip, 125 μl of lipid buffer (20 mM Hepes pH 7.4, 150 mM NaCl) was added and film was dissolved by vortexing vigorously and incubating the tubes at 70°C for 5-10 min to better dissolve the film if needed. Next, another 125 μl of lipid buffer was added for a total of 250 μl. To prevent formation of giant liposomes and obtain more uniform liposomes, liposome solutions were sonicated on a waterbath sonicator (5 times for pulse on 40 sec, pulse off 1 min). Vesicles were then aliquoted in PCR tubes (20 μl) and snap-frozen in liquid N for later use.

20 μl of liposomes were transferred into plastic tubes (S100AT3-360) and were mixed with the same volume of protein (2 μg of protein was used per sample). Liposome-protein mixtures were incubated for 30 minutes at RT and ultracentrifuge at 70.000xg for 15 minutes at RT. Supernatant (SN) contained the not-interacting fraction of proteins whereas pellet (P) contained the fraction of proteins interacted with liposomes. SN (approximately 40 μL) was transferred into a clean eppendorf tube and mixed with 4x sample buffer. Pellet fraction was resuspended with the same volume of lipid buffer and subsequently mixed with 4x sample buffer. All samples were then incubated at 95°C for 5 min, spun down and stored at -20°C.

## Materials and Methods

---

### 3.5.6. SDS polyacrylamide gel electrophoresis (SDS-PAGE)

Sodium dodecylsulfate polyacrylamide gel electrophoresis (SDS-PAGE), a widely used technique for separating proteins according to their electrophoretic mobility, which correlates with their sizes, was performed in order to separate proteins according to their molecular weight. The separating gels can be casted at different concentrations in order to analyze proteins of varying molecular masses. The stacking gel was cast using 3% acrylamide, whereas the separating gel was contained 8-14% acrylamide, depending on the experiment. Ammonium persulfate (APS) and N,N,N',N'-tetramethylethylenediamine (TEMED) were added shortly before usage to start polymerization of the gel matrix. Isopropanol was added on top of the separation gel layer to ensure a smooth interface between the gels, and removed before adding the stacking gel. After protein samples were mixed with 4x sample buffer containing 10%  $\beta$ -Mercaptoethanol, they were denatured by boiling at 95°C for 5 minutes, spun down and loaded onto the SDS-gel. The samples and the molecular marker (ladder) were run at 80 – 100 V in 1xSDS-PAGE running buffer and then further processed either for Western Blot (WB) experiments or Coomassie blue protein staining.

**Table 3.16.** Composition of SDS Polyacrylamide Gels

Components	Separation gel 12 %	Separation gel 10 %	Separation gel 8 %	Stacking gel 3 %
30 % AA/BA mix	3 ml	2.5 ml	2 ml	0.33 ml
Ultrapure water	2.5 ml	3 ml	3.5 ml	1.625 ml
4x stacking or separation buffer	1.875 ml	1.875 ml	1.875 ml	0.625 ml
10 % (w/v) APS	75 $\mu$ l	75 $\mu$ l	75 $\mu$ l	37.5 $\mu$ l
TEMED	7.5 $\mu$ l	7.5 $\mu$ l	7.5 $\mu$ l	3.75 $\mu$ l

## Materials and Methods

---

### 3.5.7. Immunoblotting (Western Blot)

Immunoblotting method was performed to detect specific proteins after their size-separation by SDS-PAGE. Negatively charged proteins were transferred from the polyacrylamide gel to a nitrocellulose membrane (GE Healthcare, Amersham Protran 0.2 NC) using an electric field and blotting chambers (BioRad). Two blotting sponges, blotting papers (Whatmann paper), the nitrocellulose membrane and the polyacrylamide gel containing proteins were assembled in a protein transfer cassette after soaking in blotting buffer. Air bubbles were removed thoroughly during the assembly. Proteins were transferred at 110V for 90 min at 4 °C using the wet blotting system.

After the transfer, membranes were stained reversibly with ponceau stain for 10 minutes at RT followed by short washes with ponceau destain solution to assess the protein transfer and equal protein loading. After the Ponceau was completely destained, membrane was blocked with Odyssey blocking buffer (Blotto, LI-COR) diluted 1:1 in TBS for 1 h at RT, following its incubation with primary antibody dilution solution in Odyssey blocking buffer overnight at 4 °C. Next day membranes were washed three times in 1x TBS containing 0.05 % (v/v) Tween-20 at RT. The primary antibody solution was recycled and fluorescently conjugated secondary antibodies (IRDye 800CW, LI-COR) were incubated in Odyssey blocking buffer for 1 hour at RT. After the membrane was washed in 1x TBS, protein levels on the membrane were detected with the LI-COR Odyssey Fc Imaging system.

### 3.5.8. Coomassie staining of SDS-polyacrylamide gels

If polyacrylamide gels were not subjected to immunoblotting they were stained with Coomassie stain for 10 minutes at RT. Unspecific background staining was removed with repeated coomassie destain washes overnight at RT.

## Materials and Methods

---

### 3.5.9. PIP-strip

PIP-strip membranes, purchased from Echelon Biosciences (Salt Lake City, UT), were blocked in 5 ml TBS-T with 3% BSA for 1 h at room temperature with gentle shaking ~100 rpm. After decanting off the blocking buffer, membrane was incubated with 0.5 µg/ml of purified GST-PH-PH (KIF1A) domain for 3h at room temperature. Blot was washed with 10 ml of TBS-T for 10 minutes three times. Afterwards blot was incubated with GST antibody at 4 °C overnight. Next day, blot was washed again three times with TBS-T and incubated with an HRP-coupled secondary antibody for 1h. After three more washes with TBS-T, ECL substrate with chemiluminescent detection was used to detect the bound protein. 1 ml of ECL solution was added on the membrane, incubated for 1 min and then chemiluminescent detection was used.

### 3.5.10. Mass Spectrometry analysis of the immunoprecipitation experiment

The protein eluates from Arl8b-mCherry or KIF1A-EGFP immunoprecipitation experiments in developing iNs were prepared for mass spectrometry analysis: Dithiothreitol (DTT) was added to the samples (pH 8) to a final concentration of 5 mM, incubated at 55°C for 30 minutes. After samples cooled down, Chloroacetamide (CAA) was added to a final concentration of 40 mM, incubated in the dark for 30 min at RT. After the samples were alkylated, they were loaded on an SDS-gel and run for only 1-1,5 cm and visualized by Coomassie staining. Coomassie was destained overnight and samples were further processed at the FMP Mass Spectrometry Facility for MS/MS analysis. Each experiment consisted of two lanes on the acrylamide gel corresponding to negative controls (GFP- virus expression in KIF1A IP and mCherry- virus expression in Arl8b IP) and IP samples.

### 4. Results

#### 4.1. Human induced pluripotent stem (iPS) cell-derived neurons (iNs) as a model system to study presynaptic biogenesis

##### 4.1.1. Human iPSCs can be efficiently differentiated into excitatory cortical neurons

As a model system to study presynaptic biogenesis, I established and optimized a previously described single-step differentiation protocol that generates excitatory cortical neurons from human iPSCs (Zhang et al., 2013). The iPSC line, provided by the MDC Stem Cell Facility, contains a Neurogenin-2 (Ngn2) expression cassette under a Doxycycline (Dox)-inducible promoter at their safe harbor locus. Thus, upon Dox treatment, forced expression of Ngn2 induces direct reprogramming of the stem cells into neuronal lineage (**Figure 4.1.a and b**). The Ngn2 cassette also encodes for the enhanced green fluorescent protein (eGFP) followed by a nuclear localisation signal (NLS) and puromycin resistance cassette to allow for their detection and selection, respectively. The day after cell seeding (Day 0), Ngn2 expression is induced by Dox treatment. At day 2, puromycin selection is performed. The following day, primary mouse glia are co-seeded with the differentiating iPSCs to support neuronal cell growth. Dox is kept in the media until day 10 to ensure that the neuronal differentiation cassette remains active, afterwards the media is replaced with growth medium containing fetal bovine serum (FBS) and consequently cells gradually lose their nuclear GFP signal. As shown in bright field microscopy images, from day two on iNs show extended neurite formations and at day 10 they gain neuronal morphology as indicated by smaller cell bodies and axon and dendrite processes (**Figure 4.1.C**).

## Results

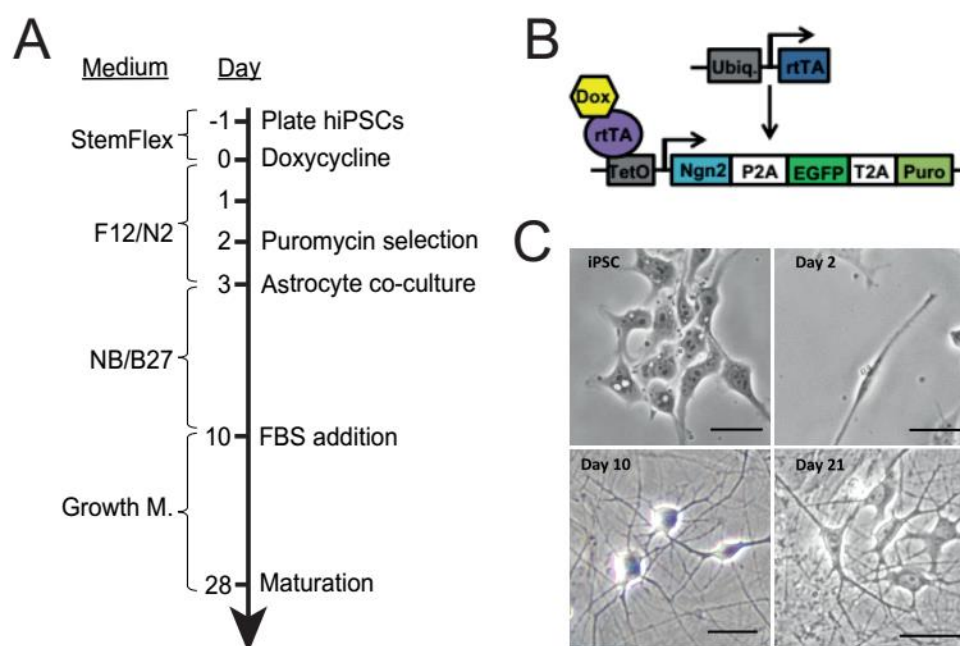


**Figure 4.1. Excitatory cortical neurons are generated from human iPSCs.** (A) Timeline for neuronal differentiation. Expression of the Ngn2 cassette is activated at day 0 by Dox treatment. Astrocyte cultures are prepared from mouse cortices at P0 or P1 and added to the differentiating iNs at day 3 to support neuronal growth and survival. Neurons are in the development stage until day 21 and are mature at day 28. (B) Expression constructs used for neuronal differentiation (adapted from (Zhang et al., 2013)). Both cassettes are placed in the safe harbor locus of the WT iPS cell line. Dox binds to rtTA and enables gene transcription by activating the tetracycline response element (TetO). Starting from day 1, cells with transcription activation show nuclear eGFP expression. On day 2 cells that fail to activate the Ngn2 cassette are discarded with puromycin selection. (C) Bright field images of human iPSCs and iPSC-derived iNs at day 2, 10 and 21 during neuronal differentiation. Scale bars, 50  $\mu$ m.

### 4.1.2. Characterization of developing and mature iNs

Differentiating iNs start expressing neuronal markers MAP2,  $\beta$ -3 Tubulin (TUJ1) and NeuN as well as presynaptic markers Synaptotagmin 1 (Syt1), Synaptophysin (Syp), Synapsin 1 among others as early as day 6 and their expression increases over the time of differentiation process. Expression of postsynaptic proteins starts later at day 21, and similar to presynaptic markers, increases over time (**Figure 4.2**). Despite the fact that differentiating iNs can be kept in the culture longer than 60 days, we searched for an optimal time point to study presynaptic biogenesis on this system. We determined days 12-15 as the presynaptic development time interval since at this time of differentiation iNs express presynaptic proteins but not yet

## Results

postsynaptic ones. We assumed the maturity stage as day 28 and after since iNs express high amounts of pre- and postsynaptic markers from this timepoint on.

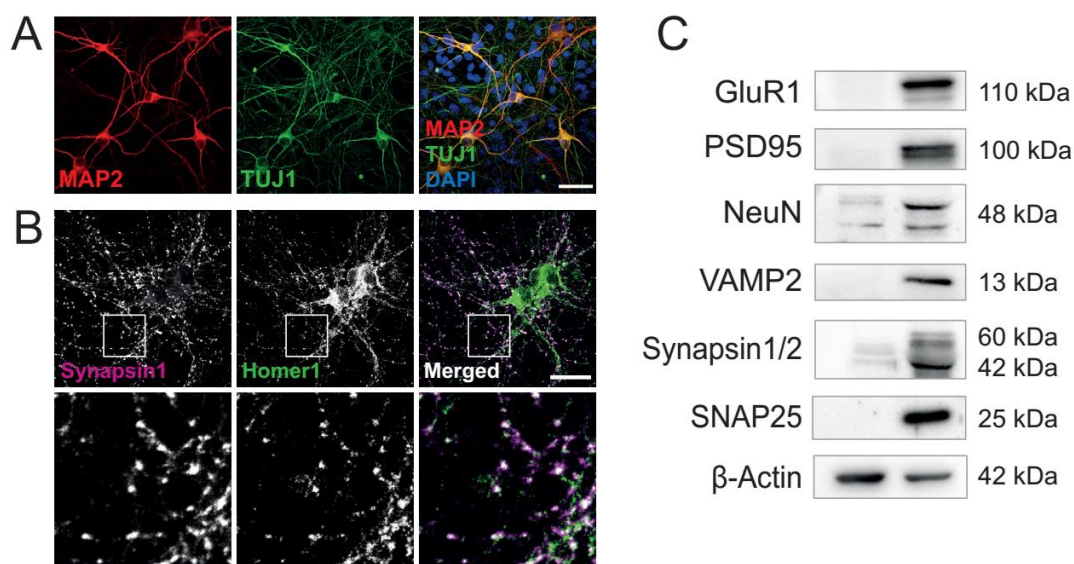


**Figure 4.2. Human iNs express neuronal markers and form pre- and postsynaptic specializations.** Human iPSC-derived cortical neurons were analyzed at 28 days after initiation of neuronal differentiation for expression of neuronal markers. (A) Expression of neuronal markers TUJ1 ( $\beta$ 3 Tubulin) and MAP2 was analyzed using immunofluorescence microscopy. Cell nuclei were counterstained with DAPI. Scale bar, 50  $\mu$ m. (B) Expression of the presynaptic Synapsin 1 the postsynaptic Homer 1 were analyzed using immunofluorescence microscopy. Lower panel demonstrates high magnifications of selected areas. Colocalization of both markers represent mature synapses. Scale bar, 30  $\mu$ m. (C) Expression of the neuronal marker NeuN, presynaptic markers VAMP2, Synapsin 1/2, SNAP25 and postsynaptic markers GluR1 and PSD95 were analyzed using comparative Western Blot analysis of the non-differentiated human iPSCs and iNs at day28.  $\beta$ -Actin served as loading control. Molecular weights are indicated on the right side of the blot in kilodaltons (kDa).

## Results

After confirming the pre- and postsynaptic protein expression on the established iN system, I continued the characterization of iNs by determining their presynaptic activity using pHluorin live imaging to monitor exo- and endocytosis of SVs upon different stimulations (**Figure 4.3**). In the Syp-pHluorin construct, pHluorin tag is fused to the luminal domain of the SV protein Syp. When this construct is expressed in neurons, pHluorin is quenched since within the SVs pH is at pH 5.5. Upon stimulation SVs fuse with the plasma membrane and pHluorin is unquenched at the neutral pH (7.4) of the extracellular medium, resulting in an increase in fluorescence. Fluorescence level then decreases after endocytic retrieval and re-acidification of internalized membranes. I transfected iNs with Syp-pHluorin construct on day 28 and analyzed the kinetics of the SV protein Syp exo-/ endocytosis in response to stimulations on day 32 at the following frequencies respectively: 40APs at 10 Hz, 100APs at 20 Hz and 200 APs at 40 Hz.

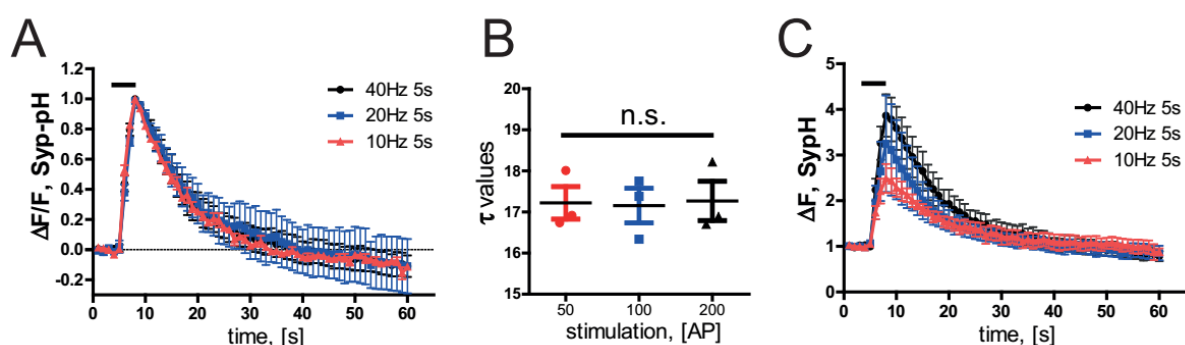


**Figure 4.3. pHluorin exo-endocytosis in iNs at DIV 28 at room temperature.** (A) Time course of Syp-pHluorin endocytosis/reacidification in response to 200 APs (40 Hz, 5s), 100 APs (20 Hz, 5s) or 50APs (10 Hz, 5s). (B) Endocytic time constants ( $\tau$ ) remain significantly unaltered between different stimulation conditions. (C) Time course of Syp-pHluorin exocytosis rates in response to 200 APs (40 Hz, 5s), 100 APs (20 Hz, 5s) or 50APs (10 Hz, 5s). Data represent mean  $\pm$  SEM.

## Results

---

### 4.2. Different components of the presynaptic compartment are co-transported along the axons of developing iNs to the nascent presynapse

There has been long debate on whether different components of the presynapse, such as presynaptic adhesion proteins, synaptic vesicle (SV) proteins, proteins of the active zone (AZ) or voltage-gated calcium channels (CaVs) are transported along the axons of developing neurons via independent mechanisms or they are present on the same organelles and are co-trafficked to axon terminals. To address this question, live imaging experiments using spinning disc confocal microscopy were conducted. Developing iNs were transfected with constructs expressing SV proteins, AZ proteins or sCAMs fused with different fluorophore tags and imaged 24 hours after transfection. Using a two-channel imaging system, anterogradely or retrogradely trafficking organelles as well as the stationary ones were recorded. Using an ImageJ plugin (KymoToolbox), movements that were detected in the imaged axon fragments were translated into kymographs (**Figure 4.4.a**). Kymographs contained the time-, distance- and direction-information of all transported vesicles. The number of transport or co-transport events were detected using KymoButler, a deep-learning based kymograph analysis tool. A KymoButler sorter script (KymoFilter) was used to document all transport events and filter them depending on their directionality and speed. Finally, a Fiji script (DrawTraces) traced all co-transport events back onto original kymographs for confirmation of the analysis. These three scripts are combined to a single ImageJ plugin (DualChannelKymoAnalysis). This way, kymographs of various protein pairs were analyzed in an unbiased manner. (**Figure 4.4.a**).

## Results

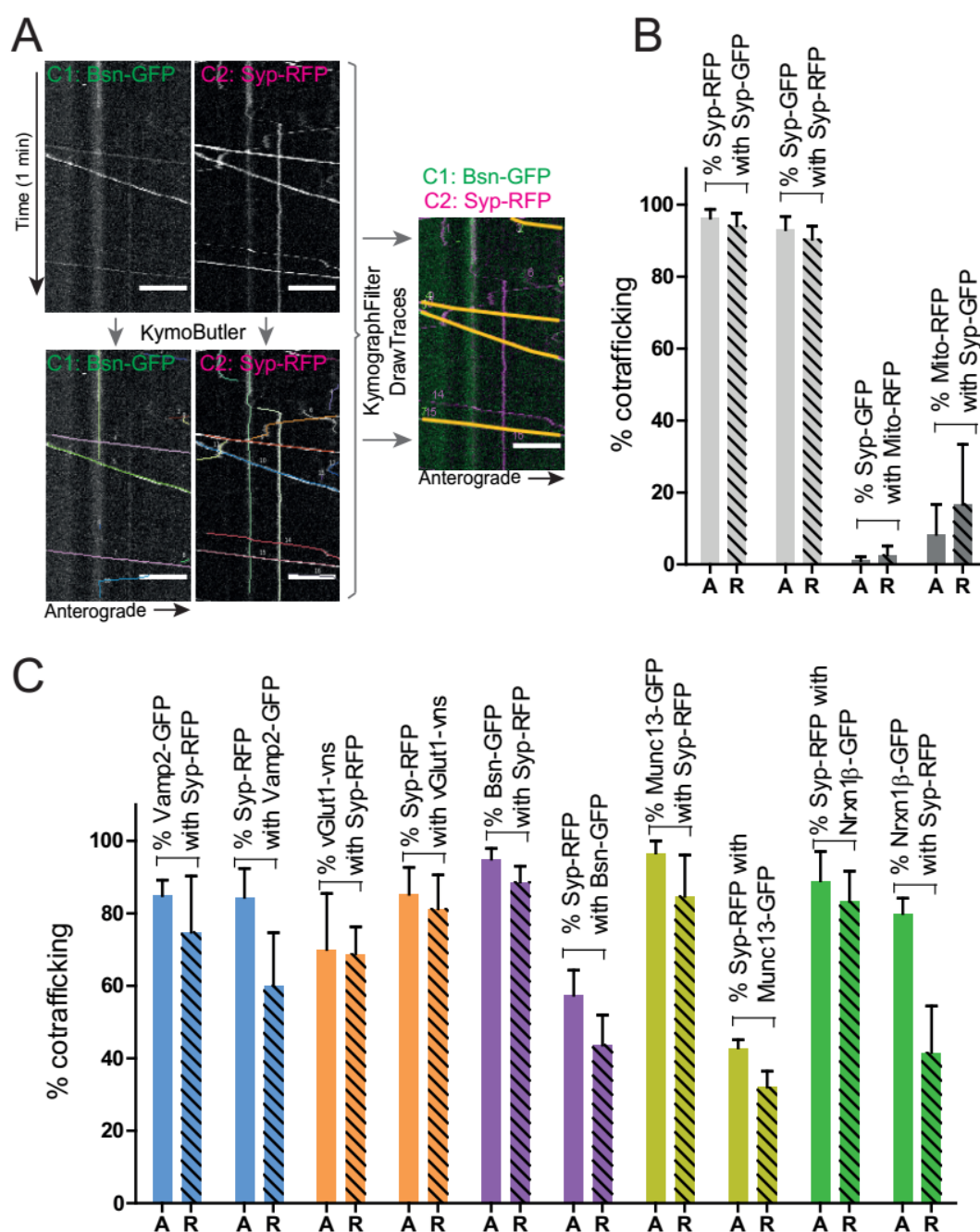


**Figure 4.4. Axonal co-transport levels of presynaptic proteins in developing iNs.** (A) Representative flowchart of two-channel live imaging strategy and used scripts and plugins for automated kymograph analysis. iNs are co-transfected with Bsn-GFP and Syp-RFP expression plasmids at day 12-13 and imaged one day after. X axis of kymographs represent a total distance of 30  $\mu$ m with anterograde transport towards the right hand side and the y axis show 1 minute time interval (Top: t = 0, bottom: t = 60 sec). (Scalebar, 10  $\mu$ m.) Kymobutler detects and highlights individual transport events detected in each channel. KymographFilter script documents all events and filters anterograde, retrograde or stationary events. DrawTraces plugin highlights co-antegradely or co-retrogradely transported vesicles on the original kymographs. (B) Positive and negative controls for two-channel live imaging. (%Syp-RFP with Syp-GFP A:  $96.26 \pm 2.444\%$ , R:  $94.16 \pm 3.392\%$ , %Syp-GFP with Mito-RFP A:

## Results

---

1.077 $\pm$  1.077%, R: 2.563%  $\pm$  2.563%). (C) Co-antero- or retrograde transport between Syp-RFP and indicated SV (Vamp2 and vGlut1), AZ (Bsn and Munc13-1) and presynaptic adhesion (Nrnx1 $\beta$ ) proteins. (%Vamp2-GFP with Syp-RFP A: 84.91  $\pm$  4.276%, R: 74.81  $\pm$  15.47%, %Syp-RFP with Vamp2-GFP A: 84.45  $\pm$  7.944%, R: 60.10%  $\pm$  14.54%; %vGlut-venus with Syp-RFP A: 70.03  $\pm$  15.42%, R: 68.89  $\pm$  7.396%, %Syp-RFP with %vGlut-venus A: 85.29  $\pm$  7.442%, R: 81.22%  $\pm$  9.394%; %Bsn-GFP with Syp-RFP A: 95.00  $\pm$  2.887%, R: 88.69  $\pm$  4.325%, %Syp-RFP with Bsn-GFP A: 57.38  $\pm$  6.915%, R: 43.66%  $\pm$  8.310%; %Munc13-GFP with Syp-RFP A: 96.67  $\pm$  3.333%, R: 84.72  $\pm$  11.37%, %Syp-RFP with Munc13-GFP A: 42.92  $\pm$  2.153%, R: 32.08%  $\pm$  4.350%; %Nrnx1 $\beta$ -GFP with Syp-RFP A: 88.99  $\pm$  8.091%, R: 83.33  $\pm$  8.333%, %Syp-RFP with Nrnx1 $\beta$ -GFP A: 79.92  $\pm$  4.273%, R: 41.67%  $\pm$  12.73%. (B and C) Data represent mean  $\pm$  SEM, n=3 independent experiments from at least 3 replicates with  $\geq$  8 videos per experiment. A: Anterograde, R: retrograde.

To rule out the introduction of transport-artefacts due to overexpression of fluorophore tagged proteins, I applied a positive control sample where the same protein (Syp) is expressed being fused to two different fluorophore tags and imaged in two different channels. Analysis of vesicle trafficking resulted in almost 100% co-transport of these proteins (**Figure 4.4.b**). Similarly, to rule out crosstalk of fluorescence emissions between two channels, I applied a negative control experiment. Co-expressing a SV protein (Syp-GFP) with a mitochondrial protein (Mito-RFP) showed almost no co-transport events. Additionally, when kymographs were generated from one channel, no crosstalk was observed in the second channel, and vice versa. Additionally, when plotting the co-transport rates I calculated the percent of co-transporting vesicles for each of the two proteins analyzed. This approach prevented missing out on any important data. For instance, only 1% of Syp-GFP containing vesicles co-traffic with Mito-RFP, however 5% of Mito-RFP organelles co-traffic with Syp-GFP. The difference in numbers originates from differences in the total number of organelles: in the specified case, there are many more Syp-GFP organelles in axons than Mito-RFP organelles. This difference should be taken into consideration especially when expressing two proteins that differ greatly in their copy numbers, such as SV and AZ proteins.

After verification of the functionality of the read-out, each of the proteins of interest were co-expressed with Syp and the level of co-trafficking between each pair was analyzed (**Figure 4.4.c**). As expected, SV proteins vGlut1 or VAMP2 showed a very high degree of co-transport with Syp. In both cases, more than 70% of the protein pairs were anterogradely co-transported. Analysis of the AZ proteins Bassoon and Munc13 also yielded high level of co-transport with Syp. Almost all vesicles positive for Munc13 or Bassoon were co-transported with Syp (more than 95% in each case), whereas only about half of all Syp vesicles in the

## Results

---

axon were also positive for Bsn or Munc13 (57% and 43%, respectively). This difference in cotransport rates possibly originates from the differences in copy numbers of these proteins: AZ proteins Bassoon and Munc13 are expressed at lower levels compared to SV proteins such as Syp. The presynaptic adhesion protein Neurexin 1 $\beta$  also displayed high levels of cotransport level with Syp. These data suggest that in iNs presynaptic precursor vesicles (PVs) carry not only SV and AZ proteins to presynaptic sites but also sCAMs.

While live imaging of developing axons is a powerful technique to study axonal transport, it is conceivable that over-expressing proteins of interest might not reflect the physiological conditions in neurons due to the expressed copy number of proteins being much higher than that of endogenous proteins. To overcome this problem, I generated an iPSC cell line with a targeted insertion of eGFP at the C terminus of the SV protein Syp. For targeted insertion of the eGFP tag, I used a Crispr/Cas9 knock-in (KI) approach. I designed a guide RNA which targets the stop codon of *SYP* gene and cloned it in a plasmid expressing Cas9. Additionally I designed homology regions at the upstream and downstream of the nucleotide to be targeted for the eGFP fusion. I transfected the iPSCs with both constructs, sorted the transfected cells and selected single colonies. Successfully generated KI cells containing the eGFP in both alleles were identified by PCR, and validated by immunostaining (**Figure 4.5**). Use of differentiated Syp-eGFP KI iNs in live imaging experiments and immunostainings avoids using over-expression of constructs and thus potential artefacts arising from it.

## Results

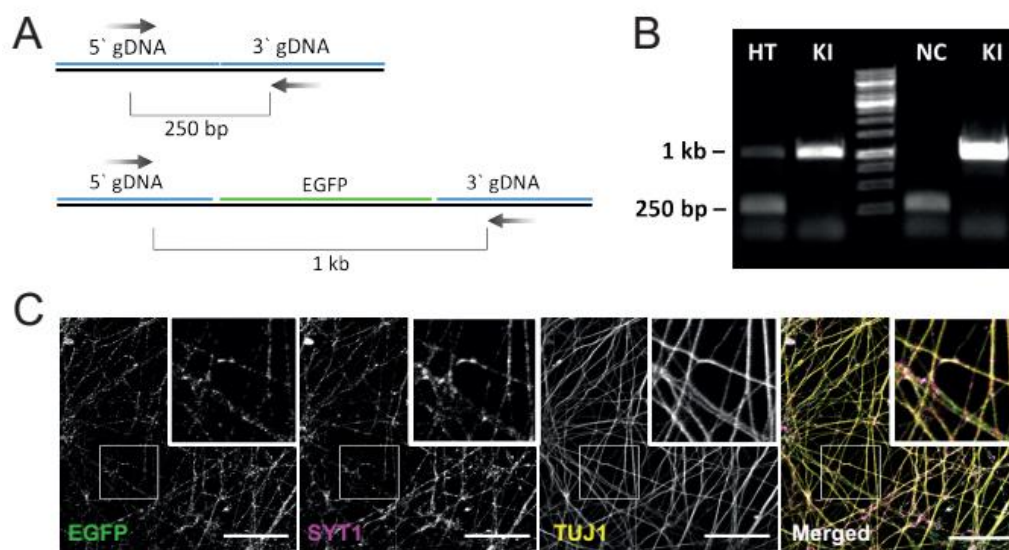


**Figure 4.5. Endogenously labelled Syp-eGFP iPSCs are generated using Crispr/Cas9.** (A) Genomic DNA was isolated from expanded clones and the region spanning the nucleotides targeted by Cas9 was amplified by PCR. Scheme shows predicted sizes of DNA bands to be amplified in WT (top) and Syp-GFP (bottom) cells. (B) Agarose gel showing WT, heterozygous KI and homozygous KI clones. HT: Heterozygous, KI: full knock-in clones, NC: negative control (WT). (C) Expression of eGFP-tagged endogenous Syp was confirmed by co-immunostaining with GFP antibody and Syp antibody. Scale bar, 10 μm.

After generation of endogenous Syp-eGFP KI iPSCs, I transfected developing iNs with plasmids encoding SV or AZ proteins to quantify the fraction of co-transport with endogenous Syp-vesicles. Since fluorescence signals of endogenous Syp are weaker than those of overexpressed proteins, I avoided expressing the second protein in the RFP (568) channel due to potential crosstalk between the two channels. Hence, the second protein of interest was always imaged in the iRFP (647) channel.

## Results

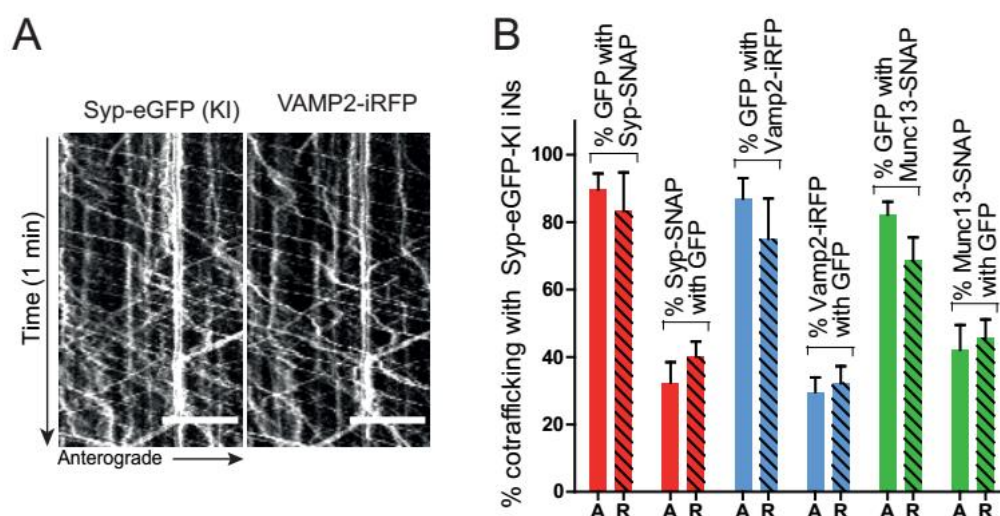


**Figure 4.6. Axonal co-transport levels of endogenous Syp-eGFP with presynaptic proteins in developing iNs.** (A) Representative kymographs showing transport of endogenous Syp-eGFP vesicles with VAMP2-iRFP. X axis shows distance, with right hand side pointing towards anterograde direction, y axis represents time (1 min). (Scale bar, 10  $\mu$ m). (B) Graph shows quantification of kymographs. Co-antero- or retrograde transport between Syp-eGFP (KI) and indicated SV (Syp and Vamp2) and AZ (Munc13-1) proteins. (%GFP with Syp-SNAP A: 89.72  $\pm$  4.722%, R: 83.33  $\pm$  11.39%, %Syp-SNAP with GFP A: 32.35  $\pm$  6.131%, R: 40.08%  $\pm$  4.493%; %GFP with Vamp2-iRFP A: 86.94  $\pm$  6.092%, R: 75.00  $\pm$  11.98%, %Vamp2-iRFP with GFP A: 29.65  $\pm$  4.274%, R: 32.22%  $\pm$  5.067%; %GFP with Munc13-SNAP A: 82.22  $\pm$  3.792%, R: 68.61  $\pm$  6.877%, % Munc13-SNAP with GFP A: 42.17  $\pm$  7.290%, R: 45.60%  $\pm$  5.548%. Data represent mean  $\pm$  SEM (n=6 independent experiments with  $\geq$  6 videos per experiment). A: Anterograde, R: retrograde.

Analysis of co-trafficking between endogenous Syp-eGFP and overexpressed SV or AZ proteins resulted in high levels of co-transport, similar to the results observed upon co-overexpression of both proteins. Around 90% of endogenous Syp vesicles anterogradely co-transported with Syp-SNAP (**Figure 4.6.b**). Similarly, endogenous Syp vesicles anterogradely co-transported with the SV protein Vamp2 and the AZ protein Munc13 at very high levels (87% and 82%, respectively) (**Figure 4.6.a and b**). These data suggest that in iNs endogenous Syp traffics with both SV and AZ proteins towards axon terminals.

## Results

### 4.3. KIF1A is the main kinesin driving anterograde transport of presynaptic vesicles

#### 4.3.1. KIF1A co-traffics with presynaptic proteins in the developing axon

Defining the kinesin which drives the anterograde transport of PVs is fundamental to discover other yet unknown regulators of PV transport and consequently to understand the general regulation of the transport machinery. In prior studies KIF1A has been implicated as the main driver of SV protein transport in axons (Hummel and Hoogenraad, 2021; Okada et al., 1995), while KIF5B has been suggested to be responsible for driving the transport of AZ proteins and SNARE proteins (Cai et al., 2007; Shapira et al., 2003). Since we have identified a high degree of co-transport between these proteins, I first analyzed whether presynaptic proteins are co-trafficked with KIF1A (**Figure 4.7**). Expressing KIF1A-EGFP with Syp-RFP resulted in a very high level of co-antegrade transport between these proteins. Importantly, the AZ protein Munc13 also co-transported with KIF1A, suggesting that it might be the main driver of PV transport in developing human iNs.

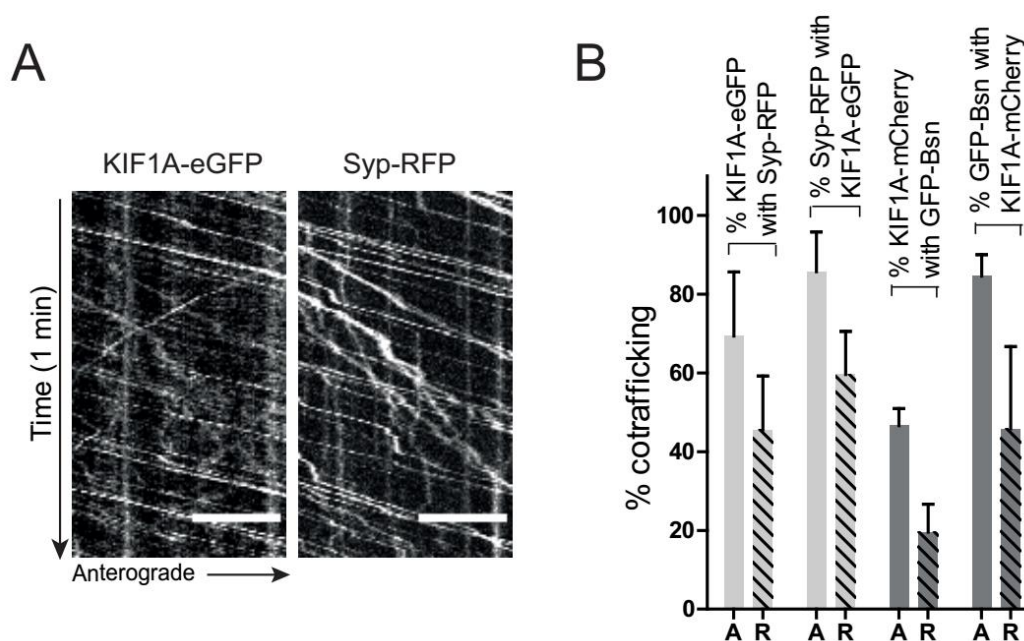


**Figure 4.7. KIF1A co-transport with PVs in developing axons.** (A) Representative kymographs showing transport of KIF1A-eGFP with Syp-RFP. X axis shows distance, with right hand side pointing towards anterograde direction, y axis represents time (1 min). (Scale bar, 10  $\mu$ m). (B) Graph shows quantification of kymographs. Co-antegrade- or retrograde transport between KIF1A-eGFP and Syp-RFP (%KIF1A-eGFP with Syp-RFP A:  $69.35 \pm$

## Results

---

16.28%, R: 46.56 ± 13.65%, %Syp-RFP with KIF1A-eGFP A: 85.71 ± 10.10%, R: 59.58% ± 10.95%; %KIF1A-mCherry with Bsn-eGFP A: 46.58 ± 4.377%, R: 19.58 ± 7.083%, %Bsn-eGFP with KIF1A-mCherry A: 84.58 ± 5.417%, R: 45.83% ± 20.83%. Data represent mean ± SEM (n=4 independent experiments with ≥ 6 videos per experiment). A: Anterograde, R: retrograde.

### 4.3.2. Lentiviral shRNA-mediated knockdown of KIF1A depletes SV and AZ proteins from presynapses in iNs.

After the co-trafficking analysis, I used a loss of function approach and generated lentiviral shRNAs against human KIF1A or KIF5B genes. iNs were transduced with lentiviruses encoding shRNAs against a non-targeting control sequence, KIF1A or KIF5B at early development (day 0 - day 2) and were differentiated for at least one week. Developing iNs were lysed and the successful knockdown of KIF1A or KIF5B were validated with immunoblot (**Figure 4.8.a and b**). After the lentivirally transduced WT or Syp-eGFP KI iPSCs started to differentiate into iNs, the effects of loss of either kinesin were analyzed by comparing the levels of anterogradely transported endogenous Syp (**Figure 4.8.c and d**). Furthermore, levels of presynaptic material reaching to and accumulating at mature synapses in each condition were compared by immunostaining of pre- and postsynaptic components in mature neurons (**Figure 4.8.e-g**).

## Results

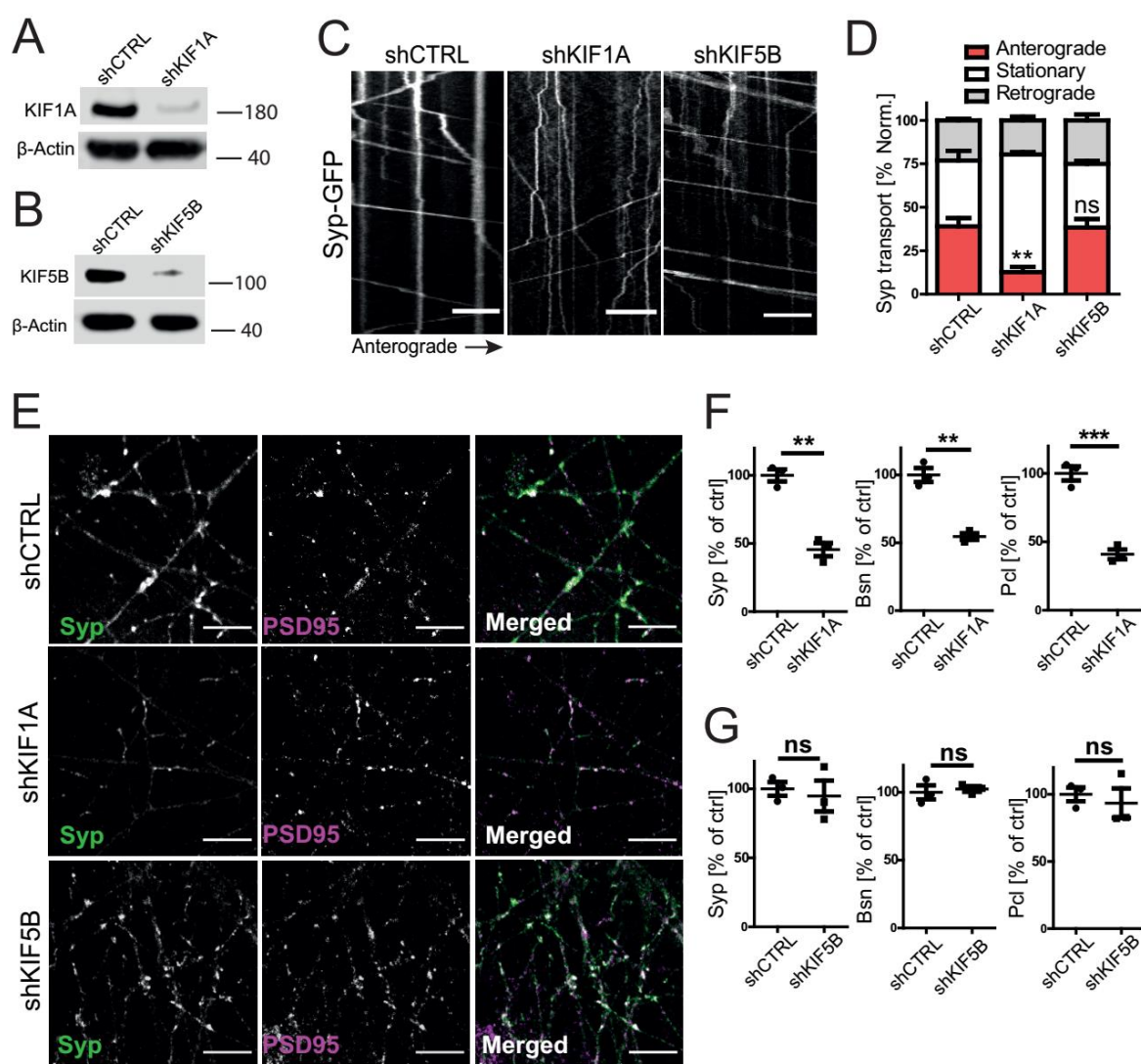


**Figure 4.8. shRNA-mediated knockdown of KIF1A results in significant decrease in levels of anterogradely transported presynaptic proteins and a strong phenotype at synaptic sites of mature human neurons.** (A) Immunoblot of iN lysates transduced with ctrl or KIF1A shRNA probed with KIF1A antibody. (B) Immunoblot of iN lysates transduced with ctrl or KIF5B shRNA probed with KIF5B antibody. (A and B)  $\beta$ -Actin served as loading control. Molecular weights are indicated on the right side of the blot in kilodaltons (kDa). (C) Kymographs showing trajectories of endogenous Syp-GFP spots in iNs transduced with shRNAs against KIF1A or KIF5B axons. X axis represents length of the axon and y axis represents time (total 1 min). (Scale bar, 10  $\mu$ m.) (D) Quantifications of anterogradely transported percentage of Syp vesicles in control condition, KIF1A knockdown or KIF5B knockdown. (shCTRL, 39.02  $\pm$  4.726%; shKIF1A, 12.68  $\pm$  3.038 %; shKIF5B, 38.39  $\pm$  4.843; n = 3 independent experiments with  $\geq$  6 videos per experiment, one-way analysis of variance (ANOVA) followed by Dunnett's post-test; p<0.0001 \*\*\*\*; p<0.01 \*\*; p>0.05 ns). (E) Representative confocal images of iNs transduced with lentiviruses expressing shRNAs against CTRL, KIF1A or KIF5B and immunostained with antibodies against Syp (presynaptic) and PSD95 (postsynaptic). Scale bar, 10  $\mu$ m. (F and G) Fluorescence level of Syp is significantly decreased in shKIF1A iNs, compared to shCTRL or shKIF5B. (F) shCTRL, 100.0  $\pm$  4.456 %; shKIF1A, 45.53  $\pm$  4.847 %; Bsn: shCTRL, 100.0  $\pm$  5.163 %, shKIF1A, 54.61  $\pm$  2.434 %; Pcl: shCTRL, 100.0  $\pm$  8.320 %, shKIF1A, 60.44  $\pm$  5.851 %. (G) Syp: shCTRL,

## Results

---

100.0 ± 4.933%; shKIF5B, 94.83 ± 11.19%; Bsn: shCTRL, 100.0 ± 5.163 %, shKIF5B, 102.5 ± 2.052 %; Pcl: shCTRL, 100.0 ± 6.807, shKIF5B, 87.31 ± 7.219 %. (F and G) n = 3 independent experiments with ≥100 synaptic puncta per experiment; t test; \*P < 0.05). Data represent mean ± SEM.

Axons of developing neurons lacking KIF1A showed a drastic decrease in the anterogradely transported Syp-carrying organelles, and a corresponding increase in the ratio of stationary organelles (**Figure 4.8c and d**). The retrogradely transported organelle population remained unaltered. KIF5B loss, on the other hand, did not lead to a change in the number of either anterogradely or retrogradely moving organelles. These results suggest that KIF1A loss stalls anterograde transport of PVs whereas KIF5B does not have a direct effect.

In a second set of experiments, mature neurons transduced with shRNAs against control, KIF1A or KIF5B were fixed at day 30 and immunostained with antibodies against pre- and postsynaptic components. Mature synapses were defined as puncta which were positive for both pre- and postsynaptic markers. The intensity of pre- and postsynaptic proteins at mature synapses were compared in control and knockdown conditions. Neither the knockdown of KIF1A nor KIF5B resulted in a detectable intensity change of postsynaptic components (**Figure 4.8e-g**). In contrast, the intensity of presynaptic proteins at mature synapses was significantly decreased upon depletion of KIF1A. This decrease was observed not only for the SV protein Syp but also for the AZ proteins Bassoon and Piccolo. We conclude that KIF1A is responsible for driving the anterograde axonal transport of not only SV proteins but also of AZ proteins.

## Results

### 4.3.3. Genetically engineered *KIF1A*<sup>-/-</sup> iNs phenocopy the KIF1A knockdown phenotype

To verify the presynaptic depletion phenotype shown with KIF1A knockdown, we collaborated with the MDC Stem Cell Facility and generated CRISPR/Cas9 KIF1A knockout (KO) iPSCs. The frameshift created in exon 4 of KIF1A was verified by genomic DNA sequencing (by the MDC, data not shown) and complete loss of the protein was demonstrated by Western Blot and immunostaining (**Figure 4.9.a and b**).

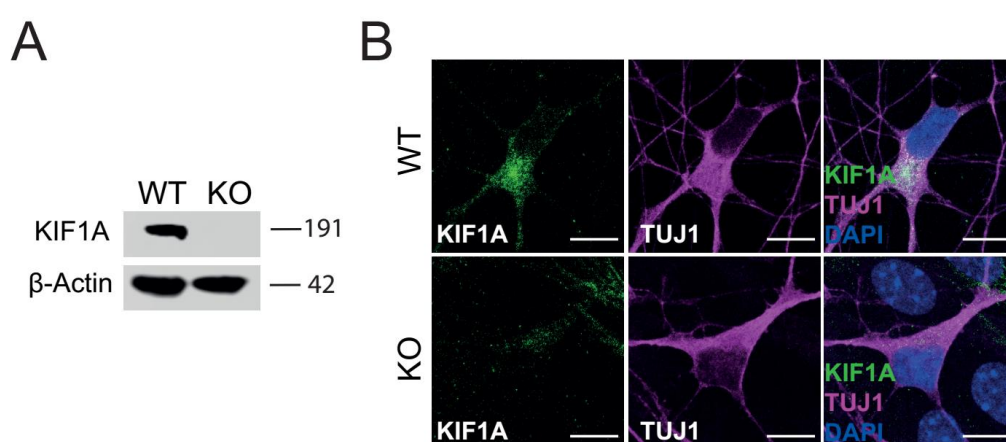


**Figure 4.9. KIF1A KO iPSC line was generated by using CRISPR/Cas9.** (A) Comparative Western Blot analysis of the WT line and the KIF1A KO clone (clone 14) confirmed the ablation of KIF1A expression in clone 14. Detection of  $\beta$ -Actin served as loading control. Molecular weights are indicated on the right in kilodaltons (kDa). (B) Representative immunofluorescence microscopy images of KIF1A and a neuronal marker (TUJ1) expression in the iNs derived by the WT iPSC line (upper panel) and the generated KIF1A KO cell lines (lower panel). Cell nuclei were counterstained with DAPI. (Scale bar, 10  $\mu$ m.)

KIF1A KO iPSCs displayed increased cell death during the first two weeks of neuronal differentiation compared to WT iPSCs. However, the morphology of the remaining KO cells appeared similar to WT cells at the stem cell stage or during development. When KIF1A KO iNs were transfected with Syp-eGFP or Bsn-eGFP at their developing stage, similar to KIF1A KD iNs, they also showed a severe reduction in their ratio of anterogradely transported presynaptic vesicles (**Figure 4.10**). The ratio of anterogradely transported Syp-eGFP vesicles

## Results

decreased almost five times and a consequent increase in the stationary pool of the vesicles was observed, indicating stalled transport of PVs.

To validate that the lack of KIF1A is the cause for the decrease in the anterograde transport of presynaptic proteins, KIF1A was overexpressed from the initiation of neuronal reprogramming until the day of live imaging. Importantly, lentiviral re-expression of full-length KIF1A (FL-KIF1A) fully rescued anterograde transport in developing KO-iNs to WT transport levels. On the other hand, re-expressing a KIF1A construct lacking its C terminal PH domain ( $\Delta$ PH-KIF1A) did not rescue the transport phenotype, consistent with a role for membrane lipids in KIF1A function and with earlier studies (Hummel and Hoogenraad, 2021; Klopfenstein and Vale, 2004).

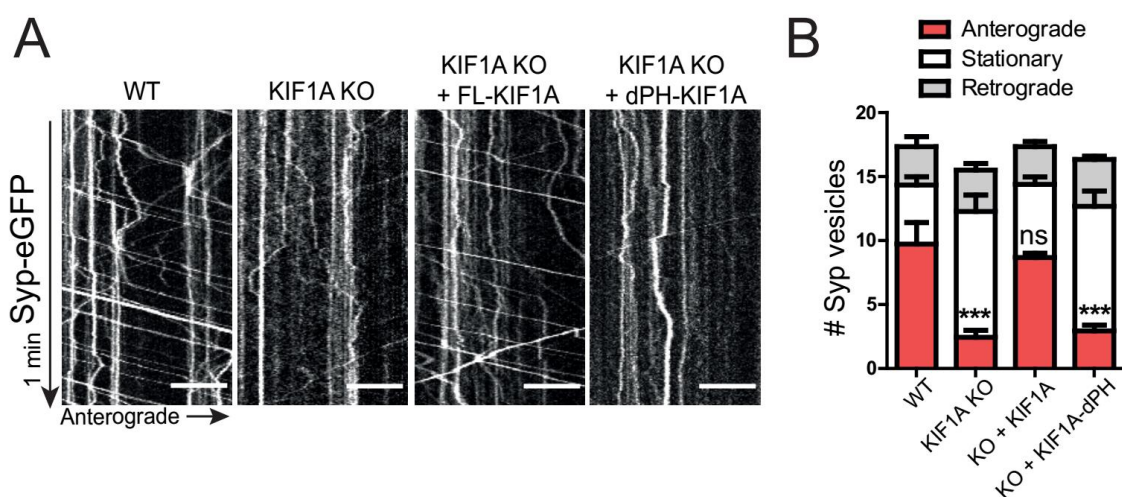
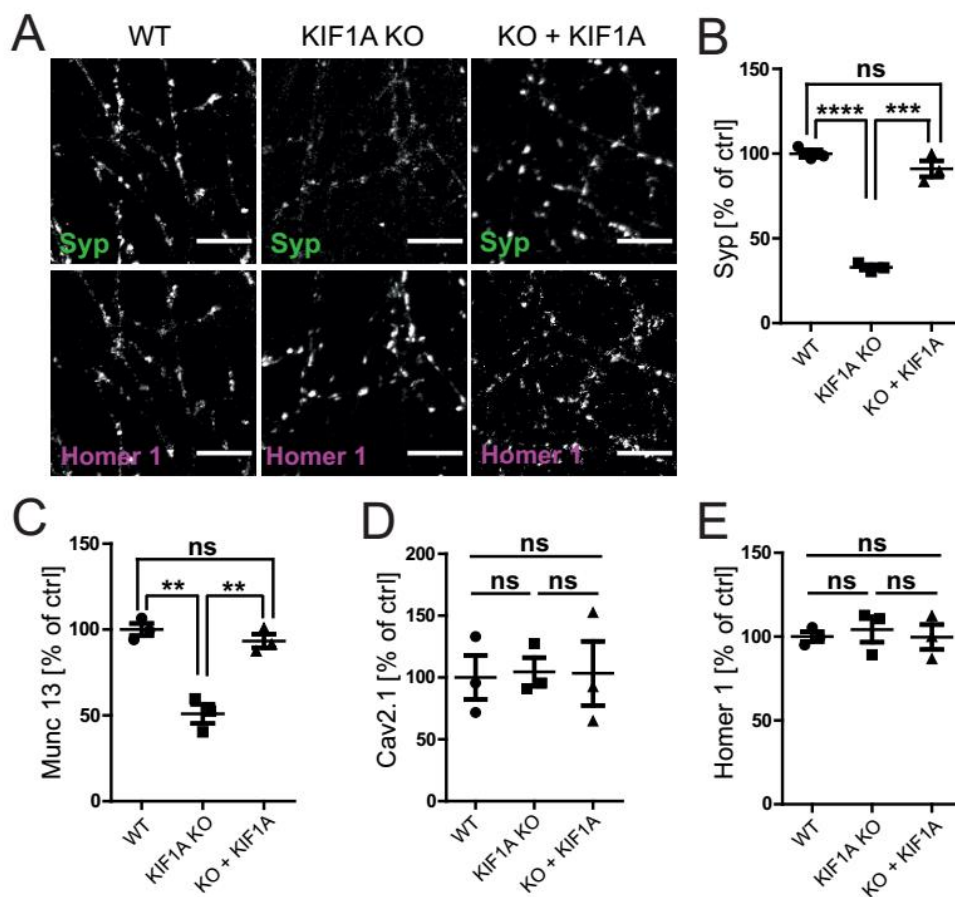


**Figure 4.10. KIF1A KO iNs show decreased ratio of anterogradely transported presynaptic proteins.** (A) Kymographs showing trajectories of overexpressed Syp-GFP spots in WT or KIF1A KO iNs with KO iNs also co-expressing either full length FL-KIF1A or PH domain lacking  $\Delta$ PH-KIF1A constructs. The kymograph of WT axons demonstrate movement in both anterograde (arrow) and retrograde direction with few stationary events (vertical lines). Kymograph analysis of KIF1A KO axons show that anterograde transport events are decreased and many Syp-GFP puncta become stationary. Overexpression of FL-KIF1A rescued the number of transport vesicles to WT levels. Expression of  $\Delta$ PH-KIF1A did not rescue the axonal transport loss in KO iNs. X axis represents the distance and y axis represents time (total 1 min). (Scale bar, 10  $\mu$ m.) (B) Anterograde Syp transport is significantly decreased upon KIF1A loss. Quantifications of number of anterogradely moving Syp-eGFP vesicles: WT,  $9.722 \pm 1.684\%$ ; KIF1A KO,  $2.444 \pm 0.5472\%$ ; KO + KIF1A,  $8.667 \pm 0.3333\%$ ; KO +  $\Delta$ PH-KIF1A,  $2.944 \pm 0.4444\%$ . (n = 3 independent experiments with  $\geq 8$  videos per experiment; one-way analysis of variance (ANOVA) followed by Dunnett's post-test;  $p < 0.0001$  \*\*\*\*;  $p < 0.01$  \*\*;  $p > 0.05$  ns). Data represent mean  $\pm$  SEM.

## Results

The observed depletion of presynaptic proteins transported towards axon terminals should result in a consequent decrease in the amount of these proteins reaching to mature synapses. To test this, we differentiated WT or KIF1A KO iNs until day 30 and immunostained them with antibodies against pre- and postsynaptic components. As a rescue condition, KIF1A KO iNs transduced with a full-length KIF1A expression lentivirus was included in the experiment. Mature synapses were defined as puncta that is positive for both pre- and postsynaptic markers. Our analysis showed that KIF1A loss resulted in a significant decrease in the intensity levels of the SV protein Syp and the AZ protein Munc 13 whereas it did not change the intensity of the postsynaptic protein Homer 1 (**Figure 4.11**). Importantly, fluorescence intensity levels of the presynaptic calcium channel Cav2.1 were not altered upon KIF1A loss, indicating that these proteins might not be included in the cargoes of PVs that are transported by KIF1A. We conclude that KIF1A is responsible for driving the anterograde axonal transport of SV proteins and AZ proteins, but not likely of Cavs.



## Results

### Figure 4.11. Complete loss of KIF1A using CRISPR/Cas9 results in a strong depletion of fluorescence levels of SV and AZ proteins but not Cavs at synaptic sites of mature human neurons.

(A) Representative confocal images of WT or KIF1A KO iNs or KIF1A KO iNs transduced with a lentivirus expressing full-length KIF1A and immunostained with antibodies against Syp (presynaptic) and Homer 1 (postsynaptic). Scale bar, 10  $\mu$ m. (B, C, D and E) Fluorescence levels of the SV protein Syp and the AZ protein Munc13 significantly decreased in KIF1A KO iNs, whereas levels of Calcium channel Cav2.1 remained unaltered. Postsynaptic Homer1 intensity remained unchanged. (B) Syp levels (% normalized): WT,  $100.0 \pm 2.143$  %; KIF1A KO,  $32.89 \pm 1.499$ %; KO + KIF1A,  $91.10 \pm 4.745$ %. (C) Munc 13 levels (% normalized): WT,  $100.0 \pm 17.85$ %; KIF1A KO,  $50.90 \pm 5.641$ %, KO + KIF1A,  $93.33 \pm 3.953$ %. (D) Cav2.1 levels (% normalized): WT,  $100.0 \pm 4.933$ %; KIF1A KO,  $104.6 \pm 11.46$ %; KO + KIF1A,  $103.3 \pm 25.87$ %. (E) Homer 1 levels (% normalized): WT,  $100.0 \pm 2.987$ %; KIF1A KO,  $104.2 \pm 7.543$ %; KO + KIF1A,  $99.74 \pm 7.424$ % (B, C, D and E) n = 3 independent experiments with  $\geq 100$  synaptic puncta per experiment; t test; \*P < 0.05). Data represent mean  $\pm$  SEM.

### 4.3.4. Immunoprecipitation of KIF1A followed by MS/MS reveals interaction partners of KIF1A in developing iNs

Validating that KIF1A is the main kinesin that drives the anterograde transport of presynaptic precursor vesicles in the axon was crucial in our search for other candidate markers of these organelles and regulators of the transport machinery. Therefore, to uncover interaction partners of KIF1A, I transduced iPSCs with lentiviral KIF1A-eGFP under the control of the human Synapsin1 promoter and differentiated them for 12 days. At this time of development of iNs, the presynapse begins to be formed, in contrast to the postsynaptic compartment. The transport rate of presynaptic proteins in the axon is comparably high at this stage. Therefore, at this timepoint capturing the maximum number of transport organelles is possible. I immunoprecipitated KIF1A-eGFP using magnetic beads with covalently bound anti-GFP-nanobodies, verified a successful pulldown and proceeded with MS/MS analysis (**Table 4.1**).

**Table 4.1. KIF1A-eGFP MS/MS reveals interaction partners in developing neurons (selected hits).**

	Intensity Ctrl	Intensity KIF-IP	iBAQ Ctrl	iBAQ KIF-IP	LFQ intensity ratio KIF-IP/Ctrl
<b>KIAA1279</b>	161130	54171000	4603.8	1547800	18.616.000
<b>SHB</b>	34920000	18512000	1343100	711990	10.864.000
<b>Arl1</b>	89590	29160000	12799	4165700	9.714.500

## Results

---

	Intensity Ctrl	Intensity KIF-IP	iBAQ Ctrl	iBAQ KIF-IP	LFQ intensity ratio KIF-IP/Ctrl
<b>Rab35</b>	1807200	25688000	150600	2140600	9.226.100
<b>Rab3A</b>	125210	27089000	9631.8	2083800	9.024.600
<b>Arl3</b>	153970	23204000	13997	2109400	7.730.200
<b>DENND4B</b>	0	7734400	0	175780	7.685.000
<b>SNX8</b>	42793	23011000	1945.2	1046000	7.666.100
<b>WDR91</b>	0	12742000	0	554000	6.750.700
<b>Fam83H</b>	1601700	6709100	26695	111820	6.173.700
<b>TAB2</b>	1395200	299440	77512	16635	5.345.300
<b>ASAP3</b>	0	1562800	0	97675	5.182.400
<b>VPS4A</b>	62246	14661000	2489.8	586440	4.884.200
<b>SYP</b>	210290	12669000	30041	1809800	4.220.500
<b>PIKfyve</b>	1404600	3533900	20964	52744	3.511.300
<b>Rab21</b>	703850	9067400	54142	697490	3.306.500
<b>Arl8a/b</b>	155610	9816400	14147	892400	3.270.300
<b>JIP4</b>	40655000	77608000	615980	1175900	2.672.900
<b>Fam83D</b>	0	4821100	0	160700	2.325.800
<b>SNX1</b>	66437	6424100	4429.1	428270	2.140.100
<b>Rab12</b>	0	5810900	0	341820	1.935.900
<b>FYCO1</b>	1203700	1564000	14330	18619	1.554.000
<b>SYT1</b>	460410	50936000	23021	2546800	1.377.000
<b>SNX18</b>	0	3234600	0	161730	1.346.300
<b>SNX29</b>	730480	867860	16602	19724	862.320

MS/MS analysis verified KIF1A interaction with many previously identified interactors such as microtubule-associated proteins MAP2 and KIFBP (KIAA1279P). Interestingly, several SV proteins also came up on the list (Syp, Rab3 and Syt1) further showing a close proximity of KIF1A with presynaptic proteins. The previously reported KIF1A adaptor protein MADD/DENN, lysosomal adaptor proteins Arl8a/b and FYCO1 were also identified. In addition, PIKfyve, a kinase that generates PI(3,5)P<sub>2</sub> from PI3P was identified as interaction partner of KIF1A.

## Results

---

### 4.4. Arl8 is a marker of PVs and regulates their axonal trafficking

#### 4.4.1. PVs co-transport with lysosomal membrane proteins in the developing axon

Arl8 is a lysosomal kinesin adaptor that was previously shown to be present on PVs, regulating their anterograde transport in *D. melanogaster* (Vukoja et al., 2018). Importantly, Arl8 is identified as one of the interaction partners of KIF1A in developing neurons (**Table 4.1**). To validate their interaction, iPSCs were transduced with an Arl8b-mCherry expressing lentivirus under the control of the human Synapsin1 promoter. Developing iNs were collected, lysed and Arl8b-mCherry was immunoprecipitated using magnetic beads with immobilized anti-RFP nanobodies. Interaction between Arl8b and KIF1A was verified by Western Blot using both an antibody against KIF1A which detected the endogenous KIF1A and by using a GFP antibody which detected the overexpressed pool of KIF1A-eGFP (**Figure 4.12a**). Interestingly, SV proteins Syp and Syt1 were found as interaction partners of Arl8b, further strengthening the hypothesis that Arl8 is a marker of PVs and a possible component of the axonal transport machinery.

If Arl8 is a marker of PVs in the axons of mouse hippocampal neurons and in *drosophila* motoneurons, a similar machinery might be conserved in human neurons as well. To test this, co-transport experiments expressing Arl8b-mCherry together with either Syp-, Bassoon- or Munc13-GFP in developing iNs were performed (**Figure 4.12b**). Two-channel confocal imaging resulted in high anterograde co-transport levels between Arl8 and all three presynaptic proteins (at least 50% in all cases). This finding suggests that at least half of all human PVs contain Arl8. Of note, presynaptic proteins showed no difference in their co-transport levels between Arl8a and Arl8b (not shown).

## Results

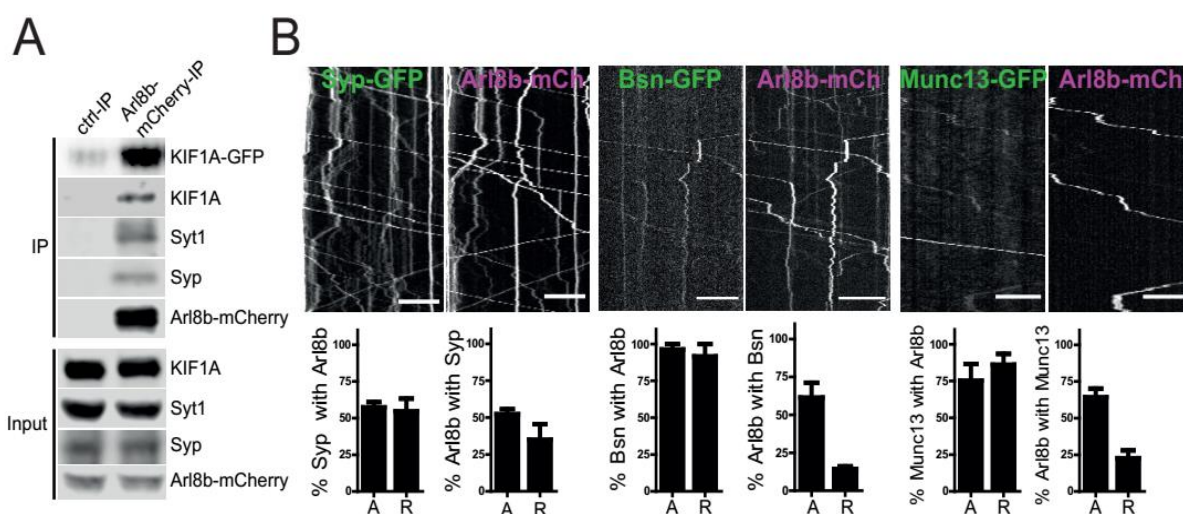


**Figure 4.12. Arl8b is a marker of PVs.** (A) Co-immunoprecipitation of Arl8b-mCherry with KIF1A from developing (day12) iNs. iNs expressing Arl8b-mCherry were lysed and subjected to affinity capture by RFP-nanotrap magnetic beads or magnetic beads as a control. Bound proteins were detected by immunoblotting. Input: 5% of total lysate. (B) Top panel: kymographs showing transport of Syp-GFP, Bsn-GFP or Munc13-GFP with Arl8b-mCherry, respectively. X-axis shows distance, with right hand side pointing towards anterograde direction; y-axis represents time (1 min). (Scale bar, 10  $\mu$ m). Bottom panel: graphs show quantification of kymographs. All co-transport levels are percent normalized. (% Syp-GFP cotransport with Arl8b-mCherry A:  $57.31 \pm 3.616$ , R:  $54.72 \pm 8.611$ ; % Arl8b cotransport with Syp A:  $52.31 \pm 3.410$ , R:  $35.05 \pm 10.49$ ; % Bsn-GFP cotransport with Arl8b-mCherry A:  $96.30 \pm 3.704$ , R:  $91.67 \pm 8.333$ ; % Arl8b cotransport with Bsn A:  $61.51 \pm 9.631$ , R:  $14.39 \pm 1.679$ ; % Munc13-GFP with Arl8b-mCherry A:  $75.30 \pm 11.32$ , R:  $86.11 \pm 7.349$ ; % Arl8b with Munc13 A:  $64.27 \pm 5.946$ , R:  $22.73 \pm 5.235$ . (n=3 independent experiments with  $\geq 6$  videos per experiment) A: Anterograde, R: Retrograde transport.

Investigating the cell biological identity of the presynaptic transport organelles has been a fundamental question. So far, by live imaging and fixed immunostaining experiments we have shown that both KIF1A and Arl8 co-transport with presynaptic proteins and regulate transport. Moreover, we found Arl8b and KIF1A to interact in developing iNs (**Table 4.1.**, **Figure 4.12**). Importantly, interaction of Arl8 with endogenous SV proteins Syp and Syt1 has also been demonstrated, further strengthening the hypothesis that Arl8 associates with PVs carrying presynaptic proteins.

Arl8 localizes on lysosomes and regulates lysosomal motility. Since PVs have Arl8 on their membranes, this indicates that they might be lysosome-related organelles. To explore

## Results

the lysosomal identity of PVs in more detail, I used iNs that contain endogenously tagged Syp-eGFP and quantified the fraction of co-transport with lysosomal proteins. Endogenous Syp organelles anterogradely moved with Arl8-iRFP and Lamp1-SNAP organelles in more than 50% of all cases (**Figure 4.13**). Similar values were observed for endogenous Lamp1 (e.g. using CRIPSR-engineered iN endogenously expressing Lamp1-eGFP) organelles co-transporting with SV proteins Syp and Syt1 (Kong, S., 2022). These results confirm the lysosomal membrane identity of PVs.

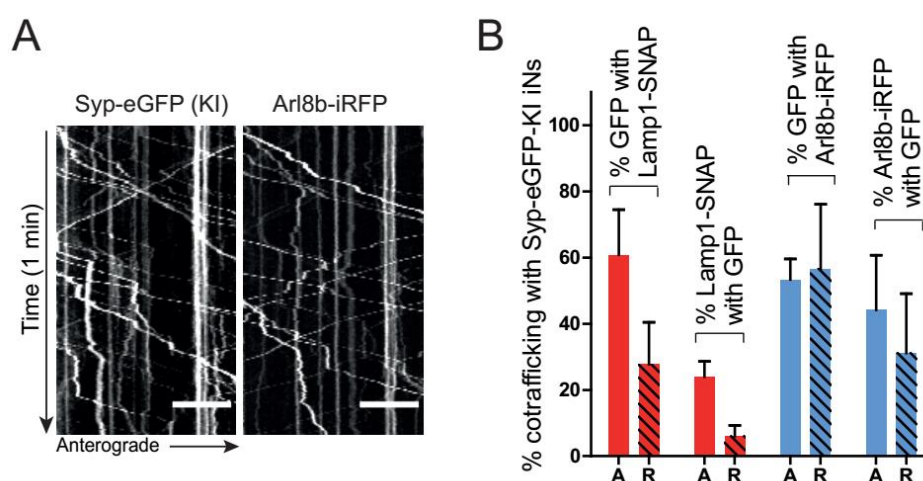


**Figure 4.13. Axonal co-transport levels of endogenous Syp-eGFP with lysosomal membrane proteins in developing iNs.** (A) Representative kymographs showing transport of endogenous Syp-eGFP vesicles with Arl8b-iRFP. X axis shows distance, with right hand side pointing towards anterograde direction, y axis represents time (1 min). (Scale bar, 10  $\mu$ m). (B) Graph shows quantification of kymographs. Co-antero- or retrograde transport between Syp-eGFP (KI) and indicated lysosomal membrane proteins. (%GFP with Lamp1-SNAP A: 60.83  $\pm$  13.63%, R: 27.78  $\pm$  12.67%, %Lamp1-SNAP with GFP A: 23.97  $\pm$  4.671%, R: 6.032%  $\pm$  3.250%; %GFP with Arl8b-iRFP A: 53.33  $\pm$  6.236%, R: 56.67  $\pm$  19.44%, %Arl8b-iRFP with GFP A: 44.17  $\pm$  16.54%, R: 31.11%  $\pm$  18.02%. Data represent mean  $\pm$  SEM (n=6 independent experiments with  $\geq$  6 videos per experiment). A: Anterograde, R: retrograde.

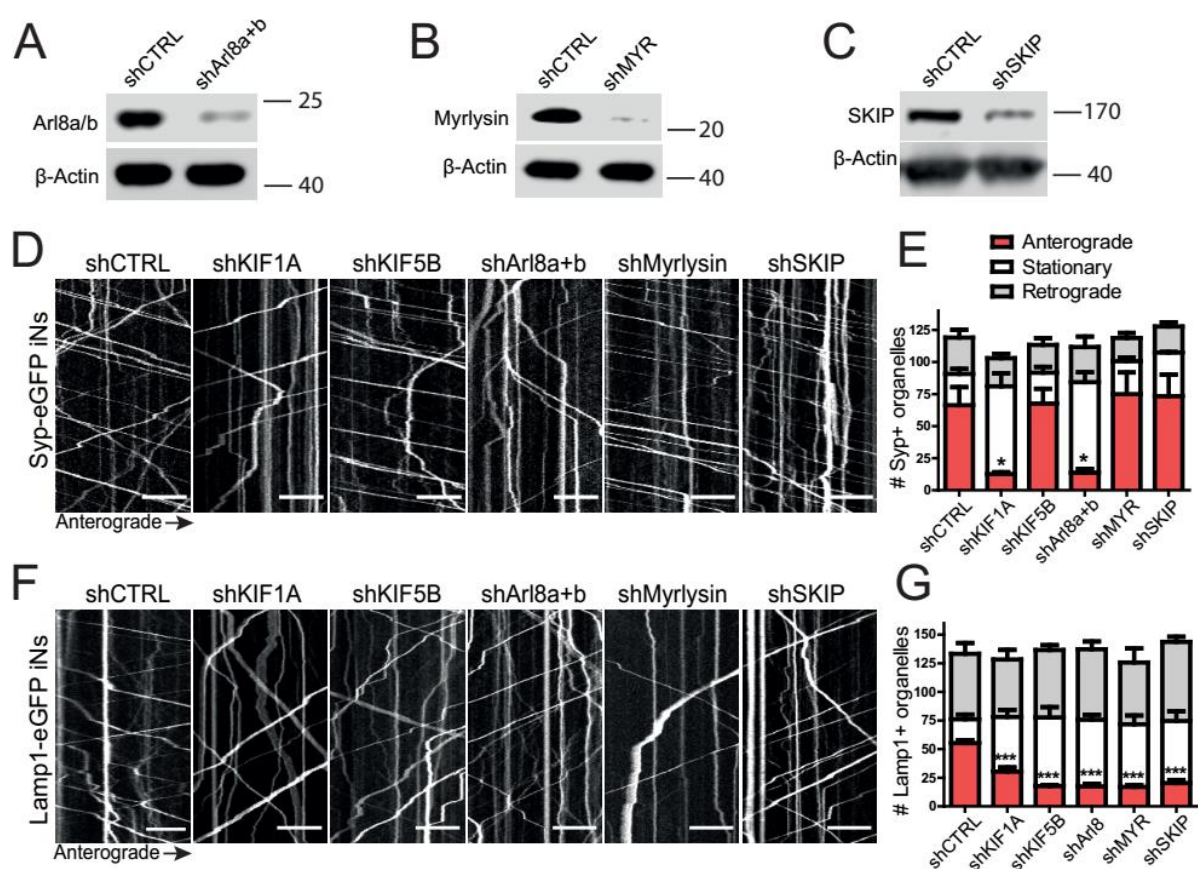
## Results

---

### 4.4.2. PV transport is regulated by Arl8 but is not dependent on KIF5B/BORC/SKIP complex

Arl8 mediates lysosomal movement in non-neuronal cells. To further investigate whether it has direct role in regulating the transport machinery of presynaptic precursor vesicles, I generated lentiviral shRNA constructs to knockdown both Arl8a and Arl8b isoforms in human neurons (**Figure 4.14a**). Additionally, previous data demonstrates that in PVs co-transport with lysosomal membrane proteins, namely Spinster in *Drosophila* and Lamp1 in mouse hippocampal neurons (Vukoja et al., 2018). We also show that endogenous Syp organelles co-transport with Lamp1 (**Figure 4.13**). This suggests that PVs have a lysosomal origin, thus, PV transport might follow known lysosomal transport mechanisms. To test this hypothesis, I designed shRNAs against proteins known to regulate lysosomal trafficking in neuronal and non-neuronal cells. BORC (BLOC-1 related complex) is an upstream regulator of Arl8 and acts as a master regulator of lysosome movement as it can regulate both KIF5B-KLC2-SKIP and KIF1A motors (Guardia et al., 2016; Pu et al., 2015). Thus, I generated shRNAs against Myrlysin, a subunit of BORC (**Figure 4.14b**). Moreover, I used shRNAs against the lysosome adaptor and Arl8 effector protein SKIP (PLEKHM2) (**Figure 4.14c**) and two kinesins which have been reported to direct lysosomal motility, KIF1A and KIF5B (**Figure 4.8 a and b**). I then quantified the ratio of anterogradely transported endogenous Syp organelles in developing axons of Syp-eGFP KI iNs. I used Lamp1-eGFP KI iNs to serve as a positive control for detecting positioning defects of *bona fide* lysosomes upon knockdown of each protein (**Figure 4.14 f and g**).

## Results



## Results

---

The ratio of anterogradely moving endogenous Lamp1 organelles drastically decreased upon depletion of KIF1A, KIF5B, Arl8a+b, Myrlysin or SKIP whereas none of these manipulations led to a change in the number of retrograde events (**Figure 4.14 f and g**). This confirmed that all tested components have a direct role in the regulation of lysosomal motility in developing axons. Surprisingly, anterograde movement of endogenous Syp was significantly reduced upon KIF1A knockdown or Arl8a and Arl8b co-knockdown, whereas it remained unchanged upon knockdown of KIF5B, Myrlysin or SKIP (**Figure 4.14 d and e**).

In a following experiment, iNs were fully differentiated to mature neurons (day 28) under the same conditions as in the previous knockdown screen, and stained using antibodies against pre- and postsynaptic markers. Puncta that were co-labeled with both markers identified synapses. iNs lacking Arl8a and Arl8b, similar to iNs lacking KIF1A (**Figure 4.8**), showed a significant depletion of presynaptic proteins at mature synapses (**Figure 4.15**). This decrease was consistent in case of SV proteins Syp, Syt1 as well as the AZ proteins Bassoon and Piccolo. We conclude that Arl8, like KIF1A, facilitates the anterograde axonal transport of SV and AZ proteins.

Loss of Arl8a and Arl8b severely impaired anterograde transport of presynaptic proteins in developing neurons and their consequent accumulation at synaptic sites in mature neurons. No such change was observed for KIF5B, Myrlysin or SKIP loss. In line with previous studies (De Pace et al., 2020), this argues that even though PVs contain certain lysosomal markers, their transport mechanism seems to be independent of the conventional lysosome transport machinery which involves the BORC/KIF5B /SKIP ensemble.

## Results

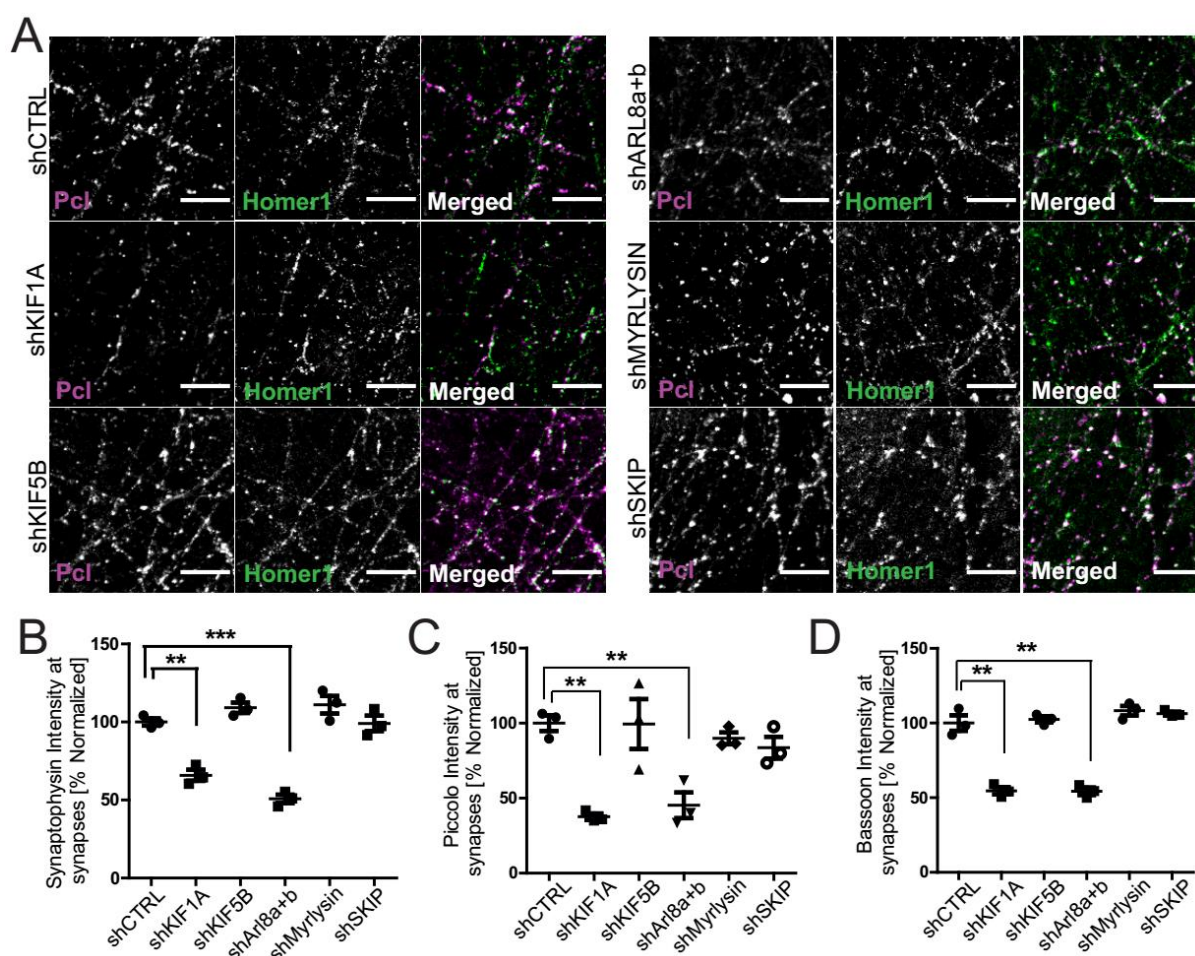


**Figure 4.15. Co-knockdown of Arl8a and Arl8b phenocopies the presynaptic depletion observed upon KIF1A loss.** (A) Representative confocal images of WT iNs transduced with lentiviruses expressing CTRL, KIF1A, KIF5B, Arl8a+b, Myrlysin or SKIP shRNAs, fixed at day 28 and immunostained with antibodies against Piccolo (presynaptic) and Homer1 (postsynaptic). (Scale bar, 10  $\mu$ m.) (B, C and D) Quantifications of fluorescence intensities of presynaptic Syp, Piccolo or Bassoon in mature iNs. (B) % normalized intensity of Syp: shCTRL, 100.0  $\pm$  2.286%; shKIF1A, 65.83  $\pm$  3.550%; shKIF5B, 109.1  $\pm$  3.358%; shArl8a+b, 50.77  $\pm$  2.694%; shMyrlysin, 111.1  $\pm$  5.612%; shSKIP, 99.10  $\pm$  4.924%. (C) % normalized intensity of Piccolo: shKIF1A, 37.63  $\pm$  2.159%; shKIF5B, 99.46  $\pm$  16.63%; shArl8a+b, 45.26  $\pm$  8.564%; shMyrlysin, 89.88  $\pm$  3.988%; shSKIP, 83.71  $\pm$  7.245%. (D) % normalized intensity of Bassoon: shKIF1A, 54.61  $\pm$  2.434%; shKIF5B, 102.5  $\pm$  2.052%; shArl8a+b, 54.30  $\pm$  2.460%; shMyrlysin, 108.3  $\pm$  3.191%; shSKIP, 106.4  $\pm$  1.254%. (B, C and D) n = 3 independent experiments with  $\geq$ 100 synapses per experiment; t test; \*P < 0.05). Data represent mean  $\pm$  SEM.

## Results

### 4.4.3. Arl8a/b double KO iPSCs validate the presynaptic loss observed in Arl8 knockdown iNs

To confirm the severe effects of shRNA mediated co-knockdown of Arl8a and Arl8b on developing human neurons, I generated an Arl8a and Arl8b double knockout (dKO) iPSC line using Crispr/Cas9. I designed guideRNA constructs to target the first exon of each gene. First, I transfected cells with the plasmid encoding the guide RNA against Arl8b and Cas9. After analyzing the KO scores of each clone, I re-transfected the Arl8b KO clones with a plasmid encoding the guideRNA against Arl8a and Cas9 expression and generated dKO iPSCs which were validated by Western Blot and immunostaining using an Arl8 antibody which recognizes both isoforms of Arl8 (**Figure 4.15a**). To avoid any possible off-target effect deriving from clonal selection during Crispr workflow, I used three different independent dKO lines in experiments with KO cells and included a non-targeted line (clone 27) to compare with WT cells.

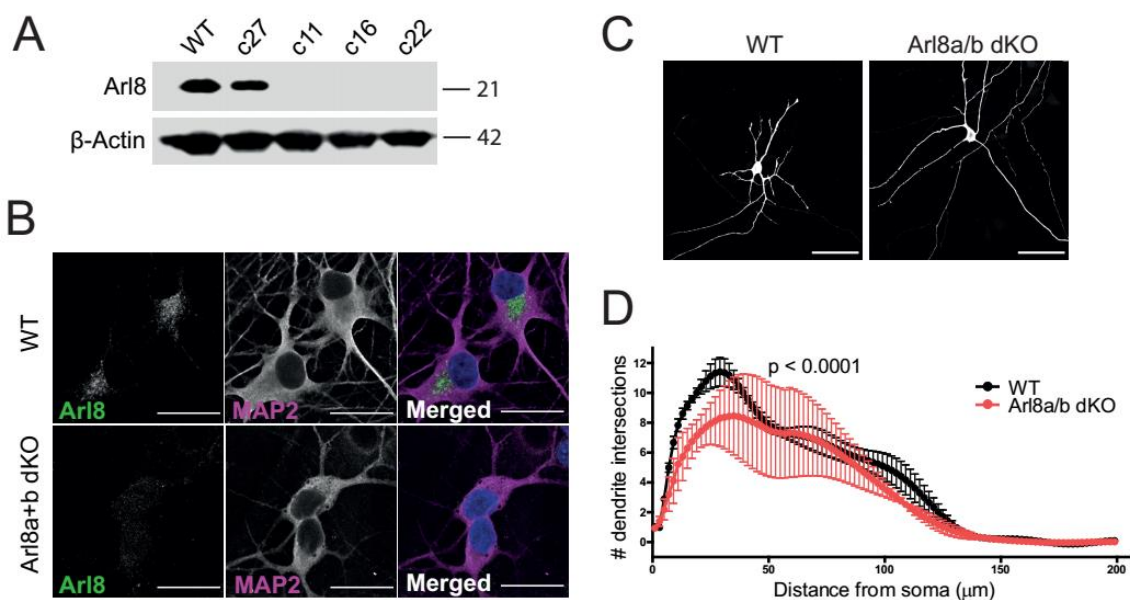


**Figure 4.16. Arl8a and Arl8b double knockout iPSCs were generated using Crispr/Cas9.** (A) Comparative Western Blot analysis of the parental cell line (WT), the Arl8a+b double KO clones (clones 11, 16 and 22) as well as a non-targeted clone (clone 27) confirmed the ablation of Arl8 expression in clones 11, 16 and 22. Detection of  $\beta$ -Actin served as loading control. Molecular weights are indicated on the right in kilodalton (kDa). (B) Complete ablation of Arl8 was demonstrated using immunofluorescence microscopy. To verify loss of both isoforms, an Arl8

## Results

---

antibody recognizing both Arl8a and Arl8b was used. iNs were fixed and stained at day 21. Cells were counterstained with the neuronal marker MAP2 and with DAPI. Scale bar, 25  $\mu\text{m}$ . (C) WT or Arl8a/b dKO iPSCs were differentiated for 21 days, transfected with GFP plasmids for sholl analysis and fixed two days post-transfection. Scale bar, 50  $\mu\text{m}$ . (D) Quantification of Sholl analysis. Arl8a/b dKO iNs show fewer dendritic intersections.  $n=60$  for each condition derived from three separate iN cultures.  $n=3$  independent experiments; t test;  $*P < 0.0001$ . Data represent mean  $\pm$  SEM.

Upon Ngn2 activation Arl8a/b dKO iPSCs were successfully differentiated to iNs. They expressed neuronal markers and did not show morphological abnormalities. **(Figure 4.16b)**. From the beginning to the end of the differentiation process, although more apparent in early differentiation, Arl8a/b dKO neurons showed increased cell death compared to WT neurons. Interestingly, Sholl analysis revealed that Arl8a/b dKO iNs contained fewer dendritic branches compared to WT iNs, indicating a developmental delay **(Figure 4.16 c and d)**.

To test whether presynaptic anterograde transport depletion caused by Arl8a/b co-knockdown is also observed in Arl8a/b dKO cells, I transfected WT or KO iNs with presynaptic proteins during development (day 10-12) and imaged them 24 hours post-transfection. A marked decrease in anterograde transport, similar to the knockdown condition was detected in dKO neurons **(Figure 4.17)**. This defect in anterograde Syp transport was rescued to control levels by co-overexpression of Arl8a and Arl8b, further validating that the phenotype is indeed caused by Arl8a/b loss, and it is not an off-target effect.

## Results

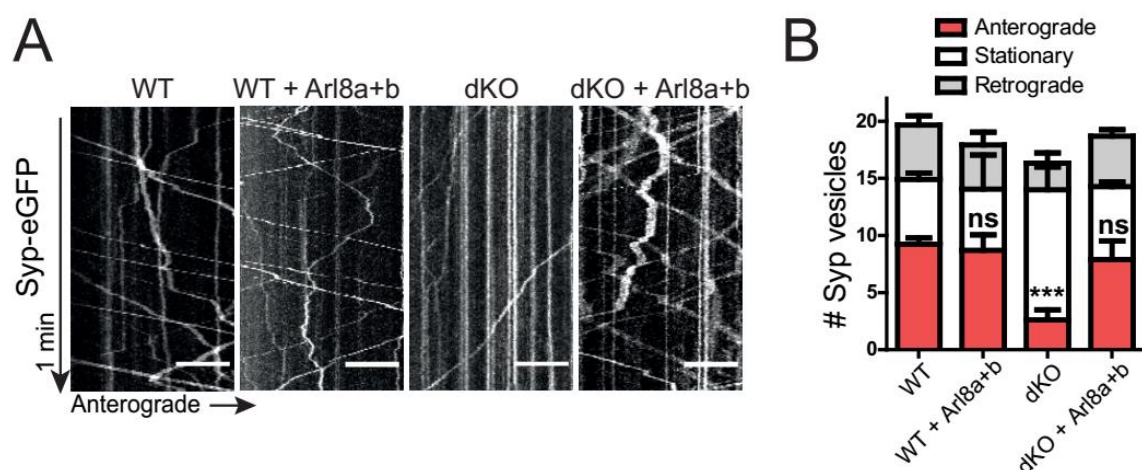


**Figure 4.17. Arl8a/b dKO iNs show Arl8-dependent regulation of PV transport.** (A) Kymographs showing trajectories of Syp-GFP vesicles in WT or Arl8a/b dKO iNs. dKO iNs show decreased anterograde (pointed arrow) directed movements which is rescued to WT levels upon lentiviral administration of Arl8a and Arl8b at the start of differentiation. X axis represents length of the axon and y axis represents time (total 1 min). (Scale bar, 10  $\mu$ m.) (B) Quantifications of number of anterogradely moving Syp-eGFP vesicles: WT,  $9.222 \pm 0.5556$ ; WT + Arl8a+b,  $8.694 \pm 1.368$ ; Arl8a/b dKO,  $2.611 \pm 0.8731$ ; Arl8a/b dKO + Arl8a+b,  $7.889 \pm 1.637$ . (n = 3 independent experiments with  $\geq 8$  videos per experiment; one-way analysis of variance (ANOVA) followed by Dunnett's post-test;  $p < 0.0001$  \*\*\*;  $p < 0.01$  \*\*,  $p > 0.05$  ns). Data represent mean  $\pm$  SEM.

Moreover, Arl8a/b dKO iNs showed significantly lower intensity in the fluorescence levels of endogenous SV or AZ proteins at mature synapses (**Figure 4.18**). This depletion of presynaptic material at mature synapses was completely rescued when cells were transduced with a lentivirus overexpressing Arl8b at the day when differentiation was initiated. Of note, overexpression of Arl8b in WT cells did not alter the fluorescence levels of presynaptic proteins at mature synapses. This finding confirmed that Arl8 is essential for presynaptic biogenesis in human iNs.

## Results

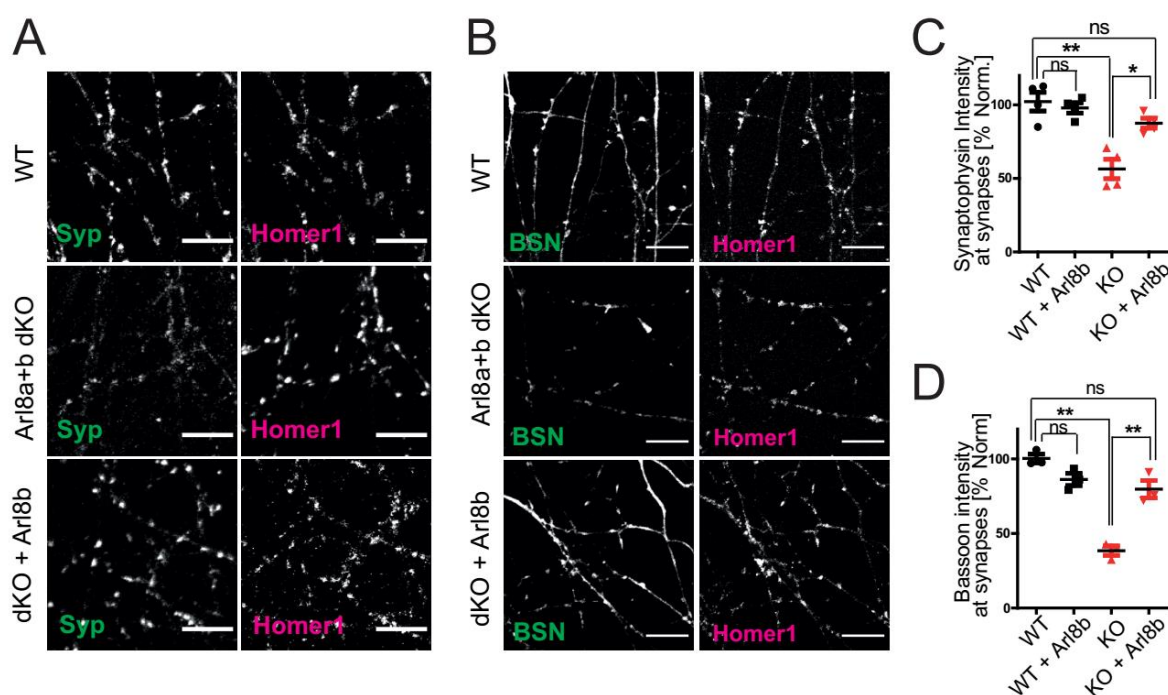


**Figure 4.18. Arl8a/b dKO iNs phenocopy the presynaptic depletion observed in Arl8a/b co-knockdown neurons.** (A) Representative confocal images of WT or Arl8a/b dKO iNs with or without lentiviral overexpression of Arl8b, fixed at day 30 and immunostained with antibodies against Syp (presynaptic) and Homer1 (postsynaptic). (Scale bar, 10  $\mu$ m.) (B) Confocal images of WT or Arl8a/b dKO iNs with or without lentiviral overexpression of Arl8b, immunostained for Syp (presynaptic) and Homer1 (postsynaptic). (Scale bar, 10  $\mu$ m.) (C and D) Fluorescence intensity of Syp (C) and Bassoon (D) puncta are significantly decreased in dKO iNs compared to WT. Percent normalized values: (C) Syp puncta: WT, 102.2  $\pm$  6.368%; WT + Arl8a+b, 97.97  $\pm$  3.491%; Arl8a/b dKO, 56.44  $\pm$  6.566%; Arl8a/b dKO + Arl8a+b, 87.60  $\pm$  3.365%. (D) Bsn puncta: WT, 100.3  $\pm$  2.906%; WT + Arl8a+b, 86.27  $\pm$  4.102%; Arl8a/b dKO, 38.50  $\pm$  3.138%; Arl8a/b dKO + Arl8a+b, 79.72  $\pm$  5.849% (C and D) n = 3 independent experiments with  $\geq$ 100 synapses per experiment; t test; \*P < 0.05). Data represent mean  $\pm$  SEM.

### 4.4.4. Depletion of Arl8 in iNs results in decreased levels of stimulation-induced Ca<sup>2+</sup>

We have confirmed that genetic loss of Arl8a and Arl8b leads to decreased levels of anterograde axonal transport of PVs in developing human neurons and consequently the amount of the presynaptic material arrives at the mature synapses also decreases. Next we asked whether Arl8a/b loss affects activity of iNs. Neuronal activity causes rapid changes in intracellular free calcium. To track and image the activity of human neurons, we used an ultra-sensitive protein calcium probe (GCaMP7f) fused to a specific protein-based binder of PSD-95 (Xph20) (Rimbault et al., 2021). This allowed us image neuronal activity in a targeted and

## Results

regulated manner since GCaMP7 was enriched at the synapses and the expression of the sensor was regulated by a regulation system that was designed to avoid overexpression of the synthetic binder compared to its endogenous target. Mature iNs were transfected at day 30 and stimulated and imaged at day 34. A 10 Hz stimulation was applied for 10 seconds resulting a plateau in the fluorescence levels. Changes in total calcium influx upon stimulation at 10 Hz for 10 seconds were determined by measuring the area under the curve (AUC), which was significantly reduced in *Arl8a/b* dKO iNs (**Figure 4.19**). Importantly, initial calcium levels (pre-stimulation) were not significantly different in the two conditions.

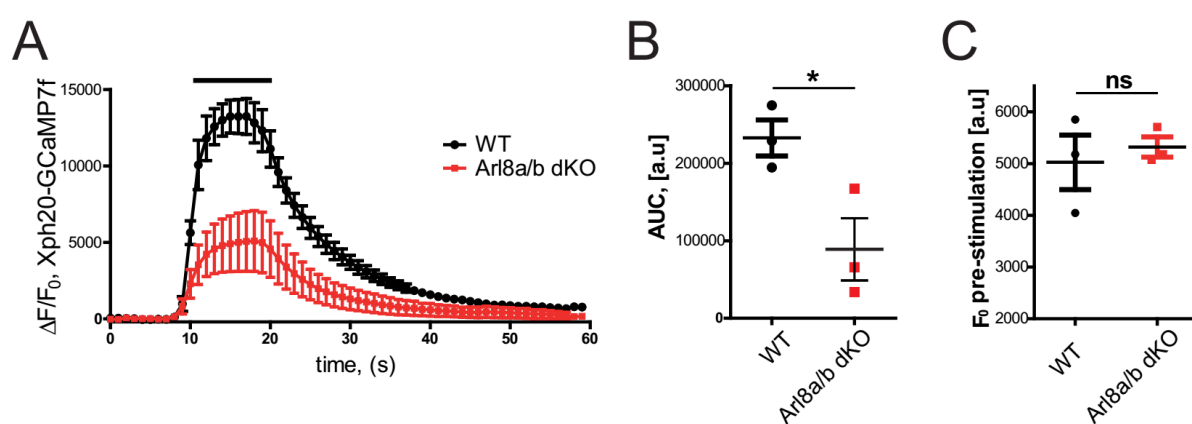


**Figure 4.19. Postsynaptically localized calcium probe Xph20-CGAMP7f reveals that upon 100 AP stimulation  $Ca^{++}$  levels are significantly decreased in *Arl8a/b* dKO iNs at DIV 34.** (A) Mean  $\Delta F/F_0$  response of Xph20-CGAMP7f to 100 AP (10 Hz, 10s) stimulation in WT or *Arl8a.b* dKO iNs. Black line indicates duration of stimulation. (B) Area under the curve (AUC) significantly decreased upon loss of *Arl8a/b*. WT:  $232.658 \pm 23.222$ ; *Arl8a/b* dKO:  $88.943 \pm 40.199$ . (C) Basal  $Ca^{++}$  levels were not altered upon *Arl8a/b* depletion. WT:  $5025 \pm 527.1$ ; *Arl8a/b* dKO:  $5320 \pm 196.3$ . All data represent mean  $\pm$  SEM.

## Results

---

### 4.6. KIF1A drives the transport of synaptic PVs via its interaction with Arl8 and PI(3,5)P<sub>2</sub>

#### 4.6.1. PH domain of KIF1A is essential for driving anterograde transport of PVs

To elucidate the cell biological identity of presynaptic transport organelles, I initially aimed to identify marker proteins that are specific to PVs. Although MS/MS of KIF1A identified many interesting interaction partners, attempts for detecting a candidate for such a marker remained unsuccessful. On the other hand, KIF1A could not transport PVs towards axon terminals when lacking its PH domain. For that experiment, I generated a KIF1A construct lacking the C terminal PH domain. I transfected WT or KIF1A KO iNs either with full-length KIF1A or with PH-lacking dPH-KIF1A. After 24 hours dPH-KIF1A did not rescue the transport deficit caused by KIF1A loss (**Figure 4.10**). This indicated an important role of the PH domain of KIF1A in directing its cargo recognition and transport. In fact, if the PH domain indeed binds to specific phospholipids as previously shown (Klopfenstein and Vale, 2004), it could unravel the lipid identity of the transport organelles.

When KIF1A-dPH was expressed in WT iNs, the membrane-localization of full-length KIF1A was completely lost and KIF1A was instead dispersed in the axoplasm (**Figure 4.20 a and b**). Another construct containing only the C terminal part, starting from the CC3 domain ending with the PH domain of KIF1A (named KIF1A-tail), however, resulted in very striking membrane localization, verifying that this part of the protein is crucial for recruitment of KIF1A to its cargoes. It also showed very high levels of co-transport with its cargo, Syp-RFP vesicles. Thus, KIF1A indeed either failed to recognize its cargo or could not bind to membranes without its PH domain.

## Results

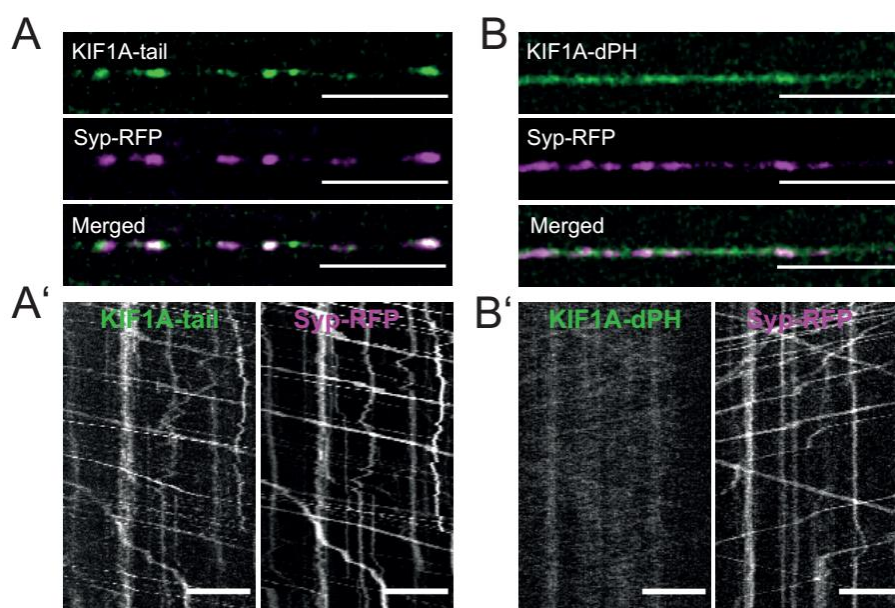


**Figure 4.20. Lipid binding PH domain of KIF1A is required for membrane recruitment.** (A, B, A' and B') WT iNs are transfected either with KIF1A-tail and Syp-RFP (A and A') or with KIF1A-dPH and Syp-RFP (B and B') and imaged 24h post-transfection. Morphology of KIF1A domains in developing iN axons (A and B) and kymographs belonging to the same axons are shown. X axis represent distance (Direction right: Anterograde) and Y axis represent time (1 min). (Scale bars, 10  $\mu$ m.)

### 4.6.2. A PIP Kinase inhibitor screen reveals specific phosphoinositides recognized by the PH domain of KIF1A

Our next question concerned the specific lipid identity of the transport organelles. If the PH domain indeed binds to specific PIPs, PVs are also expected to co-transport with them in developing axons. To address this, I first overexpressed previously validated PIP sensors together with presynaptic proteins in developing iNs to observe any axonal co-transport events. I used EGFP-FYVE-FYVE (Hrs), a PI(3)P sensor, PH-PH (FAPP), a PI(4)P sensor, and EGFP-PH-PH (PLC d), a sensor for PI(4,5)P<sub>2</sub> (**Figure 4.21**). While PI(4)P localization was restricted to somatodendritic regions and almost completely absent from axons and therefore resulted in no axonal co-transport with Syp, PI(3)P and PI(4,5)P<sub>2</sub> were detected in all cellular compartments. Occasional axonal co-transport of PI(3)P and Syp was observed. The PI(4,5)P<sub>2</sub> signal was too dispersed to detect any co-transport events as it labelled the whole plasma membrane, thus no specific co-transport with Syp was detected.

## Results

---

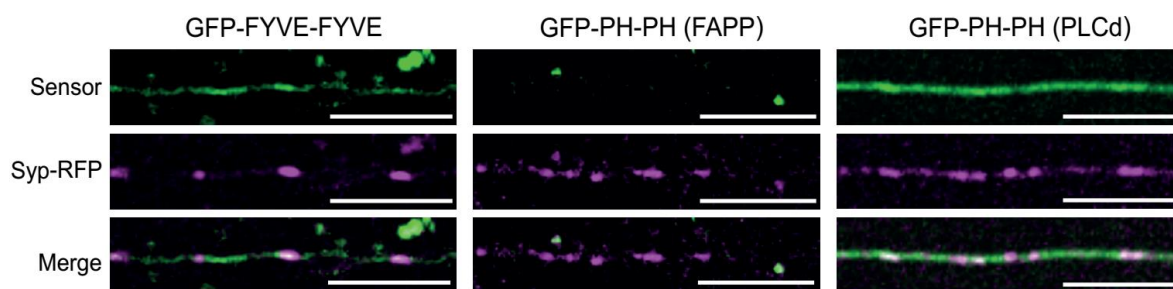


**Figure 4.21.** PIP sensors were screened to detect levels of co-transport between Synaptophysin and PI(3)P, PI(4)P or PI(4,5)P<sub>2</sub>. Syp-RFP was co-expressed in developing iNs either with the PI(3)P sensor GFP-FYVE-FYVE, the PI(4)P sensor GFP-PH-PH (FAPP) or the PI(4,5)P<sub>2</sub> sensor GFP-PH-PH (PLCd). (Scale bars, 10  $\mu$ m.)

Attempts for detecting co-transport event using PIP sensors did not lead to any conclusions regarding a potential PIP identity of PVs. Thus, to determine whether PV transport is affected by specific loss of any PIP, I then set up a lipid kinase inhibitor screen. I treated Syp-eGFP KI iNs with three different previously validated inhibitors against VPS34 to deplete PI(3)P: VPS34IN1, SAR405 and Compound19. Next, I used an inhibitor against PI4KIII $\beta$  to deplete PI(4)P, an inhibitor against PIKfyve to deplete levels of PI(3,5)P<sub>2</sub> and three inhibitors against PI4P5K to deplete PI(4,5)P<sub>2</sub>. The number of anterogradely transported Syp vesicles were significantly decreased in case of either PI(3)P or PI(3,5)P<sub>2</sub> depletion whereas other treatments did not change the ratios of antero- or retrogradely transporting vesicles (**Figure 4.22 a and b**).

## Results

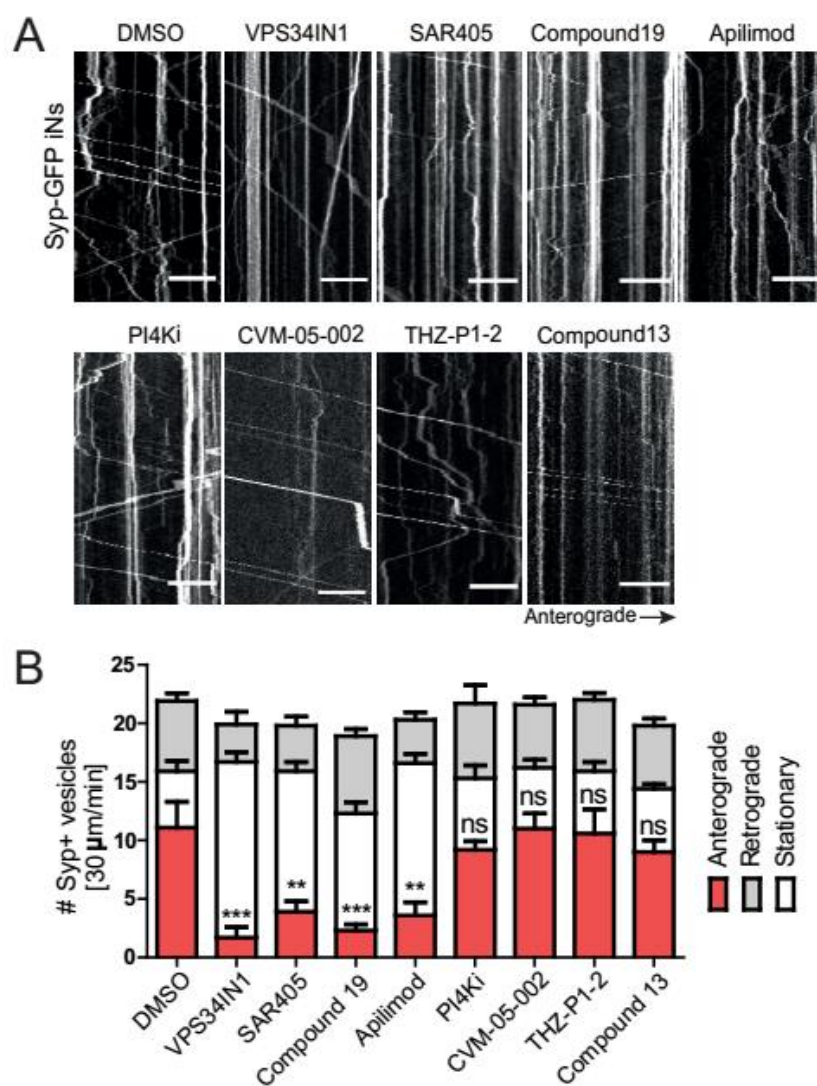


**Figure 4.22. Depletion of PI(3)P or PI(3,5)P<sub>2</sub> levels inhibits anterograde transport of endogenous Syp vesicles in developing iNs.** (A) Lipid kinases producing specific PIPs were inhibited using pharmacological treatments. Kymographs show endogenous Syp-eGFP vesicles upon each treatment. X axis represent distance (Direction right: Anterograde) and Y axis represent time (1 min). (Scale bars, 10 μm.) iNs were incubated with the inhibitors for 30 minutes at following concentrations: VPS34IN1 (10 μM), SAR405 (3 μM), Compound 19 (3uM), Apilimod (100 nM), PI4KIIIβ-inhibitor (PIKi) (2 μM), CVM-05-002 (10 μM), THZ-P1-2 (1 μM), Compound 13(10 μM). (B) Quantification of endogenous Syp-eGFP vesicles moving anterogradely or retrogradely or remaining stationary. Bars show average number of Syp vesicles per video (2 minutes) over 30 μm length of axon. Quantifications of the number of anterogradely transporting Syp vesicles per video: DMSO, 11.10 ± 2.205; VPS34-IN1, 1.700 ± 0.888; SAR405, 3.900 ± 0.9000; Compound19, 2.300 ± 0.5148; Apilimod, 3.600 ± 1.122; PI4Ki, 9.200 ± 0.7348; CVM-05-002 11.000 ± 1.304; THZ-P1-2, 10.60 ± 2.064; Compound19, 9.000 ± 1.000. (n = 5 independent experiments with ≥ 6 videos per experiment; one-way analysis of variance (ANOVA) followed by Dunnett's post-test; p<0.0001 \*\*\*\*; p<0.01 \*\*; p>0.05 ns). Data represent mean ± SEM.

## Results

---

This finding narrowed the possible specific PIPs on PVs recognized by KIF1A to two, being either PI(3)P or PI(3,5)P<sub>2</sub>. MS/MS analysis of KIF1A IP in developing neurons revealed PIKfyve, the kinase which produces the PI(3,5)P<sub>2</sub>, as an interaction partner of KIF1A (**Table 4.1**), suggesting a possible link between PIKfyve and KIF1A. To test whether PIKfyve plays a role in KIF1A function via its enzymatic activity, iNs were transfected with KIF1A-tail and Syp-RFP constructs and live-imaged 24 hours later after being treated for 30 minutes with DMSO, VPS34-IN1 or Apilimod. Under steady-state conditions, the KIF1A-tail is associated with membranes and shows a vesicular pattern. However, a remarkable portion of the expressed KIF1A-tail dispersed into the axoplasm after Apilimod treatment for 30 minutes, depleting the membrane-associated KIF1A by 50% (**Figure 4.23**). Of note, this deficiency in membrane recruitment was not observed upon treatment with VPS34 inhibitor VPS34-IN1.

The number of KIF1A vesicles also slightly and insignificantly decreased upon VPS34-IN1 treatment, which likely reflects that PI(3)P serves as a substrate for PI(3,5)P<sub>2</sub> synthesis. Therefore, diminished anterograde transport of PVs upon VPS34 inhibition could be an indirect effect due to eventual loss of PI(3,5)P<sub>2</sub> levels.

Similar to the observation in developing iNs, time-lapse confocal imaging of HeLa cells expressing KIF1Atail-GFP were treated with DMSO or Apilimod. Approximately 20 minutes after the addition of Apilimod into the imaging buffer, KIF1Atail-GFP started to solubilize and at the end of the 30 minute treatment it almost completely dispersed into cytoplasm, whereas it remained vesicular in the DMSO condition (**Figure 4.23 e**). These results suggest that removal of KIF1A from membranes as a result of the PI(3,5)P<sub>2</sub> depletion upon Apilimod treatment is observed in different cells, and is not limited to neurons.

## Results

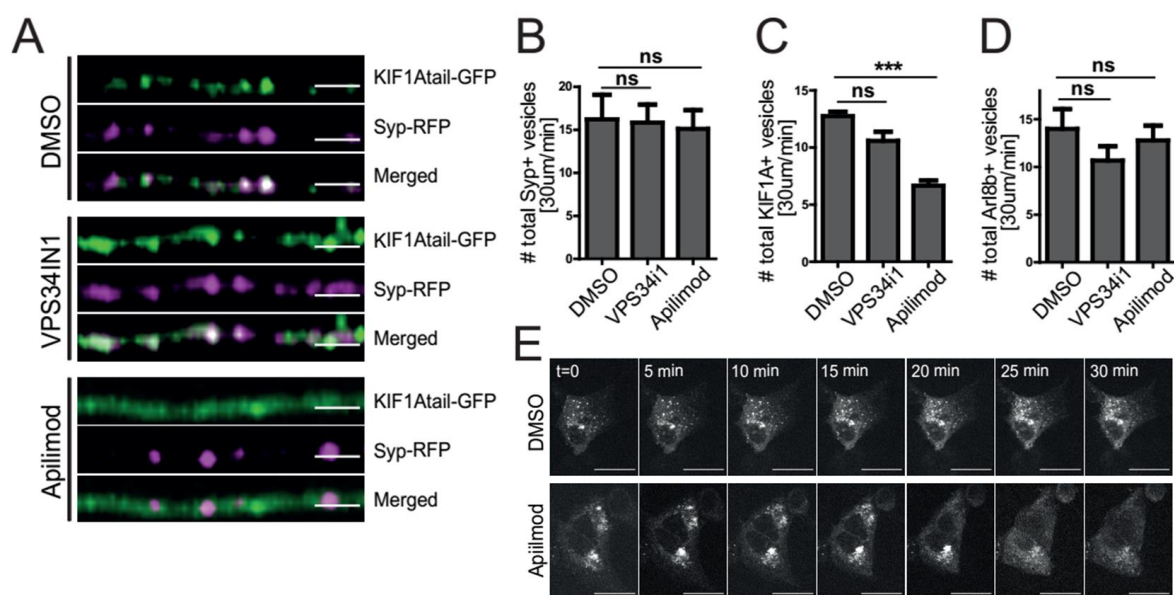


**Figure 4.23. KIF1A cannot be recruited to membranes of PVs upon Apilimod treatment.** (A) Axons transfected with Syp-RFP and KIF1Atail-GFP and incubated with DMSO, VPS34-IN1 or Apilimod for 30 minutes before imaging. DMSO and VPS34-IN1 conditions demonstrate vesicular KIF1Atail-GFP localization in the axons whereas Apilimod treatment leads to dispersion of KIF1Atail in axoplasm. (Scale bars, 2.5 µm.) (B, C and D) Quantifications of total number of (anterogradely or retrogradely moving or stationary) vesicles upon different inhibitor treatments. Bars represent average number of total vesicles per video (2 minutes) over 30µm length of axons. (B) Total number of Syp-RFP vesicles: DMSO, 16.22 ± 2.850; VPS34-IN1, 15.83 ± 2.088; Apilimod, 15.10 ± 2.178. (C) Total number of KIF1A-eGFP vesicles: DMSO, 12.75 ± 0.3819; VPS34-IN1, 10.58 ± 0.7949; Apilimod, 6.667 ± 0.4410. (D) Total number of Arl8b-mCherry vesicles: DMSO, 14.00 ± 2.082; VPS34-IN1, 10.67 ± 1.503; Apilimod, 12.78 ± 1.556). (n = 3 independent experiments with ≥ 8 videos per experiment; one-way analysis of variance (ANOVA) followed by Dunnett's post-test; p<0.0001 \*\*\*\*; p<0.01 \*\*; p>0.05 ns). Data represent mean ± SEM. (E) Time-lapse confocal microscopy demonstrating the localization of KIF1Atail-GFP construct in HeLa cells upon 30-minute incubation with DMSO or 100 nM Apilimod.

To test whether the striking reduction in KIF1A membrane recruitment upon depletion of PI(3,5)P<sub>2</sub> is conserved between different species, I repeated the experiment using mouse hippocampal neurons under the same conditions. Very similar to what has been observed in human iNs, KIF1A dissociated from Syp-positive PVs after 30 minutes of incubation with Apilimod (**Figure 4.24**) whereas it remained attached to Syp-positive membranes in cells treated with DMSO or VPS34-IN1, verifying that PI(3,5)P<sub>2</sub> is essential for membrane binding of KIF1A.

## Results

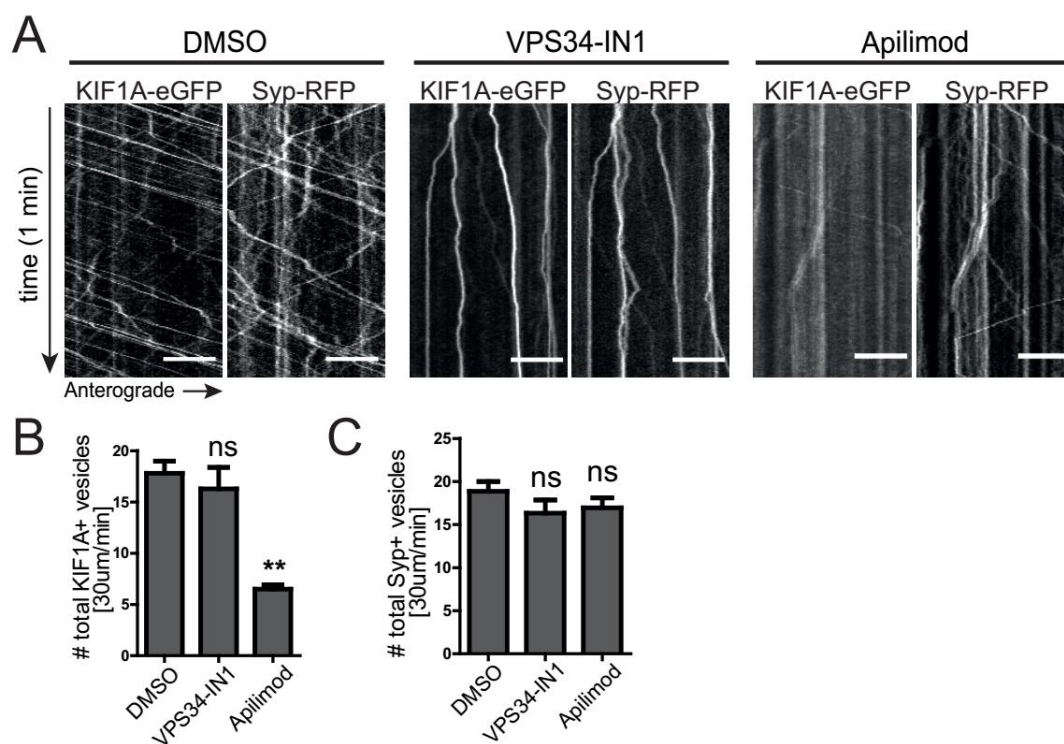


**Figure 4.24. Primary hippocampal neurons confirm the reduction of KIF1A membrane recruitment upon Apilimod treatment.** (A) Lipid kinases VPS34 and PIKfyve producing PI(3)P and PI(3,5)P<sub>2</sub> were inhibited using VPS34-IN1 (1  $\mu$ M) or Apilimod (100 nM) for 30 minutes. Kymographs show KIF1A<sub>tail</sub>-GFP and Syp-RFP vesicles upon each treatment. X axis represent distance (Direction right: Anterograde) and Y axis represent time (1 min). (Scale bars, 10  $\mu$ m.) (B and C) Quantification of Syp (B) or KIF1A (C) vesicles moving anterogradely or retrogradely or remaining stationary. Bars show average number of vesicles per video (2 minutes) over 30  $\mu$ m length of axon. (B) Total number of KIF1A-eGFP vesicles: DMSO, 17.80  $\pm$  1.193; VPS34-IN1, 16.28  $\pm$  2.096; Apilimod, 6.500  $\pm$  0.4194 (C) Total number of Syp vesicles: DMSO, 128.87  $\pm$  1.129; VPS34-IN1, 16.33  $\pm$  1.528; Apilimod, 16.94  $\pm$  1.156. (n = 3 independent experiments with  $\geq$  6 videos per experiment; one-way analysis of variance (ANOVA) followed by Dunnett's post-test; p<0.0001 \*\*\*\*; p<0.01 \*\*; p>0.05 ns). Data represent mean  $\pm$  SEM.

## Results

### 4.6.3. Lentiviral knockdown of PIKfyve verifies that PI(3,5)P<sub>2</sub> is essential for PV transport

The use of pharmacological inhibitors to manipulate certain molecules and signaling pathways in cells, albeit being advantageous in screening for fast and robust effects, has limitations in terms of enzyme specificity and possible off-target effects. To investigate results of PI(3,5)P<sub>2</sub> loss more specifically, I carried out genetic manipulations and generated lentiviral shRNAs against the kinase which produces this phosphoinositide, PIKfyve, and imaged iNs following their co-transfection with plasmids expressing KIF1A<sub>tail</sub>-GFP and Syp-RFP (**Figure 4.25**).

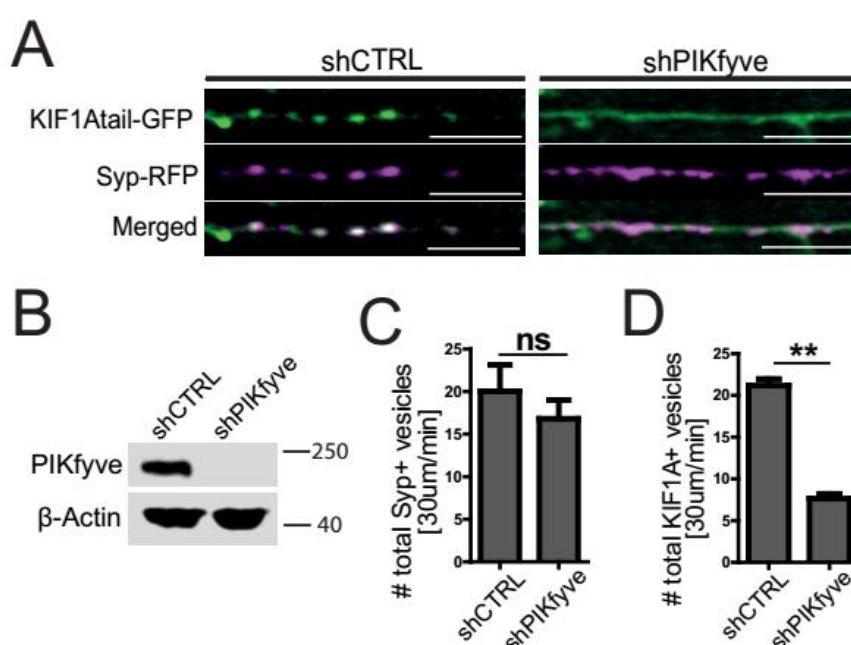


**Figure 4.25. Lentiviral knockdown of PIKfyve inhibits recruitment of KIF1A to membranes of precursor vesicles.** (A) Axons demonstrating localization of KIF1A and Syp in cells under shCTRL or shPIKfyve conditions. iNs at day 12 were transfected with Syp-RFP and KIF1A<sub>tail</sub>-GFP and imaged 24h post-transfection. Upon PIKfyve knockdown a high portion of the expressed KIF1A dispersed into axoplasm. (Scale bars, 10  $\mu$ m.) (B) Comparative Western Blot analysis of iNs transduced with lentivirus encoding either control shRNA or shRNA against PIKfyve at day 1 and lysed at day 15 confirmed the successful depletion of PIKfyve levels upon its knockdown. Detection of  $\beta$ -Actin served as loading control. Molecular weights are indicated on the right in kilodaltons (kDa). (C and D) Quantifications of total number of Syp or KIF1A vesicles moving anterogradely, retrogradely or remaining stationary. Bars show average number of vesicles per video (2 minutes) over 30  $\mu$ m length of axon. (C) Total Syp vesicles: shCTRL, 20.02  $\pm$  3.082; shPIKfyve, 16.81  $\pm$  2.186. (D) Total KIF1A vesicles: shCTRL, 21.17  $\pm$  0.7719; shPIKfyve, 7.643  $\pm$  0.5548. (n = 3 independent experiments with  $\geq$  8 videos per experiment; t test; \*P < 0.05). Data represent mean  $\pm$  SEM.

## Results

---

Supporting our previous observations using the PIKfyve inhibitor Apilimod, knockdown of PIKfyve in iNs also lead to a significant decrease in the total number of KIF1A positive organelles in the axons (**Figure 4.25**). In fact, the effect was even more striking in case of genetic loss of PIKfyve. As expected, Syp remained on membranes but failed to be anterogradely transported (**Figure 4.25**). This finding confirmed that axonal transport and KIF1A localization phenotypes previously observed in iNs treated with Apilimod are specific effects caused by PI(3,5)P<sub>2</sub> depletion.

### 4.6.4. Liposome sedimentation assays show that the KIF1A PH domain directly binds to PI(3,5)P<sub>2</sub>

Demonstrating the decrease in KIF1A membrane recruitment by lack of PI(3,5)P<sub>2</sub> directly by *in vitro* biochemical assays would uncover the phosphoinositide binding preference of the PH domain. To get an initial hint on potential lipid binding preferences of this domain, I performed a PIP-strip assay, in which the PIP-strip membrane containing different phosphoinositides was incubated with the purified GST-PH-PH (KIF1A) domain. Binding was detected using an antibody against GST (**Figure 4.26 a and b**). The experiment showed weak binding of the PH domain to PI(4)P, PI(5)P, PI(3,4)P<sub>2</sub> and PI(4,5)P<sub>2</sub> and stronger binding to PI(3,5)P<sub>2</sub> and PI(3,4,5)P<sub>3</sub>. No binding was detected for PE, PC or PS. Overall, while validating that some portion of the PH domain can bind to phosphoinositides, the PIP-strip approach remained insufficient in revealing specific binding preferences of the PH domain of KIF1A.

## Results

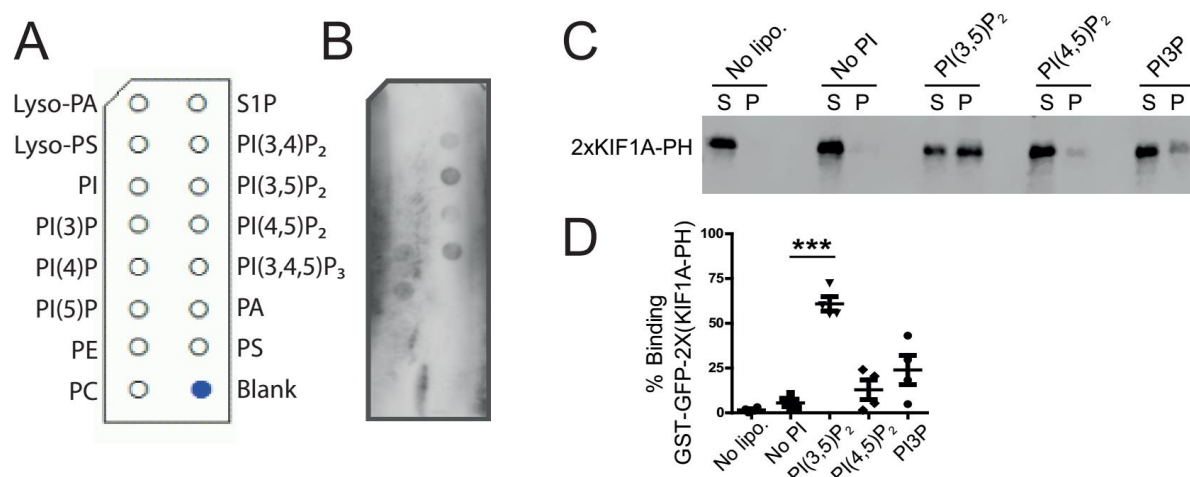


**Figure 4.26. PI(3,5)P<sub>2</sub> binding of KIF1A PH domain was verified by *in vitro* assays.** (A) PIP-Strip membrane was incubated with 0.5 µg/ml of purified GST-GFP-PH-PH (KIF1A) domain. Different lipids on the membrane were shown on the left and right hand sides of lipid dots. (B) After incubation with domain and detection with GST antibody, PIP-Strip membrane showed interactions of PH domain with PI(3,5)P<sub>2</sub>, PI(3,4,5)P<sub>3</sub> and to a lower extent with PI(4)P, PI(5)P, PI(3,4)P<sub>2</sub> and PI(4,5)P<sub>2</sub>. (C) Representative blot from liposome-sedimentation assay demonstrating that purified GST-GFP-PH-PH (KIF1A) domain interacts strongly with PI(3,5)P<sub>2</sub>. (S: supernatant, P: pellet) (D) Quantifications of liposome sedimentation assay show significant binding to PI(3,5)P<sub>2</sub> (No liposomes, 1.665 ± 0.6454%; No PI, 5.527 ± 2.065%; PI(3,5)P<sub>2</sub>, 60.86 ± 4.026%; PI(4,5)P<sub>2</sub>, 12.88 ± 5.525%; PI(3)P, 23.97 ± 8.144% (n = 4 independent experiments; one-way analysis of variance (ANOVA) followed by Dunnett's post-test; p<0.0001 \*\*\*\*; p<0.01 \*\*; p>0.05 ns). Data represent mean ± SEM.

To determine the binding preference of KIF1A more specifically, I performed a liposome pelleting assay where I prepared liposomes containing PC, PS, PE, Cholesterol and 10% PIPs (PI(3,5)P<sub>2</sub>, PI(4,5)P<sub>2</sub> or PI(3)P). Following incubation of the purified domain with liposomes and ultracentrifugation, the fraction of the domain interacting with PIPs was found in the pellet whereas the non-interacting fraction of the protein remained in the supernatant part (**Figure 4.26 c and d**). A negative control without any liposomes verified that no portion of the domain was found in the pellet independent of the presence of liposomes. Another negative control where the PH domain was incubated with liposomes containing no PIPs further validated that there was no non-specific binding to other components of liposomes. To quantify the binding ratios, the fraction of the domain detected in the pellet was divided by the total amount of protein (supernatant + pellet). These results demonstrated that the KIF1A PH domain had a strong preference for binding to PI(3,5)P<sub>2</sub> with 70% of the protein ending up in the pellet fraction, which was followed by PI(3)P with 25% and PI(4,5)P<sub>2</sub> with 10%. The only

## Results

---

significant enrichment in the pellet fraction was detected in case of liposomes containing PI(3,5)P<sub>2</sub>, confirming that the PH domain of KIF1A specifically recognizes and interacts with PI(3,5)P<sub>2</sub>.

### 4.7. PIKfyve activity is required for anterograde PV transport

#### 4.7.1. KIF1A requires Arl8 and PI(3,5)P<sub>2</sub> to drive anterograde transport of PVs in developing neurons

The neuronal kinesin KIF1A, together with the lysosomal small GTPase Arl8 and the endosomal phosphoinositide PI(3,5)P<sub>2</sub> are markers for presynaptic PVs in developing iNs. A central question therefore is how they regulate the PV transport. To gain more insights into how these proteins interact with PLVs and regulate their transport, I performed live-imaging experiments using KIF1A KO or Arl8a/b dKO iNs.

First, I co-transfected WT or Arl8a/b dKO iNs with plasmids expressing KIF1A<sub>tail</sub>-GFP and Syp-RFP at day 12. Following imaging of axonal transport of both proteins, quantifications showed, similar to the results obtained upon depletion of PI(3,5)P<sub>2</sub>, a significant inhibition in membrane recruitment of KIF1A. As seen in the axon images (**Figure 4.27a**), Arl8a/b dKO caused KIF1A<sub>tail</sub>-GFP to be mainly dispersed in the axon, indicated by its decreased co-localization with Syp-labeled membranes. In fact, the remaining membrane-bound KIF1A decreased by 50% compared to the initial population of KIF1A positive vesicles (**Figure 4.27 b**). To validate that this decrease in membrane-bound KIF1A was due to Arl8 loss, I co-transfected the Arl8a/b dKO iNs with either the constitutively active Arl8b(QL)-Myc or the GDP-locked Arl8b(TN)-Myc expressing plasmids. Membrane-binding deficiency observed in KIF1A<sub>tail</sub>-GFP was completely rescued when a GTP-locked Arl8b mutant was co-expressed whereas the phenotype was not rescued using the GDP-locked form of Arl8b was used. This result showed that KIF1A does not only require the presence of PI(3,5)P<sub>2</sub> on PLVs but also the presence of Arl8 on them. In addition, the GTP binding of Arl8 is essential for KIF1A to drive the anterograde axonal transport. Therefore, Arl8 should act upstream of KIF1A to enable its binding to PLVs to consequently drive their anterograde axonal transport.

## Results

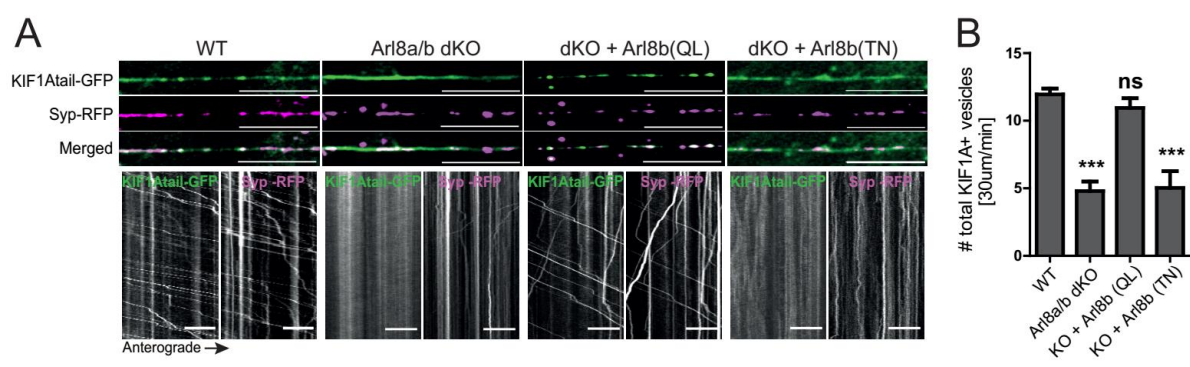


**Figure 4.27. Membrane recruitment of the tail domain of KIF1A is inhibited by Arl8a/b loss.** (A) Upper panel: axons demonstrating localization of KIF1Atail and Syp in WT or Arl8a/b dKO iNs. iNs at day 12 were co-transfected either only with Syp-RFP and KIF1Atail-GFP or additionally with GTP-locked Arl8b (QL) or GDP-locked Arl8b (TN) and imaged 24h post-transfection. (Scale bars, 10  $\mu$ m.) Lower panel: kymographs showing movements of KIF1Atail-GFP and Syp-RFP vesicles under each condition. X axis represent distance (Direction right: Anterograde) and Y-axis represent time (1 min). (Scale bars, 10  $\mu$ m.) (B) Quantifications show that the number of KIF1A vesicles significantly decrease upon Arl8 a/b depletion. Bars demonstrate average number of vesicles per video (2 minutes) over 30  $\mu$ m length of axon. Total KIF1A vesicles: WT,  $11.95 \pm 0.4311$ ; Arl8a/b dKO,  $4.800 \pm 0.7000$ ; dKO + Arl8b (QL),  $10.95 \pm 0.7089$ ; dKO + Arl8b (TN),  $5.028 \pm 1.236$  ( $n = 3$  independent experiments with  $\geq 6$  videos per experiment; one-way analysis of variance (ANOVA) followed by Dunnett's post-test;  $p < 0.0001$  \*\*\*\*;  $p < 0.01$  \*\*;  $p > 0.05$  ns). Data represent mean  $\pm$  SEM.

Next, we asked whether Arl8b also requires KIF1A activity to localize efficiently on vesicle membranes. If that were the case, one would expect a decrease in Arl8 positive vesicles upon KIF1A loss. To test this, I co-transfected developing WT or KIF1A KO iNs with Syp-GFP and Arl8b-mCherry plasmids and analyzed axonal localization of Arl8b in each condition. Albeit a slight decrease of the number of vesicles was observed, Arl8b-mCherry mostly remained membrane-bound upon KIF1A loss (**Figure 4.28**), indicating that KIF1A is not essential for Arl8 membrane localization. Of note, Syp transport was dramatically affected by KIF1A loss and anterograde transport was re-stored by overexpression of KIF1A in KIF1A KO cells (**Figure 4.28 a**).

Altogether these results indicate that, whereas KIF1A requires GTP binding of Arl8 to be successfully recruited to presynaptic precursor vesicles, membrane recruitment of Arl8 does not depend on the presence of KIF1A, placing Arl8 upstream to KIF1A in the PV transport machinery.

## Results

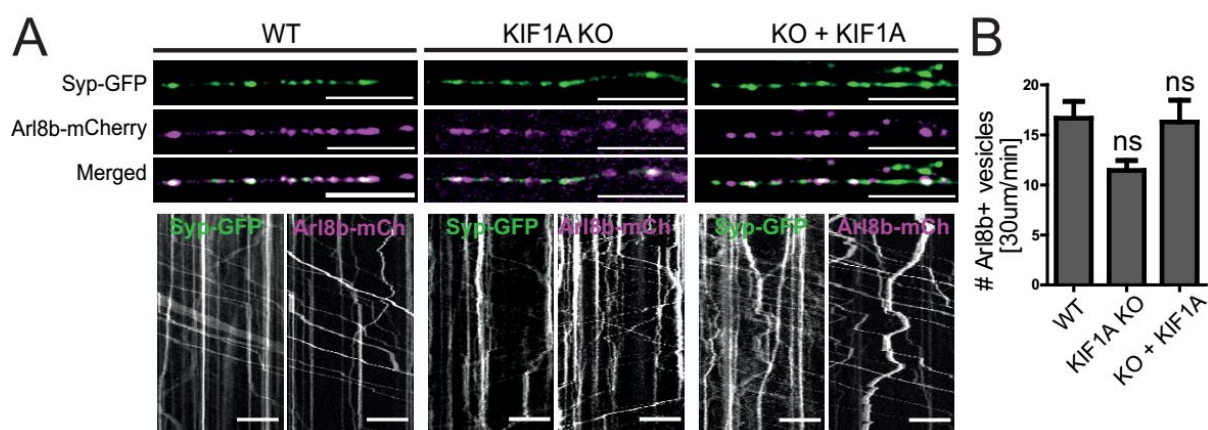


**Figure 4.28. Number of Arl8b positive vesicles in the axons are not altered with KIF1A loss.** (A) Upper panel: axons demonstrating localization of Syp and Arl8b in WT or KIF1A KO iNs. Neurons at day 12 were co-transfected either with only Syp-GFP and Arl8b-mCherry or with also KIF1A-Myc and imaged 24h post-transfection. (Scale bars, 10  $\mu$ m.) Lower panel: kymographs showing movements of Syp-GFP and Arl8b-mCherry vesicles in each condition. X-axis represent distance (Direction right: Anterograde) and Y-axis represent time (1 min). (Scale bars, 10  $\mu$ m.) (B) Quantifications of the live imaging experiment showing that total number of Arl8b vesicles remain unaltered in KIF1A KO cells. Bars demonstrate average number of vesicles per video (2 minutes) over 30  $\mu$ m length of axon. (WT,  $16.67 \pm 1.678$ ; KIF1A KO,  $11.44 \pm 0.9876$ ; KO + KIF1A,  $16.28 \pm 2.182$ ;  $n = 3$  independent experiments with  $\geq 6$  videos per experiment; one-way analysis of variance (ANOVA) followed by Dunnett's post-test;  $p < 0.0001$  \*\*\*\*;  $p < 0.01$  \*\*;  $p > 0.05$  ns). Data represent mean  $\pm$  SEM.

Finally, I investigated whether Arl8 also, similar to KIF1A, requires PI(3,5)P<sub>2</sub> to bind to membranes. I transfected WT iNs with Arl8b and repeated the PIKfyve inhibition experiment using Apilimod treatment (**Figure 4.23 d**). Quantification for Arl8b labelled vesicles in axons showed no change in total number of vesicles upon neither VPS34-IN1 nor Apilimod treatment. Thus, presence of KIF1A or PI(3,5)P<sub>2</sub> are both dispensable for Arl8 recruitment to presynaptic precursor transport organelles.

## Results

---

### 4.7.2. Depletion of BORC induces anterograde PV transport by increasing PI(3,5)P<sub>2</sub> levels

BORC is a multi-subunit complex that regulates lysosomal motility in cells through activating Arl8. Previously we found that loss of BORC activity did not affect axonal transport dynamics of PVs (**Figure 4.14**). If anything, it caused a slight increase in the anterogradely transported fraction of Syp vesicles. This unexpected finding prompted us to further investigate possible roles of BORC on PV transport. We generated lentiviral shRNAs against two subunits of BORC complex, Myrlysin and Diaskedin, which are not shared by the BLOC1 complex. Additionally we knocked down BLOS1, which is a subunit shared by BLOC1 and BORC complexes and finally we knocked down Cappucino (CNO; BLOC1S4) a subunit which is specific to BLOC1 complex and is not shared by BORC. Transport of endogenously labelled Syp vesicles were not altered upon depletion of BORC or BLOC1 subunits in WT iNs (**Figure 4.29a and b**). In iNs depleted of Myrlysin, although the Syp transport levels per se are not affected, the anterogradely moving fraction of Arl8b as well as the level of Arl8b found on vesicles decreased. In parallel with this, co-transport levels of Syp and Arl8 as well as Munc13 and Arl8 were found to be severely decreased (**Figure 4.29c and d**). This means that in neurons depleted of BORC, a large fraction of PVs are transported independently of Arl8. This suggests that either PVs are regulated via two routes, one being independent of Arl8 activity, or BORC has other roles than activating Arl8 and it can enhance the anterograde PV transport through this pathway. Since Arl8 loss depletes almost all anterograde transport of PVs, I decided to test the latter hypothesis. To this aim, I focused on the question how BORC loss might enhance PV transport in the absence of Arl8.

## Results

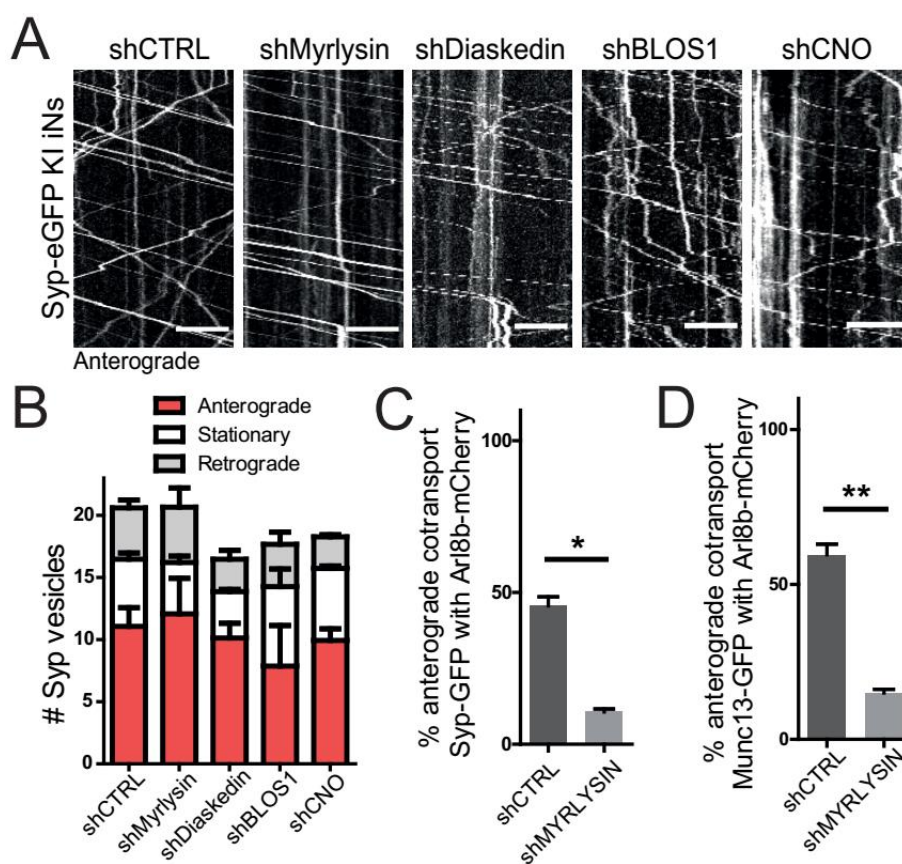


**Figure 4.29. Anterograde transport of PVs is unaltered upon shRNA-mediated depletion of BORC subunits.**

(A) Kymographs demonstrate transport of endogenous Syp-eGFP vesicles in control condition and upon knockdown of Myrlysin, Diaskedin, BLOS1 or CNO. X axis represent distance (Direction right: Anterograde) and Y-axis represent time (1 min). (Scale bars, 10  $\mu$ m.) (B) Quantifications of the number of endogenous Syp vesicles under different conditions. Bars demonstrate average number of anterogradely moving vesicles per video (2 minutes) over 30  $\mu$ m length of axon in WT iNs. Number of Syp vesicles: (shCTRL,  $11.07 \pm 1.507$ ; shMyrlysin,  $12.07 \pm 2.867$ ; shDiaskedin,  $10.13 \pm 1.179$ ; shBLOS1,  $7.867 \pm 3.275$ ; shCNO,  $10.13 \pm 0.9821$ ) (C) Quantifications of the anterogradely co-transported portion of Syp-GFP and Arl8-mCherry vesicles in WT control conditions and upon loss of Myrlysin. (shCTRL,  $45.64 \pm 2.947\%$ ; shMyrlysin,  $10.63 \pm 0.9949\%$ ) (D) Quantifications of the anterogradely co-transported portion of Munc13-GFP and Arl8-mCherry vesicles in WT control conditions and upon loss of Myrlysin. (shCTRL,  $59.59 \pm 3.420\%$ ; shMyrlysin,  $15.01 \pm 1.175\%$ ) (n = 3 independent experiments with  $\geq 6$  videos per experiment; t test; \*P < 0.05). Data represent mean  $\pm$  SEM.

## Results

---

Interestingly, loss of BORC has previously been shown to cause an increase in PI(3,5)P<sub>2</sub> levels, possibly by hyperactivating PIKfyve (Yordanov et al., 2019). Hence, a similar pathway may operate in iN and thereby regulate PV transport. To test this possibility, WT and Arl8a/b dKO iNs were first transduced with lentiviruses encoding shRNAs against control, Myrlysin, Diaskedin, BLOS1, CNO or PIKfyve sequences. At day 12 iN were transfected with Syp-RFP and KIF1A tail-GFP constructs. Following the analysis of transported vesicles, loss of Myrlysin or Diaskedin were found to indeed rescue the anterograde transport defect caused by Arl8a/b loss (**Figure 4.30a**). Importantly, the total number of KIF1A vesicles significantly decreased upon loss of Arl8a/b. Importantly, this phenotype was rescued when Myrlysin or Diaskedin were lost in addition to Arl8a/b depletion (**Figure 4.30b**). This indicates a compensatory effect of Myrlysin and Diaskedin subunits, suggesting that Arl8 loss renders neurons hypersensitive to changes in BORC. Importantly, this rescue of total membrane-bound KIF1A cannot take place when PIKfyve is depleted in Arl8a/b dKO cells, arguing that BORC acts through activating PIKfyve, placing BORC upstream of PIKfyve in the PV transport machinery.

## Results

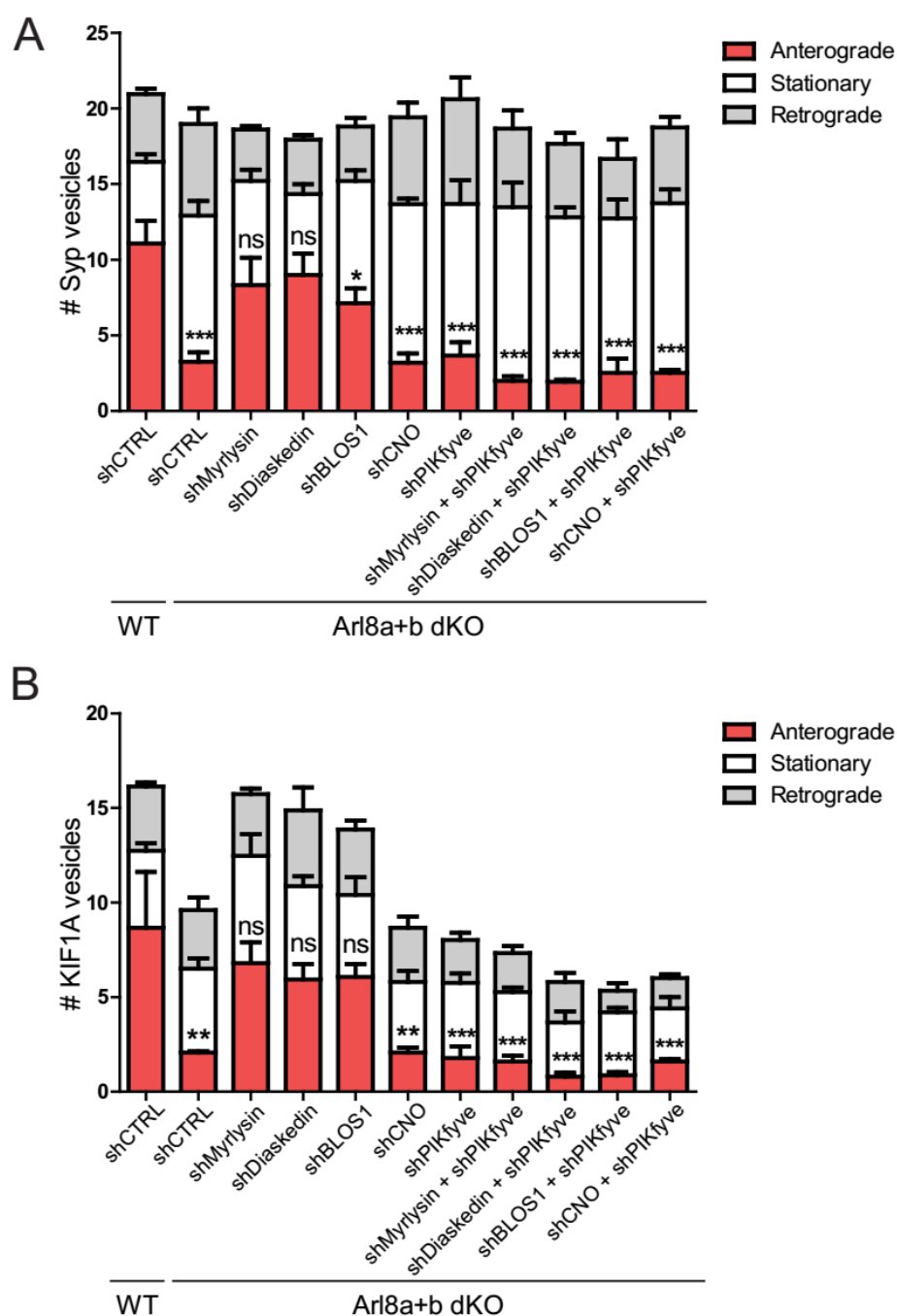


**Figure 4.30. In the absence of Arl8a/b, loss of BORC increases anterograde PV transport and membrane recruitment of KIF1A.** Quantifications of the number of Syp-RFP or KIF1Atail-GFP vesicles under different conditions. Bars demonstrate average number of anterogradely moving vesicles per video (2 minutes) over 30  $\mu$ m length of axon in Arl8a/b dKO iNs. (A) Number of Syp-RFP vesicles. (WT: shCTRL,  $11.07 \pm 1.507$ ; Arl8a+b dKO: shCTRL,  $3.250 \pm 0.6292$ ; shMyrlysin,  $8.333 \pm 1.805$ ; shDiaskedin,  $9.000 \pm 1.400$ ; shBLOS1,  $7.133 \pm 0.9821$ ; shCNO,  $3.200 \pm 0.600$ ; shPIKfyve,  $3.667 \pm 0.8819$ ; shMyrlysin + shPIKfyve,  $2.000 \pm 0.3055$ ; shDiaskedin + shPIKfyve,  $1.933 \pm 0.1333$ ; shBLOS1 + shPIKfyve,  $2.533 \pm 0.9404$ ; shCNO + shPIKfyve,  $2.533 \pm 0.1764$ ) (B) Number of KIF1A vesicles (WT: shCTRL,  $8.667 \pm 2.949$ ; Arl8a+b dKO: shCTRL,  $2.067 \pm 0.06667$ ; shMyrlysin,  $6.800 \pm 1.102$ ; shDiaskedin,  $5.933 \pm 0.8110$ ; shBLOS1,  $6.067 \pm 0.6766$ ; shCNO,  $2.067 \pm 0.2667$ ; shPIKfyve,  $1.778$

## Results

---

$\pm 0.6186$ ; shMyrlysin + shPIKfyve,  $1.600 \pm 0.3055$ ; shDiaskedin + shPIKfyve,  $0.800 \pm 0.2000$ ; shBLOS1 + shPIKfyve,  $0.8667 \pm 0.1764$ ; shCNO + shPIKfyve,  $1.600 \pm 0.1155$ ) ( $n = 3$  independent experiments with  $\geq 6$  videos per experiment; one-way analysis of variance (ANOVA) followed by Dunnett's post-test;  $p < 0.0001$  \*\*\*\*;  $p < 0.01$  \*\*;  $p > 0.05$  ns). Data represent mean  $\pm$  SEM.

Moreover, **Figure 4.30** demonstrates that although the total number of Syp vesicles remains constant, the number of anterogradely transported Syp vesicles change similar to KIF1A vesicles. In WT cells depletion of different subunits of BORC does not affect anterograde transport, whereas in Arl8a/b dKO cells depletion of Myrlysin or Diaskedin rescues diminished anterograde transport to WT levels. Importantly, this rescue does not happen when PIKfyve is lost. Whether BORC loss results in a direct hyperactivation of PIKfyve, or it leads to an increase in PI(3,5)P<sub>2</sub> levels via inhibiting a phosphatase such as MTMR2, or else there is a complex mechanism regulating the lipid levels and subsequently the transport machinery remains unclear and future studies are needed to understand these molecular mechanisms.

### 5. Discussion

During the course of this work, we investigated the components of the core machinery that mediate axonal transport of presynaptic precursor organelles (PVs) in developing human neurons. I show that the lysosomal small GTPase Arl8a/b is crucial for mediating presynaptic PV transport, in coordination with the kinesin 3 family motor protein KIF1A. Importantly, KIF1A is recruited to its cargo, presynaptic PVs, via its PH domain which specifically binds to the endolysosomal phosphoinositide PI(3,5)P<sub>2</sub>. Depletion of this membrane phospholipid by inhibition or genetic depletion of PIKfyve, its upstream kinase, prevents membrane recruitment of KIF1A and consequently inhibits anterograde PV transport. Therefore, KIF1A requires to interact not only with Arl8 but also with PI(3,5)P<sub>2</sub> in order to ensure efficient cargo recruitment and successful delivery of presynaptic proteins to axon terminals. This work not only elucidates the molecular mechanisms regulating presynapse formation in developing human neurons including characterization of the transport machinery of presynaptic transport organelles in detail, but also for the first time demonstrates the phosphoinositide identity of these organelles.

#### 5.1. Different components of the presynaptic compartment are delivered collectively to axon terminals

Transport vesicles carrying presynaptic proteins to axon terminals have been long-debated. A number of studies have argued that different presynaptic components are carried on distinct vesicles to reach the presynaptic sites, and each of these different types of vesicles use distinct molecular motors and adaptor proteins to regulate their transport. For instance, some of the AZ proteins, namely Piccolo, Bassoon and RIM binding proteins, were postulated to be co-transported in 80nm diameter electron-dense Piccolo-Bassoon transport vesicles (PTVs) and these vesicles used KIF5 as their molecular motors. Other SV-associated proteins, like Syt1 and Syp, on the other hand, were claimed to be transported via SV-like smaller and clear-cored vesicles which used KIF1A to mediate their transport. Other presynaptic proteins like the AZ protein Munc13 and SV-associated protein Synapsin 1 are not contained on neither of these vesicles (Maas et al., 2012b; Shapira et al., 2003). Other, more recent studies have suggested that different components of the presynaptic compartment are likely transported together either on a single type of organelle, or on clusters of carrier organelles, the latter

## Discussion

---

being named 'presynaptic transport units' (Ahmari et al., 2000; Tao-Cheng, 2007; Vukoja et al., 2018). These studies have used live imaging and EM immunolabeling approaches to detect multiple presynaptic proteins transported in a coordinated manner along the axons of different species and have reported transport carrier aggregates in the axons containing both SV and AZ proteins (Bury and Sabo, 2011; Tao-Cheng, 2007). This hypothesis provides considerable advantage for developing neurons since a single vesicle or vesicle cluster could potentially carry the stoichiometric amounts of material to build a presynapse. Despite the undeniable contribution all these studies have provided, the presynaptic protein content and cell biological identity of these precursor carriers remain incompletely understood. In this work we have established an unbiased approach to quantitatively demonstrate the amount of co-trafficking between molecules from different presynaptic building blocks and have concluded that different presynaptic proteins co-traffic to a high extent in order to assemble a functional presynapse.

In order to study co-trafficking of presynaptic proteins, we developed and used a human stem-cell derived model system in which stem cells are directly reprogrammed into neural lineage. We used human neurons at early developing time points in which presynaptic protein expression was initiated. This system provides a number of advantages. First, by using stem-cell derived neurons we could ensure that developing neurons have never formed a synapse prior to our experiment, nor the stem cells inherited any expression of neural transcription factors by which the cells could acquire cues for synapse development. Second, we were able to design our experiments not only based on overexpression of proteins but we could also generate Crispr/Cas9 knock-in (KI) cell lines encoding endogenously tagged proteins of interest. In fact, generation of a Synaptophysin-eGFP KI iPSC line has led us monitor the endogenous Synaptophysin carrying organelles within developing human neurons for the first time. Moreover, having a model system that is amenable to genetic engineering has also helped us to study regulation of the precursor transport machinery in detail by using Crispr/Cas9 knock-out (KO) lines. Finally, to image axonal trafficking of presynaptic proteins we used a two-channel live imaging approach and developed tools for an automated analysis of trafficking events. Different from other studies, our imaging results which were plotted on kymographs were analyzed using a deep-learning based kymograph analysis tool. Trafficking events were filtered and co-trafficking events were calculated using scripts generated in this project. This approach resulted in objective conclusions of a collection of experiments.

## Discussion

---

Our trafficking experiments have shown that SV proteins are found to be co-traveling with each other towards nascent presynapses, shown by the high extent of co-transport between Syp, vGlut1 and Vamp2 proteins both at the overexpressed levels and endogenous levels. Moreover, SV proteins co-transport with the AZ proteins Bassoon and Munc13 with a co-transport rate of higher than 94% in case of either protein. Interestingly, the SV protein Syp also co-transport to a very high extent with the synaptic adhesion molecule Nrxa1 $\beta$  (co-transport rate higher than 88%). These results clearly demonstrate that proteins belonging to different building blocks of the presynapse are in fact present on the same vesicles or clusters of vesicles and carried along the developing axons to build a presynaptic compartment, thereby supporting the *transport packet model*. The difference in rates of co-transport between different presynaptic proteins, especially when taking their different copy numbers into consideration, suggests a heterogeneous population of PVs, most of which carrying both SV proteins, AZ proteins and sCAMs; some having low amount of AZ proteins; and some only carrying SV proteins. Recently a minor fraction of AZ proteins have been shown to be synthesized by local translation at close proximity to the presynaptic compartment (Hafner et al., 2019), although this has only been reported at mature synapses undergoing plastic modulation. Therefore, further analyses are needed to understand whether local protein synthesis can also supply AZ proteins at nascent synapses during development.

Our results are contradictory to several previous studies which have argued for the transport of SV and AZ proteins on distinct carriers (Maas et al., 2012b; Shapira et al., 2003). It is important to note that the previous studies likely remained limited in uncovering the presynaptic material carried by the PTVs, mostly due to the limitations in molecular insights. For instance, AZ protein Bassoon and SNARE proteins Syntaxin and SNAP-25 have been reported to interact with each other but Bassoon and Synaptophysin have not. These experiments likely reflect the interactions taking place in presynaptic sites rather than carrier organelles as these organelles are of low amounts and have a rather transient nature (Shapira et al., 2003; Zhai et al., 2001). Similarly, the kinesin 1 KIF5B has been identified as the driver of PTVs solely based on interaction studies with very limited loss of function experiments. Finally, time-lapse microscopy of the axonally transported presynaptic proteins with kinesins would have been needed to strengthen the hypothesis of multiple distinct carriers. Importantly, different species and neuronal types have been used in different studies and the possibility remains that axonal transport mechanisms vary between species and neuron types. Our results, besides being compatible with many others (Bury and Sabo, 2011; Klassen et al., 2010; Tao-Cheng, 2007; Vukoja et al., 2018), remain limited to reflect a collection of

## Discussion

---

experiments performed on stem-cell derived human excitatory cortical neurons. Since these neurons essentially are derived from a cell line, it would be critical to test the main findings of this study in different organisms and different neuron types.

Presynaptic biogenesis requires all presynaptic proteins to be delivered to nascent synapses in a coordinated manner. We included many of these proteins in our study and reported that SV, AZ and nCAM proteins are transported towards axon terminals collectively on PVs by KIF1A. It is important to note that our trafficking experiments did not include Cav proteins, whose clustering at the AZ is crucial for controlling the speed and strength of neurotransmitter release. Cavs might use a different transport mechanism since the levels of Cav2.1 at the synapses of mature neurons remained unaltered upon loss of KIF1A. Compared to other presynaptic elements, there is surprisingly very little known about the transport and clustering of Cavs. Hence, studying axonal transport of Cav-carrying organelles in detail is of great importance for future studies. Interestingly, a presynaptic Neurexin, Nrnx1 $\beta$ , is trafficked together with the SV protein Syp to a very high extent in developing neurons. Axonal transport of Neurexin by KIF1A has been suggested in other recent studies (Oliver et al., 2022). However, whether Neurexins are lost from presynaptic compartments in KIF1A deficient neurons and to what extent is an important question to address in future studies, considering their roles as essential synaptic organizers.

Although with fast live-imaging we can detect whether two proteins transport together or independently along axons, confocal microscopy reaches only to resolutions of 180nm laterally and 500nm axially (Hell, 2015), which cannot separate between single PVs which are expected to be between 40 to 100nm in diameter. Therefore, from these experiments we cannot conclude whether these multiple different proteins reside on a single organelle or instead on multiple organelles that are co-transported. Similarly, we also cannot estimate the copy numbers of proteins present on transport organelles. Future experiments are needed to address these questions. For instance, super-resolution imaging on the endogenously-labeled proteins following live-fixing of anterogradely trafficking organelles would give insights into the nanoscale organization of the transport organelles as with this method 20-40 nm lateral resolution could be reached (Hell, 2015). Likewise, applying FIB-SEM on the transport organelles following live-fixation could address their ultrastructure in detail.

### 5.2. Arl8a and Arl8b regulate PV motility in developing human neurons

Arl8 is the first small GTPase that has been shown to localize to lysosomal membranes in mammalian cells. Having two isoforms in humans, Arl8a and Arl8b, it directly regulates lysosomal positioning. The striking finding that Arl8 mutant animals show presynaptic biogenesis phenotypes has featured Arl8 a novel role on the organismal level (Klassen et al., 2010; Vukoja et al., 2018). In our study we have investigated the role of Arl8 in detail using developing and mature iNs and have demonstrated that it is not only a marker of PVs but also a regulator of their transport.

Axonal co-trafficking experiments show that more than 50% of Synaptophysin-containing transport vesicles (both overexpressed and endogenous labelled) also contain Arl8. This could mean that transport vesicles exist as a heterogeneous population, some of which contain Arl8 and others not. However, the loss-of-function experiments we conducted either using lentiviral shRNAs against Arl8a and Arl8b, or Crispr KO cell lines that are completely deficient of Arl8a and Arl8b counteract this explanation. If Arl8 is present on and regulates the trafficking of only a subpopulation of vesicles, which is only around 50% of the total population, its depletion would also expectedly affect the transport of 50% of the Syp-carrying vesicles. However we did not only see an almost complete loss in the number of anterogradely transported vesicles, but also a significant depletion in the level of presynaptic material which reaches presynaptic sites and build mature synapses. Thus, it is likely that there is another upstream mechanism by which Arl8 regulates PV transport in addition to its presence on PVs. As known from previous studies, roles of Arl8 are not limited to regulating lysosomal motility but also controlling late endocytic function. While Arl8 has been shown to recruit proteins which link lysosomes to microtubule motor proteins, such as SKIP (Rosa-Ferreira et al., 2018), In *Drosophila*, GTP-bound Arl8 has also been shown to recruit lysosomes to the HOPS complex regulating lysosomal fusion events. It is likely that Arl8 is responsible for mediating a similar fusion event in the maturation process of PVs, perhaps right after their biogenesis in neuronal somata or in the AIS. Alternatively, the interaction of Arl8 with PVs might be spatiotemporally regulated, such that binding of GTPase active Arl8 is initially required for PV transport but it can later dissociate from the KIF1A/PV complex. Indeed, GTP-bound Arl8 has been previously shown to be required for initiating axonal presynaptic precursor vesicle transport in *C. elegans* by releasing KIF1A auto inhibition (Niwa et al., 2016).

## Discussion

---

Two Arl8 isoforms, Arl8a and Arl8b have more than 90% similarity at the protein level. Therefore, they might compensate for each other's loss in single knockdown or knockout conditions. Indeed, single Arl8b knockout iNs show only a mild anterograde transport phenotype (not shown), while complete loss of Arl8a and Arl8b together results in a dramatic decrease of the number of anterogradely transported PVs with only very rare anterograde transport events remaining. Furthermore, fluorescent intensities of endogenous SV and AZ markers at mature synapses decrease to less than half. Importantly both the stalled Syp transport and the depletion in the level of presynaptic material at mature synapses can be rescued with re-expression of only Arl8b from the beginning of the neuronal differentiation process. Of note, re-expression of GTPase inactive Arl8b cannot rescue either of the phenotypes, indicating that GTPase activity of Arl8 is essential to drive the transport of presynaptic PVs.

Complete Arl8 deficiency is lethal at the organism level (Hashimoto et al., 2019; Vukoja et al., 2018), however there have been Arl8 deficient cell lines reported (Guardia et al., 2016). All three Arl8a/b double KO cell lines we generated resulted in more cell death compared to WT lines when differentiated to iNs, especially during the first week of differentiation which represents the initial neuronal differentiation phase. Additionally, Arl8 dKO neurons showed reduced dendritic branching, pointing out a neurodevelopmental phenotype.

Arl8a/b dKO iNs showed a dramatic decrease in their anterograde axonal transport of PVs, confirming our observations upon lentiviral knockdown of Arl8a and Arl8b. In a recent study, Arl8 mutant *Drosophila* motoneurons showed an accumulation of presynaptic precursor vesicles in neuronal cell bodies, as a result of axonal transport deficiency (Vukoja et al., 2018). Surprisingly, Arl8a/b double KO iNs we generated did not show such somatic aggregation. This might have two main explanations. First, since differentiation of stem cells into mature neurons requires comparably long time in culture (approximately 30 days), vesicles that start to aggregate in the neuronal soma or within the AIS might get degraded. This would conceivably be a way for neurons to maintain their cellular homeostasis. To look into this in more detail, neurons could be stained for presynaptic markers following inhibition of protein degradation. Second, neurons derived from different organisms might acquire different fine-tuning of their system. For instance, previous mouse models of KIF1A<sup>-/-</sup> also reported somatic accumulation of vesicle clusters, which were not detected in our human iN model (Yonekawa et al., 1998). Lastly, our model is based on *in vitro* differentiation of a cell line, which might not fully recapitulate what is happening on an organismal level. Therefore, although the main

## Discussion

---

phenotypes reported in different model systems might be largely comparable, it should not be expected to demonstrate the exact same outcomes to the same extent.

Although we reported a significant decrease in the presynaptic SV and AZ protein levels at the synapses of Arl8a/b deficient iNs, this did not completely explain the functional importance of Arl8a/b in regulating the presynaptic assembly. We hypothesized that Arl8a/b deficiency would negatively affect the level of synaptic transmission since it would prevent accumulation of sufficient presynaptic material at mature synapses. Neural activity causes rapid changes in intracellular free calcium. Genetically encoded calcium sensors, such as GCaMPs which are a synthetic fusion of green fluorescent protein (GFP), calmodulin (CaM), and M13 (a peptide sequence from myosin light-chain kinase) are widely used to track the activity of neuronal populations and to probe excitation of neuronal compartments (Chen et al., 2013). Since we have reported that Arl8a/b loss affects only the presynaptic compartment but does not seem to affect the postsynaptic protein levels, we reasoned that the absence of Arl8a/b will have a negative impact on SVs release and consequently will reduce the  $Ca^{2+}$  influx at the postsynaptic sites. Thus, we decided to compare levels of  $Ca^{2+}$  at the postsynapse and used a calcium sensor, GCaMP7f-Xph20, localizing specifically to postsynapse. Arl8a/b deficient neurons showed a significant decrease in their total levels of stimulation-induced  $Ca^{2+}$  whereas the basal  $Ca^{2+}$  levels were unaltered; indicating that Arl8 loss indeed resulted in less glutamate release due to inadequate presynaptic SV and AZ protein accumulation in mature Arl8a/b dKO iNs

### 5.3. PVs have a lysosomal identity although they are different than *bona fide* lysosomes

The fascinating finding that Arl8 acts as a marker of PVs and regulates their trafficking has led us re-visit a crucial question: what is the cell biological nature of presynaptic transport organelles? Following their synthesis, nascent secretory proteins exit the ER and accumulate in ER-Golgi intermediate compartments distributed throughout the somatodendritic area. After their exit from this compartment, nascent proteins can take either of the two routes: They can traffic to the somatic Golgi apparatus and to Golgi outposts (GOs) in the most proximal segments of dendrites. GOs are small discrete Golgi units separated from the main perinuclear

## Discussion

---

Golgi structure. Alternatively, they may directly traffic to recycling endosomes, hence using a Golgi-independent pathway to reach the plasma membrane. Many studies in the past have claimed that PVs were Golgi-derived vesicles (Maas et al., 2012b; Shapira et al., 2003). However, this conclusion might be too general with evidence from various studies indicating involvement of other mechanisms. First, although GOs are crucial for assembly of the postsynaptic compartment (Horton and Ehlers, 2003; Horton et al., 2005), Golgi structures have only been detected in axons of the peripheral nervous system (Cornejo et al., 2020). Second, components of the endolysosomal system are found both in dendrites and in axons and there are indications that the endolysosomal system and autophagy in neurons might regulate synaptic transmitter release and participate in synaptic plasticity processes (Andres-Alonso et al., 2021; Ferguson, 2018). Third, dendrites and axons greatly differ in their immediate reliance on the secretory pathway. Disruption of Golgi function using BFA treatment or inhibitory mutants of COP I machinery components and protein kinase D (PKD) (a protein regulating membrane fission at the TGN) prevents dendritic growth and maintenance whereas they have no significant effect on axonal outgrowth (Horton et al., 2005; Ye et al., 2007).

Our results show that presynaptic Syp co-traffics with lysosomal membrane proteins such as Lamp1 and Arl8b in axons. Partial co-movement between these proteins in a retrograde fashion is expected, as this would likely reflect the portion of PVs that are delivered back to the cell body for degradation. However, the fact that lysosomal proteins and Syp start their co-transport at the AIS and move towards axon terminals together strongly suggests that they either reside on a single transport organelle or within the same organelle cluster. We show that endogenous Syp co-transport anterogradely with Lamp1 and Arl8b in more than 50% of the cases. Likewise, endogenous Lamp1 vesicles also co-transport anterogradely with SV proteins Syp and Syt1 in more than 50% of the cases. These results using endogenously labelled SV or lysosomal proteins verify previous quantifications which used overexpressed proteins. Overall, levels of co-transport between lysosomal proteins and SV proteins, both using overexpression as well as endogenous tagging, are lower than the fractions of co-transported presynaptic proteins with each other. This suggests a heterogeneity in the PV population, such that not all PVs contain lysosomal membrane proteins. One exception for this has been observed in co-transport levels between the lysosomal small GTPase Arl8 and AZ proteins Munc13 and Bassoon which showed very high anterograde cotransport rates with Arl8. This high co-trafficking between AZ proteins and Arl8 possibly stems from their low copy numbers in cells, so that almost all AZ-carrying transport vesicles also have Arl8 identity. Of note, we report that transport rates of presynaptic proteins with Arl8a or Arl8b highly similar.

## Discussion

---

Our results indicate that the transport machinery of *bona fide* lysosomes, which uses KIF5B/BORC/SKIP ensemble, does not regulate transport of PVs. Knockdown of either of these proteins neither altered the transport of endogenous Syp vesicles nor had an effect on the presynaptic material arriving at mature synapses. Contrary to these findings, genetic loss of either Arl8a/b or KIF1A greatly diminished the ratio of anterogradely moving endogenous Syp. Thus, different regulators play role in PV transport. Further experiments conducted in our lab have supported these findings. First, only less than 10% of the anterogradely-moving endogenous Syp contained lysosomal LysoTracker or SiR-Lysosome, suggesting that this fraction of Syp organelles are almost never acidic (indicated by LysoTracker activity) nor contain active Cathepsin D (sensed by SiR Lysosome) (Kong, S., 2022). Second, using a pHluorin-conjugated Lamp1 construct, we compared the pH values of somatic, anterogradely moving and retrogradely moving organelles that were co-labelled with Syp and Lamp1. Anterograde transporting population of PVs were significantly less acidic than the somatic or retrogradely transporting vesicles (Kong, S., 2022). Overall, these results indicate that presynaptic PVs, albeit containing lysosomal membrane protein identity, are distinct from lysosomes and are regulated via different mechanisms.

Another indication showing that PVs are derived from the endolysosomal system arises from their membrane identity. Anterograde PV transport is heavily diminished upon depletion of two specific phosphoinositides: PI(3)P and PI(3,5)P<sub>2</sub>, both of which are historically defining endosomal and lysosomal PIP-identity. Further biochemical and genetic experiments showed that PVs have a PI(3,5)P<sub>2</sub> identity, which is essential for their recognition and transport by KIF1A (discussed in detail in section 5.4). PI(3,5)P<sub>2</sub> is found in endosomes, multivesicular bodies (MVBs), lysosomes and autophagic compartments and the conversion of PI(3)P to PI(3,5)P<sub>2</sub> at the limiting membrane of late endosomes is crucial for endosomal maturation along the late endosome/lysosome pathway. The fact that PI(3,5)P<sub>2</sub> is sufficient for KIF1A binding to PVs, raises questions regarding meaning of PV transport inhibition upon PI(3)P depletion. PI(3)P is the only substrate that the PI-5-kinase PIKfyve can use to synthesize PI(3,5)P<sub>2</sub>. Since blocking the PI(3)P synthesis by VPS34 inhibition will eventually decrease the amount of substrate required to yield PI(3,5)P<sub>2</sub>, decrease of PI(3)P is also expected to indirectly affect the PV transport. However in our experiment, lipid kinase inhibitors, including VPS34 inhibitors, were applied for relatively short time (max. 30 minutes) which would possibly not be sufficient to fully deplete the PI(3,5)P<sub>2</sub> levels. Thus, a milder phenotype was expected in anterograde PV transport upon PI(3)P depletion. Since this was not the case, it is possible that PI(3)P has a direct role in PV identity. It cannot be ruled out that PVs might undergo

## Discussion

---

maturation steps as they move from the AIS to axon terminals. Perhaps, similar to other members of the endolysosomal system, PVs also convert their PI(3)P to PI(3,5)P<sub>2</sub> either in the soma or during their early transport at the AIS (Ferguson, 2018; Wallroth and Haucke, 2018). The critical role of PI(3)P might explain the diminished PV transport upon depletion of PI(3)P levels. It is also conceivable that upon PI(3)P depletion immature PVs containing presynaptic proteins accumulate in the cell body and proximal axon. Nevertheless, future studies are required to clarify the PI(3)P-dependence of PVs.

### 5.4. KIF1A PH domain is essential to drive anterograde transport of PVs

Earlier studies have already suggested a role for KIF1A in driving the transport of PVs (Hummel and Hoogenraad, 2021; Niwa et al., 2016; Okada et al., 1995; Oliver et al., 2022; Vukoja et al., 2018; Yonekawa et al., 1998). In this work, we confirm the KIF1A dependence of PVs in their anterograde axonal transport. We show that KIF1A is transported with SV and AZ proteins at very high levels. Furthermore, complete loss of KIF1A in human neurons diminishes the anterograde transport of PVs and severely impairs the presynaptic protein levels at mature synapses. In KIF1A KO neurons, incomplete delivery of presynaptic proteins to axon terminals results in mature synapses containing significantly low levels of SV or AZ proteins, whereas postsynaptic protein levels remain unaffected.

The presynaptic phenotype observed in cultured human neurons is similar to that in cultured neurons from embryonic KIF1A KO mice. Of note, electron micrographs from neuronal somata in KIF1A deficient mice result in an accumulation of SV-like clear-cored vesicles. These vesicles have been claimed to make up the population of PVs which could not be delivered to axon terminals. Parallel to this, a recent study using knockdown of KIF1A in cultured mouse neurons also reports somatic accumulation of a SV protein, Rab3 (Hummel and Hoogenraad, 2021). In our hands, endogenous stainings of various presynaptic (SV, AZ or Cav) proteins in KIF1A KO neurons did not show any significant accumulation of such proteins in cell bodies of mature iNs. Various studies have suggested that the DLK pathway works antagonistic to Arl8 and KIF1A in presynaptic assembly and the DLK signaling becomes activated when KIF1A (Unc-104)'s function is lost (Li et al., 2017; Wu et al., 2013). The interplay between DLK and KIF1A has been extensively studied in *Drosophila* NMJ, where

## Discussion

---

authors have shown that an axon damage signaling pathway is triggered via the fly homologue of DLK (*Wnd*) upon impairment of Unc-104 (fly homolog of KIF1A) (Li et al., 2017). This leads to restricted level of expression of SV and AZ proteins (shown with Vglut and Brp), counteracting their excess accumulation in cell bodies while causing the observed defects in presynapse structure and function. When we treated KIF1A KD iNs with a pharmacological inhibitor against DLK for 24 hours, we could indeed regain some level of accumulated SV proteins in somata, indicating that the DLK signaling pathway is activated upon KIF1A loss (**Appendix B, Figure S2**). To understand how exactly DLK activity might be important in maintaining synaptic homeostasis, further research is needed.

Our study has shown that the C-terminal PH domain of the KIF1A motor protein is a phosphatidylinositol lipid binding domain which specifically interacts with PI(3,5)P<sub>2</sub>. A KIF1A construct lacking the PH domain (KIF1A-dPH) loses its vesicle-binding ability and this deletion renders KIF1A cytoplasmic. In contrast, another KIF1A construct consisting of only the C-terminal tail part, CC3 and PH domains (KIF1A-tail) expresses in cells as vesicular and transports with Syp to a very high extent. Thus, KIF1A requires its PH domain to bind membranes. Does the PH domain have any preference towards a specific phosphoinositide, and if so, can this phosphoinositide unravel a specific membrane identity of PVs? A liposome pelleting assay demonstrated that KIF1A PH domain preferentially interacts with liposomes containing PI(3,5)P<sub>2</sub>, although low amount of interaction with PI(3)P and PI(4,5)P<sub>2</sub> has been observed as well. In developing axons, inhibition of PIKfyve by using a specific inhibitor, Apilimod, causes the cargo-binding tail domain of KIF1A to become soluble, indicating that KIF1A PH domain no longer binds to the cargo's membrane. This finding is further supported by genetic manipulations, using lentiviral shRNAs against PIKfyve. Similar to Apilimod treatment, knockdown of PIKfyve renders the KIF1A-tail construct soluble, as seen by the significant reduction in the total number of KIF1A decorated vesicles in axons. PV transport levels and levels of presynaptic material at mature synapses are heavily affected by PIKfyve loss. These results collectively indicate that the PH domain of KIF1A interacts with PI(3,5)P<sub>2</sub> on the membranes of PVs.

Before this study, the PH domain of KIF1A has never been shown to interact with PI(3,5)P<sub>2</sub>. In fact, earlier studies have suggested that KIF1A PH domain binds to another PIP<sub>2</sub>, which is PI(4,5)P<sub>2</sub> (Klopfenstein and Vale, 2004) to transport PVs in *C. elegans*. A membrane floatation assay was conducted using the mini Unc104-motor, which is the fusion of the motor domain of Unc104 and the PH domain. Mini Unc104-motor bound preferentially to liposomes

## Discussion

---

composed of 10% PI(4,5)P<sub>2</sub>/90% phosphatidyl choline (PC) compared with other phosphoinositide such as PI(3)P (35%), PI(4)P (25%) and PI(3,4,5)P<sub>2</sub> (20%) or acidic phospholipids such as PA (less than 20% binding) (Klopfenstein and Vale, 2004). In a more recent study, PH domain of *C. elegans* Unc104 was used in a liposome pelleting assay and approximately 60% of the purified protein was found to bind to PI(4,5)P<sub>2</sub> whereas only 25% of the protein was bound to PI(4)P (Kumar et al., 2010). It should be noted that neither of these studies included PI(3,5)P<sub>2</sub> in their experiments. In our liposome pelleting assay, we used the human PH domain of KIF1A fused to an N-terminal GST tag to improve stability. We used two repeated PH domains separated from one another by a linker sequence to improve binding affinity. Our liposomes were prepared using a more complex mixture of ingredients in order to mimic physiological, especially lysosomal membranes. Thus, they contained PC, PE and cholesterol instead of only PC. Next, due to the previously gathered evidence that PVs could be lysosome related, we aimed to include lysosomal PIs to our test samples. Therefore we used not only PI(4,5)P<sub>2</sub> and PI(4)P but also included PI(3)P, PI(3,4)P<sub>2</sub> (not shown in the main figure) and PI(3,5)P<sub>2</sub> in our liposome pelleting assay. Surprisingly, the highest amount of binding of PH domain was observed in case of PI(3,5)P<sub>2</sub> containing liposomes (61%) which was followed by PI(3)P (24%) and PI(4,5)P<sub>2</sub> (13%). Moreover, we tested the effects of pharmacological inhibition of lipid kinases on KIF1A membrane binding in non-neuronal and neuronal cells. Only depletion of PI(3,5)P<sub>2</sub> levels by Apilimod treatment resulted in the dispersion of the PH domain of KIF1A from the membranes. Thus, although PI(4,5)P<sub>2</sub> binding of KIF1A PH domain was partly recapitulated by our liposome pelleting assay, our results overall indicate that binding efficiencies of the PH domain of KIF1A/Unc104 might vary in different organisms.

Many studies emphasize on the role of KIF1B $\beta$ , a paralog of KIF1A, in driving PV transport. KIF1A and KIF1B $\beta$  are structurally highly similar and they both are expressed in neurons, are able to interact with presynaptic proteins and both knockout mouse models show reduced density of SVs in the nerve terminals (Niwa et al., 2016; Yonekawa et al., 1998; Zhao et al., 2001). In our experiments, shRNA mediated depletion of both kinesin motor proteins resulted in decreased anterograde transport of PVs, with a stronger phenotype upon KIF1A loss (**Appendix B, Figure S1**). Nevertheless, combined loss of KIF1A and KIF1B $\beta$  did not show a more dramatic loss in PV transport compared to single knockdowns. Furthermore, reduction in PV transport rates and presynaptic protein levels were already reduced dramatically in KIF1A KO iNs. When KIF1B $\beta$  was additionally depleted in KIF1A KO iNs, the extent of cell death was very high, resulting in very low number of surviving neurons in culture.

## Discussion

---

Therefore, we used KIF1A KO iNs in our experiments instead of generating KIF1A and KIF1B $\beta$  double KO iPSCs. So far, there are a number of remaining questions regarding the role of KIF1B $\beta$  in PV transport in iNs: does complete genetic ablation of KIF1B $\beta$  result in similar presynaptic phenotypes, does KIF1B $\beta$  also interact with Arl8 and does its PH domain also interact with PI(3,5)P<sub>2</sub>? Future experiments are needed to answer these questions.

Our knockout and knockdown experiments show that upon complete loss of KIF1A (or KIF1A KO and KIF1B $\beta$  knockdown), a minor fraction of anterogradely transported PVs remain. Moreover, certain level of presynaptic material reaches to synaptic sites. This would argue that perhaps there are additional mechanisms that drive axonal PV transport in these conditions. Kinesin superfamily includes 45 mammalian genes producing a myriad of proteins (Lawrence et al., 2004; Miki et al., 2001 (Lawrence et al., 2004; Miki et al., 2001)). This might allow for other kinesins to compensate for the loss of some, such as KIF1A. This redundancy in kinesin function would most likely cast a role for the classical kinesin KIF5, as already mentioned in several studies in the context of axonal presynaptic protein transport (Shapira et al., 2003; Zhai et al., 2001).

### 5.5. PIKfyve activity is required for KIF1A to drive efficient transport of PVs

Our results show that depletion of PI(3,5)P<sub>2</sub> levels in developing neurons either by treating them with a specific PIKfyve inhibitor or by using an shRNA-mediated knockdown of PIKfyve abolishes PV transport. Syp, a SV protein carried on PVs, becomes stationary and can no longer be trafficked to axon terminals. The transport of KIF1A, the kinesin that is responsible for Syp transport in axons, is also stalled. Furthermore, KIF1A becomes dispersed in the cytoplasm instead of residing on stationary axonal vesicles upon PI(3,5)P<sub>2</sub> depletion. Further supported by biochemical experiments, this demonstrates that KIF1A requires the PI(3,5)P<sub>2</sub> on PVs in order to bind them and drive their anterograde transport.

We show that Arl8, KIF1A and PI(3,5)P<sub>2</sub> are three essential elements of the PV transport machinery. The fact that Arl8 is able to bind PVs even in the absence of KIF1A whereas KIF1A membrane-binding was depleted in the absence of Arl8 places Arl8 upstream of KIF1A in the initiation of PV transport. Furthermore, knowing that the membrane-binding

## Discussion

ability of KIF1A is heavily affected by changes in PI(3,5)P<sub>2</sub> levels, we conclude that PVs require to have a PI(3,5)P<sub>2</sub> identity prior to their interaction with KIF1A. In other words, PI(3,5)P<sub>2</sub> identity is essential for initiation of their anterograde axonal transport. Finally we questioned whether Arl8 is affected by depletion of PI(3,5)P<sub>2</sub> levels. Both PIKfyve inhibition or knockdown experiments demonstrate that Arl8 remains on PVs in either condition. These findings suggest that cargo binding of KIF1A is achieved by coincidence detection of both Arl8 and PI(3,5)P<sub>2</sub> (**Figure 5.1**).

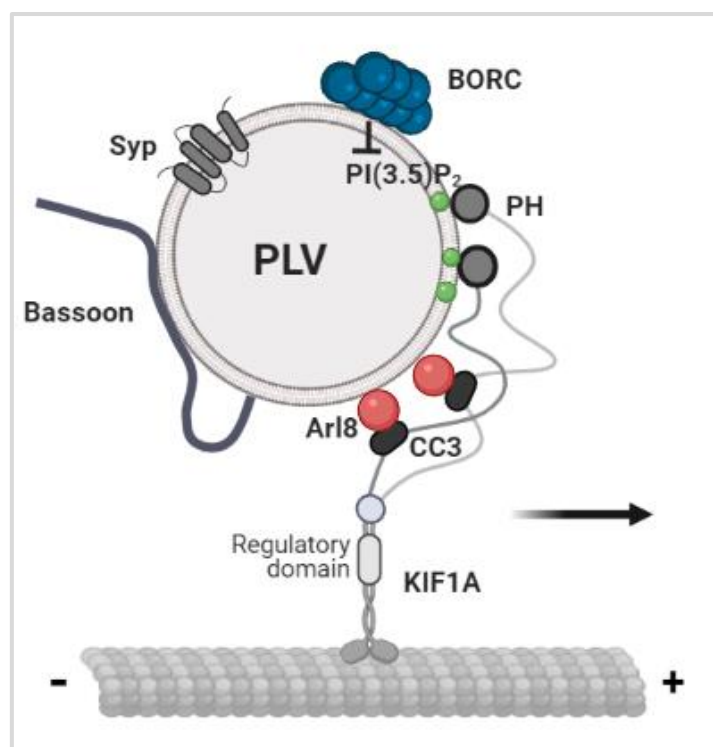


**Figure 5.1. Schematic representation for PV transport machinery.** PVs are presynaptic precursor transport organelles carrying SV proteins (shown Syp) and AZ proteins (shown Bassoon) in the axons of developing neurons. Their transport is driven by KIF1A and regulated by Arl8a/b which interacts with KIF1A on its CC3 domain, and PI(3,5)P<sub>2</sub> which binds the PH domain of KIF1A. BORG inhibition induces PI(3,5)P<sub>2</sub> production and sustains anterograde PV transport.

## Discussion

---

BORC is an upstream regulator of Arl8. It directs lysosomal motility and works upstream to PIKfyve. Interestingly, shRNA mediated depletion of BORC subunits Myrlysin and Diaskedin did not result in a depletion of PV transport. This finding was counterintuitive since depletion of either Myrlysin or Diaskedin decreased axonal Arl8 transport. In neurons where subunits of BORC were depleted, the majority of PVs were transported independently of Arl8. Moreover, in Arl8a/b dKO neurons, levels of anterograde PV transport were partially rescued upon BORC knockdown, indicating that perhaps BORC loss triggers an Arl8a/b-independent mechanism to enhance anterograde PV transport. To validate further that this rescue in anterograde transport is BORC dependent, we also depleted BLOS-1, a subunit shared by BORC and BLOC complexes, and CNO, a subunit specific for BLOC complex. Loss of CNO in Arl8a/b dKO neurons did not lead to any increase anterograde PV transport, indicating that this rescue observed in PV transport is specific to the depletion of BORC activity.

In a recent study, genetic loss of Myrlysin or Diaskedin have been shown to increase PI(3,5)P<sub>2</sub> levels in non-neuronal cells, perhaps by hyperactivating PIKfyve (Yordanov et al., 2019). These findings drive the hypothesis, that hyperactivation of PIKfyve by loss of BORC might at least partially compensate for inactivation of Arl8 due to BORC loss and thus effects of BORC loss on axonal anterograde PV transport are negligible. Hyperactivation of PIKfyve and thus increase in the PI(3,5)P<sub>2</sub> levels on PV membranes -one of the two elements of KIF1A recruitment to PV membranes and initiation of anterograde transport- might compensate for decreased Arl8 activity, the 2nd element of KIF1A recruitment to PV membranes and initiation of anterograde transport. Indeed, a partial rescue of anterograde PV transport was achieved with BORC knockdown in iNs with a Arl8a/b dKO background, an effect which was not observed when PIKfyve was silenced. Therefore, BORC might indeed direct a mechanism which regulates PI(3,5)P<sub>2</sub> levels and thus counteracts the effect of decreased Arl8 activity on KIF1A recruitment and PV transport.

Our understanding of how PIKfyve is regulated is limited, with only two major kinases, AMPK and AKT having been reported to cause PIKfyve activation (Hill et al., 2010; Liu et al., 2013). In parallel to this, cells genetically depleted of Diaskedin have shown higher intrinsic AMPK activity and ERK signalling (Yordanov et al., 2019). Therefore, a mechanism by which BORC loss enhances PIKfyve activity via AMPK is at least conceivable.

In addition to the hypothesis that BORC might regulate PI(3,5)P<sub>2</sub> levels by hyperactivating PIKfyve, there are also other possibilities which could directly affect the lipid

## Discussion

---

levels. The myotubularin family is a large group of protein tyrosine/dual specificity phosphatase-like phosphatases which could act as regulators of the highly active PI metabolism in cells, where interconversions of the eight PI species is controlled by a set of specific kinases and phosphatases (**Figure 1.9**). Four family members, MTM1, MTMR1, MTMR2 and MTMR4 have been suggested to use PI(3,5)P<sub>2</sub> as a substrate, in addition to PI(3)P *in vitro* (Tronchere et al., 2004). MTM1 and MTMR2 phosphoinositide phosphatases were additionally shown to hydrolyze PI3P and PI(3,5)P<sub>2</sub> in mammalian cells (Tronchere et al., 2004; Vaccari et al., 2011). MTMR2 phosphatase activity is positively regulated by its interaction with MTMR13 (Set-binding-factor; Sbf2) (Berger et al., 2006). In addition, Fig4 is a 5-phosphatase involved in the dephosphorylation of PI(3,5)P<sub>2</sub>, a predicted substrate of MTMR2. In addition to its 5-phosphatase activity, Fig4 also activates Fab1, the yeast homolog of PIKfyve (Duex et al., 2006). Although these studies suggest a role for MTM1 and MTMR2 in dephosphorylation of PI(3,5)P<sub>2</sub>, so far there is no PI(3,5)P<sub>2</sub>-specific phosphatase known. Nevertheless, if BORC activates the phosphatase hydrolyzing PI(3,5)P<sub>2</sub>, silencing of BORC might trigger the inhibition of this phosphatase which results in accumulation of PI(3,5)P<sub>2</sub> and a subsequent decrease in PI(3)P levels. Studies involving use of proximity labelling of PVs in the presence and absence of BORC in Arl8a/b dKO neurons will likely contribute to widen our knowledge on the phosphatase that functions in the PV transport machinery. Identifying how BORC might alter PI(3,5)P<sub>2</sub> levels is of particular interest since it would reveal a novel role for this multisubunit complex.

Our model of PV transport machinery illustrates the presynaptic precursor vesicles carrying SV proteins but also AZ proteins along the axons. The motility of PVs along axons is regulated by Arl8, which interacts with KIF1A through its CC3 domain, and the endolysosomal phosphoinositide PI(3,5)P<sub>2</sub>, which binds KIF1A via its PH domain. BORC regulates PV transport negatively such that in the absence of Arl8 BORC inhibition induces PI(3,5)P<sub>2</sub> production and sustains anterograde PV transport. Finally, when KIF1A is recruited to PVs, it drives their transport towards axon terminals (**Figure 5.1**). The importance of the regulators of PV transport have been confirmed in other cells and species. For instance the PI(3,5)P<sub>2</sub>-binding of KIF1A was validated in HeLa cells by live-tracking of KIF1A PH domain upon Apilimod treatment. Furthermore, cultured mouse hippocampal neurons lost anterograde PV transport and KIF1A binding to PVs upon PI(3,5)P<sub>2</sub> depletion. Similarly, critical roles of Arl8 in regulating presynaptic assembly have been shown in Arl8 mutant *Drosophila* and *C. elegans* (Klassen et al., 2010; Vukoja et al., 2018). These results suggest that PV transport machinery seem to be a general mechanism conserved through species. However, it is important to note

## Discussion

---

that in this thesis the neuronal model system primarily used for establishing the described mechanism was based on transdifferentiated human stem cells into cortical neurons only. Different types of synapses display characteristic features such as the number and size of AZs, the size and organization of the SV pools, or release probability (Jahn and Fasshauer, 2012; Jin and Garner, 2008; Südhof, 2017a). To understand how presynaptic biogenesis takes place and is regulated in different neuronal types, different neuronal differentiation protocols resulting in populations of GABAergic neurons or motor neurons (Bianchi et al., 2018; Yang et al., 2017) as well as different model organisms should be used in future studies.

Finally, our studies in developing human neurons were restricted to a short period in which expression of presynaptic proteins was initiated. Our experiments did not focus on later stages of development in which less PVs were transported as synaptogenesis had already taken place. This difference in the abundance of PVs suggests that a certain intrinsic steady-state set point is reached towards the final stage of neuronal development. Additionally, different components of the presynaptic compartment are of different copy numbers per synapse. Thus, the composition of PVs might change from development to the mature nervous system and might be subject to plastic modulation. Setting and adjusting synaptic weight likely involves feedback control mechanisms in order for neurons to reach a steady-state set point and to undergo plastic remodeling when needed, for example in case of rewiring of neuronal networks or during long-term forms of homeostatic plasticity (Rizalar et al., 2021). A possible component of such feedback control mechanism might be Wallenda (Wnd)/DLK signaling, a pathway implicated in the axonal transport and presynaptic delivery of presynaptic proteins. This pathway could involve post-translational, translational, or transcriptional mechanisms in the neuronal cell bodies since hyperactive DLK signaling in KIF1A/Unc104 mutant flies results in decreased presynaptic protein expression (Li et al., 2017) (also see section 5.4). How exactly this pathway functions and whether additional mechanisms take place to adjust synaptic weight remains to be elucidated.

### 6. Conclusion

Neurons communicate with each other through synapses and therefore synapses are crucial for various processes such as information processing, learning and memory. When an AP reaches the presynaptic terminal, it causes neurotransmitters to be released from the presynaptic neuron into the synaptic cleft. The released neurotransmitters then attach to the receptors on the postsynapse of another neuron, mediating the transfer of information. This process is dependent on various molecular machineries that have to be tightly regulated to not only generate but also maintain a functional synapse. Thus, mechanisms regulating presynaptic biogenesis also have to be tightly regulated to ensure the establishment of a functional nascent synapse in developing neurons and to maintain neuronal plasticity in mature neuronal networks.

In the axons of developing neurons, the main components of the presynaptic compartment are present on vesicular carrier organelles named precursor vesicles (PVs) and are carried to sites of presynaptic biogenesis. In this thesis, I investigated the components of the core machinery of the presynaptic transport organelles and the regulation of presynaptic protein transport in the developing neurons. Our study demonstrates that PVs carry different components of the presynaptic compartment collectively towards axon terminals. Axonal transport of PVs is driven by the neuronal kinesin motor protein KIF1A and is regulated by the lysosomal small GTPase Arl8. PVs partially co-transport towards axon terminals with lysosomal proteins, although they are different from *bona fide* lysosomes. Importantly, KIF1A required its PH domain to be efficiently recruited to its cargo, presynaptic PVs. PH domain of KIF1A binds to the endolysosomal phosphoinositide PI(3,5)P<sub>2</sub>, indicating that PVs might originate from endosomes. Depletion of PI(3,5)P<sub>2</sub> by inhibition or genetic depletion of PIKfyve, its upstream kinase, prevents membrane recruitment of KIF1A and consequently inhibits the anterograde PV transport. Thus, presence of both Arl8 and PI(3,5)P<sub>2</sub> are essential in order to ensure efficient cargo recruitment and successful delivery of presynaptic proteins to axon terminals.

This work sheds light on the molecular mechanisms regulating presynaptic biogenesis in developing human neurons including characterization of the transport machinery of presynaptic transport organelles in detail and for the first time demonstrates the phosphoinositide identity of these precursor organelles.

### 7. References

1. Acuna, C., Liu, X., and Südhof, T.C. (2016). How to Make an Active Zone: Unexpected Universal Functional Redundancy between RIMs and RIM-BPs. *Neuron* 91, 792-807.
2. Ahmari, S.E., Buchanan, J., Smith, S.J., and (2000). Assembly of presynaptic active zones from cytoplasmic transport packets. *Nature Neuroscience* 3, 445–451.
3. Andres-Alonso, M., Kreutz, M.R., and Karpova, A. (2021). Autophagy and the endolysosomal system in presynaptic function. *Cell Mol Life Sci* 78, 2621-2639.
4. Antonny, B., Beraud-Dufour, S., Chardin, P., and Chabre, M. (1997). N-terminal hydrophobic residues of the G-protein ADP-ribosylation factor-1 insert into membrane phospholipids upon GDP to GTP exchange. *Biochemistry* 36, 4675-4684.
5. Balla, T. (2013). Phosphoinositides: tiny lipids with giant impact on cell regulation. *Physiol Rev* 93, 1019-1137.
6. Berger, P., Berger, I., Schaffitzel, C., Tersar, K., Volkmer, B., and Suter, U. (2006). Multi-level regulation of myotubularin-related protein-2 phosphatase activity by myotubularin-related protein-13/set-binding factor-2. *Hum Mol Genet* 15, 569-579.
7. Bianchi, F., Malboubi, M., Li, Y., George, J.H., Jerusalem, A., Szele, F., Thompson, M.S., and Ye, H. (2018). Rapid and efficient differentiation of functional motor neurons from human iPSC for neural injury modelling. *Stem Cell Res* 32, 126-134.
8. Biederer, T., Kaeser, P.S., and Blanpied, T.A. (2017). Transcellular Nanoalignment of Synaptic Function. *Neuron* 96, 680-696.
9. Biederer, T., Sara, Y., Mozhayeva, M., Atasoy, D., Liu, X., Kavalali, E.T., and Südhof, T.C. (2002). SynCAM, a synaptic adhesion molecule that drives synapse assembly. *Science* 297, 1525-1531.
10. Bolino, A., Bolis, A., Previtali, S.C., Dina, G., Bussini, S., Dati, G., Amadio, S., Del Carro, U., Mruk, D.D., Feltri, M.L., *et al.* (2004). Disruption of *Mtmr2* produces CMT4B1-like neuropathy with myelin outfolding and impaired spermatogenesis. *J Cell Biol* 167, 711-721.
11. Boucrot, E., Henry, T., Borg, J.P., Gorvel, J.P., and Meresse, S. (2005). The intracellular fate of *Salmonella* depends on the recruitment of kinesin. *Science* 308, 1174-1178.
12. Bresler, T., Shapira, M., Boeckers, T., Dresbach, T., Futter, M., Garner, C.C., Rosenblum, K., Gundelfinger, E.D., and Ziv, N.E. (2004). Postsynaptic density assembly is fundamentally different from presynaptic active zone assembly. *J Neurosci* 24, 1507-1520.
13. Burton, P.R., and Paige, J.L. (1981). Polarity of axoplasmic microtubules in the olfactory nerve of the frog. *Proc Natl Acad Sci U S A* 78, 3269-3273.
14. Bury, L.A., and Sabo, S.L. (2011). Coordinated trafficking of synaptic vesicle and active zone proteins prior to synapse formation. *Neural Development* 6.
15. Byrd, D.T., Kawasaki, M., Walcoff, M., Hisamoto, N., and Matsumoto, K. (2001). UNC-16, a JNK-Signaling Scaffold Protein, Regulates Vesicle Transport in *C. elegans*. *Neuron* 32, 787–800.

## References

---

16. Cai, Q., Pan, P.Y., and Sheng, Z.H. (2007). Syntabulin-kinesin-1 family member 5B-mediated axonal transport contributes to activity-dependent presynaptic assembly. *J Neurosci* 27, 7284-7296.
17. Cai, X., Xu, Y., Cheung, A.K., Tomlinson, R.C., Alcazar-Roman, A., Murphy, L., Billich, A., Zhang, B., Feng, Y., Klumpp, M., *et al.* (2013). PIKfyve, a class III PI kinase, is the target of the small molecular IL-12/IL-23 inhibitor apilimod and a player in Toll-like receptor signaling. *Chem Biol* 20, 912-921.
18. Carabalona, A., Hu, D.J., and Vallee, R.B. (2016). KIF1A inhibition immortalizes brain stem cells but blocks BDNF-mediated neuronal migration. *Nat Neurosci* 19, 253-262.
19. Chen, T.W., Wardill, T.J., Sun, Y., Pulver, S.R., Renninger, S.L., Baohan, A., Schreiter, E.R., Kerr, R.A., Orger, M.B., Jayaraman, V., *et al.* (2013). Ultrasensitive fluorescent proteins for imaging neuronal activity. *Nature* 499, 295-300.
20. Cherfils, J., and Zeghouf, M. (2013). Regulation of small GTPases by GEFs, GAPs, and GDIs. *Physiol Rev* 93, 269-309.
21. Chow, C.Y., Zhang, Y., Dowling, J.J., Jin, N., Adamska, M., Shiga, K., Szigeti, K., Shy, M.E., Li, J., Zhang, X., *et al.* (2007). Mutation of FIG4 causes neurodegeneration in the pale tremor mouse and patients with CMT4J. *Nature* 448, 68-72.
22. Chun, J., Shapovalova, Z., Dejgaard, S.Y., Presley, J.F., and Melancon, P. (2008). Characterization of class I and II ADP-ribosylation factors (Arfs) in live cells: GDP-bound class II Arfs associate with the ER-Golgi intermediate compartment independently of GBF1. *Mol Biol Cell* 19, 3488-3500.
23. Cohen, L.D., Zuchman, R., Sorokina, O., Müller, A., Dieterich, D.C., Armstrong, J.D., Ziv, T., and Ziv, N.E. (2013). Metabolic Turnover of Synaptic Proteins: Kinetics, Interdependencies and Implications for Synaptic Maintenance. *PLoS ONE* 8, e63191-e63191.
24. Cornejo, V.H., Gonzalez, C., Campos, M., Vargas-Saturno, L., Juricic, M.L.A., Miserey-Lenkei, S., Pertusa, M., Madrid, R., and Couve, A. (2020). Non-conventional Axonal Organelles Control TRPM8 Ion Channel Trafficking and Peripheral Cold Sensing. *Cell Rep* 30, 4505-4517 e4505.
25. Davydova, D., Marini, C., King, C., Klueva, J., Bischof, F., Romorini, S., Montenegro-Venegas, C., Heine, M., Schneider, R., Schröder, M.S., *et al.* (2014). Bassoon specifically controls presynaptic P/Q-type Ca<sup>2+</sup> channels via RIM-binding protein. *Neuron* 82, 181-194.
26. De Pace, R., Britt, D.J., Mercurio, J., Foster, A.M., Djavaherian, L., Hoffmann, V., Abebe, D., and Bonifacino, J.S. (2020). Synaptic Vesicle Precursors and Lysosomes Are Transported by Different Mechanisms in the Axon of Mammalian Neurons. *Cell Rep* 31, 107775.
27. Dean, C., Scholl, F.G., Choih, J., DeMaria, S., Berger, J., Isacoff, E., and Scheiffele, P. (2003). Neurexin mediates the assembly of presynaptic terminals. *Nature Neuroscience* 6, 708-716.
28. Di Paolo, G., and De Camilli, P. (2006). Phosphoinositides in cell regulation and membrane dynamics. *Nature* 443, 651-657.
29. Diefenbach, R.J., Diefenbach, E., Douglas, M.W., and Cunningham, A.L. (2002). The heavy chain of conventional kinesin interacts with the SNARE proteins SNAP25 and SNAP23. *Biochemistry* 41, 14906-14915.

## References

---

30. Dolphin, A.C., and Lee, A. (2020). Presynaptic calcium channels: specialized control of synaptic neurotransmitter release. *Nature Reviews Neuroscience* 21, 213-229.
31. Dong, X.P., Shen, D., Wang, X., Dawson, T., Li, X., Zhang, Q., Cheng, X., Zhang, Y., Weisman, L.S., Delling, M., and Xu, H. (2010). PI(3,5)P(2) controls membrane trafficking by direct activation of mucolipin Ca(2+) release channels in the endolysosome. *Nat Commun* 1, 38.
32. Dove, S.K., Cooke, F.T., Douglas, M.R., Sayers, L.G., Parker, P.J., and Michell, R.H. (1997). Osmotic stress activates phosphatidylinositol-3,5-bisphosphate synthesis. *Nature* 390, 187-192.
33. Dresbach, T., Torres, V., Wittenmayer, N., Altmann, W.D., Zamorano, P., Zuschratter, W., Nawrothki, R., Ziv, N.E., Garner, C.C., and Gundelfinger, E.D. (2006). Assembly of active zone precursor vesicles: Obligatory trafficking of presynaptic cytomatrix proteins Bassoon and Piccolo via A trans-Golgi compartment. *Journal of Biological Chemistry* 281, 6038-6047.
34. Duex, J.E., Tang, F., and Weisman, L.S. (2006). The Vac14p-Fig4p complex acts independently of Vac7p and couples PI3,5P2 synthesis and turnover. *J Cell Biol* 172, 693-704.
35. Dulubova, I., Khvotchev, M., Liu, S., Huryeva, I., Südhof, T.C., and Rizo, J. (2007). Munc18-1 binds directly to the neuronal SNARE complex. *Proceedings of the National Academy of Sciences of the United States of America* 104, 2697-2702.
36. Dumont, A., Boucrot, E., Drevensek, S., Daire, V., Gorvel, J.P., Pous, C., Holden, D.W., and Meresse, S. (2010). SKIP, the host target of the Salmonella virulence factor SifA, promotes kinesin-1-dependent vacuolar membrane exchanges. *Traffic* 11, 899-911.
37. Eggermann, E., Bucurenciu, I., Goswami, S.P., and Jonas, P. (2012). Nanodomain coupling between Ca<sup>2+</sup> channels and sensors of exocytosis at fast mammalian synapses. (Nature Publishing Group), pp. 7-21.
38. Emperador-Melero, J., and Kaeser, P.S. (2020). Assembly of the presynaptic active zone. *Curr Opin Neurobiol* 63, 95-103.
39. Ferguson, S.M. (2018). Axonal transport and maturation of lysosomes. *Curr Opin Neurobiol* 51, 45-51.
40. Fogel, A.I., Akins, M.R., Krupp, A.J., Stagi, M., Stein, V., and Biederer, T. (2007). SynCAMs organize synapses through heterophilic adhesion. *Journal of Neuroscience* 27, 12516-12530.
41. Fujimoto, K., Shibasaki, T., Yokoi, N., Kashima, Y., Matsumoto, M., Sasaki, T., Tajima, N., Iwanaga, T., and Seino, S. (2002). Piccolo, a Ca<sup>2+</sup> sensor in pancreatic  $\beta$ -cells: Involvement of cAMP-GEFII-Rim2-Piccolo complex in cAMP-dependent exocytosis. *Journal of Biological Chemistry* 277, 50497-50502.
42. Fukuda, M. (2003). Distinct Rab binding specificity of Rim1, Rim2, Rabphilin, and Noc2: Identification of a critical determinant of Rab3a/Rab27a recognition by Rim2. *Journal of Biological Chemistry* 278, 15373-15380.
43. Gabrych, D.R., Lau, V.Z., Niwa, S., and Silverman, M.A. (2019). Going Too Far Is the Same as Falling Short(dagger): Kinesin-3 Family Members in Hereditary Spastic Paraplegia. *Front Cell Neurosci* 13, 419.
44. Gary, J.D., Sato, T.K., Stefan, C.J., Bonangelino, C.J., Weisman, L.S., and Emr, S.D. (2002). Regulation of Fab1 phosphatidylinositol 3-phosphate 5-kinase pathway by

## References

---

- Vac7 protein and Fig4, a polyphosphoinositide phosphatase family member. *Mol Biol Cell* 13, 1238-1251.
45. Gasparini, S., Kasyanov, A.M., Pietrobon, D., Voronin, L.L., and Cherubini, E. (2001). Presynaptic r-type calcium channels contribute to fast excitatory synaptic transmission in the rat hippocampus. *Journal of Neuroscience* 21, 8715-8721.
  46. Goldstein, A.Y.N., Wang, X., and Schwarz, T.L. (2008). Axonal transport and the delivery of pre-synaptic components. *Current Opinion in Neurobiology* 18, 495-503.
  47. Gordon, S.L., Leube, R.E., and Cousin, M.A. (2011). Synaptophysin is required for synaptobrevin retrieval during synaptic vesicle endocytosis. *J Neurosci* 31, 14032-14036.
  48. Graf, E.R., Valakh, V., Wright, C.M., Wu, C., Liu, Z., Zhang, Y.Q., and DiAntonio, A. (2012). RIM promotes calcium channel accumulation at active zones of the *Drosophila* neuromuscular junction. *Journal of Neuroscience* 32, 16586-16596.
  49. Guardia, C.M., Farias, G.G., Jia, R., Pu, J., and Bonifacino, J.S. (2016). BORC Functions Upstream of Kinesins 1 and 3 to Coordinate Regional Movement of Lysosomes along Different Microtubule Tracks. *Cell Rep* 17, 1950-1961.
  50. Guedes-Dias, P., and Holzbaur, E.L.F. (2019). Axonal transport: Driving synaptic function. *Science* 366, eaaw9997-eaaw9997.
  51. Hafner, A., Donlin-Asp, P., Leitch, B., Herzog, E., and Schuman, E. (2019). Local protein synthesis is a ubiquitous feature of neuronal pre- and postsynaptic compartments. *Science* 364, 12.
  52. Hall, D.M., and Hedgecock, E.M. (1991). Kinesin-Related Gene *Unc-104* Is Required for Axonal Transport of Synaptic Vesicles in *C. elegans*. *Cell* 65, 837-847.
  53. Hallermann, S., Kittel, R.J., Wichmann, C., Weyhersmüller, A., Fouquet, W., Mertel, S., Oswald, D., Eimer, S., Depner, H., Schwärzel, M., *et al.* (2010). Naked dense bodies provoke depression. *Journal of Neuroscience* 30, 14340-14345.
  54. Han, Y., Kaeser, P.S., Südhof, T.C., and Schneggenburger, R. (2011). RIM determines Ca<sup>2+</sup> channel density and vesicle docking at the presynaptic active zone. *Neuron* 69, 304-316.
  55. Hasegawa, J., Strunk, B.S., and Weisman, L.S. (2017). PI5P and PI(3,5)P<sub>2</sub>: Minor, but Essential Phosphoinositides. *Cell Struct Funct* 42, 49-60.
  56. Hashimoto, K., Yamaguchi, Y., Kishi, Y., Kikko, Y., Takasaki, K., Maeda, Y., Matsumoto, Y., Oka, M., Miura, M., Ohata, S., *et al.* (2019). Loss of the small GTPase *Arl8b* results in abnormal development of the roof plate in mouse embryos. *Genes Cells* 24, 436-448.
  57. Hata, Y., Butz, S., and Südhof, T.C. (1996). *CASK*: A novel *dlg/PSD95* homolog with an N-terminal calmodulin-dependent protein kinase domain identified by interaction with neurexins. *Journal of Neuroscience* 16, 2488-2494.
  58. Hata, Y., Slaughter, C.A., and Südhof, T.C. (1993). Synaptic vesicle fusion complex contains *unc-18* homologue bound to syntaxin. *Nature* 366, 347-351.
  59. Hell, S.W. (2015). Nanoscopy with Focused Light (Nobel Lecture). *Angew Chem Int Ed Engl* 54, 8054-8066.
  60. Hendricks, A.G., Perlson, E., Ross, J.L., Schroeder, H.W., 3rd, Tokito, M., and Holzbaur, E.L. (2010). Motor coordination via a tug-of-war mechanism drives bidirectional vesicle transport. *Curr Biol* 20, 697-702.

## References

---

61. Hill, E.V., Hudson, C.A., Vertommen, D., Rider, M.H., and Tavaré, J.M. (2010). Regulation of PIKfyve phosphorylation by insulin and osmotic stress. *Biochem Biophys Res Commun* 397, 650-655.
62. Hirokawa, N., Niwa, S., and Tanaka, Y. (2010). Molecular motors in neurons: transport mechanisms and roles in brain function, development, and disease. *Neuron* 68, 610-638.
63. Hirokawa, N., Noda, Y., Tanaka, Y., and Niwa, S. (2009). Kinesin superfamily motor proteins and intracellular transport. *Nat Rev Mol Cell Biol* 10, 682-696.
64. Hofmann, I., and Munro, S. (2006). An N-terminally acetylated Arf-like GTPase is localised to lysosomes and affects their motility. *J Cell Sci* 119, 1494-1503.
65. Horn, K.E., Xu, B., Gobert, D., Hamam, B.N., Thompson, K.M., Wu, C.-L., Bouchard, J.-F., Uetani, N., Racine, R.J., Tremblay, M.L., *et al.* (2012). Receptor protein tyrosine phosphatase sigma regulates synapse structure, function and plasticity. *Journal of Neurochemistry* 122, 147-161.
66. Horton, A.C., and Ehlers, M.D. (2003). Dual Modes of Endoplasmic Reticulum-to-Golgi Transport in Dendrites Revealed by Live-Cell Imaging. *The Journal of Neuroscience* 23, 6188-6199.
67. Horton, A.C., Racz, B., Monson, E.E., Lin, A.L., Weinberg, R.J., and Ehlers, M.D. (2005). Polarized secretory trafficking directs cargo for asymmetric dendrite growth and morphogenesis. *Neuron* 48, 757-771.
68. Hsu, F., and Mao, Y. (2015). The structure of phosphoinositide phosphatases: Insights into substrate specificity and catalysis. *Biochim Biophys Acta* 1851, 698-710.
69. Hummel, J.J.A., and Hoogenraad, C.C. (2021). Specific KIF1A-adaptor interactions control selective cargo recognition. *J Cell Biol* 220.
70. Hurd, D.D., and Saxton, W.M. (1996). Kinesin mutations cause motor neuron disease phenotypes by disrupting fast axonal transport in *Drosophila*. *Genetics* 144, 1075-1085.
71. Ikonomov, O.C., Sbrissa, D., Delvecchio, K., Xie, Y., Jin, J.P., Rappolee, D., and Shisheva, A. (2011). The phosphoinositide kinase PIKfyve is vital in early embryonic development: preimplantation lethality of PIKfyve<sup>-/-</sup> embryos but normality of PIKfyve<sup>+/-</sup> mice. *J Biol Chem* 286, 13404-13413.
72. Ikonomov, O.C., Sbrissa, D., Mlak, K., Kanzaki, M., Pessin, J., and Shisheva, A. (2002). Functional dissection of lipid and protein kinase signals of PIKfyve reveals the role of PtdIns 3,5-P<sub>2</sub> production for endomembrane integrity. *J Biol Chem* 277, 9206-9211.
73. Iwasaki, K., Staunton, J., Saifee, O., Nonet, M., and Thomas, J.H. (1997). *aex-3* Encodes a Novel Regulator of Presynaptic Activity in *C. elegans*. *Neuron* 18, 613-622.
74. Jahn, R., and Fasshauer, D. (2012). Molecular machines governing exocytosis of synaptic vesicles. *Nature* 490, 201-207.
75. Jefferies, H.B., Cooke, F.T., Jat, P., Boucheron, C., Koizumi, T., Hayakawa, M., Kaizawa, H., Ohishi, T., Workman, P., Waterfield, M.D., and Parker, P.J. (2008). A selective PIKfyve inhibitor blocks PtdIns(3,5)P<sub>2</sub> production and disrupts endomembrane transport and retroviral budding. *EMBO Rep* 9, 164-170.
76. Jin, N., Chow, C.Y., Liu, L., Zolov, S.N., Bronson, R., Davisson, M., Petersen, J.L., Zhang, Y., Park, S., Duex, J.E., *et al.* (2008). VAC14 nucleates a protein complex

## References

---

- essential for the acute interconversion of PI3P and PI(3,5)P(2) in yeast and mouse. *EMBO J* 27, 3221-3234.
77. Jin, N., Lang, M.J., and Weisman, L.S. (2016). Phosphatidylinositol 3,5-bisphosphate: regulation of cellular events in space and time. *Biochem Soc Trans* 44, 177-184.
78. Jin, Y., and Garner, C.C. (2008). Molecular mechanisms of presynaptic differentiation. *Annu Rev Cell Dev Biol* 24, 237-262.
79. Kaeser, P.S., Deng, L., Fan, M., and Südhof, T.C. (2012). RIM genes differentially contribute to organizing presynaptic release sites. *Proceedings of the National Academy of Sciences of the United States of America* 109, 11830-11835.
80. Kaeser, P.S., Deng, L., Wang, Y., Dulubova, I., Liu, X., Rizo, J., and Südhof, T.C. (2011). RIM proteins tether Ca<sup>2+</sup> channels to presynaptic active zones via a direct PDZ-domain interaction. *Cell* 144, 282-295.
81. Khatter, D., Sindhvani, A., and Sharma, M. (2015). Arf-like GTPase Arl8: Moving from the periphery to the center of lysosomal biology. *Cell Logist* 5, e1086501.
82. Khvotchev, M., Dulubova, I., Sun, J., Dai, H., Rizo, J., and Südhof, T.C. (2007). Dual modes of Munc18-1/SNARE interactions are coupled by functionally critical binding to syntaxin-1 N terminus. *Journal of Neuroscience* 27, 12147-12155.
83. Klassen, M.P., Wu, Y.E., Maeder, C.I., Nakae, I., Cueva, J.G., Lehrman, E.K., Tada, M., Gengyo-Ando, K., Wang, G.J., Goodman, M., *et al.* (2010). An Arf-like Small G Protein, ARL-8, Promotes the Axonal Transport of Presynaptic Cargoes by Suppressing Vesicle Aggregation. *Neuron* 66, 710-723.
84. Klopfenstein, D.R., and Vale, R.D. (2004). The lipid binding pleckstrin homology domain in UNC-104 kinesin is necessary for synaptic vesicle transport in *Caenorhabditis elegans*. *Mol Biol Cell* 15, 3729-3739.
85. Ko, J., Na, M., Kim, S., Lee, J.R., and Kim, E. (2003). Interaction of the ERC Family of RIM-binding Proteins with the Liprin- $\alpha$  Family of Multidomain Proteins. *Journal of Biological Chemistry* 278, 42377-42385.
86. Kumar, J., Choudhary, B.C., Metpally, R., Zheng, Q., Nonet, M.L., Ramanathan, S., Klopfenstein, D.R., and Koushika, S.P. (2010). The *Caenorhabditis elegans* Kinesin-3 motor UNC-104/KIF1A is degraded upon loss of specific binding to cargo. *PLoS Genet* 6, e1001200.
87. Kwan, A.C., Dombeck, D.A., and Webb, W.W. (2008). Polarized microtubule arrays in apical dendrites and axons. *Proc Natl Acad Sci U S A* 105, 11370-11375.
88. Langemeyer, L., and Ungermann, C. (2015). BORC and BLOC-1: Shared subunits in trafficking complexes. *Dev Cell* 33, 121-122.
89. Lasek, R.J., Garner, J.A., and Brady, S.T. (1984). Axonal transport of the cytoplasmic matrix. *J Cell Biol* 99, 212s-221s.
90. Lawrence, C.J., Dawe, R.K., Christie, K.R., Cleveland, D.W., Dawson, S.C., Endow, S.A., Goldstein, L.S., Goodson, H.V., Hirokawa, N., Howard, J., *et al.* (2004). A standardized kinesin nomenclature. *J Cell Biol* 167, 19-22.
91. Lees, J.A., Li, P., Kumar, N., Weisman, L.S., and Reinisch, K.M. (2020). Insights into Lysosomal PI(3,5)P<sub>2</sub> Homeostasis from a Structural-Biochemical Analysis of the PIKfyve Lipid Kinase Complex. *Mol Cell* 80, 736-743 e734.
92. Lenk, G.M., Ferguson, C.J., Chow, C.Y., Jin, N., Jones, J.M., Grant, A.E., Zolov, S.N., Winters, J.J., Giger, R.J., Dowling, J.J., *et al.* (2011). Pathogenic mechanism of the

## References

---

- FIG4 mutation responsible for Charcot-Marie-Tooth disease CMT4J. *PLoS Genet* 7, e1002104.
93. Li, J., Zhang, Y.V., Adib, E.A., Stanchev, D.T., Klinedinst, S., Soppina, P., Jahn, T.R., Hume, R.I., Rasse, T.M., and Collins, C.A. (2017). Restraint of presynaptic protein levels by *Wnd/DLK* signaling mediates synaptic defects associated with the kinesin-3 motor *Unc-104*. *Elife* 6, 1-30.
94. Li, S.C., Diakov, T.T., Xu, T., Tarsio, M., Zhu, W., Couoh-Cardel, S., Weisman, L.S., and Kane, P.M. (2014). The signaling lipid PI(3,5)P(2) stabilizes V(1)-V(o) sector interactions and activates the V-ATPase. *Mol Biol Cell* 25, 1251-1262.
95. Li, X.M., Yang, J.M., Hu, D.H., Hou, F.Q., Zhao, M., Zhu, X.H., Wang, Y., Li, J.G., Hu, P., Chen, L., *et al.* (2007). Contribution of downregulation of L-type calcium currents to delayed neuronal death in rat hippocampus after global cerebral ischemia and reperfusion. *Journal of Neuroscience* 27, 5249-5259.
96. Liu, K.S.Y., Siebert, M., Mertel, S., Knoche, E., Wegener, S., Wichmann, C., Matkovic, T., Muhammad, K., Depner, H., Mettke, C., *et al.* (2011). RIM-binding protein, a central part of the active zone, is essential for neurotransmitter release. *Science* 334, 1565-1569.
97. Liu, Y., Lai, Y.C., Hill, E.V., Tyteca, D., Carpentier, S., Ingvaldsen, A., Vertommen, D., Lantier, L., Foretz, M., Dequiedt, F., *et al.* (2013). Phosphatidylinositol 3-phosphate 5-kinase (PIKfyve) is an AMPK target participating in contraction-stimulated glucose uptake in skeletal muscle. *Biochem J* 455, 195-206.
98. Lo, K.Y., Kuzmin, A., Unger, S.M., Petersen, J.D., and Silverman, M.A. (2011). KIF1A is the primary anterograde motor protein required for the axonal transport of dense-core vesicles in cultured hippocampal neurons. *Neurosci Lett* 491, 168-173.
99. Lu, J., Machius, M., Dulubova, I., Dai, H., Sü Dhof, T.C., Tomchick, D.R., and Rizo, J. (2006). Structural Basis for a Munc13-1 Homodimer to Munc13-1/RIM Heterodimer Switch. *PLOS Biology* 4.
100. Luo, F., Sclip, A., Jiang, M., and Südhof, T.C. (2020). Neurexins cluster Ca<sup>2+</sup> channels within the presynaptic active zone. *The EMBO Journal* 39.
101. Maas, C., Torres, V.I., Altrock, W.D., Leal-Ortiz, S., Wagh, D., Terry-Lorenzo, R.T., Fejtova, A., Gundelfinger, E.D., Ziv, N.E., and Garner, C.C. (2012b). Formation of Golgi-derived active zone precursor vesicles. *J Neurosci* 32, 11095-11108.
102. Maday, S., Wallace, K.E., and Holzbaur, E.L. (2012). Autophagosomes initiate distally and mature during transport toward the cell soma in primary neurons. *J Cell Biol* 196, 407-417.
103. Maeder, C.I., Shen, K., and Hoogenraad, C.C. (2014). Axon and dendritic trafficking. *Curr Opin Neurobiol* 27, 165-170.
104. Maffucci, T., Razzini, G., Ingrosso, A., Chen, H., Iacobelli, S., Sciacchitano, S., Quon, M.J., and Falasca, M. (2003). Role of pleckstrin homology domain in regulating membrane targeting and metabolic function of insulin receptor substrate 3. *Mol Endocrinol* 17, 1568-1579.
105. Maritzen, T., and Haucke, V. (2018). Coupling of exocytosis and endocytosis at the presynaptic active zone. (Elsevier Ireland Ltd), pp. 45-52.
106. Maschi, D., and Klyachko, V.A. (2017). Spatiotemporal Regulation of Synaptic Vesicle Fusion Sites in Central Synapses. *Neuron* 94, 65-73.e63.

## References

---

107. Maximov, A., and Bezprozvanny, I. (2002). Synaptic targeting of N-type calcium channels in hippocampal neurons. *Journal of Neuroscience* 22, 6939-6952.
108. Mayinger, P. (2012). Phosphoinositides and vesicular membrane traffic. *Biochim Biophys Acta* 1821, 1104-1113.
109. McCartney, A.J., Zhang, Y., and Weisman, L.S. (2014). Phosphatidylinositol 3,5-bisphosphate: low abundance, high significance. *Bioessays* 36, 52-64.
110. Miki, H., Setou, M., Kaneshiro, K., and Hirokawa, N. (2001). All kinesin superfamily protein, KIF, genes in mouse and human. *Proc Natl Acad Sci U S A* 98, 7004-7011.
111. Miki, T., Kaufmann, W.A., Malagon, G., Gomez, L., Tabuchi, K., Watanabe, M., Shigemoto, R., and Marty, A. (2017). Numbers of presynaptic Ca<sup>2+</sup> channel clusters match those of functionally defined vesicular docking sites in single central synapses. *Proceedings of the National Academy of Sciences of the United States of America* 114, E5246-E5255.
112. Mukherjee, K., Yang, X., Gerber, S.H., Kwon, H.B., Ho, A., Castillo, P.E., Liu, X., and Südhof, T.C. (2010). Piccolo and bassoon maintain synaptic vesicle clustering without directly participating in vesicle exocytosis. *Proceedings of the National Academy of Sciences of the United States of America* 107, 6504-6509.
113. Nakae, I., Fujino, T., Kobayashi, T., Sasaki, A., Kikko, Y., Fukuyama, M., Gengyo-Ando, K., Mitani, S., Kontani, K., and Katada, T. (2010). The arf-like GTPase Arl8 mediates delivery of endocytosed macromolecules to lysosomes in *Caenorhabditis elegans*. *Mol Biol Cell* 21, 2434-2442.
114. Nakamura, Y., Harada, H., Kamasawa, N., Matsui, K., Rothman, J.S., Shigemoto, R., Silver, R.A., DiGregorio, D.A., and Takahashi, T. (2015). Nanoscale Distribution of Presynaptic Ca<sup>2+</sup> Channels and Its Impact on Vesicular Release during Development. *Neuron* 85, 145-158.
115. Nicot, A.S., Fares, H., Payraastre, B., Chisholm, A.D., Labouesse, M., and Laporte, J. (2006). The phosphoinositide kinase PIKfyve/Fab1p regulates terminal lysosome maturation in *Caenorhabditis elegans*. *Mol Biol Cell* 17, 3062-3074.
116. Niwa, S., Lipton, D.M., Morikawa, M., Zhao, C., Hirokawa, N., Lu, H., and Shen, K. (2016). Autoinhibition of a Neuronal Kinesin UNC-104/KIF1A Regulates the Size and Density of Synapses. *Cell Rep* 16, 2129-2141.
117. Niwa, S., Tanaka, Y., and Hirokawa, N. (2008). KIF1B $\beta$ - and KIF1A-mediated axonal transport of presynaptic regulator Rab3 occurs in a GTP-dependent manner through DENN/MADD. *Nat Cell Biol* 10, 1269-1279.
118. Nyitrai, H., Wang, S.S.H., and Kaeser, P.S. (2020). ELKS1 Captures Rab6-Marked Vesicular Cargo in Presynaptic Nerve Terminals. *Cell Rep* 31, 107712.
119. Odorizzi, G., Babst, M., and Emr, S.D. (1998). Fab1p PtdIns(3)P 5-kinase function essential for protein sorting in the multivesicular body. *Cell* 95, 847-858.
120. Ohtsuka, T., Takao-Rikitsu, E., Inoue, E., Inoue, M., Takeuchi, M., Matsubara, K., Deguchi-Tawarada, M., Satoh, K., Morimoto, K., Nakanishi, H., and Takai, Y. (2002). CAST: A novel protein of the cytomatrix at the active zone of synapses that forms a ternary complex with RIM1 and Munc13-1. *Journal of Cell Biology* 158, 577-590.

## References

---

121. Okada, Y., Yamazaki, H., Sekine-Aizawa, Y., and Hirokawa, N. (1995). The Neuron-Specific Kinesin Superfamily Protein KIFIA Is a Unique Monomeric Motor for Anterograde Axonal Transport of Synaptic Vesicle Precursors. *Cell* 81, 769-780.
122. Oliver, D., Ramachandran, S., Philbrook, A., Lambert, C.M., Nguyen, K.C.Q., Hall, D.H., and Francis, M.M. (2022). Kinesin-3 mediated axonal delivery of presynaptic neurexin stabilizes dendritic spines and postsynaptic components. *PLoS Genet* 18, e1010016.
123. Pack-Chung, E., Kurshan, P.T., Dickman, D.K., and Schwarz, T.L. (2007). A *Drosophila* kinesin required for synaptic bouton formation and synaptic vesicle transport. *Nat Neurosci* 10, 980-989.
124. Park, H., Li, Y., and Tsien, R.W. (2012). Influence of synaptic vesicle position on release probability and exocytotic fusion mode. *Science* 335, 1362-1366.
125. Petzoldt, A.G., Lutzkendorf, J., and Sigrist, S.J. (2016). Mechanisms controlling assembly and plasticity of presynaptic active zone scaffolds. *Curr Opin Neurobiol* 39, 69-76.
126. Prokop, A., Landgraf, M., Rushton, E., Brodie, K., and Bate, M. (1996). Presynaptic development at the *Drosophila* neuromuscular junction: Assembly and localization of presynaptic active zones. *Neuron* 17, 617-626.
127. Pu, J., Schindler, C., Jia, R., Jarnik, M., Backlund, P., and Bonifacino, J.S. (2015). BORC, a multisubunit complex that regulates lysosome positioning. *Dev Cell* 33, 176-188.
128. Raiborg, C., Schink, K.O., and Stenmark, H. (2013). Class III phosphatidylinositol 3-kinase and its catalytic product PtdIns3P in regulation of endocytic membrane traffic. *FEBS J* 280, 2730-2742.
129. Raiborg, C., and Stenmark, H. (2009). The ESCRT machinery in endosomal sorting of ubiquitylated membrane proteins. *Nature* 458, 445-452.
130. Rimbault, C., Breillat, C., Compans, B., Toulmé, E., Vicente, F.N., Fernandez-Monreal, M., Mascalchi, P., Genuer, C., Puente-Muñoz, V., Gauthereau, I., *et al.* (2021).
131. Rizalar, F.S., Roosen, D.A., and Haucke, V. (2021). A Presynaptic Perspective on Transport and Assembly Mechanisms for Synapse Formation. *Neuron* 109, 27-41.
132. Rojas, A.M., Fuentes, G., Rausell, A., and Valencia, A. (2012). The Ras protein superfamily: evolutionary tree and role of conserved amino acids. *J Cell Biol* 196, 189-201.
133. Rosa-Ferreira, C., and Munro, S. (2011). Arl8 and SKIP act together to link lysosomes to kinesin-1. *Dev Cell* 21, 1171-1178.
134. Rosa-Ferreira, C., Sweeney, S.T., and Munro, S. (2018). The small G protein Arl8 contributes to lysosomal function and long-range axonal transport in *Drosophila*. *Biol Open* 7.
135. Roy, S. (2014). Seeing the unseen: the hidden world of slow axonal transport. *Neuroscientist* 20, 71-81.
136. Rusten, T.E., Rodahl, L.M., Pattni, K., Englund, C., Samakovlis, C., Dove, S., Brech, A., and Stenmark, H. (2006). Fab1 phosphatidylinositol 3-phosphate 5-kinase controls trafficking but not silencing of endocytosed receptors. *Mol Biol Cell* 17, 3989-4001.

## References

---

137. Sakamoto, R., Byrd, D.T., Brown, H.M., Hisamoto, N., Matsumoto, K., and Jin, Y. (2005). The *Caenorhabditis elegans* UNC-14 RUN domain protein binds to the kinesin-1 and UNC-16 complex and regulates synaptic vesicle localization. *Mol Biol Cell* 16, 483-496.
138. Sanes, J.R., and Zipursky, S.L. (2020). *Synaptic Specificity, Recognition Molecules, and Assembly of Neural Circuits*. (Cell Press), pp. 536-556.
139. Sara, Y., Biederer, T., Atasoy, D., Chubykin, A., Mozhayeva, M.G., Südhof, T.C., and Kavalali, E.T. (2005). Selective capability of SynCAM and neuroligin for functional synapse assembly. *Journal of Neuroscience* 25, 260-270.
140. Sbrissa, D., Ikonomov, O.C., and Shisheva, A. (1999). PIKfyve, a mammalian ortholog of yeast Fab1p lipid kinase, synthesizes 5-phosphoinositides. Effect of insulin. *J Biol Chem* 274, 21589-21597.
141. Sbrissa, D., Ikonomov, O.C., Strakova, J., and Shisheva, A. (2004). Role for a novel signaling intermediate, phosphatidylinositol 5-phosphate, in insulin-regulated F-actin stress fiber breakdown and GLUT4 translocation. *Endocrinology* 145, 4853-4865.
142. Scheiffele, P., Fan, J., Choih, J., Fetter, R., and Serafini, T. (2000). Neuroligin expressed in nonneuronal cells triggers presynaptic development in contacting axons. *Cell* 101, 657-669.
143. Schoch, S., Castillo, P.E., Jo, T., Mukherjee, K., Geppert, M., Wang, Y., Schmitz, F., Malenka, R.C., and Südhof, T.C. (2002). RIM1 $\alpha$  forms a protein scaffold for regulating neurotransmitter release at the active zone. *Nature* 415, 321-326.
144. Schoneberg, J., Lee, I.H., Iwasa, J.H., and Hurley, J.H. (2017). Reverse-topology membrane scission by the ESCRT proteins. *Nat Rev Mol Cell Biol* 18, 5-17.
145. Schonh, J.S., van Weering, J.R., Mohrmann, R., Schluter, O.M., Sudhof, T.C., de Wit, H., Verhage, M., and Sorensen, J.B. (2010). Rab3 proteins involved in vesicle biogenesis and priming in embryonic mouse chromaffin cells. *Traffic* 11, 1415-1428.
146. Sclip, A., and Südhof, T.C. (2020). LAR receptor phospho-tyrosine phosphatases regulate NMDA-receptor responses. *eLife* 9.
147. Shapira, M.R., Zhai, G., Dresbach, T., Bresler, T., Torres, V.I., Gundelfinger, E.D., Ziv, N.E., and Garner, C.C. (2003). Unitary Assembly of Presynaptic Active Zones from Piccolo-Bassoon Transport Vesicles. *Neuron* 38, 237-252.
148. Sharma, M. (2019). Emerging roles of Arl GTPases in regulating cellular functions. *Proceedings of the Indian National Science Academy*.
149. Sigrist, S.J., Thiel, P.R., Reiff, D.F., Lachance, P.E., Lasko, P., and Schuster, C.M. (2000). Postsynaptic translation affects the efficacy and morphology of neuromuscular junctions. *Nature* 405, 1062-1065.
150. Simms, B.A., and Zamponi, G.W. (2014). *Neuronal voltage-gated calcium channels: Structure, function, and dysfunction*. (Cell Press), pp. 24-45.
151. Soykan, T., Maritzen, T., and Haucke, V. (2016). Modes and mechanisms of synaptic vesicle recycling. *Current Opinion in Neurobiology* 39, 17-23.
152. Spafford, J.D., and Zamponi, G.W. (2003). *Functional interactions between presynaptic calcium channels and the neurotransmitter release machinery*. (Elsevier Ltd), pp. 308-314.

## References

---

153. Stagi, M., Fogel, A.I., and Biederer, T. (2010). SynCAM 1 participates in axo-dendritic contact assembly and shapes neuronal growth cones. *Proceedings of the National Academy of Sciences of the United States of America* 107, 7568-7573.
154. Stepanova, T., Slemmer, J., Hoogenraad, C.C., Lansbergen, G., Dortland, B., De Zeeuw, C.I., Grosveld, F., van Cappellen, G., Akhmanova, A., and Galjart, N. (2003). Visualization of microtubule growth in cultured neurons via the use of EB3-GFP (end-binding protein 3-green fluorescent protein). *J Neurosci* 23, 2655-2664.
155. Su, Q., Cai, Q., Gerwin, C., Smith, C.L., and Sheng, Z.H. (2004). Syntabulin is a microtubule-associated protein implicated in syntaxin transport in neurons. *Nat Cell Biol* 6, 941-953.
156. Südhof, T.C. (2017a). *Molecular Neuroscience in the 21st Century: A Personal Perspective*. (Cell Press), pp. 536-541.
157. Südhof, T.C. (2017b). *Synaptic Neurexin Complexes: A Molecular Code for the Logic of Neural Circuits*. (Cell Press), pp. 745-769.
158. Takamori, S., Holt, M., Stenius, K., Lemke, E.A., Gronborg, M., Riedel, D., Urlaub, H., Schenck, S., Brugger, B., Ringler, P., *et al.* (2006a). Molecular anatomy of a trafficking organelle. *Cell* 127, 831-846.
159. Takao-Rikitsu, E., Mochida, S., Inoue, E., Deguchi-Tawarada, M., Inoue, M., Ohtsuka, T., and Takai, Y. (2004). Physical and functional interaction of the active zone proteins, CAST, RIM1, and Bassoon, in neurotransmitter release. *Journal of Cell Biology* 164, 301-311.
160. Tanaka, Y., Niwa, S., Dong, M., Farkhondeh, A., Wang, L., Zhou, R., and Hirokawa, N. (2016). The Molecular Motor KIF1A Transports the TrkA Neurotrophin Receptor and Is Essential for Sensory Neuron Survival and Function. *Neuron* 90, 1215-1229.
161. Tang, A.H., Chen, H., Li, T.P., Metzbower, S.R., MacGillavry, H.D., and Blanpied, T.A. (2016). A trans-synaptic nanocolumn aligns neurotransmitter release to receptors. *Nature* 536, 210-214.
162. Tao-Cheng, J.H. (2007). Ultrastructural localization of active zone and synaptic vesicle proteins in a preassembled multi-vesicle transport aggregate. *Neuroscience* 150, 575-584.
163. Thomas, L.A., Akins, M.R., and Biederer, T. (2008). Expression and adhesion profiles of SynCAM molecules indicate distinct neuronal functions. *The Journal of Comparative Neurology* 510, 47-67.
164. Tomishige, M., Klopfenstein, D.R., and Vale, R.D. (2002). Conversion of Unc104/KIF1A kinesin into a processive motor after dimerization. *Science* 297, 2263-2267.
165. Tronchere, H., Laporte, J., Pendaries, C., Chaussade, C., Liaubet, L., Pirola, L., Mandel, J.L., and Payrastre, B. (2004). Production of phosphatidylinositol 5-phosphate by the phosphoinositide 3-phosphatase myotubularin in mammalian cells. *J Biol Chem* 279, 7304-7312.
166. Vaccari, I., Dina, G., Tronchere, H., Kaufman, E., Chicanne, G., Cerri, F., Wrabetz, L., Payrastre, B., Quattrini, A., Weisman, L.S., *et al.* (2011). Genetic interaction between MTMR2 and FIG4 phospholipid phosphatases involved in Charcot-Marie-Tooth neuropathies. *PLoS Genet* 7, e1002319.

## References

---

167. Vanhaesebroeck, B., Guillermet-Guibert, J., Graupera, M., and Bilanges, B. (2010). The emerging mechanisms of isoform-specific PI3K signalling. *Nat Rev Mol Cell Biol* 11, 329-341.
168. Verhey, K.J., and Hammond, J.W. (2009). Traffic control: regulation of kinesin motors. *Nat Rev Mol Cell Biol* 10, 765-777.
169. Vukoja, A., Rey, U., Petzoldt, A.G., Ott, C., Vollweiter, D., Quentin, C., Puchkov, D., Reynolds, E., Lehmann, M., Hohensee, S., *et al.* (2018). Presynaptic Biogenesis Requires Axonal Transport of Lysosome-Related Vesicles. *Neuron* 99, 1216-1232 e1217.
170. Wallroth, A., and Haucke, V. (2018). Phosphoinositide conversion in endocytosis and the endolysosomal system. *J Biol Chem* 293, 1526-1535.
171. Wang, X., Hu, B., Zieba, A., Neumann, N.G., Kasper-Sonnenberg, M., Honsbein, A., Hultqvist, G., Conze, T., Witt, W., Limbach, C., *et al.* (2009). A protein interaction node at the neurotransmitter release site: Domains of aczonin/piccolo, bassoon, cast, and rim converge on the N-terminal domain of Munc13-1. *Journal of Neuroscience* 29, 12584-12596.
172. Wang, Y., Okamoto, M., Schmitz, F., Hofmann, K., and Südhof, T.C. (1997). Rim is a putative rab3 effector in regulating synaptic-vesicle fusion. *Nature* 388, 593-598.
173. Watanabe, S., Rost, B.R., Camacho-Pérez, M., Davis, M.W., Söhl-Kielczynski, B., Rosenmund, C., and Jorgensen, E.M. (2013). Ultrafast endocytosis at mouse hippocampal synapses. *Nature* 504, 242-247.
174. Whiteford, C.C., Brearley, C.A., and Ulug, E.T. (1997). Phosphatidylinositol 3,5-bisphosphate defines a novel PI 3-kinase pathway in resting mouse fibroblasts. *Biochem J* 323 ( Pt 3), 597-601.
175. Whitley, P., Reaves, B.J., Hashimoto, M., Riley, A.M., Potter, B.V., and Holman, G.D. (2003). Identification of mammalian Vps24p as an effector of phosphatidylinositol 3,5-bisphosphate-dependent endosome compartmentalization. *J Biol Chem* 278, 38786-38795.
176. Wilhelm, B.G., Mandad, S., Truckenbrodt, S., Krohnert, K., Schafer, C., Rammner, B., Koo, S.J., Classen, G.A., Krauss, M., Haucke, V., *et al.* (2014). Composition of isolated synaptic boutons reveals the amounts of vesicle trafficking proteins. *Science* 344, 1023-1028.
177. Wu, X., Cai, Q., Shen, Z., Chen, X., Zeng, M., Du, S., and Zhang, M. (2019). RIM and RIM-BP Form Presynaptic Active-Zone-like Condensates via Phase Separation. *Molecular Cell* 73, 971-984.e975.
178. Wu, Y.E., Huo, L., Maeder, C.I., Feng, W., and Shen, K. (2013). The balance between capture and dissociation of presynaptic proteins controls the spatial distribution of synapses. *Neuron* 78, 994-1011.
179. Xu, F., Takahashi, H., Tanaka, Y., Ichinose, S., Niwa, S., Wicklund, M.P., and Hirokawa, N. (2018). KIF1Bbeta mutations detected in hereditary neuropathy impair IGF1R transport and axon growth. *J Cell Biol* 217, 3480-3496.
180. Yamaguchi, K., Tanaka, M., Mizoguchi, A., Hirata, Y., Ishizaki, H., Kaneko, K., Miyoshi, J., and Takai, Y. (2002). A GDP/GTP exchange protein for the Rab3 small G protein family up-regulates a postdocking step of synaptic exocytosis in central synapses. *Proc Natl Acad Sci U S A* 99, 14536-14541.

## References

---

181. Yang, N., Chanda, S., Marro, S., Ng, Y.H., Janas, J.A., Haag, D., Ang, C.E., Tang, Y., Flores, Q., Mall, M., *et al.* (2017). Generation of pure GABAergic neurons by transcription factor programming. *Nat Methods* 14, 621-628.
182. Ye, B., Zhang, Y., Song, W., Younger, S.H., Jan, L.Y., and Jan, Y.N. (2007). Growing Dendrites and Axons Differ in Their Reliance on the Secretory Pathway. *Cell* 130, 717-729.
183. Yonekawa, Y., Harada, A., Okada, Y., Funakoshi, T., Kanai, Y., Takei, Y., Terada, S., Noda, T., and Hirokawa, N. (1998). Defect in Synaptic Vesicle Precursor Transport and Neuronal Cell Death in KIF1A Motor Protein-deficient Mice. *JCB*.
184. Yordanov, T.E., Hipolito, V.E.B., Liebscher, G., Vogel, G.F., Stasyk, T., Herrmann, C., Geley, S., Teis, D., Botelho, R.J., Hess, M.W., and Huber, L.A. (2019). Biogenesis of lysosome-related organelles complex-1 (BORC) regulates late endosomal/lysosomal size through PIKfyve-dependent phosphatidylinositol-3,5-bisphosphate. *Traffic* 20, 674-696.
185. Yu, W., and Baas, P.W. (1994). Changes in microtubule number and length during axon differentiation. *J Neurosci* 14, 2818-2829.
186. Zala, D., Hinckelmann, M.V., Yu, H., Lyra da Cunha, M.M., Liot, G., Cordelieres, F.P., Marco, S., and Saudou, F. (2013). Vesicular glycolysis provides on-board energy for fast axonal transport. *Cell* 152, 479-491.
187. Zhai, R.G., Vardinon-Friedman, H., Cases-Langhoff, C., Becker, B., Gundelfinger, E.D., Ziv, N.E., and Garner, C.C. (2001). Assembling the Presynaptic Active Zone: A Characterization of an Active Zone Precursor Vesicle. *Neuron* 29, 131-143.
188. Zhang, Y., Pak, C., Han, Y., Ahlenius, H., Zhang, Z., Chanda, S., Marro, S., Patzke, C., Acuna, C., Covy, J., *et al.* (2013). Rapid single-step induction of functional neurons from human pluripotent stem cells. *Neuron* 78, 785-798.
189. Zhao, C., Takita, J., Tanaka, Y., Setou, M., Nakagawa, T., Takeda, S., Yang, H.W., Terada, S., Nakata, T., Takei, Y., *et al.* (2001). Charcot-Marie-Tooth Disease Type 2A Caused by Mutation in a Microtubule Motor KIF1B $\beta$ . *Cell* 105, 587-597.
190. Zhou, H.M., Brust-Mascher, I., and Scholey, J.M. (2001). Direct Visualization of the Movement of the Monomeric Axonal Transport Motor UNC-104 along Neuronal Processes in Living *Caenorhabditis elegans*. *The Journal of Neuroscience* 21, 3749-3755.
191. Ziv, N.E., and Garner, C.C. (2004). Cellular and molecular mechanisms of presynaptic assembly. *Nat Rev Neurosci* 5, 385-399.
192. Zolov, S.N., Bridges, D., Zhang, Y., Lee, W.W., Riehle, E., Verma, R., Lenk, G.M., Converso-Baran, K., Weide, T., Albin, R.L., *et al.* (2012). In vivo, Pikfyve generates PI(3,5)P<sub>2</sub>, which serves as both a signaling lipid and the major precursor for PI5P. *Proc Natl Acad Sci U S A* 109, 17472-17477.
193. Kong, S. (2022). Investigating lysosomal identity of presynaptic organelles in developing human iPSC-derived neurons. [Master's Thesis, Freie Universitaet]

## 8. Appendix

### 8.1. Appendix A: Abbreviations

AA	amino acid	DKO	double knockout
Antero	anterograde	DMEM	Dulbecco's modified Eagle's medium
AP	action potential	DMSO	dimethylsulfoxid
AraC	Cytosine $\beta$ -D-arabinofuranoside	DNA	deoxyribonucleic acid
Arf	ADP-ribosylation factor	DNase	deoxyribonuclease
Arl	Arf-like	dNTP	deoxynucleosid-triphosphate
Arl8	ADP-ribosylation factor-like protein 8	Dox	Doxycycline
A.U.	arbitrary units	DLK	Dual leucine zipper kinase
AUC	area-under-the-curve	<i>E. coli</i>	<i>Escherichia coli</i>
BDNF	Brain-derived neurotrophic factor	ECL	enhanced chemiluminescence
bp	base pairs	eGFP	enhanced green fluorescent protein
BSA	bovine serum albumin	EM	electron microscopy
<i>C. elegans</i>	<i>Caenorhabditis elegans</i>	ER	endoplasmic reticulum
Cav	voltage-gated calcium channels	et al.	and others (et alii)
CMT	Charcot-Marie-Tooth	F	fluorescence intensity
CMV	cytomegalovirus	F <sub>0</sub>	fluorescence intensity
CNQS	6-cyano-7-nitroquinoxaline-2,3-dione	FBS	fetal bovine serum
CNS	central nervous system	FCS	fetal calf serum
C-terminal	carboxy-terminal	FL	full length
<i>D. melanogaster</i>	<i>Drosophila melanogaster</i>	FYVE	Fab1, YOTB, Vac1 and EEA1
DAPI	4',6-Diamidino-2-phenylindole	fw	forward
DIV	days <i>in vitro</i>	g	gram
		Gdf7	growth differentiation factor 7

## Appendix

---

GFP	green fluorescent protein	m	milli
GST	glutathione-S-transferase	MAP2	Microtubule-associated protein 2
GTP	guanosine triphosphate		
h	hour	min	minutes
HBSS	Hanks's Balanced Salt Solution	MSX1	msh homeobox1
HEK	human embryonic kidney	MTM	myotubularin
Hepes	4-(2-hydroxyethyl) piperazine-1-ethanesulfonic acid	MVB	multivesicular body
		n.s.	not significant
		NA	Numerical aperture
HRP	horseradish peroxidase	NEAA	non-essential amino acid
Hz	Herz	NGS	normal goat serum
ICC	immunocytochemistry	N terminal	amino-terminal
IgG	Immunoglobulin G	P/S	penicillin/ streptomycin
IHC	Immunohistochemistry	PBS	phosphate buffered saline
iPSC	induced pluripotent stem cell	PCR	polymerase chain reaction
		PDL	poly-D-Lysin hydromide
iN	induced neuron	PFA	paraformaldehyde
IPTG	Isopropyl- $\beta$ -D-thiogalactopyranoside	PH	pleckstrin homology
		PI	phosphoinositide
KD	knockdown	PI(3)P	phosphatidylinositol-3-phosphate
kDa	kilodalton		
KI	knockin	PI(4,5)P <sub>2</sub>	phosphatidylinositol-4,5-bisphosphate
KIF1A	Kinesin Family Member 1A	PI(3,4)P <sub>2</sub>	phosphatidylinositol-3,4-bisphosphate
KO	knockout		
Lamp1	Lysosomal-associated membrane protein 1	PI(3,4,5)P <sub>3</sub>	phosphatidylinositol-(3,4,5)-trisphosphate
LB	Luria-Bertani Broth	PI(4,5)P <sub>2</sub>	phosphatidylinositol-4,5-bisphosphate
LV	lentivirus		
$\mu$ l	microliters	PI(4)P	phosphatidylinositol-4-phosphate
M	molar	PI(4,5)P <sub>2</sub>	phosphatidylinositol-4,5-bisphosphate
<i>M. musculus</i>	<i>Mus musculus</i>		
mCh	mCherry		

## Appendix

---

PI(5)P	phosphatidylinositol-5-phosphate	SNARE	soluble NSF attachment protein receptor
PI3K	Phosphoinositide 3-kinase	SV	synaptic vesicle
PI4K	PI 4-kinase	Syb2	Synaptobrevin
PIKfyve	Phosphoinositide Kinase, FYVE-Type Zinc Finger Containing	Syp	Synaptophysin
		Syt1	Synaptotagmin 1
PLL	poly-L-Lysin	T	endocytic time constant
PMSF	phenylmethylsulfonyl fluoride	TAE	Tris-Acetate-EDTA
		TBS	Tris buffered saline
PtdIns	Phosphatidylinositol	TEMED	N,N,N',N'-tetramethylethylenediamine
PTV	Piccolo-Bassoon transport vesicle	TGN	trans Golgi network
PV	precursor vesicle	Tuj1	Neuron-specific class III beta-tubulin
Retro	retrograde	UV	ultraviolet
rev	reverse	V	voltage
RNA	ribonucleic acid	v/v	volume per volume
ROI	region of interest	w/v	weight per volume
RT	room temperature	vGlut1	vesicular glutamate transporter
s	seconds	VAMP2	vesicle-associated membrane protein 2
scr	scrambled	WB	western blot
SDS	sodium dodecylphosphate	WT	wild type
PAGE	gel electrophoresis		
SEM	standard error of the mean		
shRNA	small hairpin RNA		

## 8.2. Appendix B: Supplemental Figures

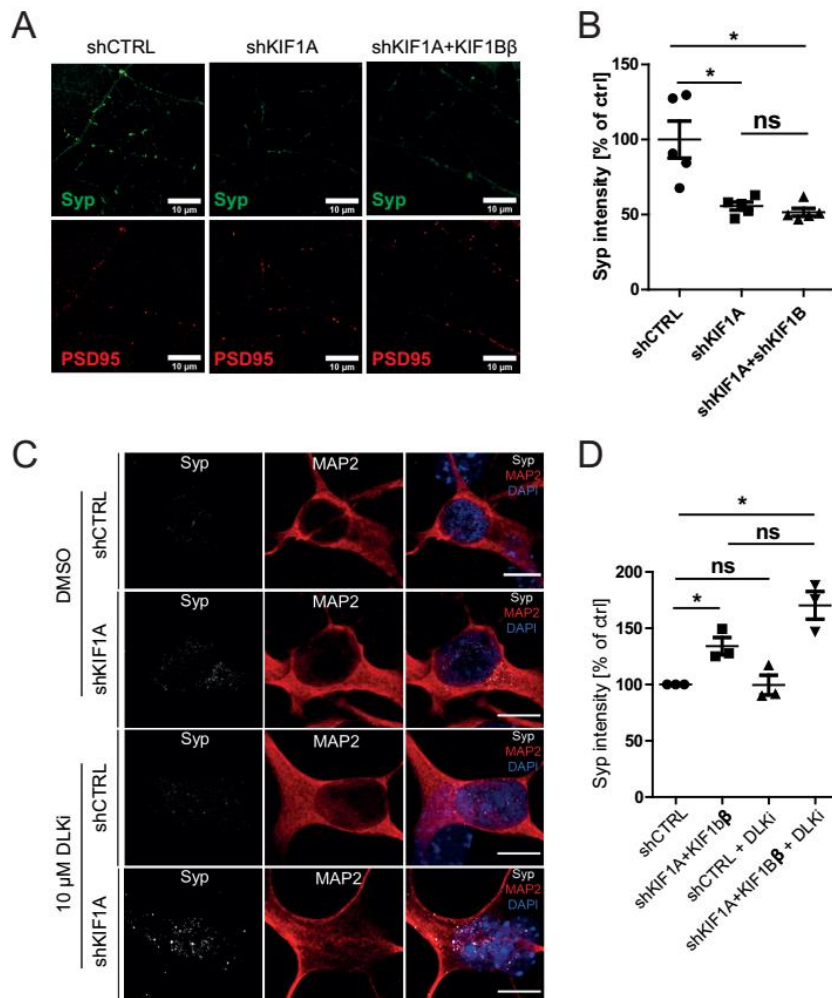


**Figure S1. Depletion of KIF1A and KIF1B $\beta$  do not have additive effects on presynapse depletion.**

(A) Representative confocal images of iNs transduced with lentiviruses expressing shRNAs against CTRL, KIF1A or KIF1A+KIF1B $\beta$  and immunostained with antibodies against Syp (presynaptic) and PSD95 (postsynaptic). Scale bar, 10  $\mu$ m. (B) Fluorescence level of Syp is significantly decreased in shKIF1A iNs, compared to shCTRL. (shCTRL, 100.0  $\pm$  12.26 %; shKIF1A, 55.63  $\pm$  2.666 %; shKIF1A + KIF1B $\beta$ , 51.58  $\pm$  2.644 %) (C) Representative confocal images of Ins somata transduced with lentiviruses expressing shRNAs against CTRL, or KIF1A+KIF1B $\beta$ , incubated 24h with DMSO or 10  $\mu$ M GNE-3511 (DLK inhibitor) and immunostained with antibodies against Syp (presynaptic) and MAP2. Scale bar, 10  $\mu$ m. (D) Accumulation of Syp in neuronal somata is slightly increased upon DLK inhibition. (DMSO: shCTRL is normalized to 100%; shKIF1A + KIF1B $\beta$ , 134.1  $\pm$  7.731 %; DLKi: shCTRL, 99.53  $\pm$  8.784%; shKIF1A + KIF1B $\beta$ , 170.3  $\pm$  12.24%) (B and D) n > 3 independent experiments with  $\geq$ 100 synaptic puncta per experiment; t test; \*P < 0.05). Data represent mean  $\pm$  SEM

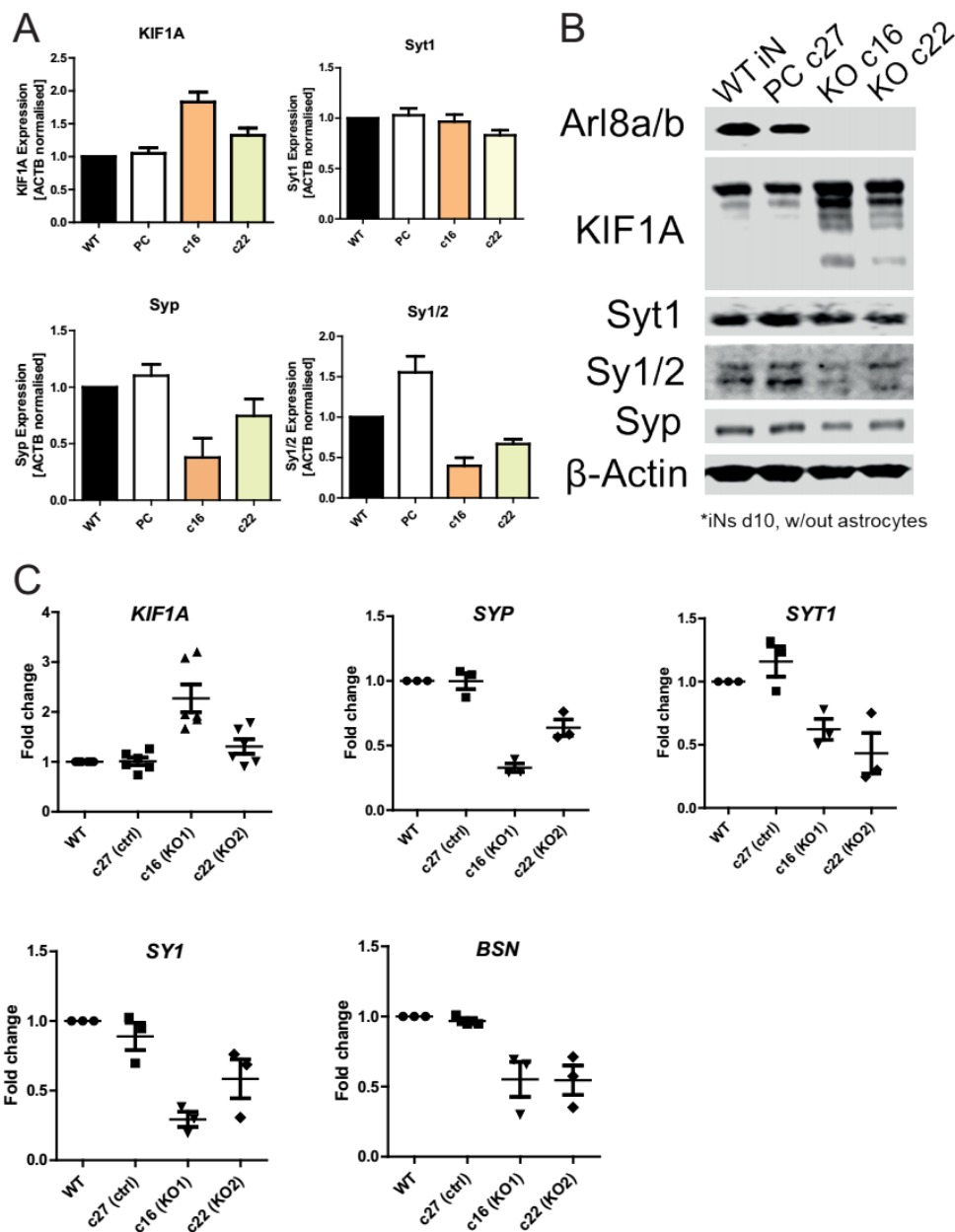


**Figure S2. Protein and mRNA levels of presynaptic proteins change in Arl8a/b dKO neurons.** (A) Graphs demonstrating that protein expression levels of KIF1A increase and Syt1, Syp and Sy1/2 decrease in Arl8a/b dKO cells. Protein levels are normalised to  $\beta$ -Actin. PC: control cell line, c16 and c22 two double KO cell lines. (B) Representative Western Blot for (A). (C) mRNA levels of KIF1A and presynaptic markers SYP, SYT1, SY1 and BSN were tested using quantitative real-time (qRT) PCR, normalized to GAPDH and compared to WT iN levels. Data are shown as mean  $\pm$  SEM (n=1 with at least 3 biological replicates).

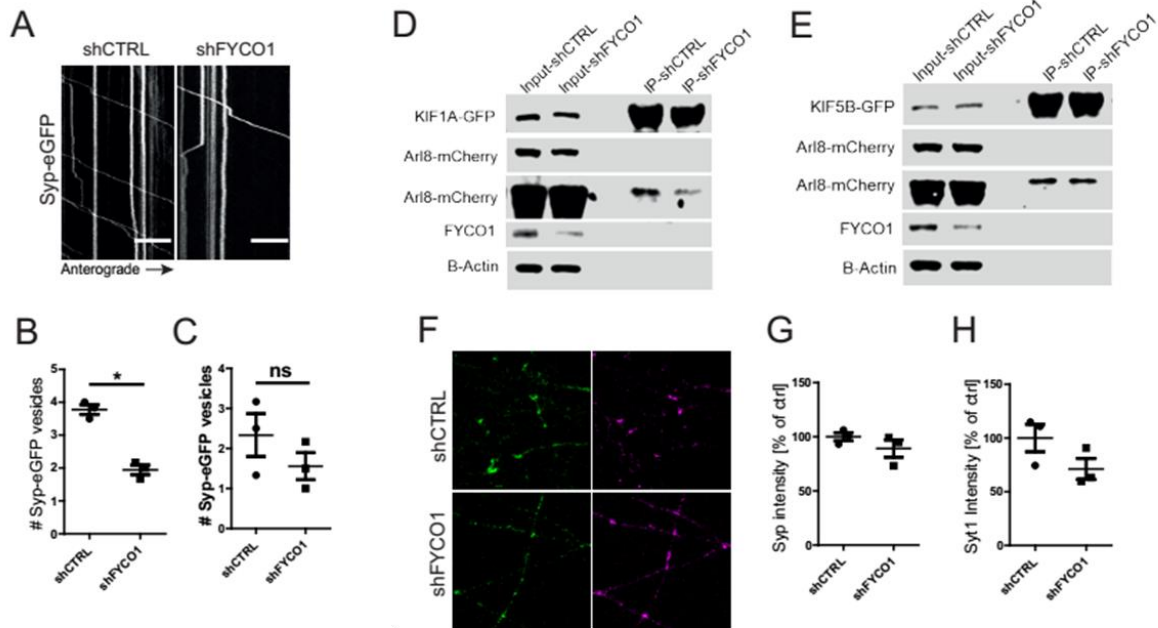


**Figure S3. FYCO1 depletion decreases anterograde PV transport and impairs KIF1A and Arl8 interaction.** (A) kymographs showing movements of Syp-GFP vesicles in shCTRL and shFYCO1 condition. X axis represent distance (Direction right: Anterograde) and Y axis represent time (1 min). (Scale bars, 10  $\mu$ m.) (B and C) Quantifications of Syp-eGFP imaging showing that number of anterogradely moving vesicles decrease but retrogradely moving vesicles do not change. Bars demonstrate average number of vesicles per video (2 minutes) over 30 $\mu$ m length of axon. (Anterograde: shCTRL,  $3.778 \pm 0.1470$ ; shFYCO1,  $1.944 \pm 0.1470$ ; Retrograde: shCTRL,  $2.333 \pm 0.5358$ ; shFYCO1,  $1.556 \pm 0.3379$ )  $n = 3$  independent experiments with  $\geq 6$  videos per experiment; one-way analysis of variance (ANOVA) followed by Dunnett's post-test;  $p < 0.0001$  \*\*\*\*;  $p < 0.01$  \*\*;  $p > 0.05$  ns). Data represent mean  $\pm$  SEM. (D and E) Co-immunoprecipitation of KIF1A-eGFP (D) or KIF5B-eGFP (E) with Arl8b-mCherry in HEKs show that levels of KIF1A-Arl8b interaction decrease upon FYCO1 knockdown whereas KIF5B-Arl8b interaction is not affected by FYCO1 loss. (F) Representative confocal images of iNs transduced with lentiviruses expressing shRNAs against CTRL or FYCO1 and immunostained for Syp (presynaptic, green) and Homer1 (postsynaptic, magenta). Scale bar, 10  $\mu$ m. (G and H) Fluorescence levels of Syp (shCTRL,  $100.0 \pm 3.712\%$ ; shFYCO1,  $89.13 \pm 8.073\%$ ) and Syt1 (shCTRL,  $100.0 \pm 12.82\%$ ; shFYCO1,  $71.4 \pm 9.816\%$ ) are slightly decreased upon FYCO1 loss.  $n=3$  independent experiments with  $\geq 100$  synaptic puncta per experiment; t test; \* $P < 0.05$ ). Data represent mean  $\pm$  SEM

### 8.3. Appendix C: List of Figures and Tables

#### 8.3.1. List of Tables

Table 3.1: Composition of buffers and media used in molecular biology experiments

Table 3.2: Buffers and solutions used in cell biological and imaging experiments

Table 3.3: Compositions of solutions used for biochemical experiments

Table 3.4: Molecular weight standards

Table 3.5: Sequences of shRNAs used in this study

Table 3.6: Primer sequences used for cloning

Table 3.7: Vector backbones used for cloning and protein expression

Table 3.8: Plasmid DNA constructs used for recombinant protein expression

Table 3.9: Primary antibodies used in this study.

Table 3.10: Secondary antibodies used in this study

Table 3.11: Phusion High-Fidelity PCR 25  $\mu$ l reaction mix

Table 3.12: Phusion High-Fidelity Touchdown PCR program

Table 3.13: guide RNA sequences used in Crispr/Cas9

Table 3.14: Primer pairs used for amplification of Crispr-targeted regions

Table 3.15: Liposome compositions for sedimentation assay

Table 3.16: Composition of SDS Polyacrylamide Gels

Table 4.1: KIF1A-eGFP MS/MS reveals interaction partners in developing neurons.

#### 8.3.2. List of Figures

Figure 1.1: Key components of the presynaptic machinery for neurotransmitter release.

Figure 1.2: Main processes in Active Zone assembly.

Figure 1.3: Illustration of axonal transport mechanism of Cav channel-carrier vesicles destined for active zone membranes.

Figure 1.4: Molecular model of an average synaptic vesicle

## Appendix

---

Figure 1.5: Domain structures of major kinesins.

Figure 1.6: Cargos, structure, and regulation of KIF1A.

Figure 1.7: Arl8 interacts with its upstream regulator BORG and its downstream effectors SKIP, HOPS complex and PLEKHM1 to regulate lysosome positioning and cargo degradation.

Figure 1.8: Compositions and roles of BORG and BLOC-1 multisubunit complexes.

Figure 1.9: Interconversion pathways of seven phosphoinositides by kinases and phosphatases.

Figure 1.10: Cryo-EM Reconstruction and domain organization of the human PIKfyve lipid kinase complex.

Figure 4.1: Excitatory cortical neurons are generated from human iPSCs.

Figure 4.2: Human iNs express neuronal markers and form pre- and postsynaptic specializations.

Figure 4.3: pHluorin retrieval in day 28 iNs at room temperature.

Figure 4.4: Axonal co-transport levels of presynaptic proteins in developing iNs.

Figure 4.5: Endogenously labelled Syp-eGFP iPSCs are generated using Crispr/Cas9.

Figure 4.6: Axonal co-transport levels of endogenous Syp-eGFP with presynaptic proteins in developing iNs.

Figure 4.7: KIF1A co-transport with PVs in developing axons.

Figure 4.8: shRNA-mediated knockdown of KIF1A results in significant decrease in levels of anterogradely transported presynaptic proteins and a strong phenotype at synaptic sites of mature human neurons.

Figure 4.9: KIF1A KO iPSC line was generated by using CRISPR/Cas9.

Figure 4.10: KIF1A KO iNs show decreased ratio of anterogradely transported presynaptic proteins.

Figure 4.11: Complete loss of KIF1A using CRISPR/Cas9 results in a strong depletion of fluorescence levels of SV and AZ proteins but not Cavs at synaptic sites of mature human neurons.

Figure 4.12: Arl8b is a marker of PVs.

## Appendix

---

Figure 4.13: Axonal co-transport levels of endogenous Syp-eGFP with lysosomal membrane proteins in developing iNs.

Figure 4.14: Knockdown screen confirms Arl8-dependent transport of PVs.

Figure 4.15: Co-knockdown of Arl8a and Arl8b phenocopies the presynaptic depletion observed upon KIF1A loss.

Figure 4.16: Arl8a and Arl8b double knockout iPSCs were generated using Crispr/Cas9.

Figure 4.17: Arl8a/b dKO iNs show Arl8-dependent regulation of PV transport.

Figure 4.18: Arl8a/b dKO iNs phenocopy the presynaptic depletion observed in Arl8a/b co-knockdown neurons.

Figure 4.19: Postsynaptically localised calcium probe Xph20-CaMP7f reveals that Arl8a/b dKO iNs have significantly decreased amounts of Ca<sup>++</sup> influx at DIV 34.

Figure 4.20: Lipid binding PH domain of KIF1A is required for membrane recruitment.

Figure 4.21: Different PIP sensors were screened to detect levels of co-transport between Synaptophysin and PI(3)P, PI(4)P or PI(4,5)P<sub>2</sub>.

Figure 4.22: Depletion of PI(3)P or PI(3,5)P<sub>2</sub> levels inhibits anterograde transport of endogenous Syp vesicles in developing iNs.

Figure 4.23: KIF1A cannot be recruited to membranes of PVs upon Apilimod treatment.

Figure 4.24: Primary hippocampal neurons confirm the reduction of KIF1A membrane recruitment upon Apilimod treatment.

Figure 4.25: Lentiviral knockdown of PIKfyve inhibits recruitment of KIF1A to membranes of precursor vesicles.

Figure 4.26: PI(3,5)P<sub>2</sub> binding of KIF1A PH domain was verified by *in vitro* assays.

Figure 4.27: Membrane recruitment of tail domain of KIF1A is inhibited by Arl8a/b loss.

Figure 4.28: Number of Arl8b positive vesicles in the axons are not altered with KIF1A loss.

Figure 4.29: Anterograde transport of PVs is unaltered upon shRNA-mediated depletion of BORG subunits.

Figure 4.30: In the absence of Arl8a/b, loss of BORG increases anterograde PV transport and membrane recruitment of KIF1A.

Figure 5.1: Schematic representation for PV transport machinery